2019年现代催化研究方法高级讲习班
西交利物浦大学，苏州，2019年7月14日

扫描探针与纳米光谱技术

杨帆

纳米与界面催化研究组(SKLC 502)

中国科学院大连化学物理研究所

Email: fyang@dicp.ac.cn; https:// fruit.dicp.ac.cn

本课程的主要内容：

- 表面科学与扫描探针显微镜简介
- 扫描隧道显微镜（STM）基本原理
- 真空基础与STM的工作原理
- STM在催化中的应用
- 原子力显微镜（AFM）基本原理
- AFM的工作原理
- AFM在催化中的应用
- 光谱，SNOM以及纳米光谱技术简介
- TERS
- IR-SNOM与AFM-IR

Books

- Introduction to Scanning Tunneling Microscopy, C. Julian. Chen, Oxford university press 1993
- Scanning tunneling Microsccopy and Spectroscopy Theory Techniques and application, Editor Dawn A. Bonell VCH 1993
- Scanning Tunneling Microscopy and spectroscopy method and application, Roland Wiesendanger, Cambridge university Press 1996
- Amplitude Modulation Atomic Force Microscopy. Ricardo Garcia, Wiley-VCH Verlag GmbH & Co. KGaA: Weinheim, Germany, 2010.

（里卡多·加西亚; 程志海; 裘晓辉, 振幅调制原子力显微术. 1 ed.; 科学出版社: 2016.）

- 辛勤，现代催化研究方法；科学出版社：2018.

一个催化过程与三项诺贝尔奖

$0{,}5N_2+1{,}5H_2 \rightarrow NH_3$

Iron Catalyst

Haber, Nobel Prize in 1918

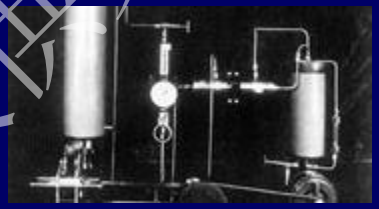

Bosch, Nobel Prize in 1931

Ertl, Nobel Prize in 2007

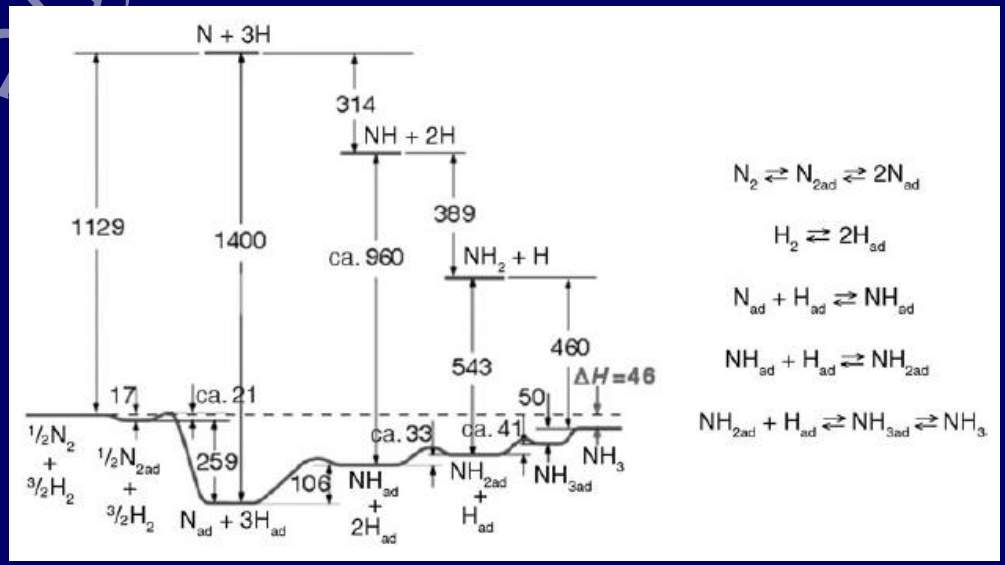

Fritz Haber

1868 - 1934

Nobel Prize 1918

Ammonia synthesis introduction from Ertl's Nobel lecture

$$N_2 + 3\,H_2 \rightarrow 2\,NH_3$$

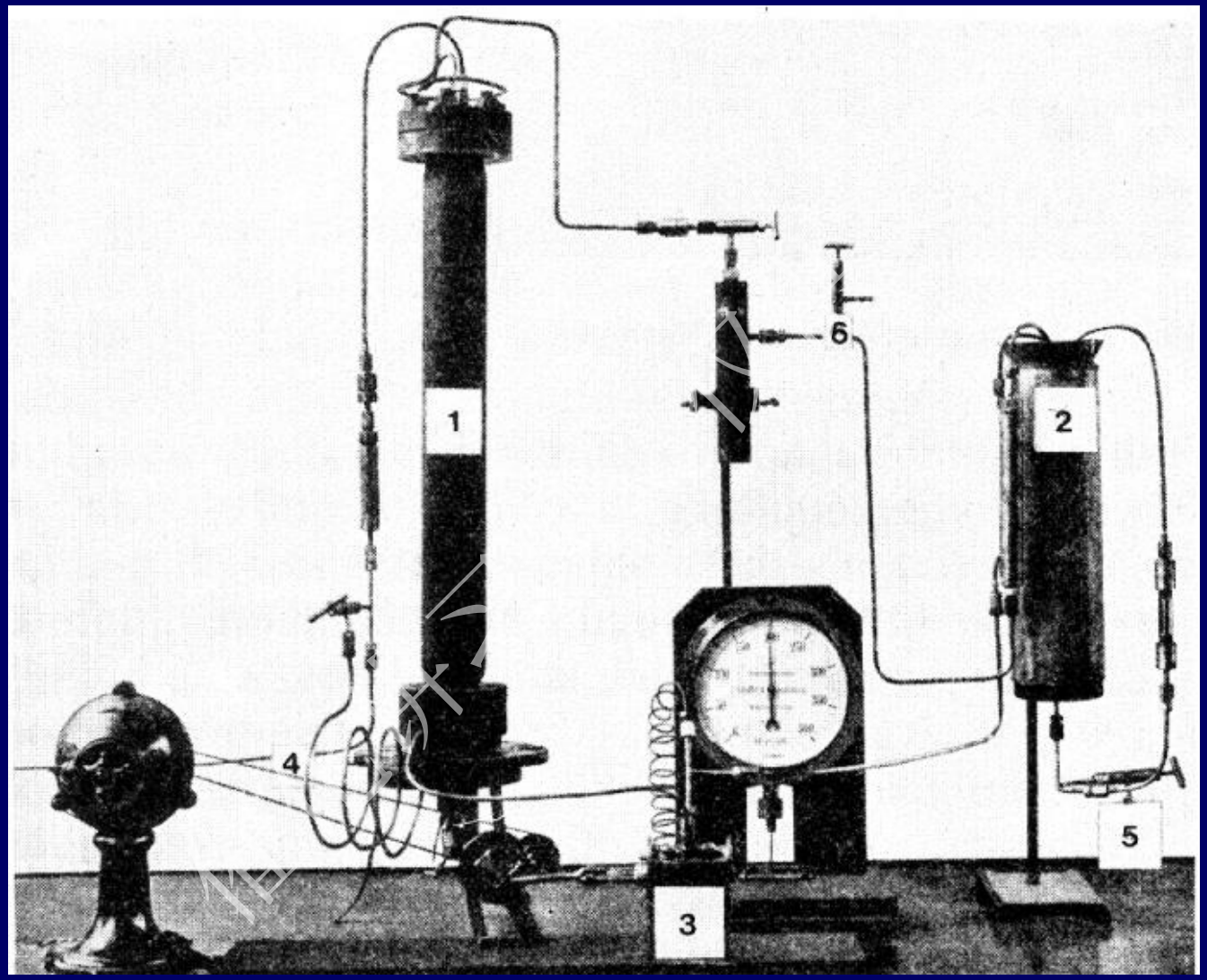

Haber & LeRossignol, 1909

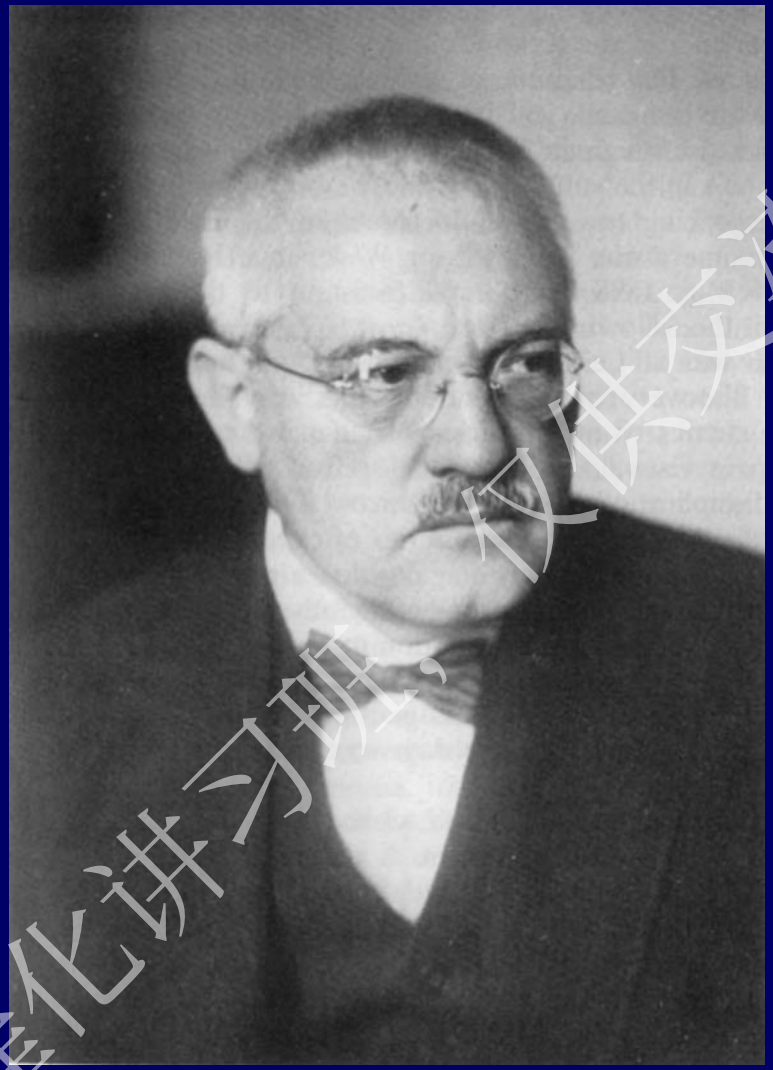

Carl Bosch
1874 - 1940

Nobel Prize 1931


催化讲习班，仅供交流

World population and ammonia production

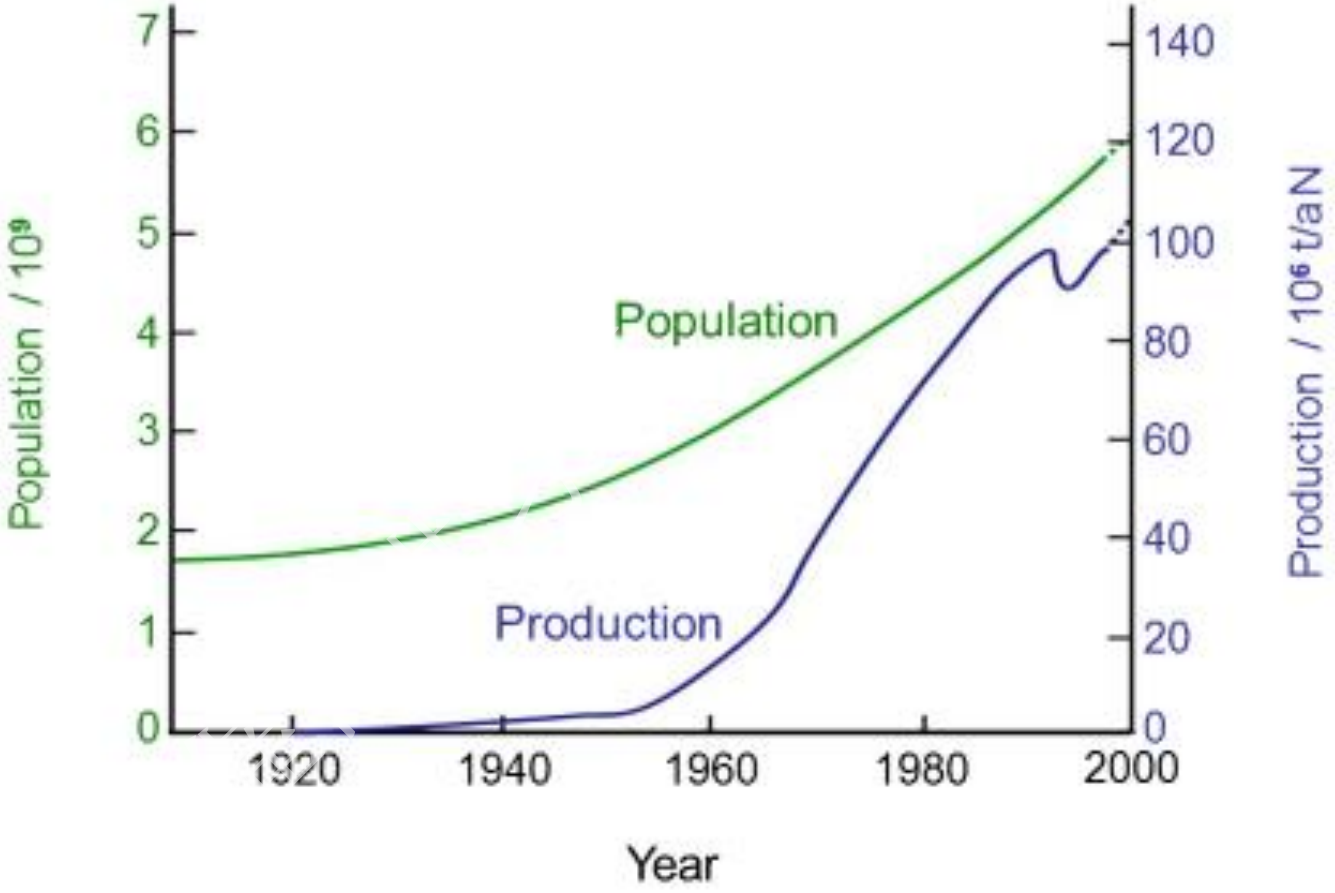

M. Appl, "Ammonia", Wiley–VCH (1999)

P.H. Emmett (1974):

„ The experimental work of the past 50 years leads to the conclusion that the rate-limiting step in ammonia synthesis over iron catalysts is the chemisorption of nitrogen. The question as to whether the nitrogen species involved is molecular or atomic is still not conclusively resolved, though, in my opinion, the direct participation of nitrogen in an atomic form seems more likely than in molecular form.“

The physical basis of heterogeneous catalysis (E. Drauglis & R.I. Jaffee, eds.), Plenum Press, New York, 1975, p. 3

Catalytic synthesis of ammonia

(Haber- Bosch process)

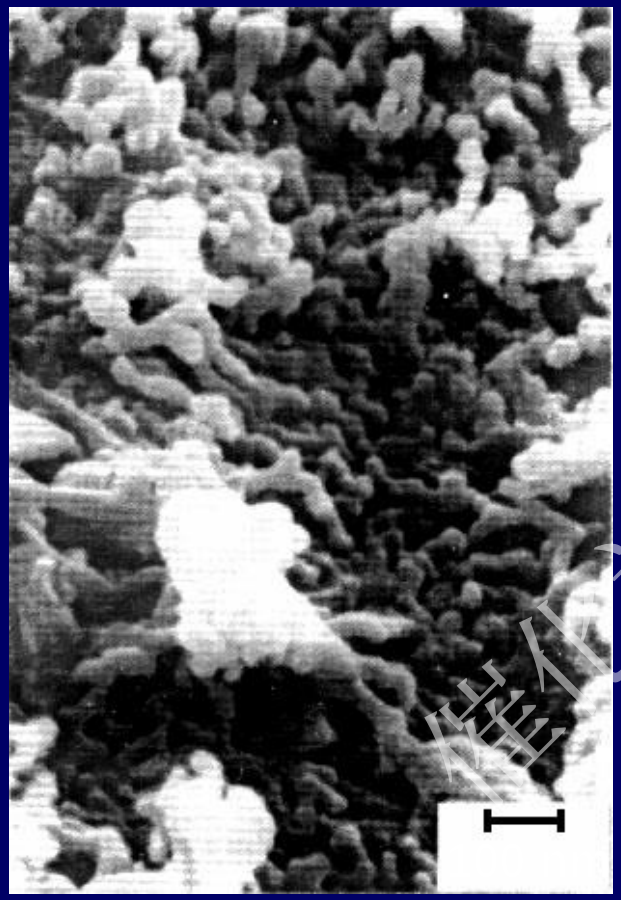

Technical conditions: $T \approx 400^{\circ}$ C, $p \approx 300$ bar
promoted iron catalyst

BASF S6-10 catalyst (at. %)

	Fe	K	Al	Ca	O
Bulk composition	40.5	0.35	2.0	1.7	53.2
Surface –					
unreduced	8.6	36.2	10.7	4.7	40.0
reduced	11.0	27.0	17.0	4.0	41.0
cat. active spot	30.1	29.0	6.7	1.0	33.2

G. Ertl, D. Prigge, R. Schlögl & D. Weiss, J.Catal. **79** *(1983), 359*

Irving Langmuir
1881 – 1957
Nobel Prize 1932

"Most finely divided catalysts must have structures of great complexity. In order to simplify our theoretical consideration of reactions at surfaces, let us confine our attention to reactions on plane surfaces. If the principles in this case are well understood, it should then be possible to extend the theory to the case of porous bodies. In general, we should look upon the surface as consisting of a checkerboard ..."

I. Langmuir, *Trans. Faraday Soc.* **17** (1922), 607

传统的表面催化研究

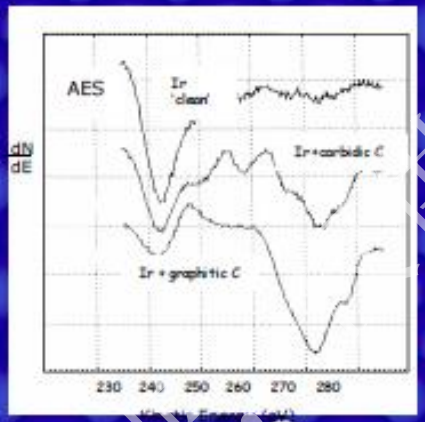

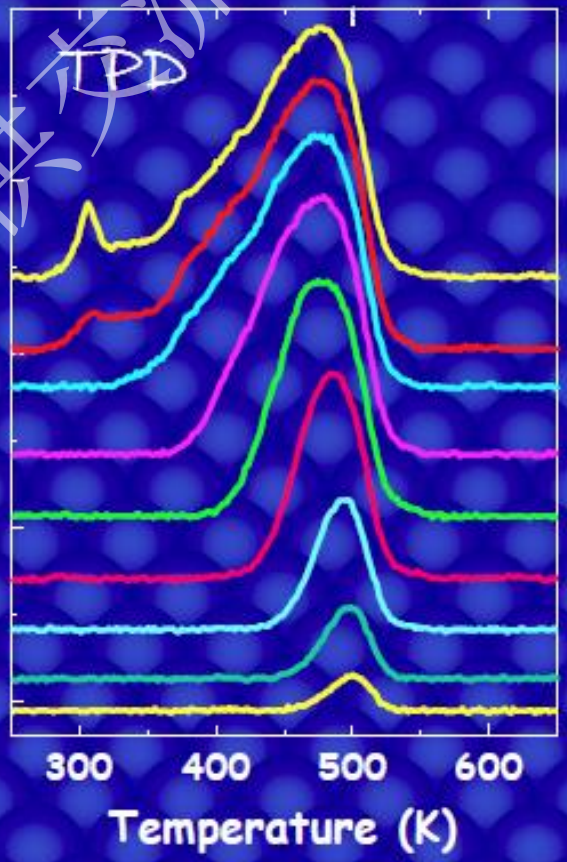

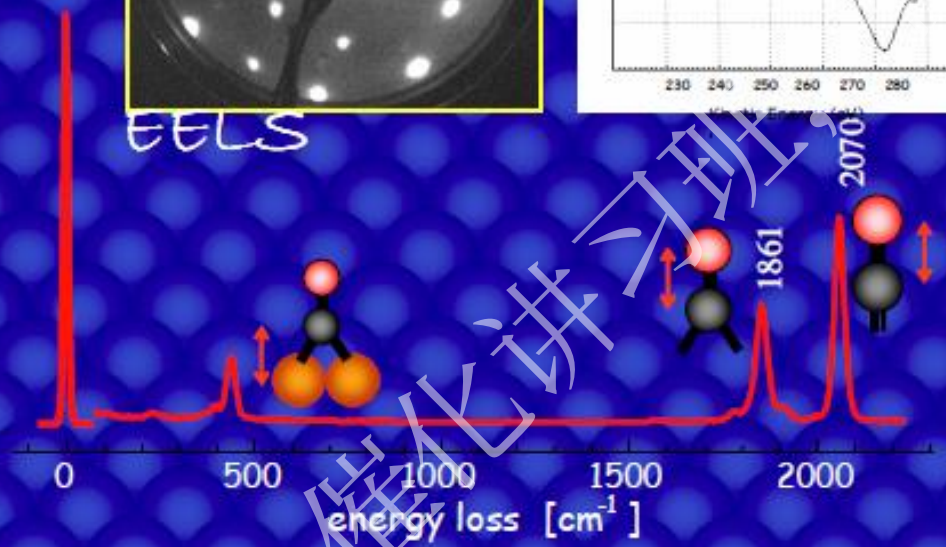

为表面催化过程提供一个定量的描述

N / Fe (100)

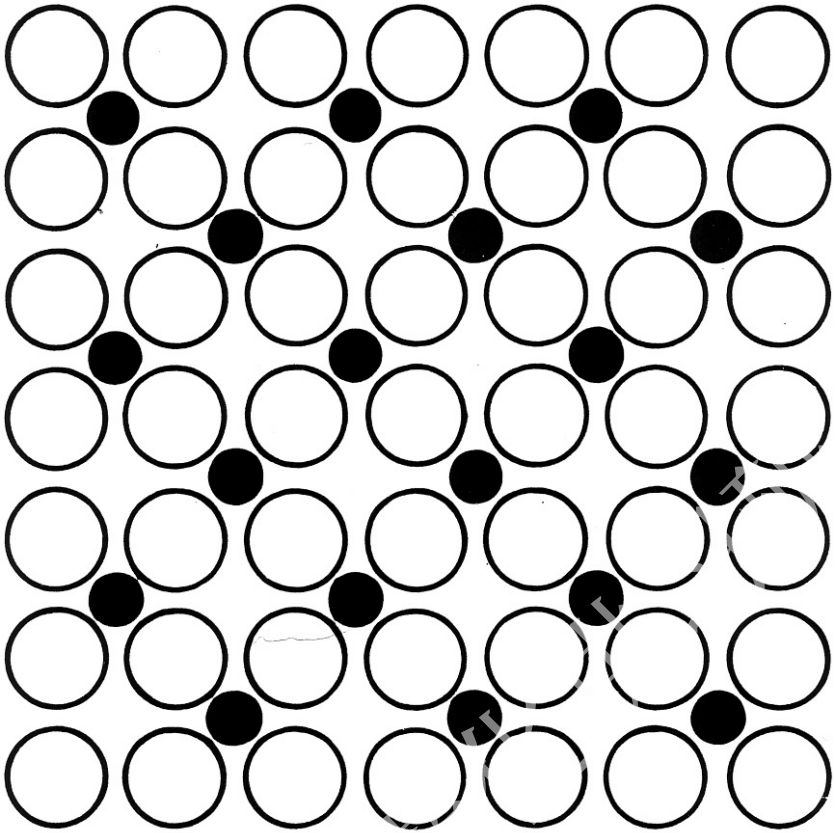

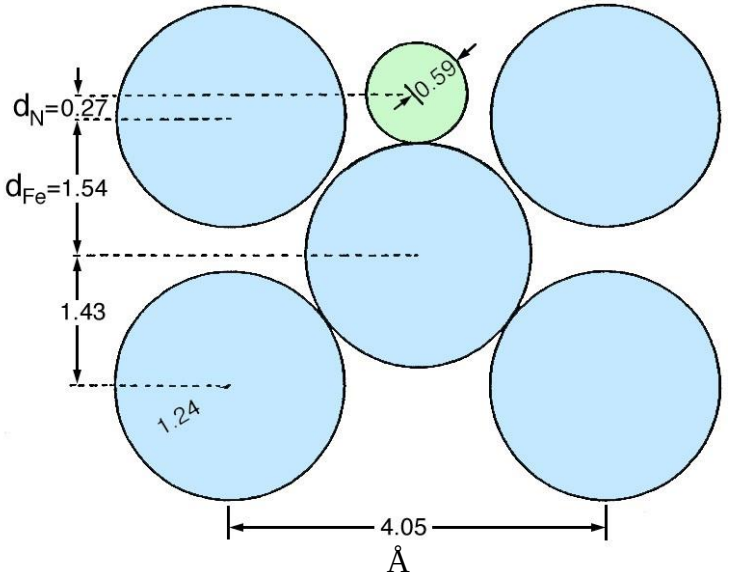

R. Imbihl, R.J. Behm, G. Ertl, W. Moritz, Surface Sci. **123** *(1982), 129.*

Ammonia synthesis introduction from Ertl's Nobel lecture

Dissociative nitrogen adsorption on Fe single crystal surfaces

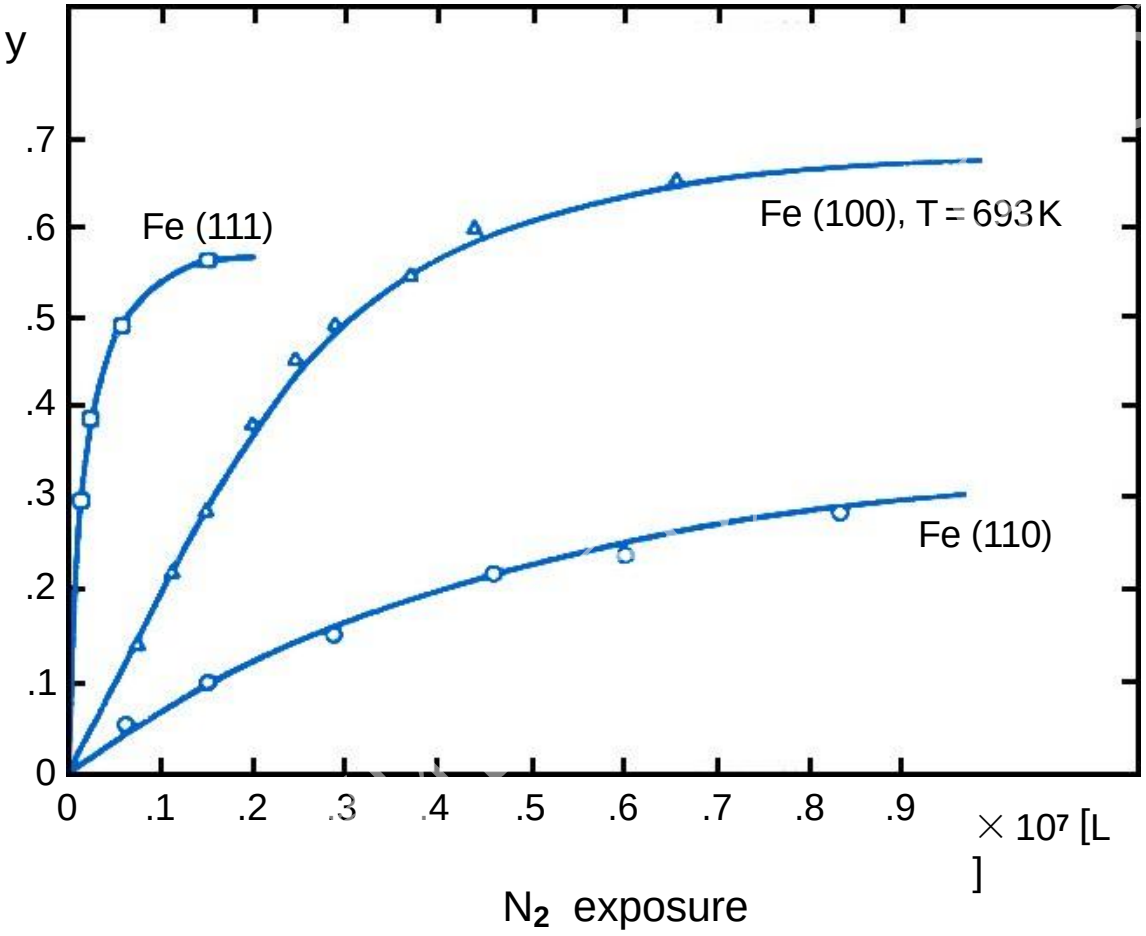

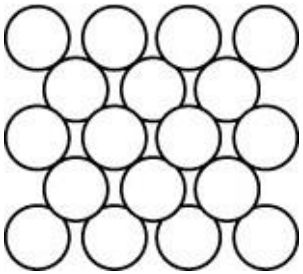

Fe (110)

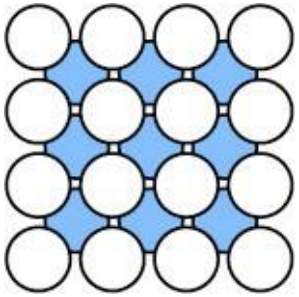

Fe (100)

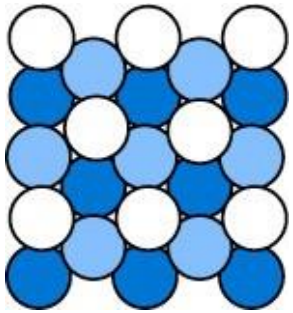

Fe (111)

F. Bozso, G. Ertl, M. Grunze & M. Weiss, J. Catal. **49** *(1977), 18;* **50** *(1977), 519*

Ammonia synthesis introduction from Ertl's Nobel lecture

Mechanism of catalytic ammonia synthesis

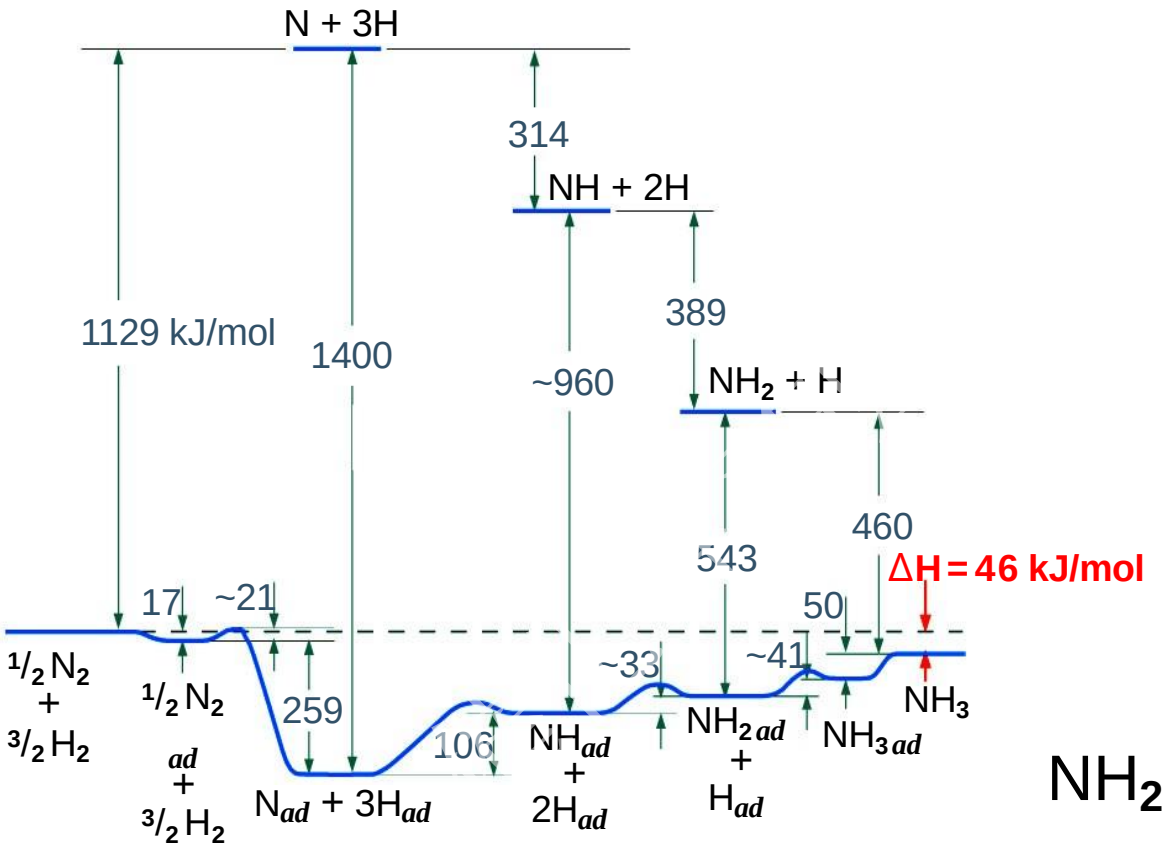

$$N_2 \rightleftarrows N_{2\,ad} \rightleftarrows 2N_{ad}$$

$$H_2 \rightleftarrows 2H_{ad}$$

$$N_{ad} + H_{ad} \rightleftarrows NH_{ad}$$

$$NH_{ad} + H_{ad} \rightleftarrows NH_{2\,ad}$$

$$NH_{2\,ad} + H_{ad} \rightleftarrows NH_{3\,ad} \rightleftarrows NH_3$$

G. Ertl, Catal.Rev.Sci.Eng. **21** *(1980), 201*

Ammonia synthesis introduction from Ertl's Nobel lecture

Catalytic synthesis of ammonia: Microkinetics

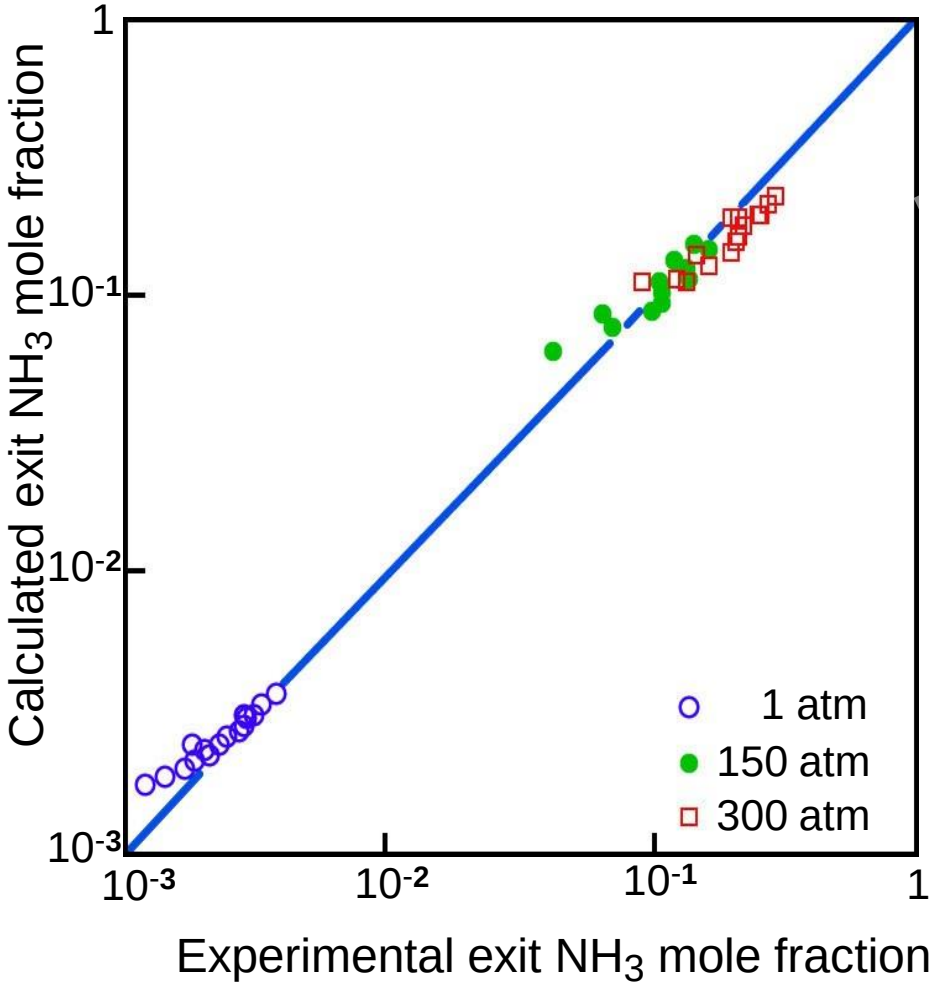

$$N_2 + 3\,H_2 \rightleftarrows 2\,NH_3$$

promoted iron catalyst

P. Stoltze and J.K. Nørskov,

Phys. Rev. Lett. ***55*** *(1985), 2502*

J. Catal. ***110*** *(1988), 1*

常用的现代表面科学手段

Low Energy Electron Diffraction (LEED)

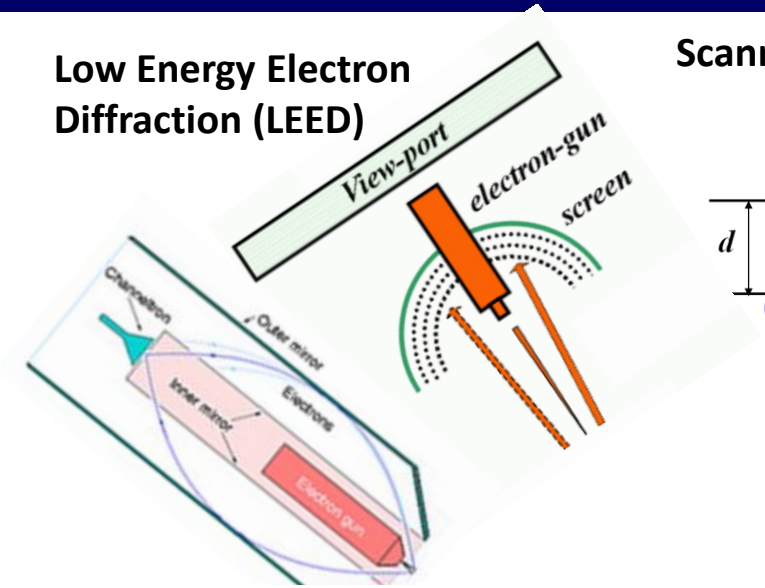

Scanning Tunneling Microscopy (STM)

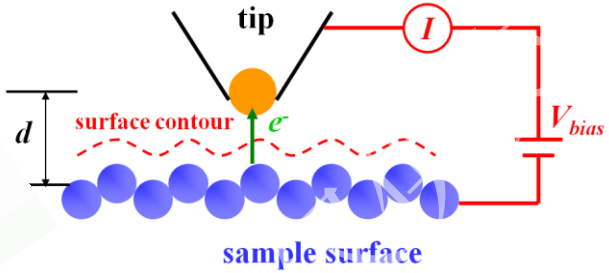

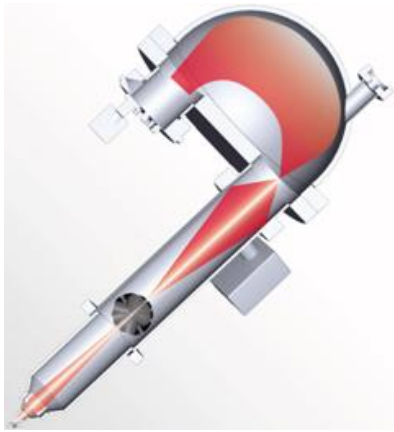

Photoelectron Spectroscopy (XPS, UPS)
Ion scattering spectroscopy (ISS)

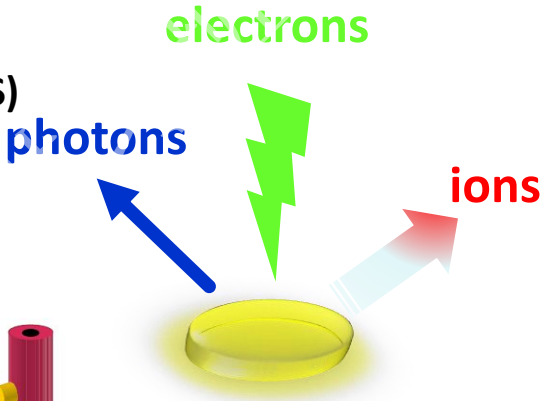

Auger Electron Spectroscopy (AES)

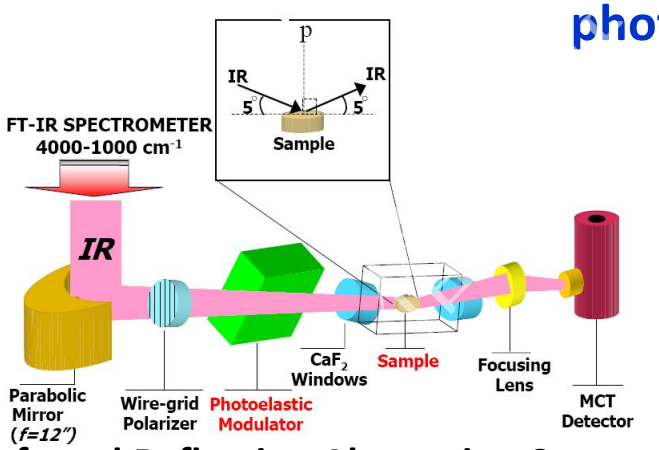

Infrared Reflection Absorption Spectroscopy (IRAS)

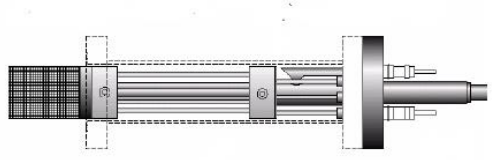

Temperature Programmed Desorption/Reaction (TPD/TPR)

High Resolution Electron Energy Loss Spectroscopy (HREELS)

表面催化1.0: 平整单晶表面的模型催化

原子尺度的构效关系

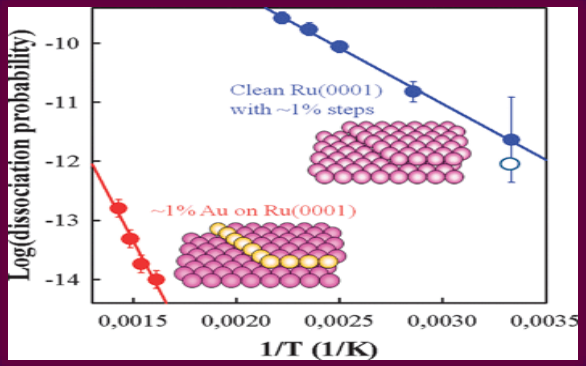

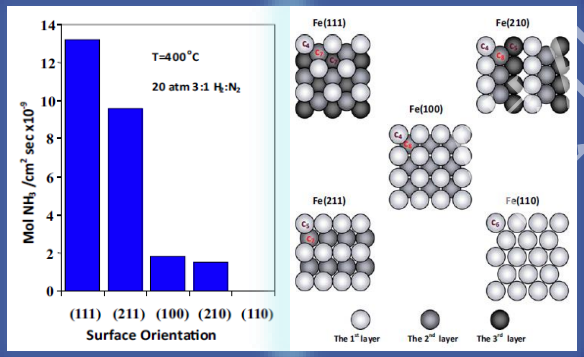

分子尺度的反应动力学与反应机理

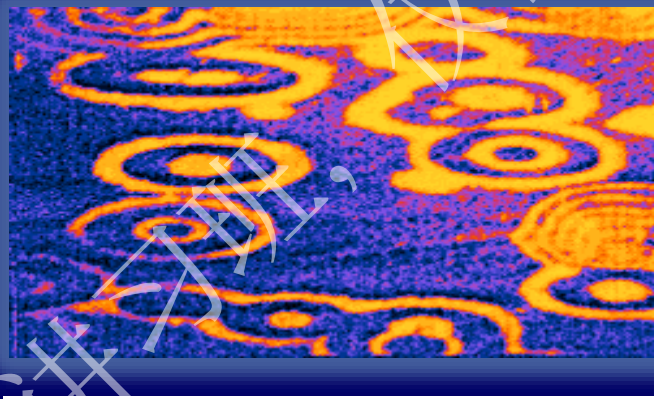

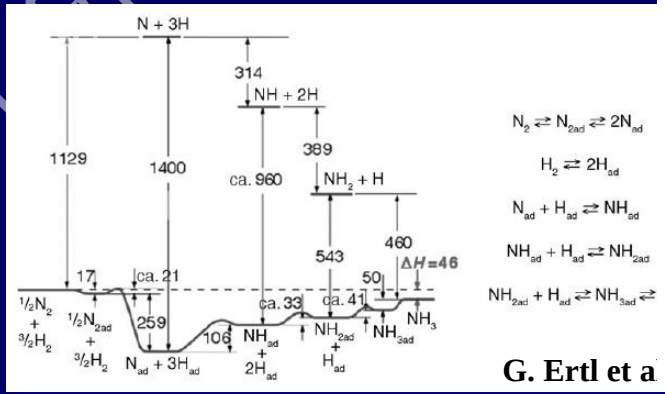

G. Ertl et a

“From the century of the rate equation to the century of the rate constants: a revolution in catalytic kinetics and assisted catalyst design”

-- Michel Boudart

多相催化的基本特性

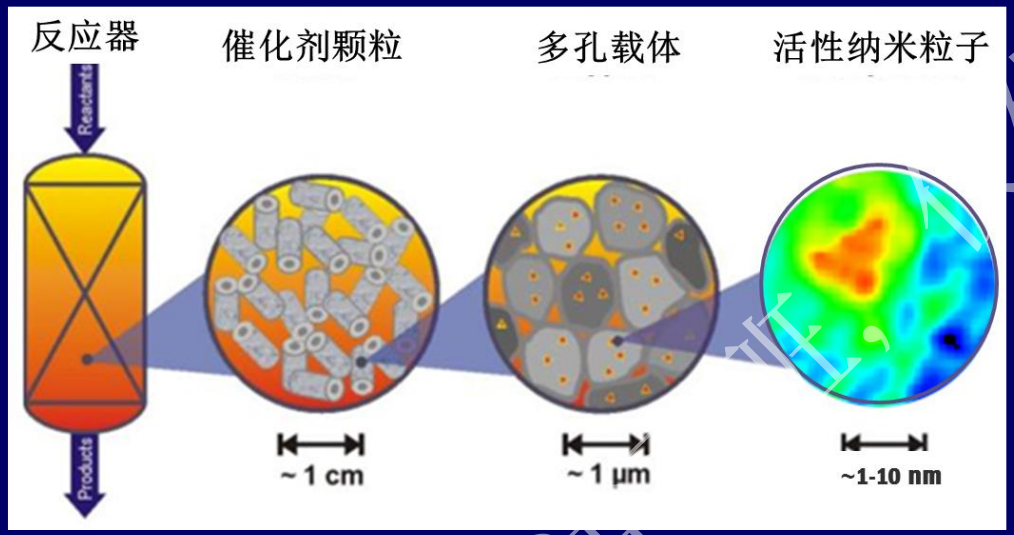

典型的工业催化反应装置示意图

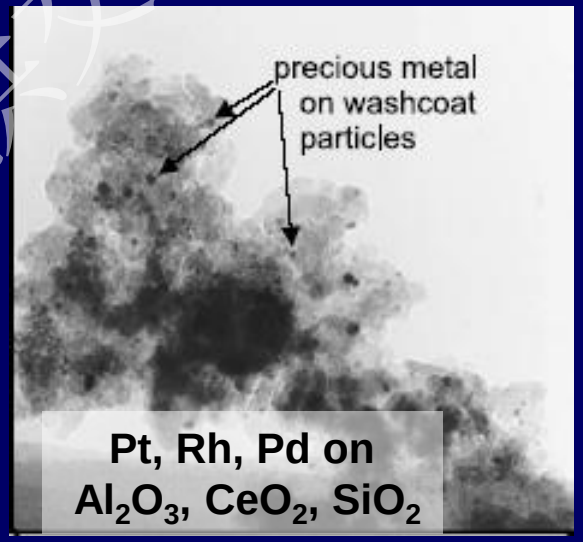

车载三效催化剂

多相催化是发生在纳米尺度、多组分协同作用、动态变化的固体表界面上的化学反应过程。

Surface Science

Catalysis

10^{-14} bar

Pressure Gap

10^{3} bar

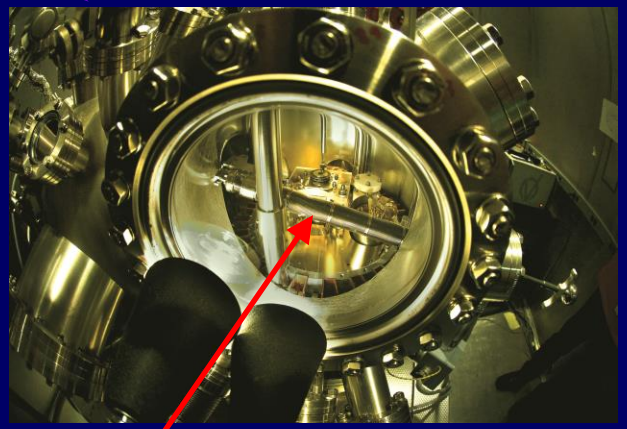

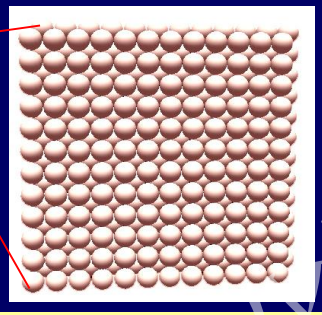

2007 Nobel Laureate

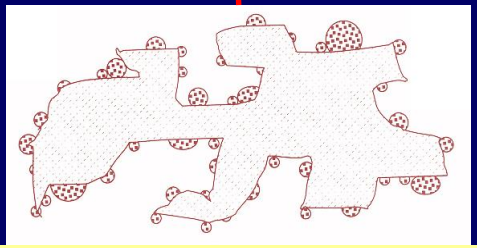

planar model catalyst: well characterized with atomic understanding

powder catalyst: difficult to characterize and involving complex phenomena at multiple scales

Material Gap

size effect, support effect, etc.

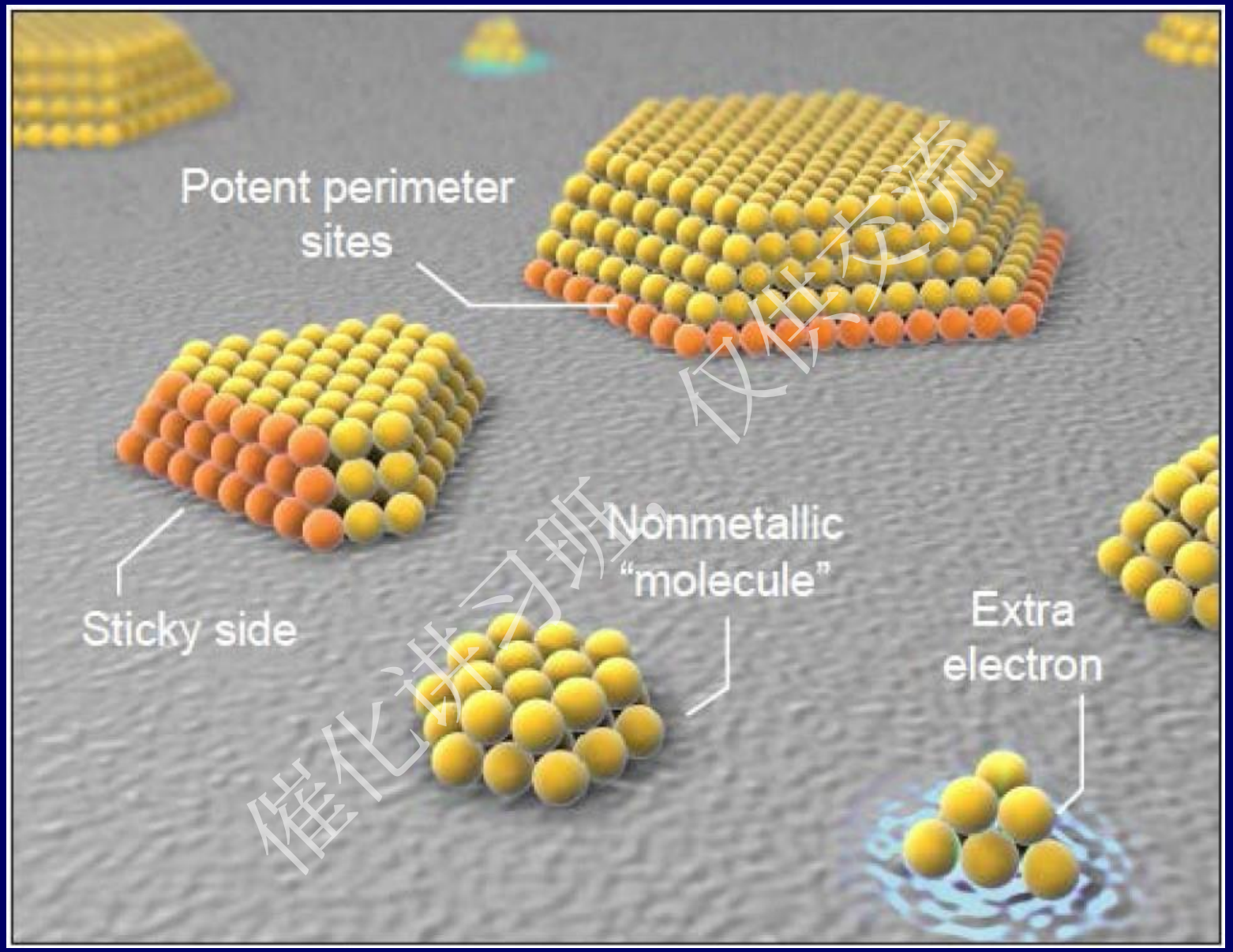

A. Cho, Science 299 (2003) 1684

多相催化研究面临的挑战

对能源和资源高效利用的重大需求，使催化研究面临新挑战

❑强调对化学反应的调控

❑对于新催化剂的研制，追求实现温和条件下的高转化率、接近100%的选择性和尽可能高的稳定性

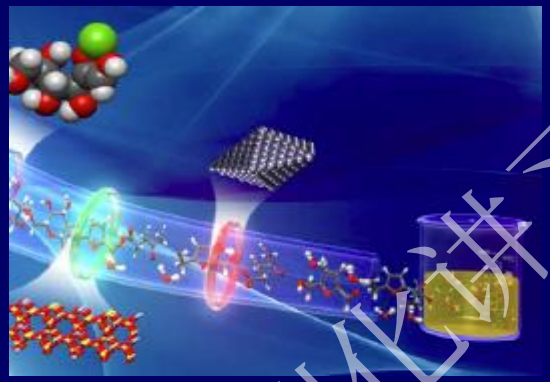

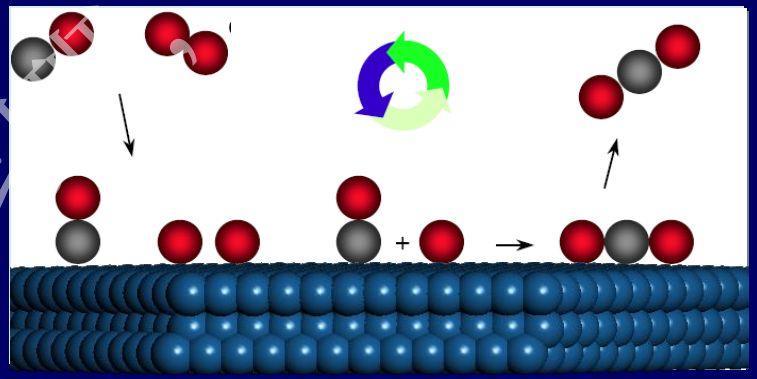

- ❑ 在原子尺度上设计、构筑有效的催化体系
- ❑ 在分子尺度上揭示反应物向产物的转化过程
- ❑ 发展表征工具——原位、实时、高空间分辨地表征工作态催化剂

The Scanning Tunneling Microscope works like a record player…

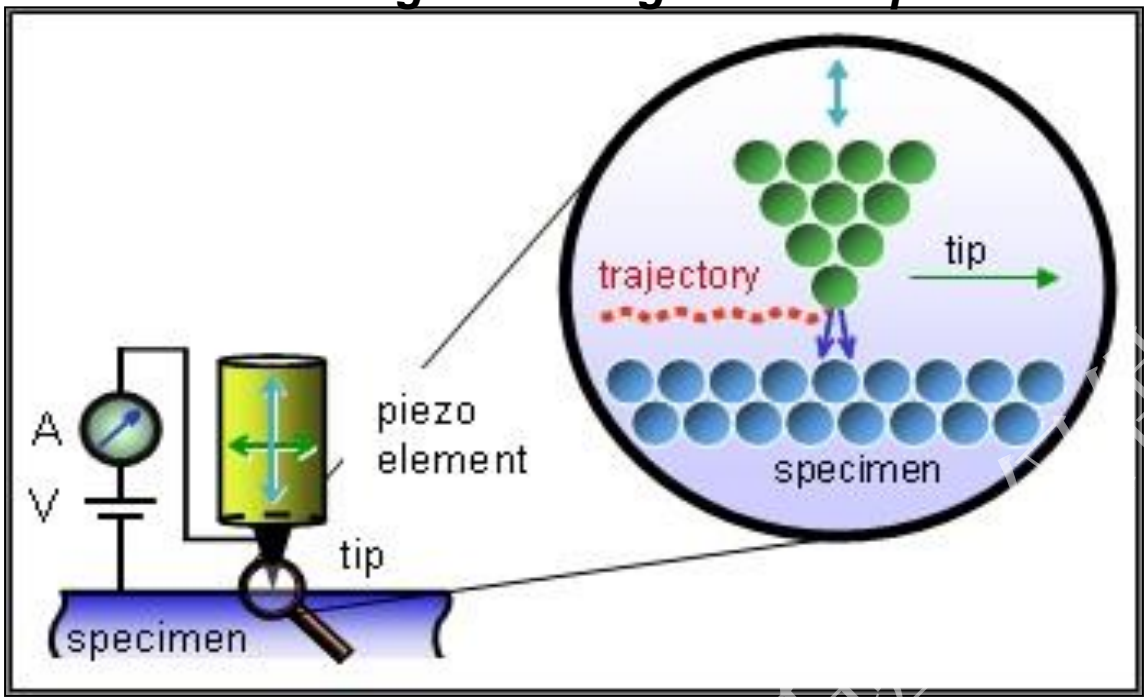

Gerd Binnig

Heinrich Rohrer

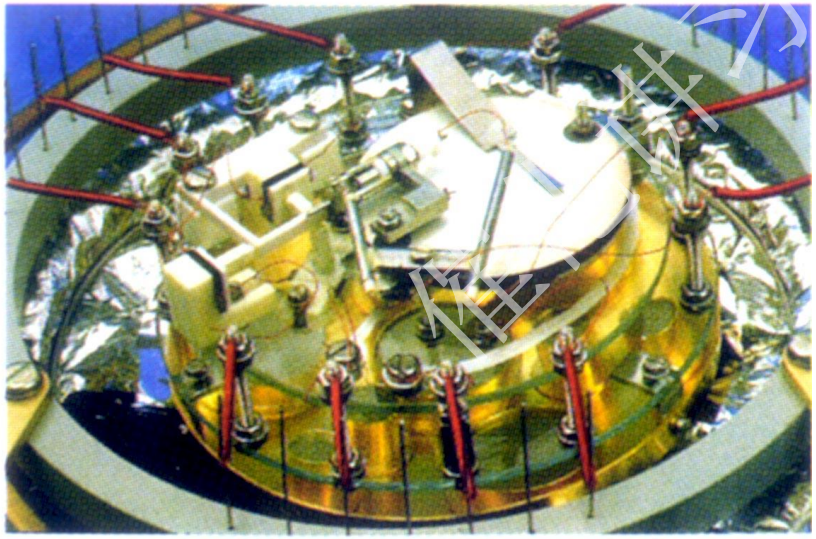

分辨率: 约0.01纳米

1981年

APL 40, 178 (1982)

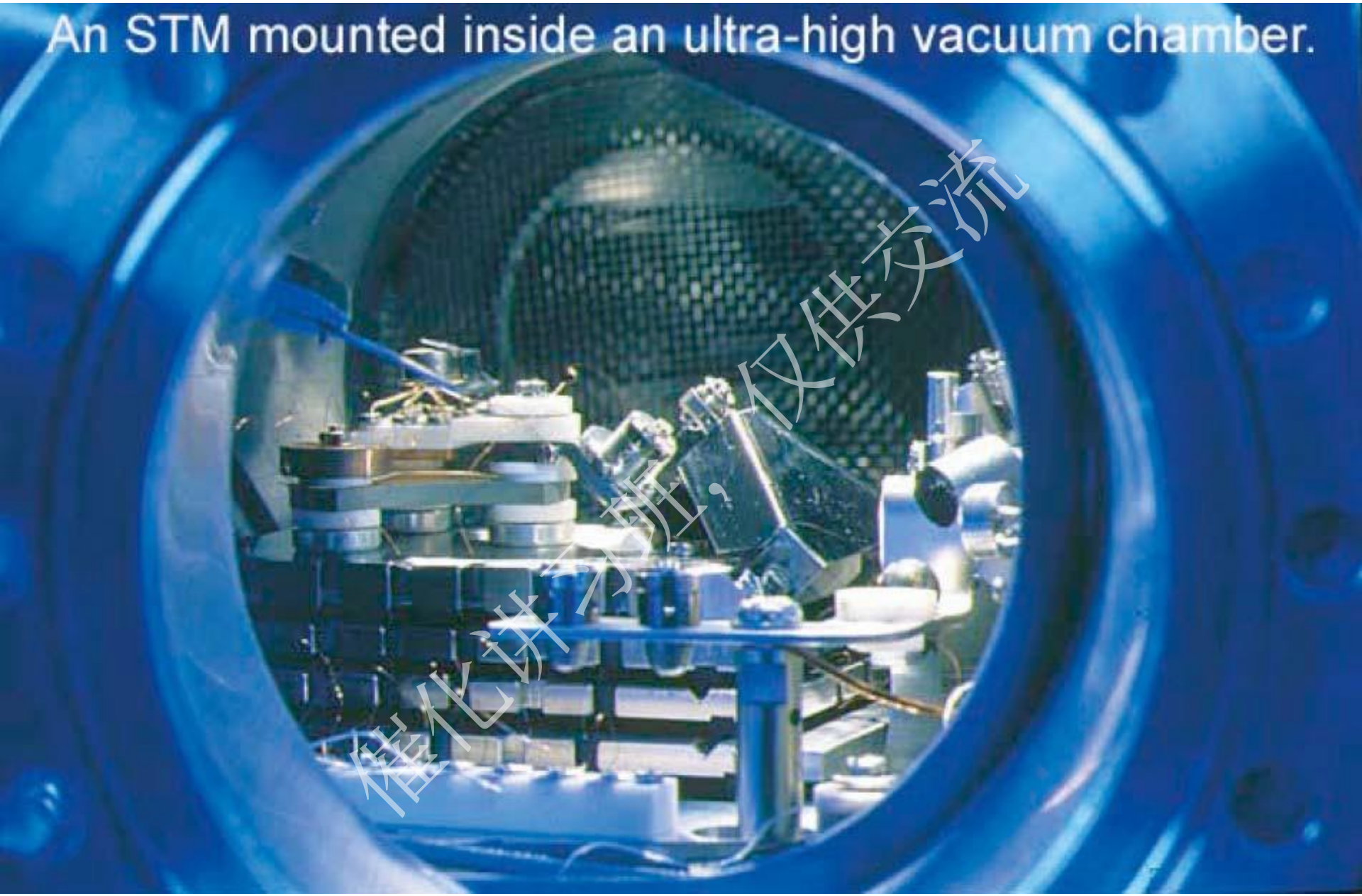

1st STM

一亿倍是多大?

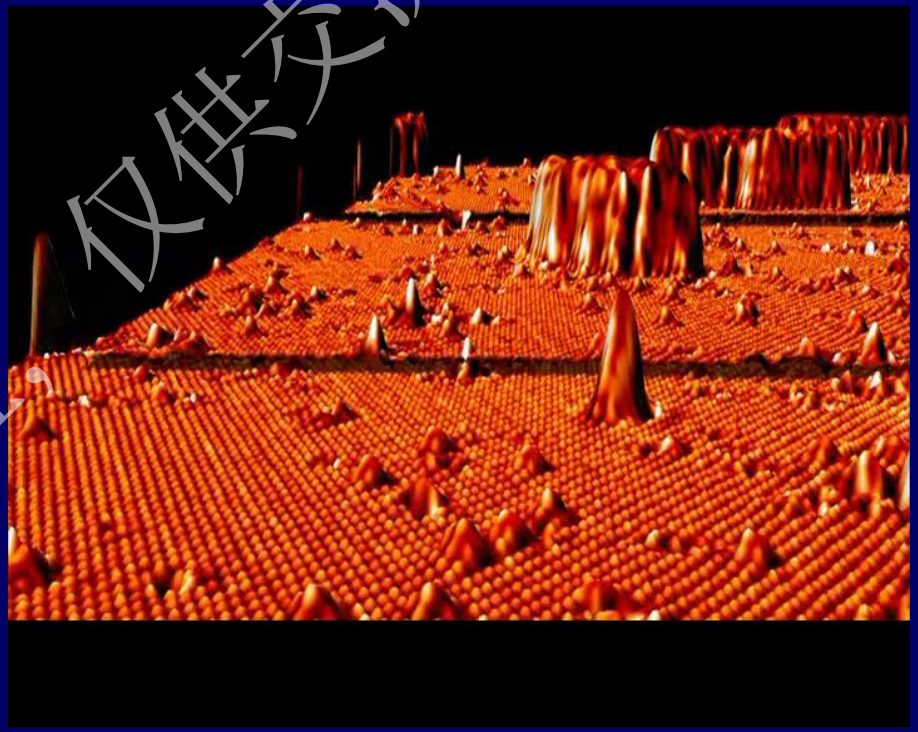

放大一亿倍

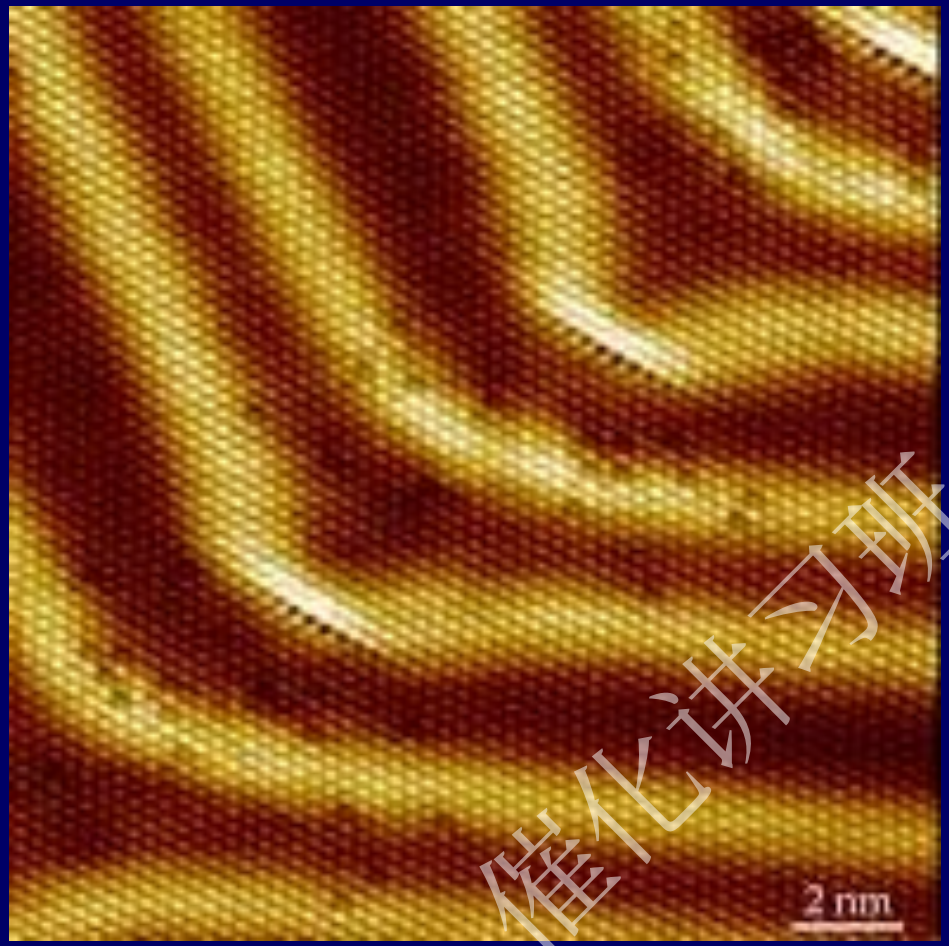

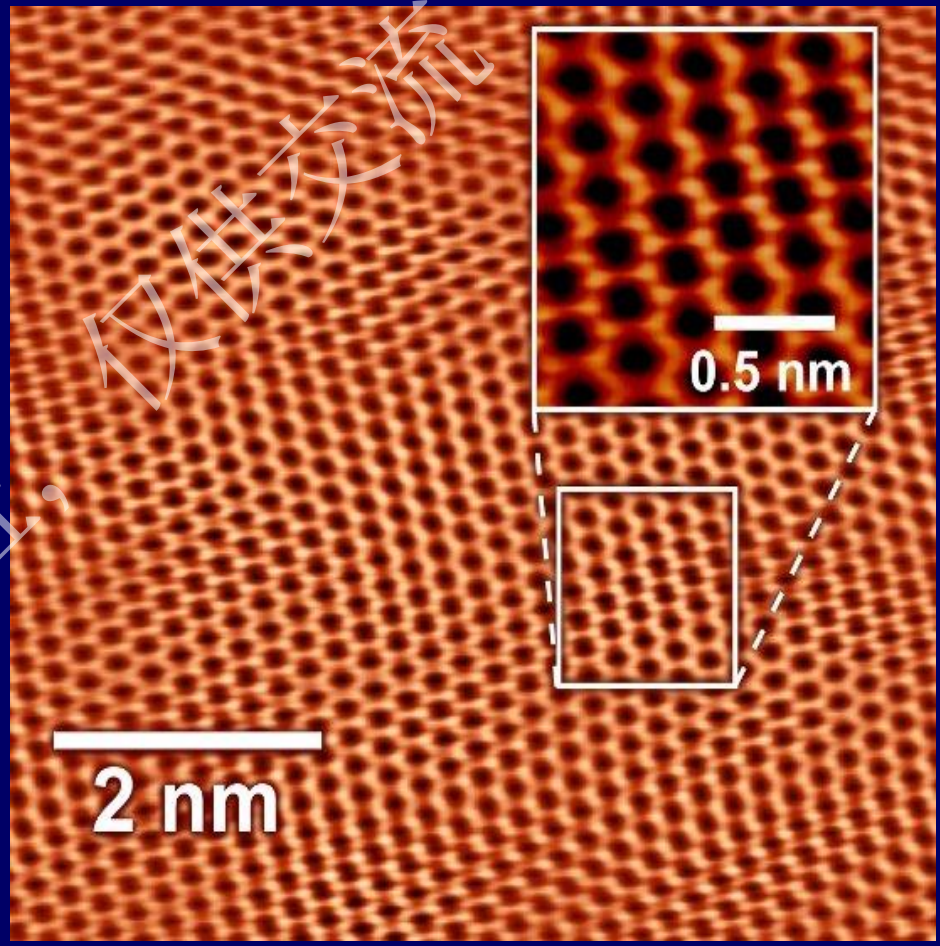

金

石墨烯

纳米赛车

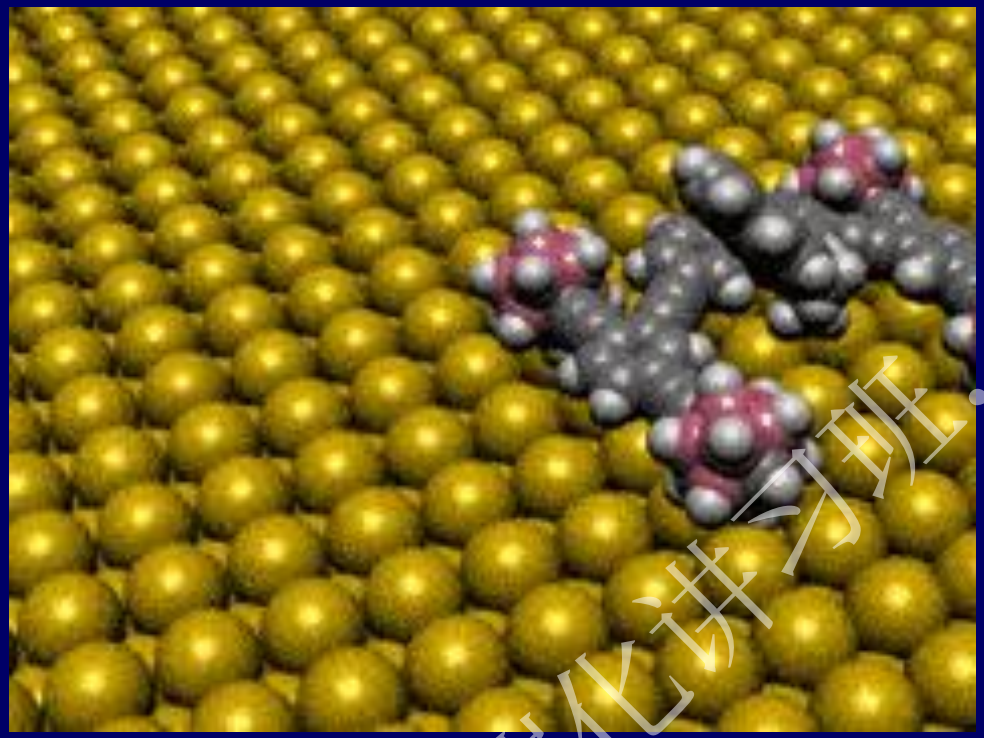

用原子拍电影

世界上最小的电影

STM 的基本原理

STM的基本原理-量子隧穿

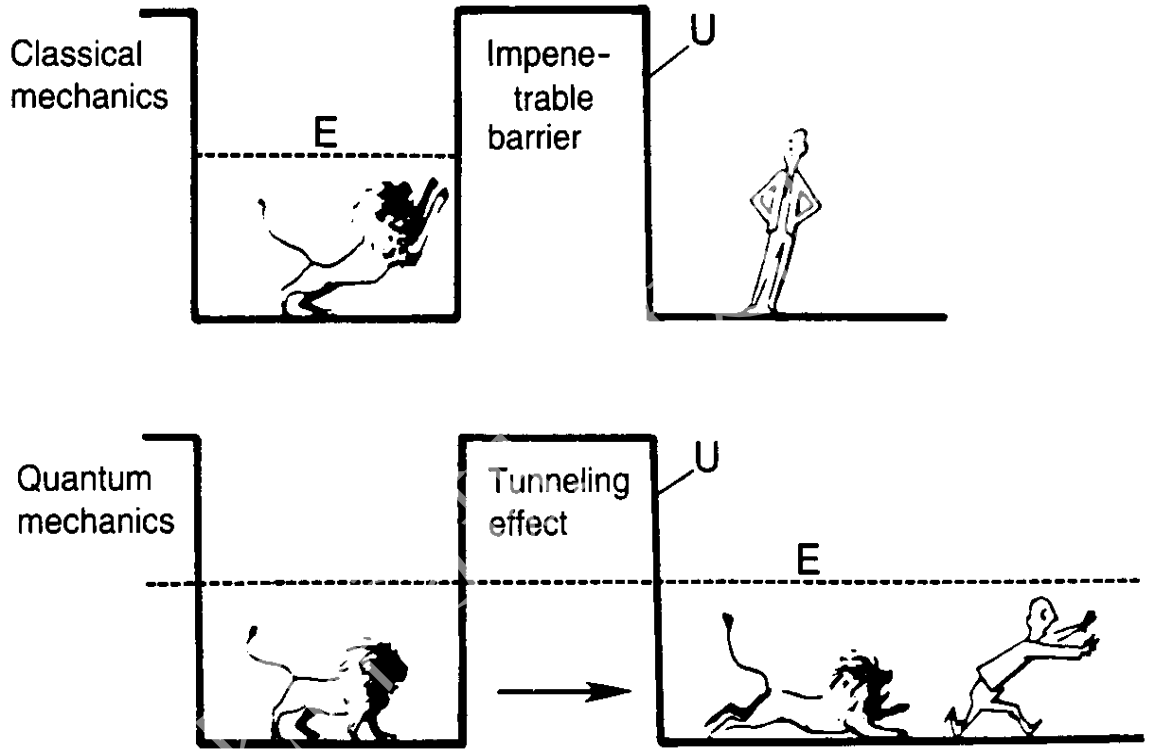

Chen, C.J. In *Introduction to Scanning Tunneling Microscopy*; Oxford University Press: New York, 1993; p 3.

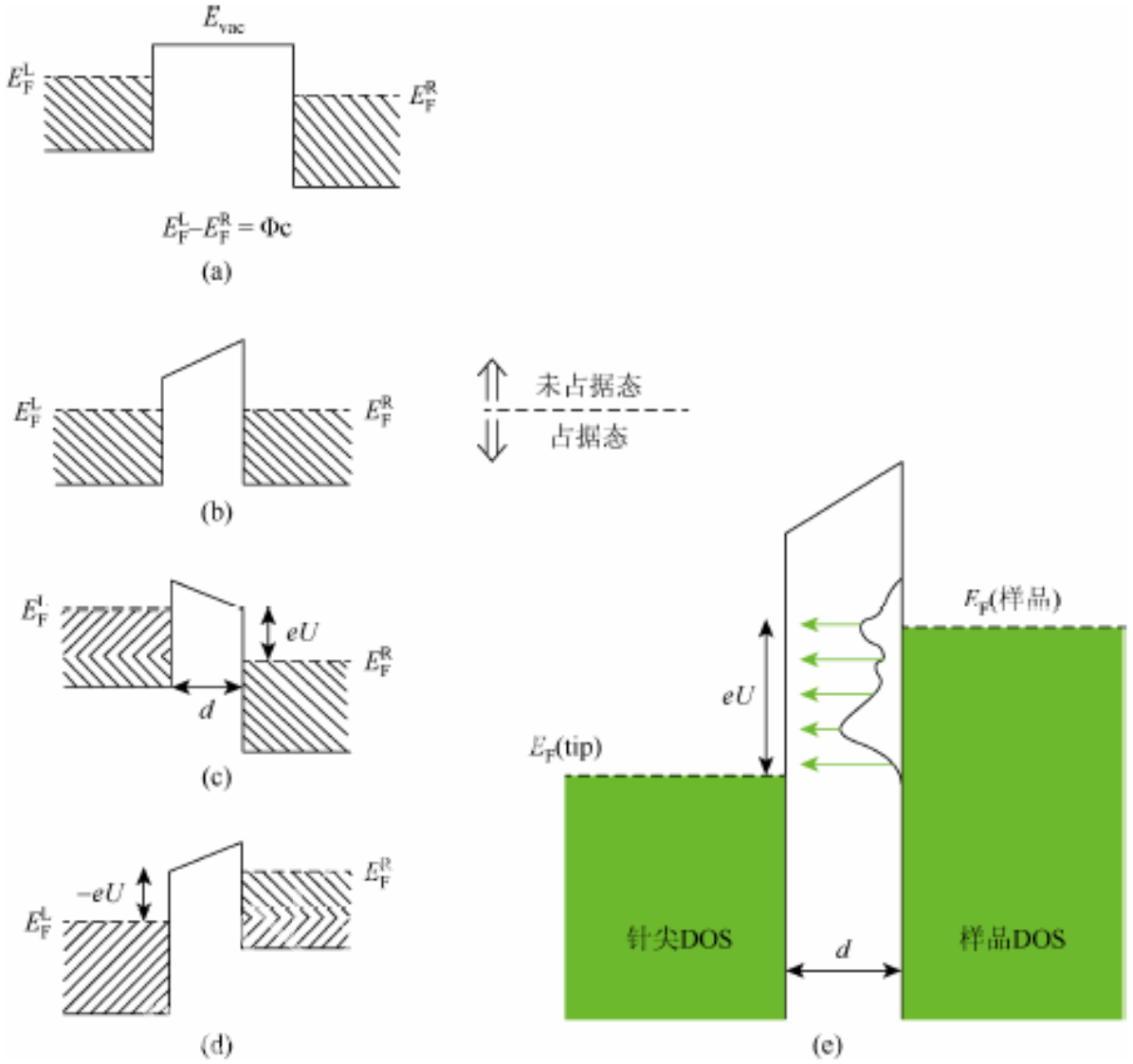

图 12-2　两个金属电极间费米能级和真空能级的相对位置，以及电子流动过程[15]

（a）两个金属相互靠近但不连通；（b）两个金属间以导线连通；（c）右侧金属相对于左侧金属被施加了一个正偏压 eU；（d）改变（c）的偏压方向，隧穿方向发生反转；（e）将左侧金属视为针尖，右侧金属视为样品，即为隧穿结示意图。通过施加偏压来改变费米能级位置，即可打开一个能量窗口发生电子从样品占据态到针尖未占据态的隧穿

Tunneling Energy Diagram

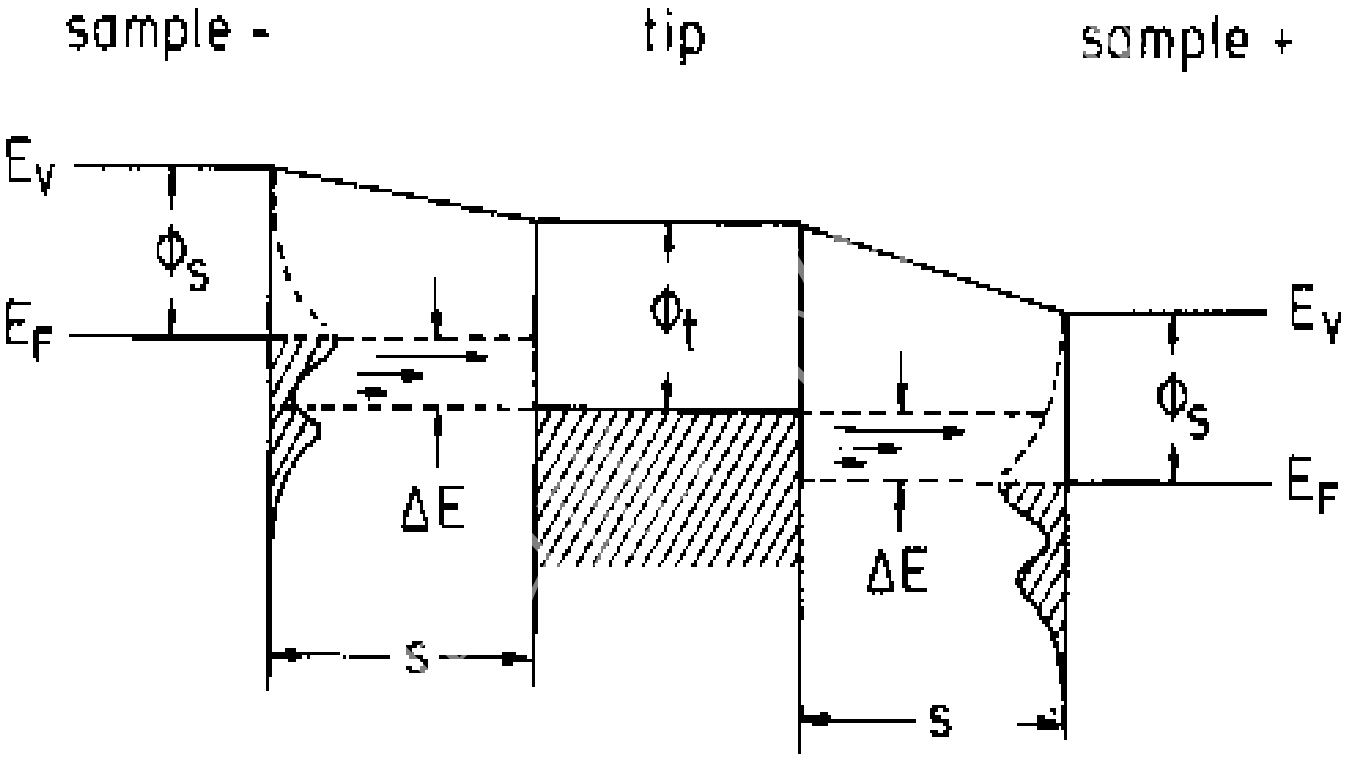

Behm, R.J.; Hosler, W. In *Chemistry and Physics of Surfaces VI*; Vanselow, R., Howe, R., Eds.; Springer: Berlin, 1986; p 361.

Modeled as a 1-D square well…

$$\Psi(z) = \Psi(0)e^{-\kappa z} \qquad \kappa = \frac{\sqrt{2m(\phi - E)}}{\hbar}$$

$$I_t \propto \int_{E_F}^{E_F + eV} \underbrace{\rho_s(E, \vec{r})}_{\text{Sample DOS}} \underbrace{\rho_T(E - eV, \vec{r})}_{\text{Tip DOS}} \underbrace{T(E, eV, \vec{r})}_{\text{Transmission factor b/t tip and sample}} dE$$

$$I = \frac{E}{\phi} e^{-2z\sqrt{2m\phi/\hbar}} = e^{-Az\sqrt{\phi}}$$

In the limit of E<<ϕ

For small bias voltages: $I = V_{bias} e^{-z\sqrt{\phi}}$

So for a work function of 4 eV with δz= 1Å, I changes by an order of magnitude.

STM 的工作原理

Scanning Tunneling Microscope(STM)

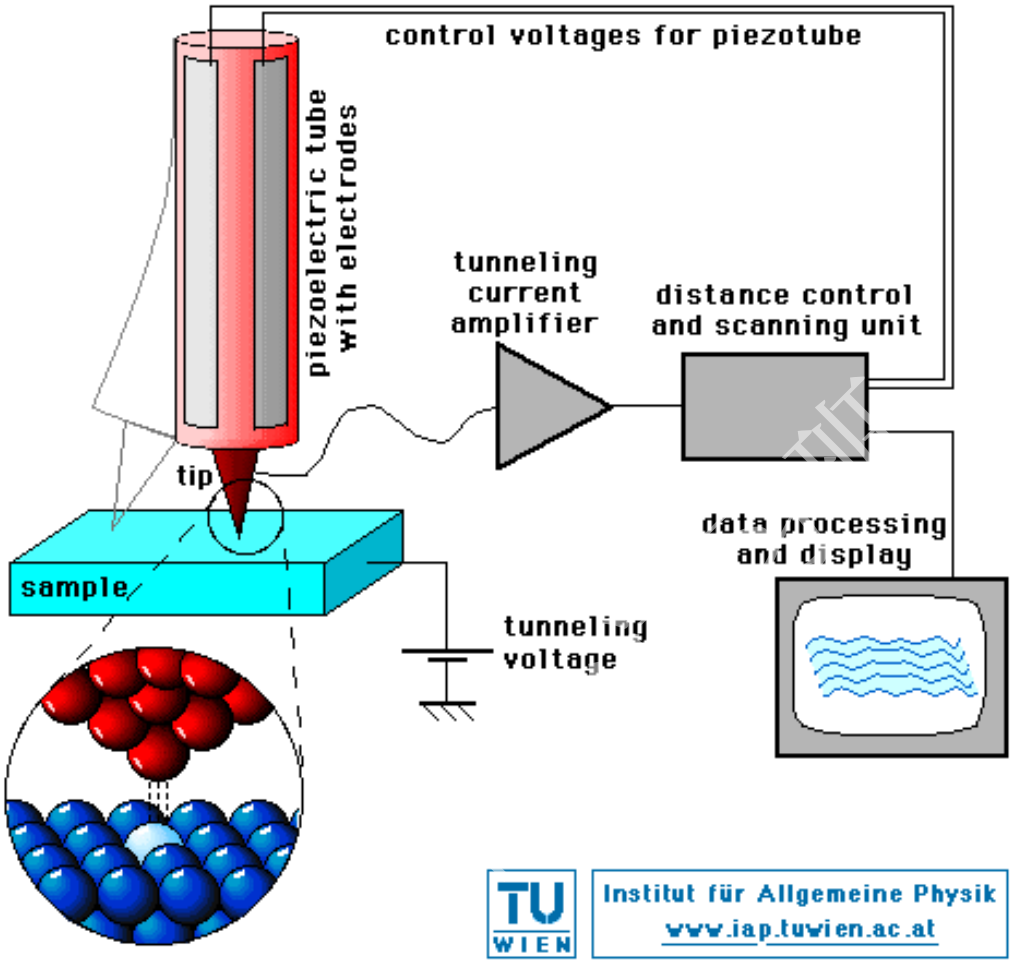


Createc LT-STM (2012)

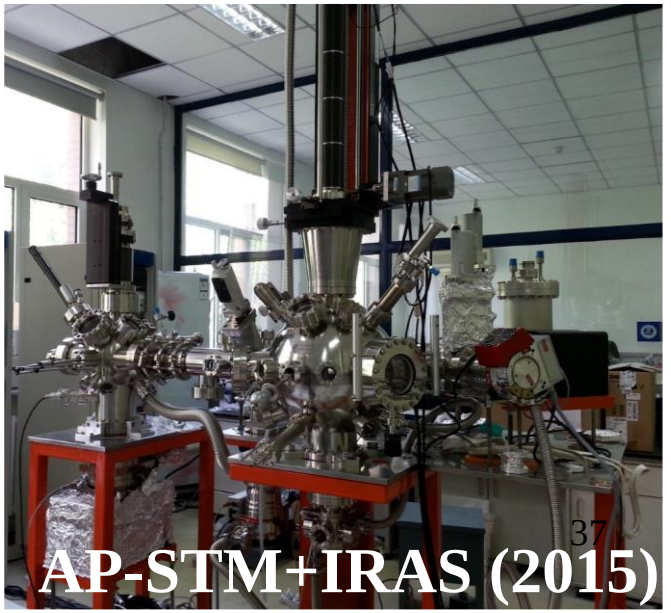
AP-STM+IRAS (2015)

How STM works

- Overlap of tip and sample wavefunctions
- Difference in tip and sample work functions causes electrons to tunnel through vacuum barrier
- An applied bias maintains potential difference between tip and sample, thus maintaining tunneling current
- Three functions of a microscope: Coarse approach；X-Y scanning；Z-feedback

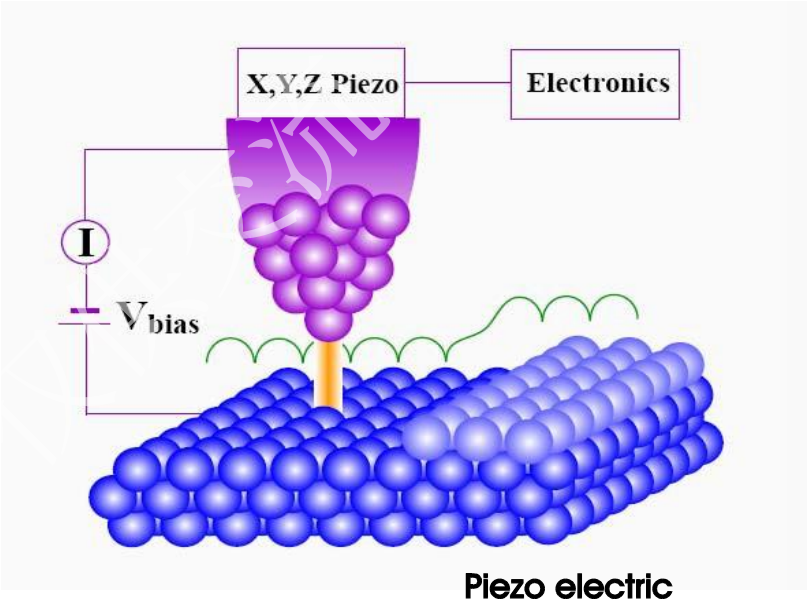

STM Movements

To get the distance between the tip and the sample down to a couple of Angstroms where the tunneling current is at a measurable level, STMs use feedback servo loops and converse piezoelectricity.

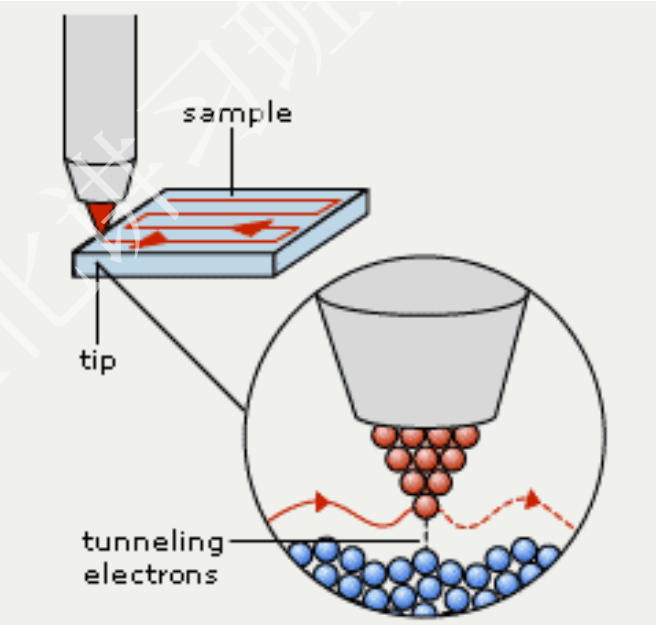

STM Instrumentation

The structure of an STM

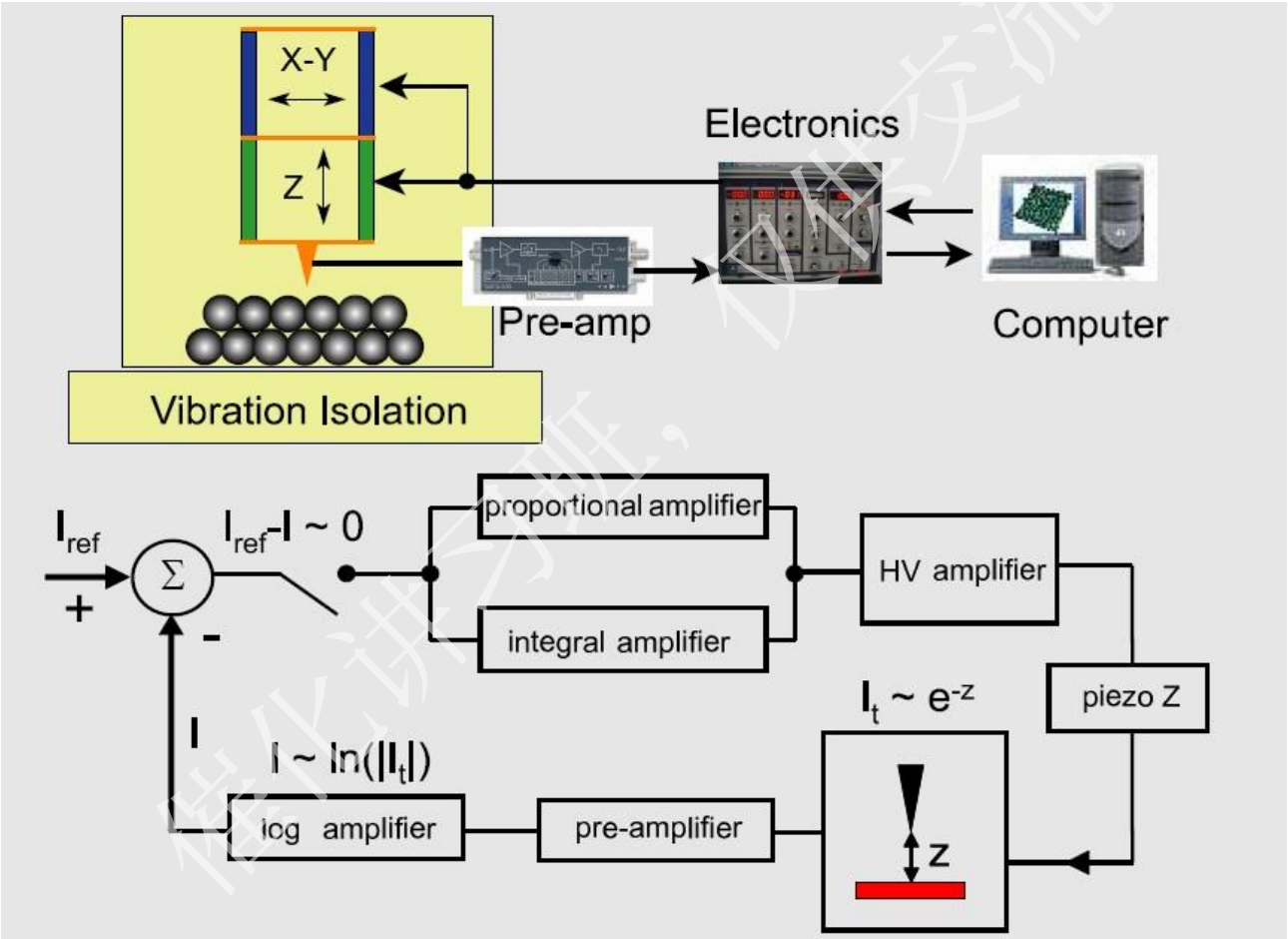

压电效应

Piezoelectricity is the ability of certain crystals to produce a voltage when subjected to mechanical stress. When you apply an electric field to a piezoelectric crystal, the crystal distorts. This is known as converse piezoelectricity. The distortions of a piezo is usually on the order of micrometers, which is in the scale needed to keep the tip of the STM a couple Angstroms from the surface.

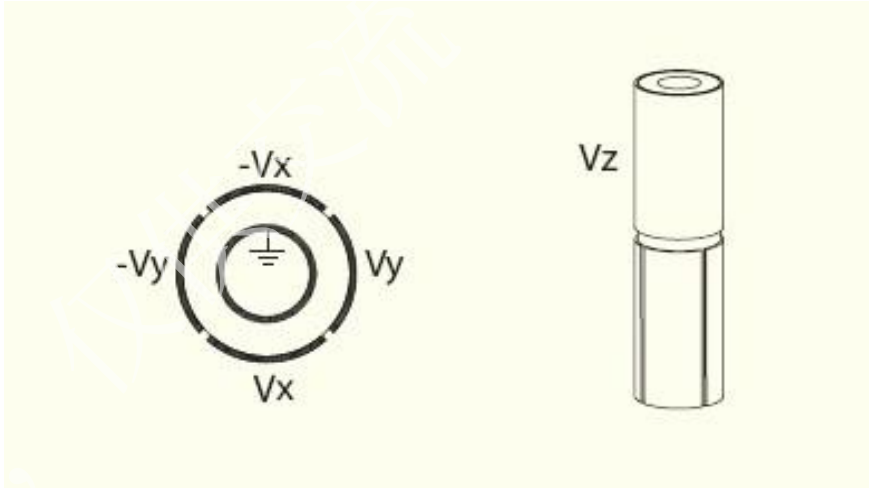

$$V_x = \frac{\pi D t}{2\sqrt{2} d_{31} L^2} x$$

$$V_y = \frac{\pi D t}{2\sqrt{2} d_{31} L^2} y$$

$$V_z = \frac{t}{d_{31} L} z$$

Typically $V = 0.01\,V \sim 100\,V$

1V~1Å

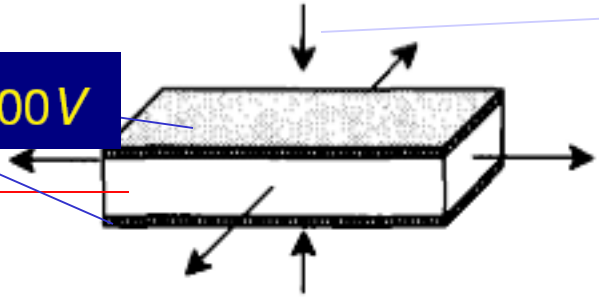

STM Instrumentation

Coarse approach

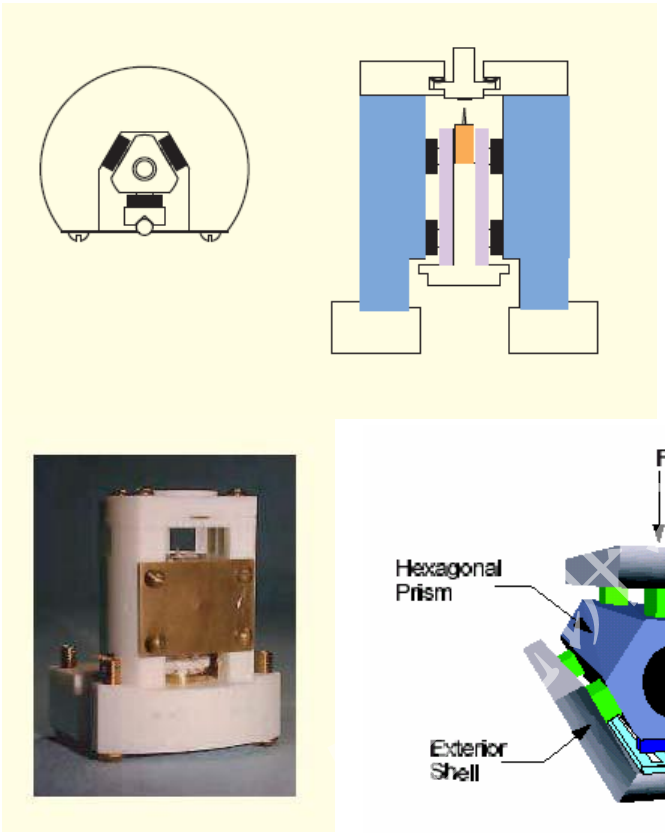

Pan type piezo walker

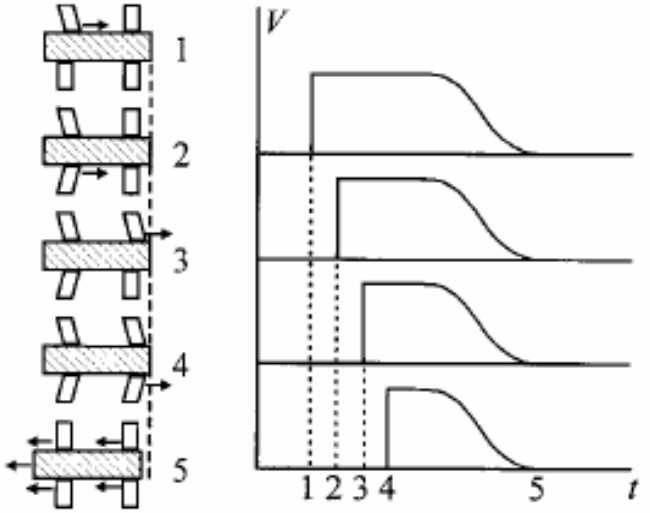

This part is from Prof. Chen Xi's ppt slides

STM Instrumentation

Coarse approach

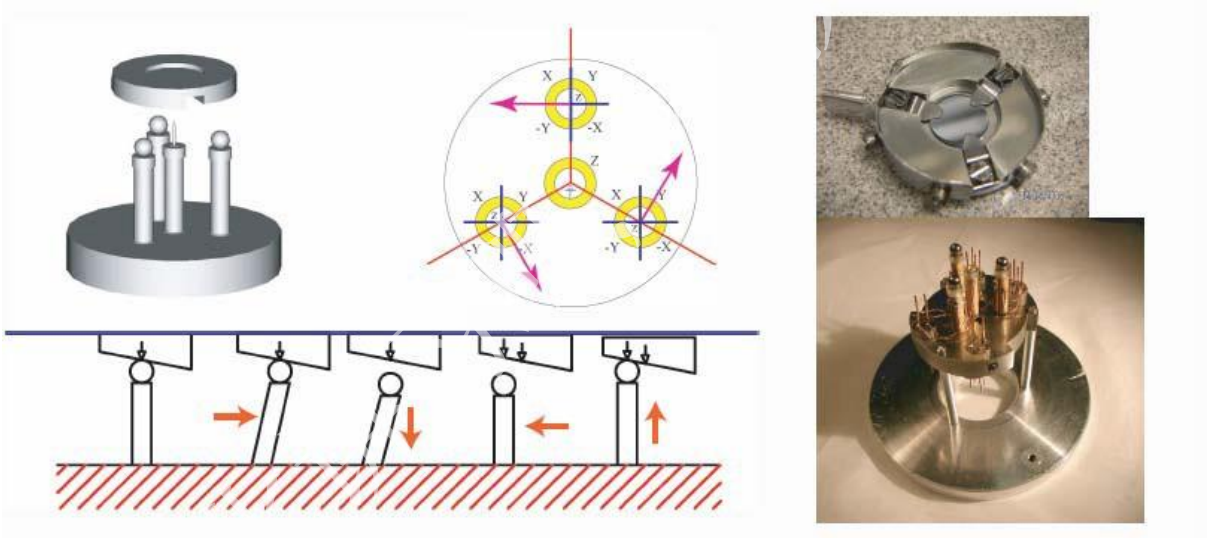

Besocke type

STM-Instrumentation

Three functions of a microscope:

Coarse approach

X-Y scanning

Z-feedback

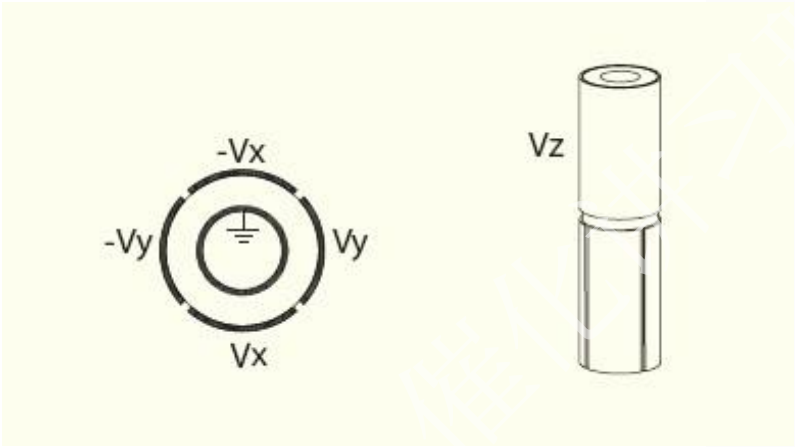

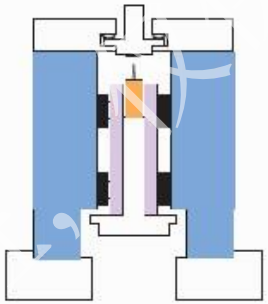

STM-Instrumentation

Design considerations

- Scanning range ~ micron
- Sensitivity: displacement per volt

Low sensitivity

Higher spatial resolution
More invulnerable to noise

- Resonance frequency
- Scanning speed

STM-Instrumentation

Design considerations

Vibration

General Rules

- Low noise environment
- Vibration isolation
- Rigid design

STM-Instrumentation

Vibration

Low noise environment

- Basement with solid foundation
- Turn off mechanical pumps, turbo pumps
- Acoustic-isolation room

With solid foundation

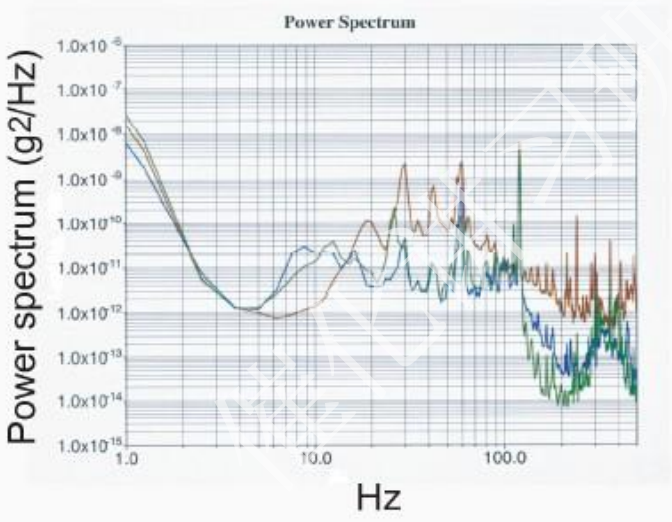

Without solid foundation

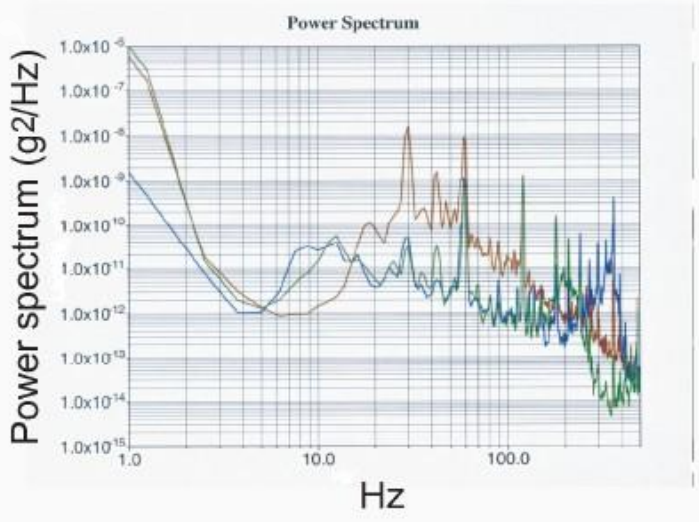

STM-Instrumentation

Vibration

Vibration isolation

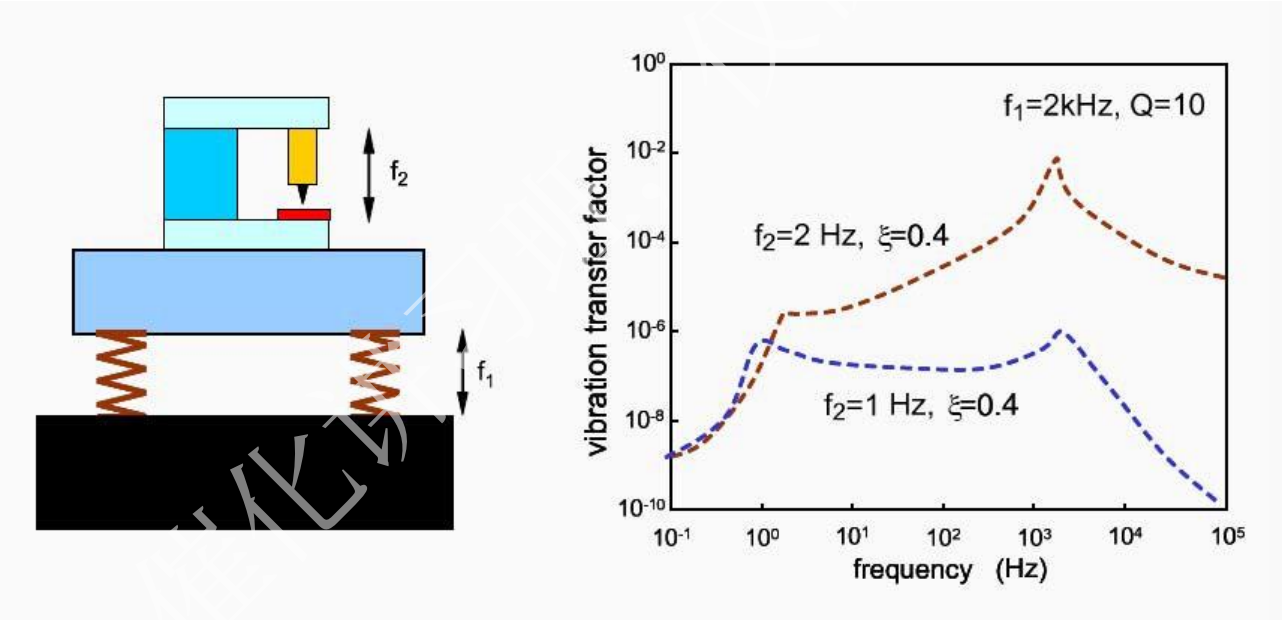

STM-Instrumentation

Vibration

Vibration isolation

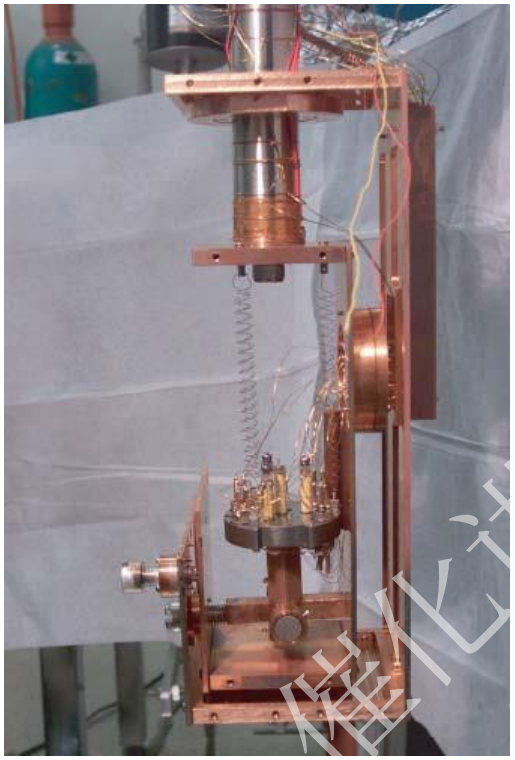

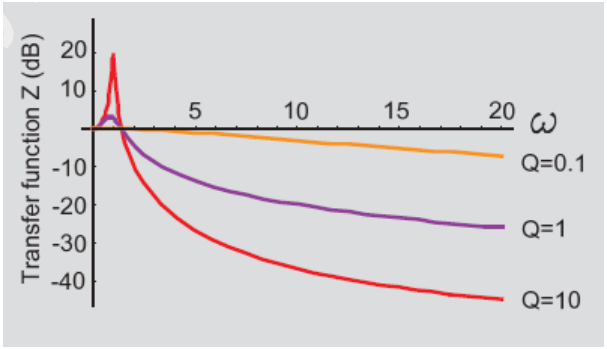

STM-Instrumentation

Vibration

Rigid design

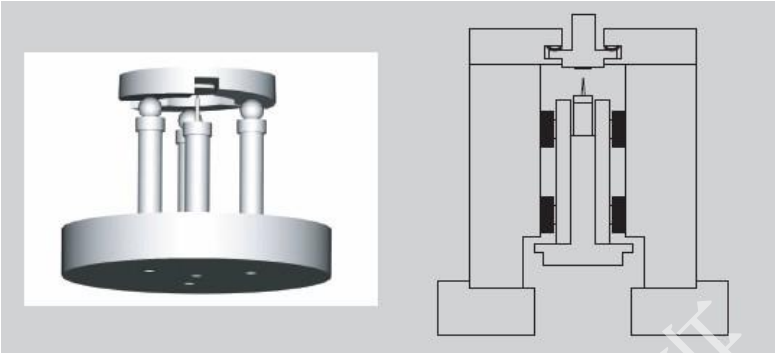

$$f \sim 0.2 \sqrt{\frac{E}{\rho}\frac{D}{L^2}}$$

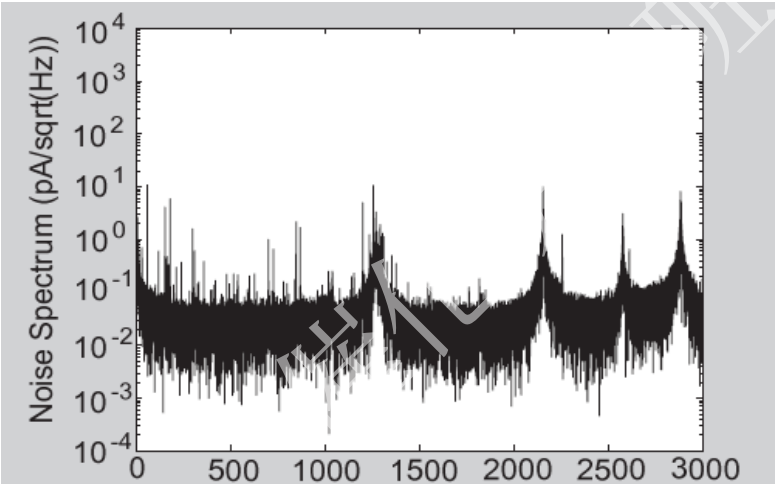

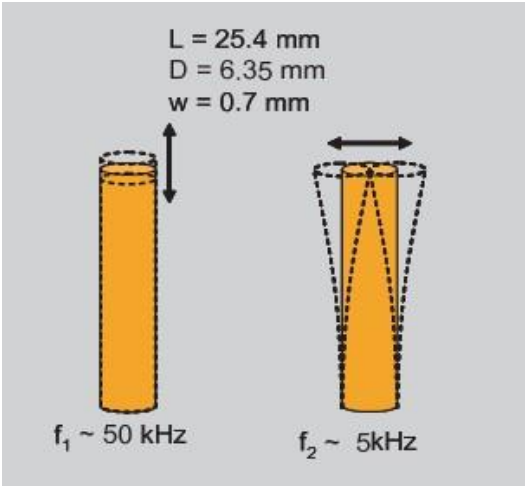

STM-Instrumentation

Vibration

Rigid design

Rigid design→ High speed

128 × 128 image, 25 images/sec

⇓

f > 40kHz

STM Instrumentation

Electronics

- Selectable gain $10^7 \sim 10^{10}\, V/A$
- Noise $i_{TSND} = \sqrt{\left(\frac{e_n}{R_f}\right)^2 + i_n^2 + \left(\frac{4k_BT}{R_f}\right)^2 + (2\pi C_{in} e_n)^2}$
- Bandwidth 256×256 size @5kHz:
  $256 \times 256 \times 1\,ms \sim 1 minute$
- Size

Pre-amplifier

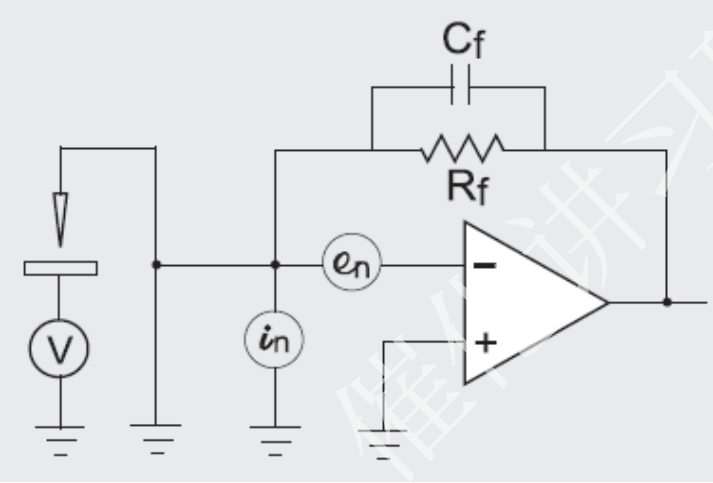

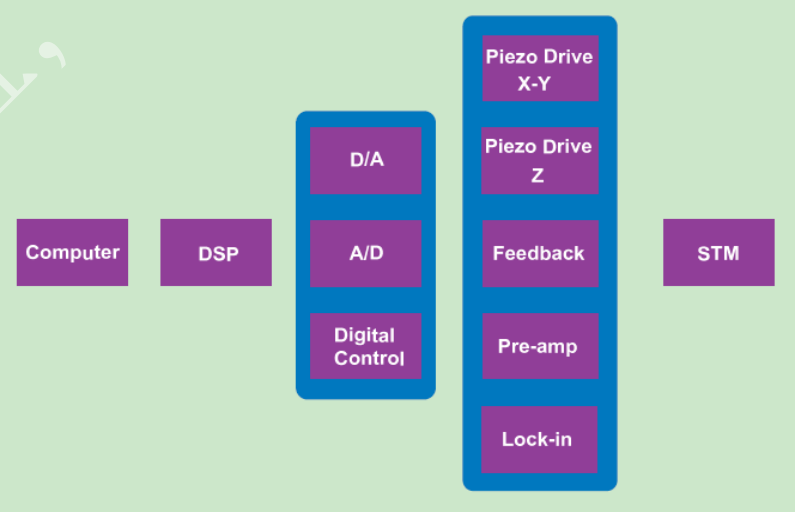

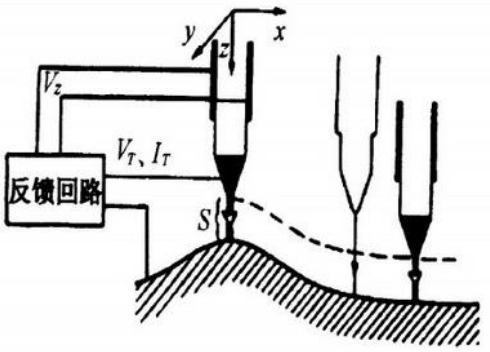

恒电流模式

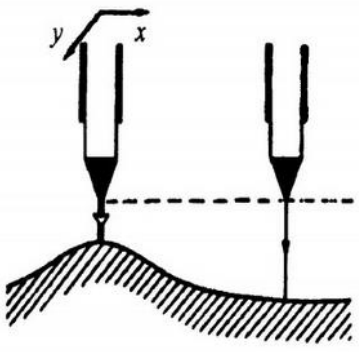

恒高度模式

➢**基本操作模式：**

恒电流模式：表面起伏大的样品

恒高度模式：表面起伏不大的样品

Constant Height Mode

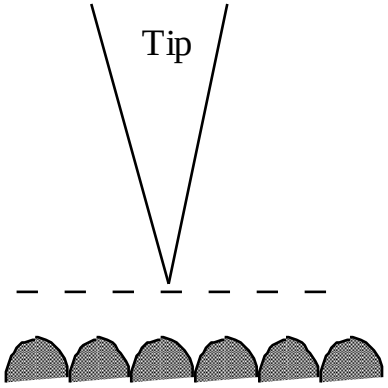

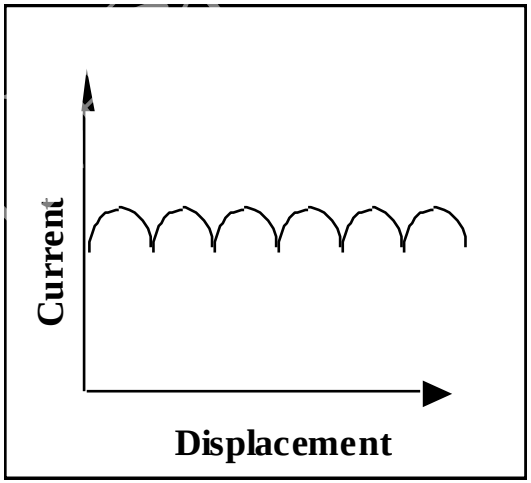

Current

Original & Processed Trace

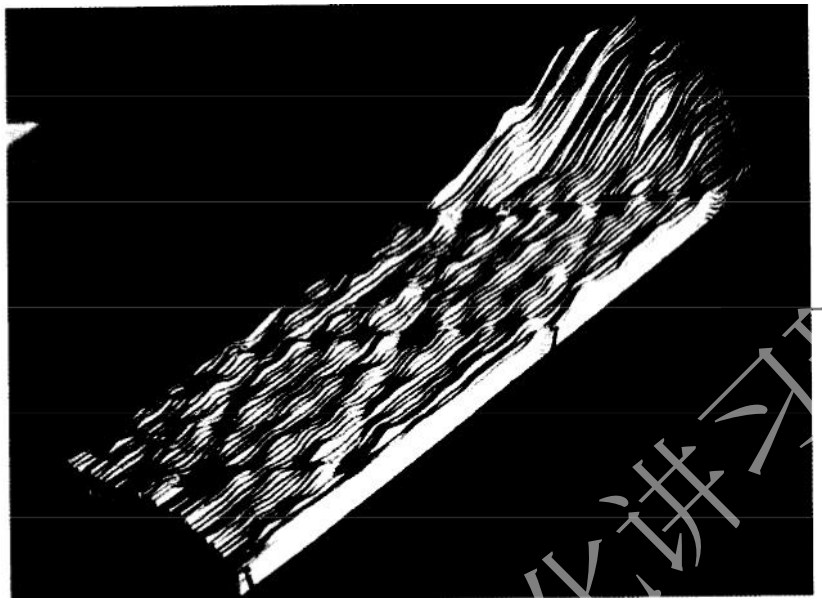

Si(111) trace taken in 1983

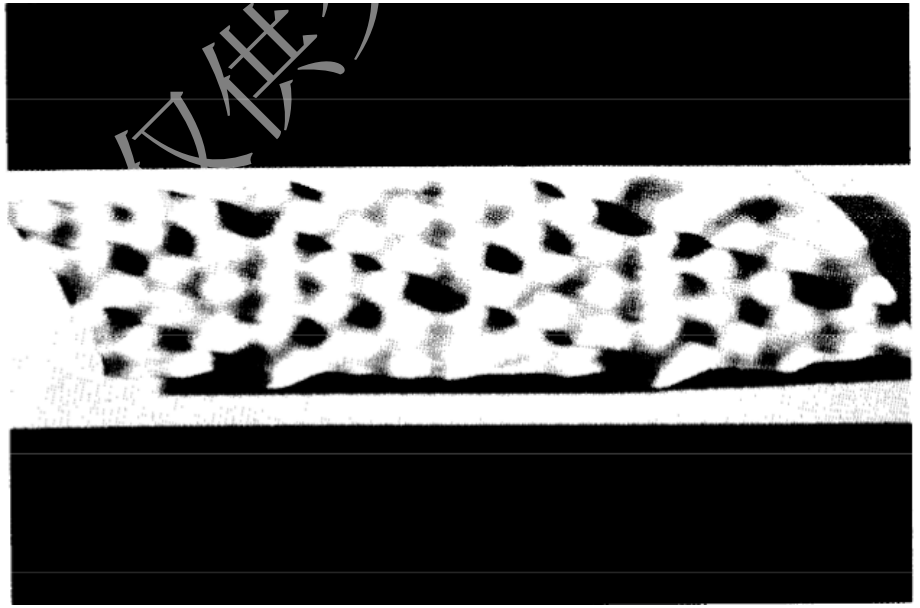

Computer processed version of the same trace of Si(111)

How to Process a Trace

The trace (1) can be interpreted as a grid which can be shown as a grayscale picture (2).

1  2 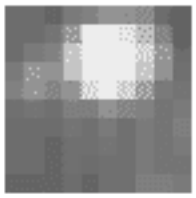 3 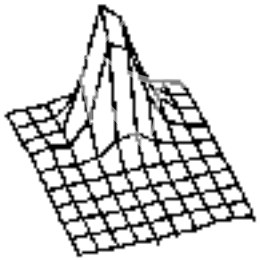 4 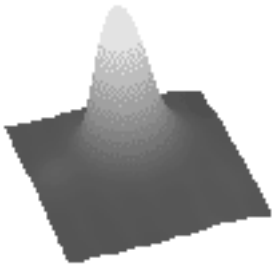

The grayscale picture can be interpreted as a contour map (3) which can then be averaged out to make smooth (4) and finally colored (below).

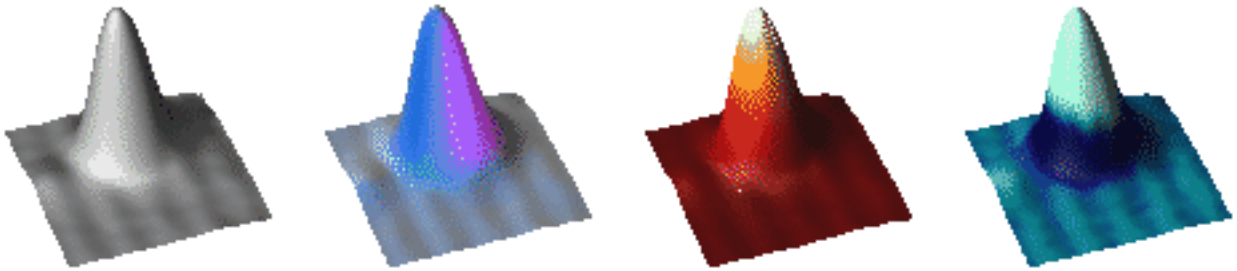

真空量度单位

- 1标准大气压=760mmHg=760(Torr)
- 1标准大气压=$1.013x10^5$ Pa
- 1Torr=133.3Pa

真空区域的划分

目前尚无统一规定，常见的划分为：

粗真空 $10^{5}-10^{3}\ pa(760-10Torr)$

低真空 $10^{3}-10^{-1}\ pa(10-10^{-3}Torr)$

高真空 $10^{-1}-10^{-6}\ pa(10^{-3}-10^{-8}Torr)$

超高真空 $10^{-6}-10^{-10}\ pa(10^{-8}-10^{-12}Torr)$

极高真空 $<10^{-10}\ pa(<10^{-12}Torr)$

Mean Free Path Calculation

The mean free path equation depends upon the temperature and pressure as well as the molecular diameter.

For pressure P_0 = 760 mmHg = 29.92 inHg = 101.3 kPa

and temperature **T** = 300 K = 26.8500000 C = 80.3300000 F,

Molecules of diameter 3 x 10^{-10} meters (angstroms)

should have a mean free path of $\lambda = \frac{RT}{\sqrt{2}\pi d^2 N_A P}$ = 1.022563 x 10^ -7 m

which is 340.854651 times the molecular diameter

and 29.6818655 times the average molecular separation of 0.3445079 x 10^ -8 m.

STM 在催化中的应用

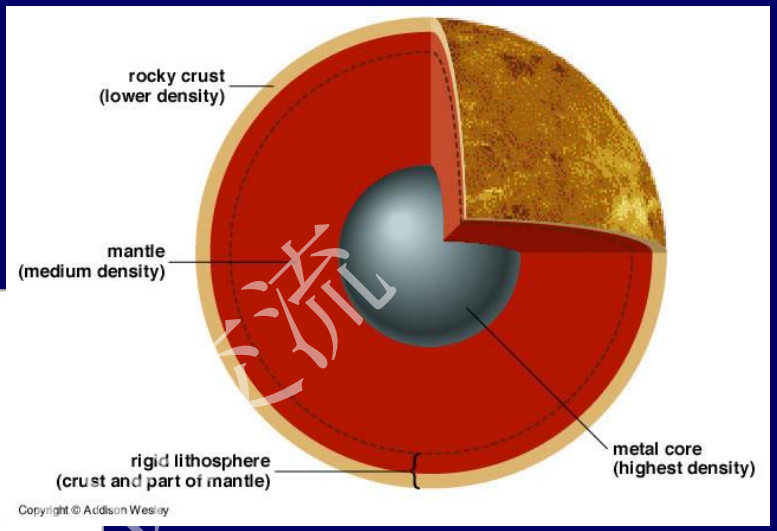
rocky crust
(lower density)
mantle
(medium density)
metal core
(highest density)
rigid lithosphere
(crust and part of mantle)
Copyright © Addison Wesley

Outline

- 1. 结构确认
  - 晶面的原子排列，如不同晶面，如表面重构；
  - 非均匀表面的缺陷，台阶，缺陷；

- 2. 电子结构表征
  - 表面局域态密度探测；
  - 功函数；

- 3. 分子吸附，活化与表界面反应
  - 吸附与活化的活性中心位点；
  - 活性吸附物种的指认；

1.1 表面结构确认

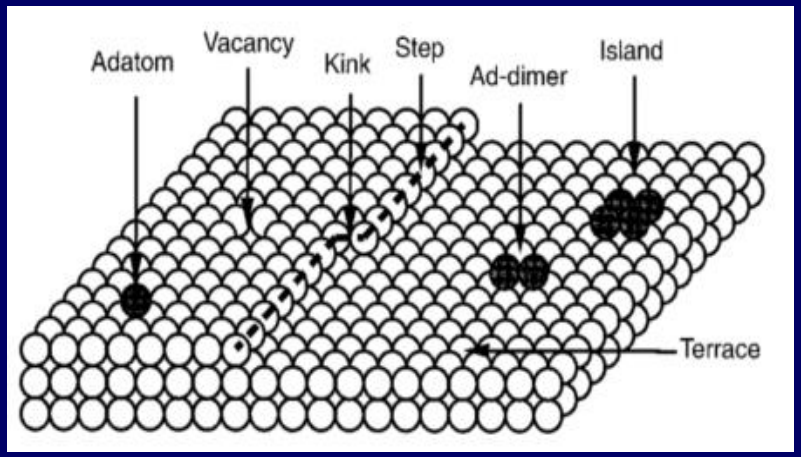

表面的T-S-K 模型：

1. 台面；
2. 台阶；
3. 拐角；
4. 空位；
5. 吸附原子与表面纳米岛

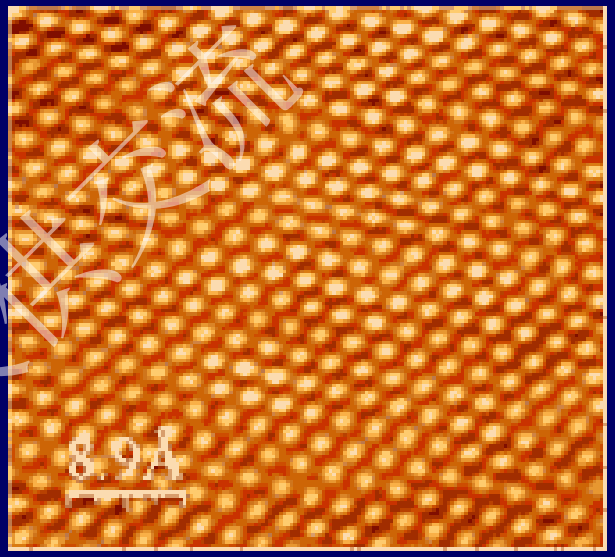

STM image of a HOPG surface

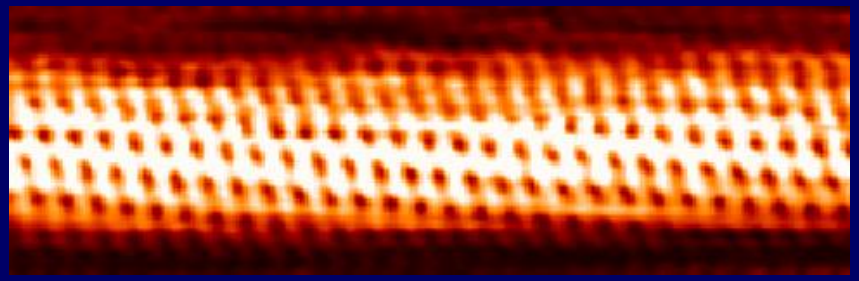

STM image of a carbon nanotube

Wilder, J. W. G., Venema, L. C., Rinzler, A. G., Smalley, R. E. & Dekker, C. (1998). *Nature*. **391**, 59–62.

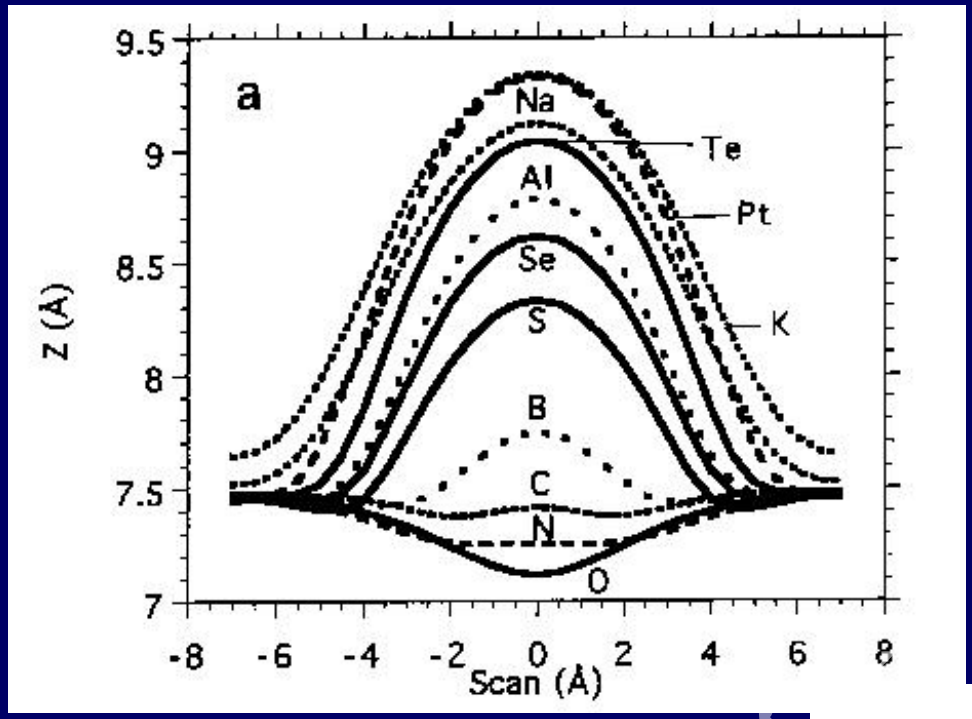

Chemical contrast…

Not everything in STM is a bump.

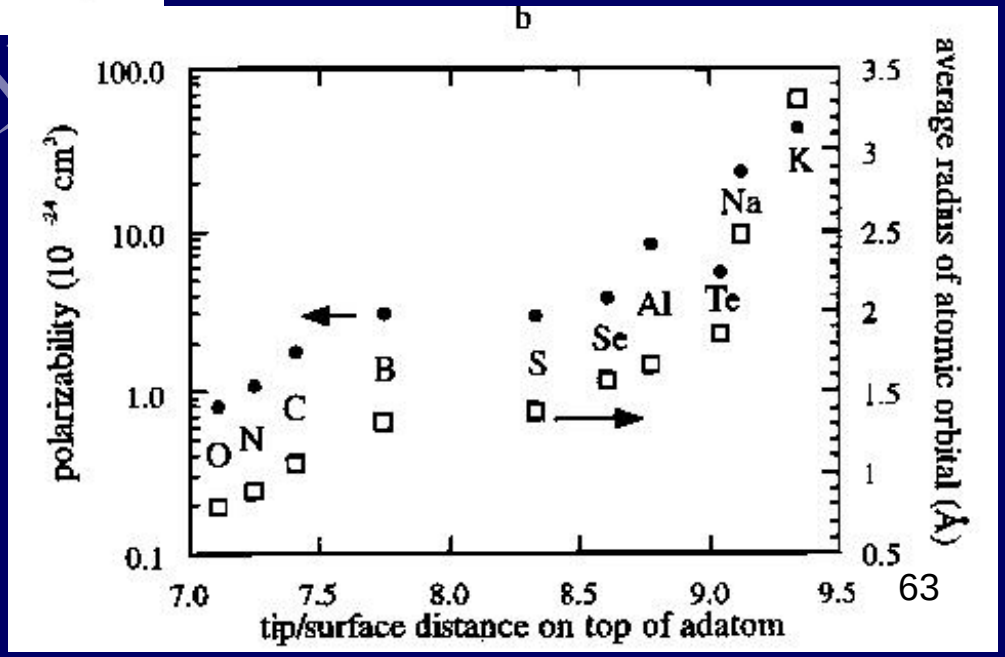

Sautet, Chem. Rev. 97 (1997) 1097.

Oh Where, Oh Where Has My Xenon Gone? Oh Where, Oh Where Can He Be? (Xenon on Nickel (110))

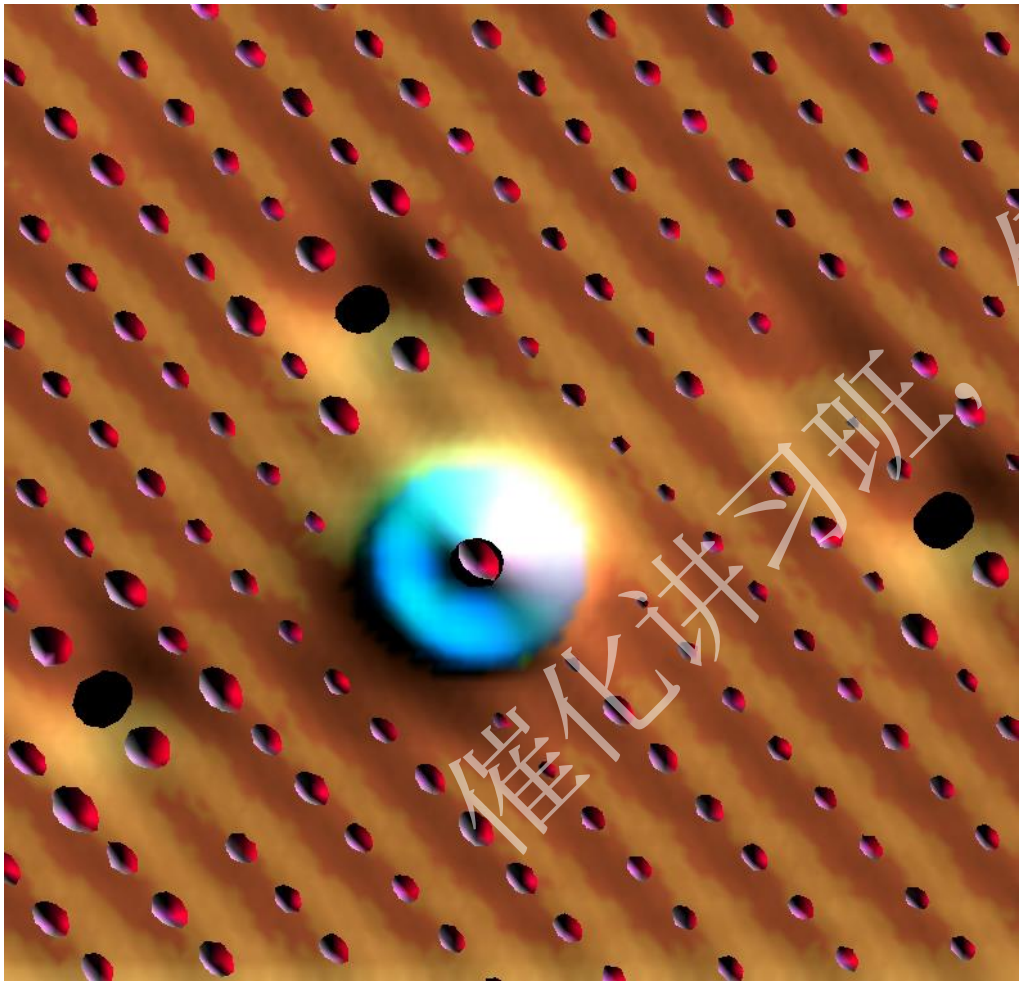

The artists were known to supplement their income with daytime jobs as scientists and here we see their touch being applied to just such a daytime endeavor. The issue was 'Where does xenon bind on a metal surface?' (a burning issue if ever there was one). Here we see not one, but two images overlayed directly on top of one another. The rectangular array of the little magenta bumps are the tops of nickel atoms from one image poking up through the other image (you can do that with the computer). The images are of the same area of the nickel surface, just with and without the xenon atom (the big light blue bump in the center). Defects in the nickel surface are used to get precise registration information so the two images can be correctly overlayed. The computer was used to chop off the top of the xenon atom in order to peer through to the image of the surface without the xenon. When you look through the hole in the xenon atom you see a nickel atom located directly beneath. Evidently, xenon binds to the on-top site.

D.M. Eigler,IBM

1.2 表面缺陷结构：CeO_2

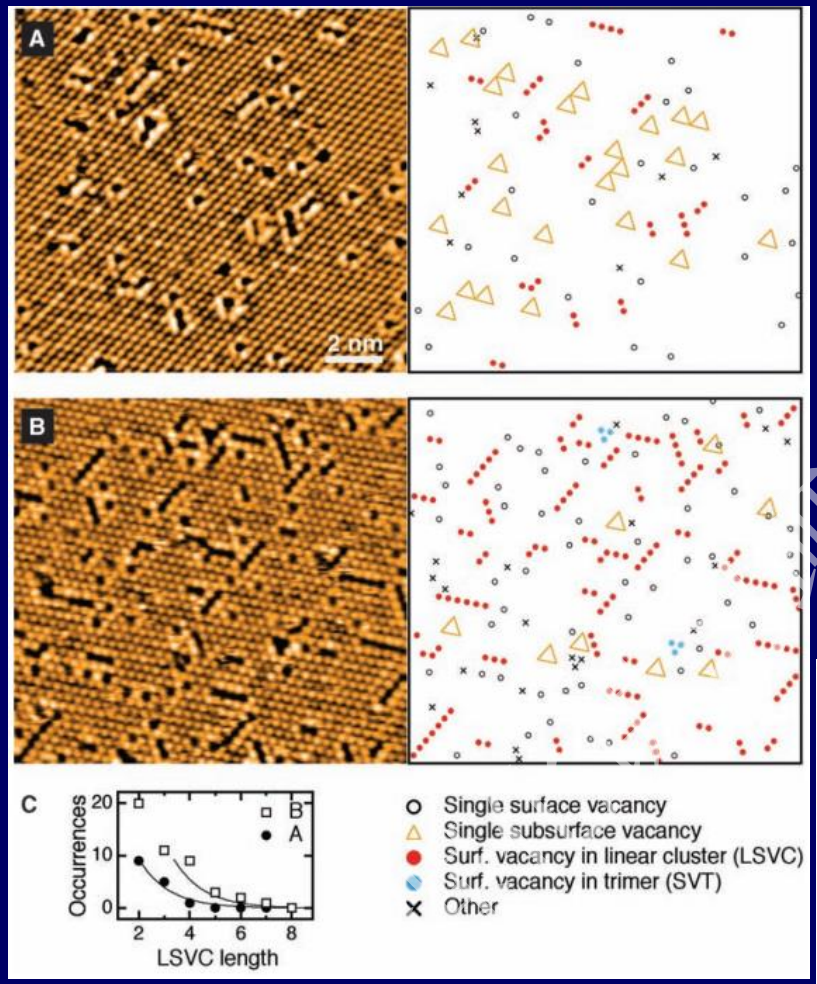

不同缺陷的观察与统计

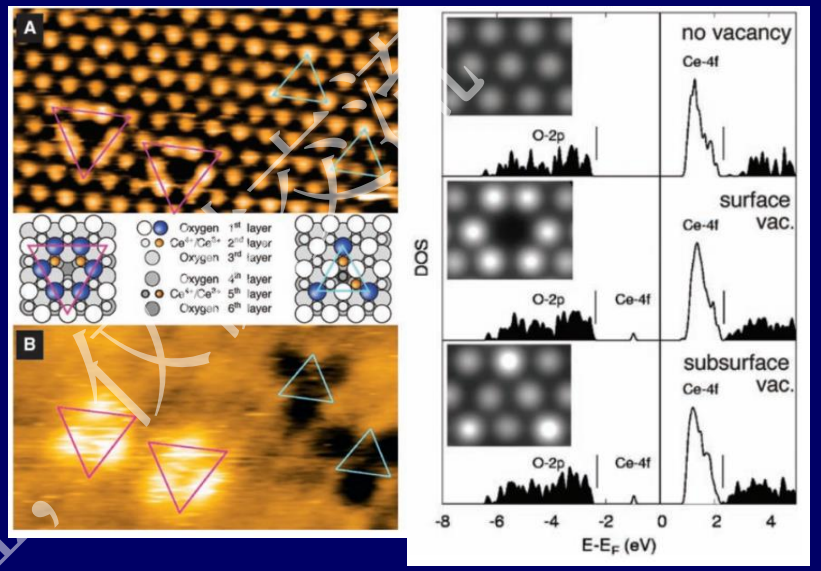

表层氧缺陷与次表层缺

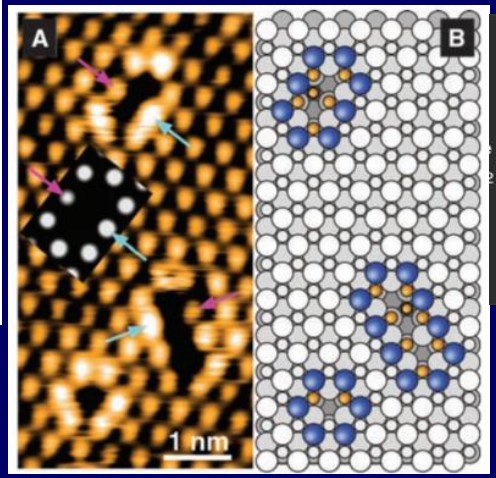

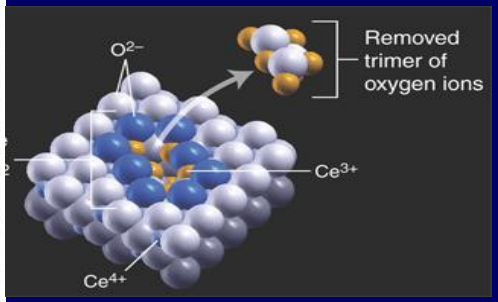

缺陷团簇利于三价铈的暴露

Science, 2005, 309, 752–755.

Oxygen vacancies on/in $CeO_2(111)$

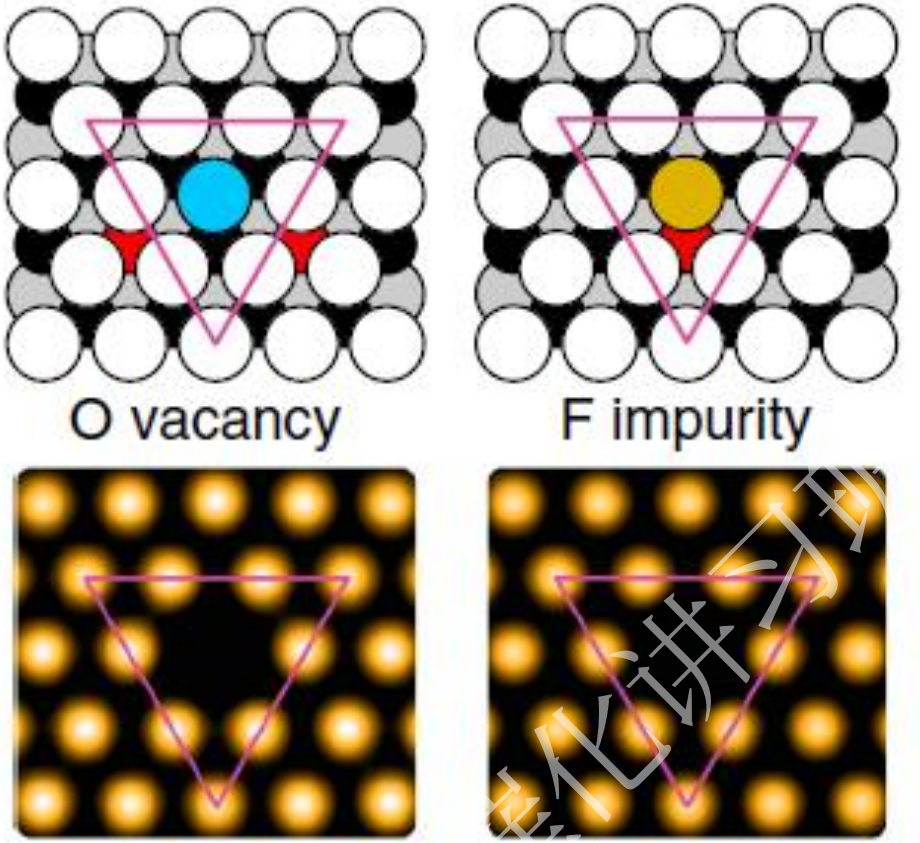

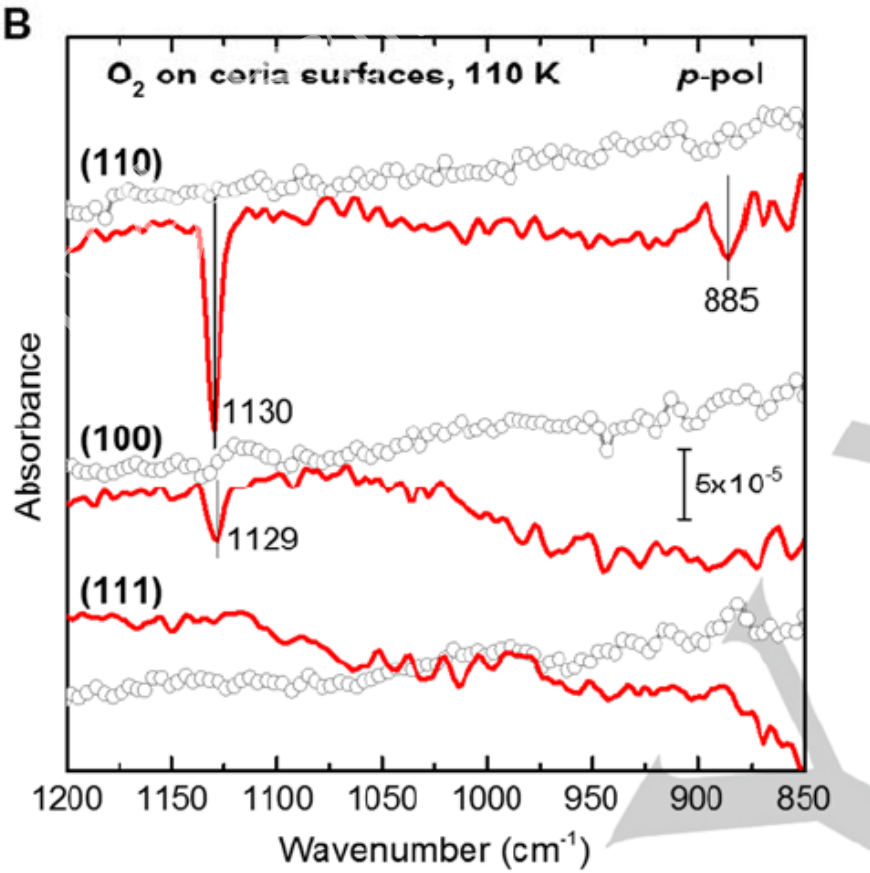

Yang, C.; Wang, Y.; Wöll, C.; Sauer, J. et al. Angew. Chem. Int. Ed. 2017, 56, 16399-16404.
Kullgren, J.; Hermansson, K. et al. Phys. Rev. Lett. 2014, 112, 156102.

Esch, F.; Comelli, G.; Rosei, R. *Science* 2005, *309*, 752.
Jerratsch, J.-F.; Freund, H.-J. et al. J. *Phys Rev Lett* 2011, *106*.

1.4 表面重构

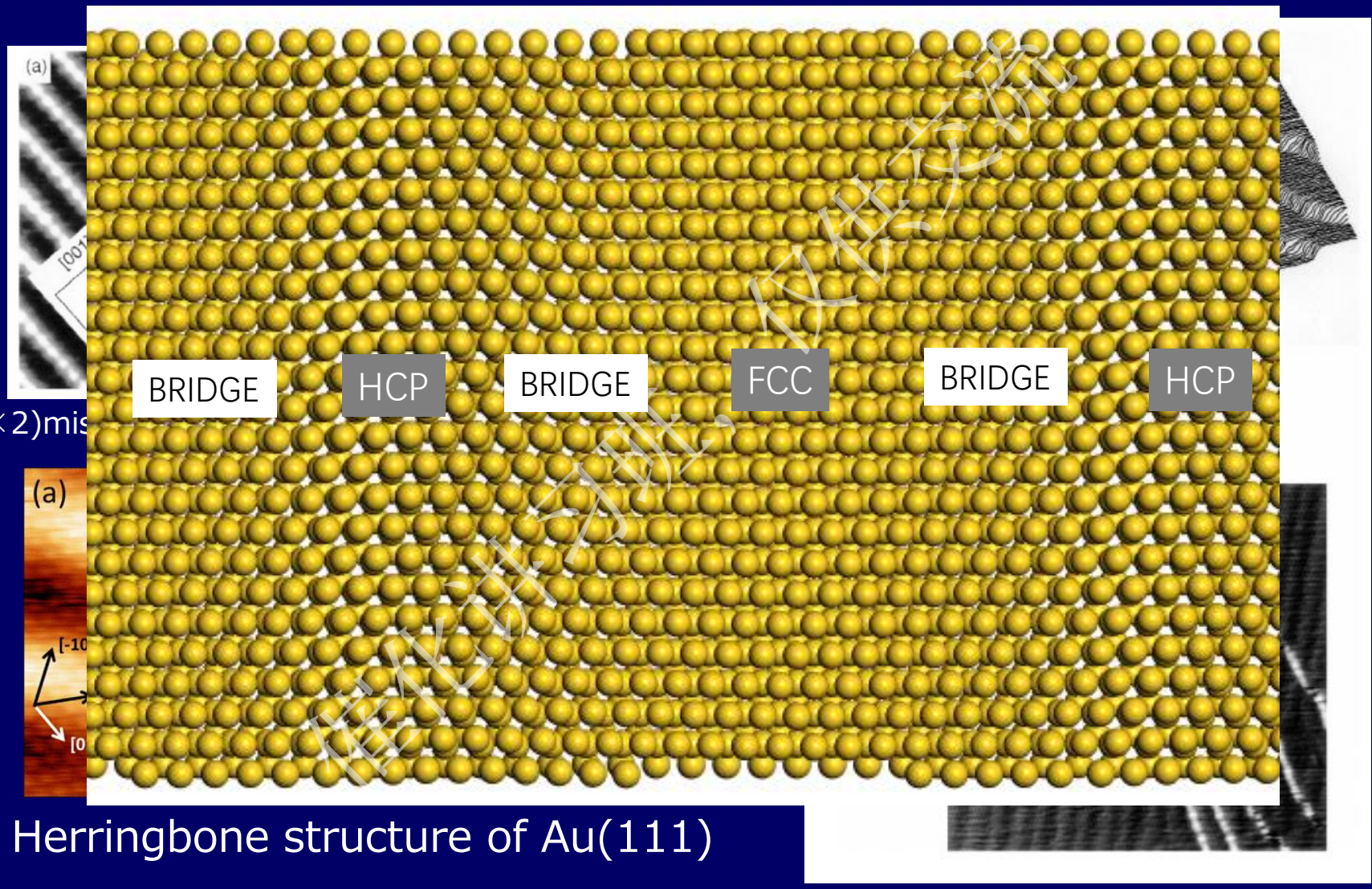

Herringbone structure of Au(111)

- Barth, J. V., Brune, H., Ertl, G. & Behm, R. J. (1990). *Phys. Rev. B*. **42**, 9307–9318.
- Besenbacher, F. (1996). *Rep. Prog. Phys.* **59**, 1737.

2. 电子结构： 扫描隧道谱(STS)

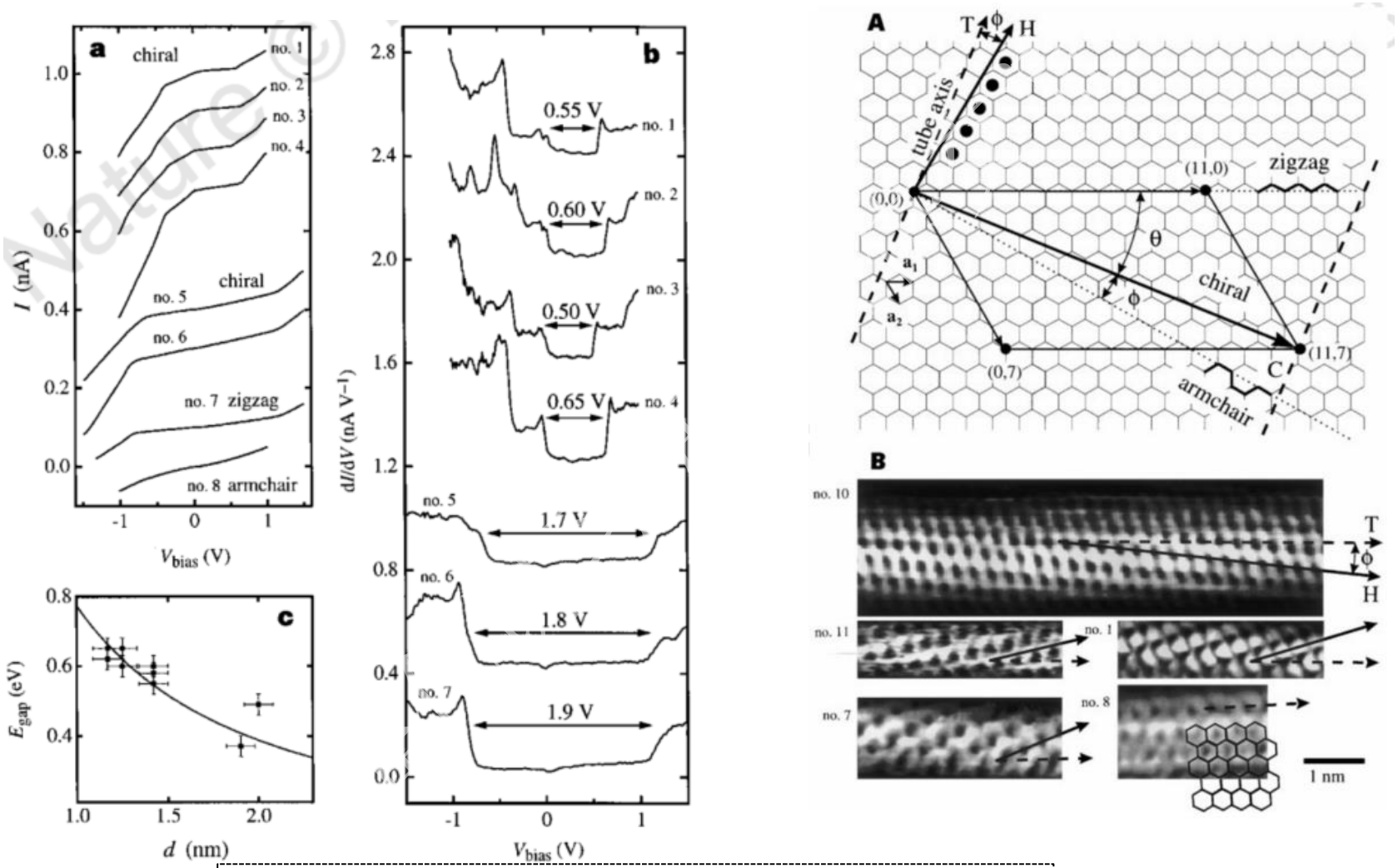

手性敏感的碳纳米管电子结构

Wilder, J. W. G., Venema, L. C., Rinzler, A. G., Smalley, R. E. & Dekker, C. (1998). *Nature*. **391**, 59–62.

Catalysis by Gold

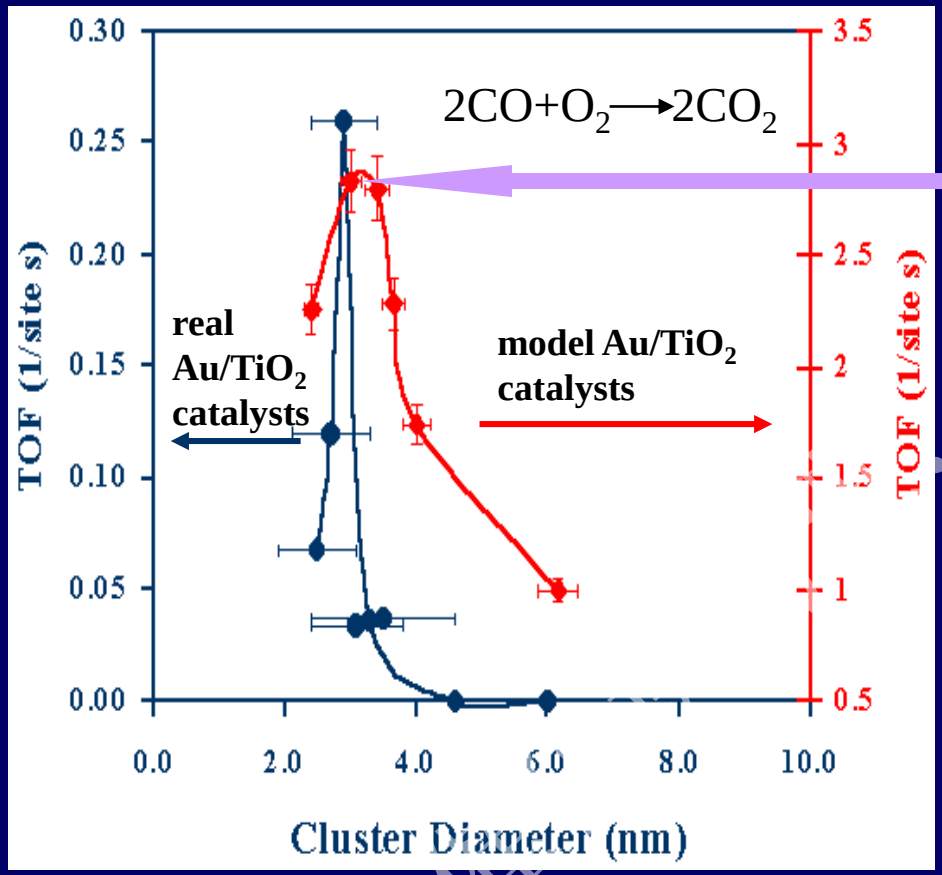

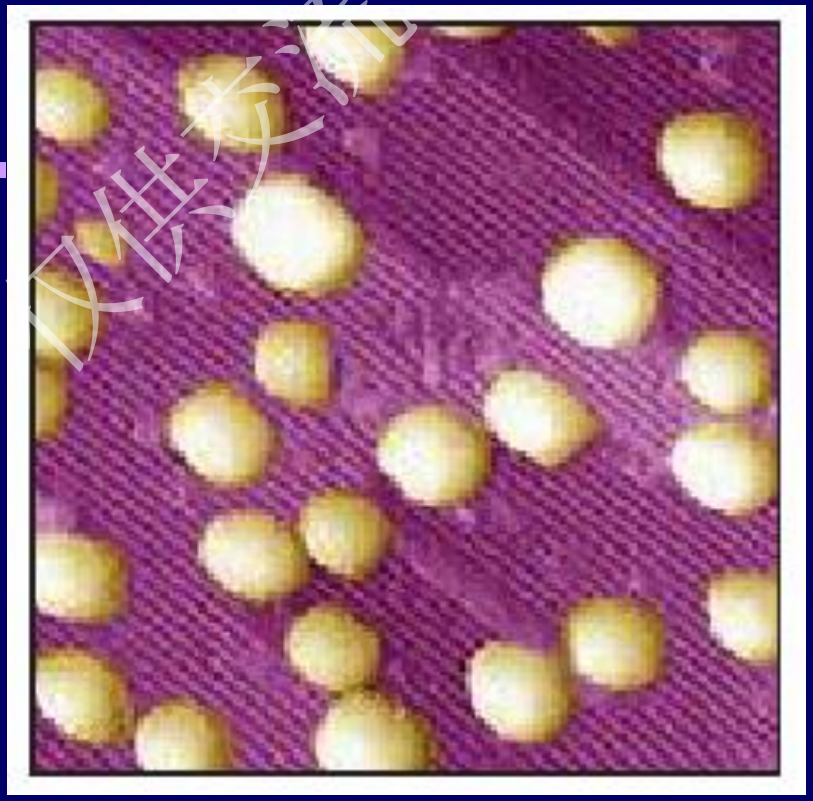

30 nm × 30 nm

G.R. Bamwenda, S. Tsubota, T. Nakamura and M. Haruta, *Catal. Lett.* **44**, 83 (1997)
M. Valden, X. Lai and D. W. Goodman, *Science* **281**, 1647 (1998)

Au clusters supported on TiO_2(110) exhibit a remarkable catalytic reactivity for CO oxidation at room temperature and have the maximum activity when the cluster size is around 3 nm.

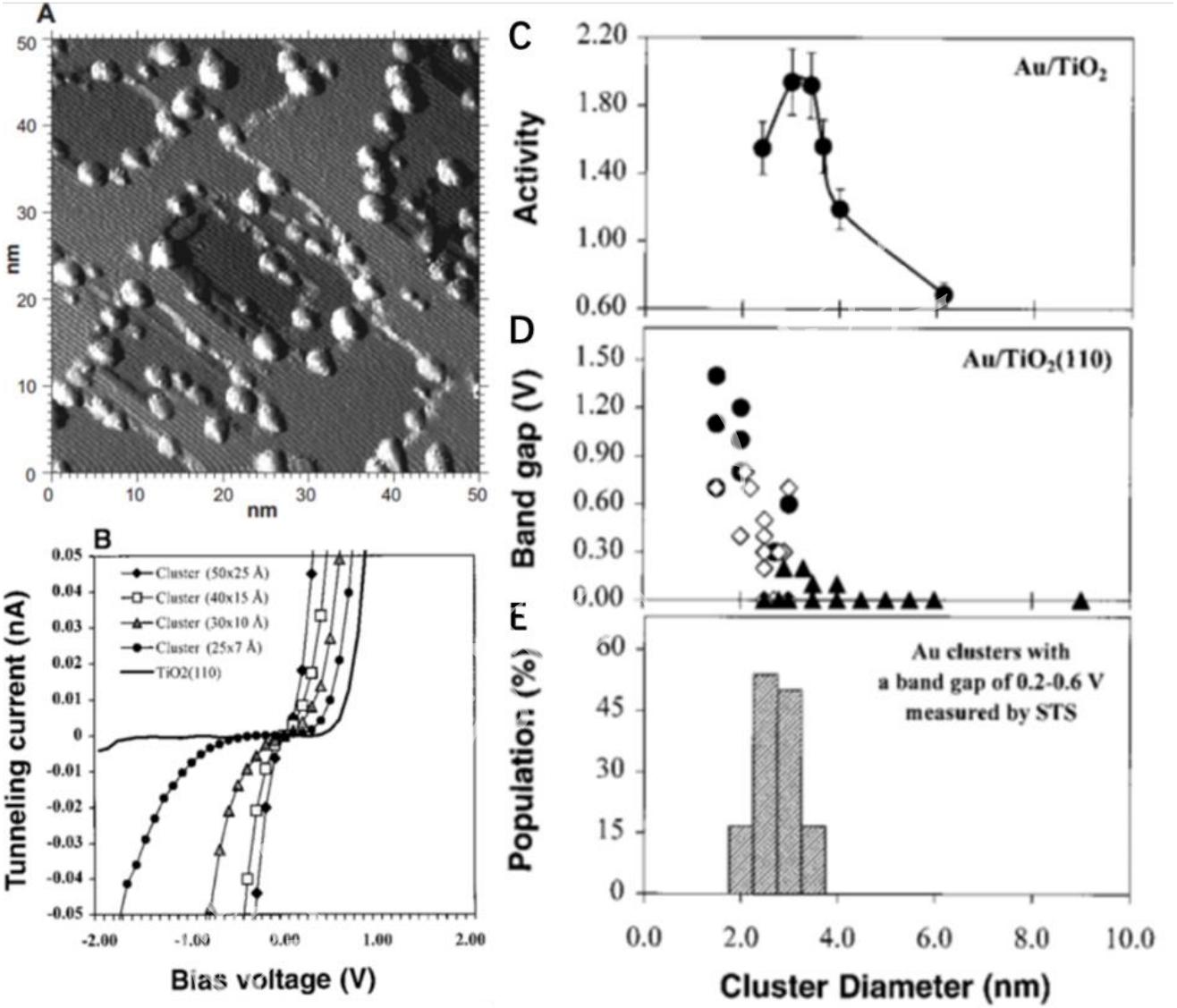

TiO2(110)表面Au纳米粒子的STM图像(A)，不同尺寸Au纳米粒子的STS谱(B)，CO氧化活性(C)， 带隙值（D），以及带隙为0.2-0.6V的Au纳米粒子在Au/TiO2表面的比例。

Valden, M., Lai, X. & Goodman, D. W. (1998). *Science*. **281**, 1647–1650.

局域功函数测量：dI/dz or d(lnI)/dz

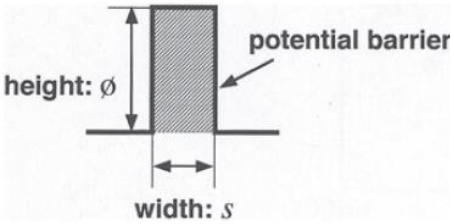

tunneling current:

$$I \propto V\exp(-1.02 \times s(\text{Å})\sqrt{\phi(\text{eV})})$$

$$\downarrow$$

$$\phi\,(\text{eV}) \approx 0.95\left(\frac{d\ \ln I}{ds\,(\text{Å})}\right)^2$$

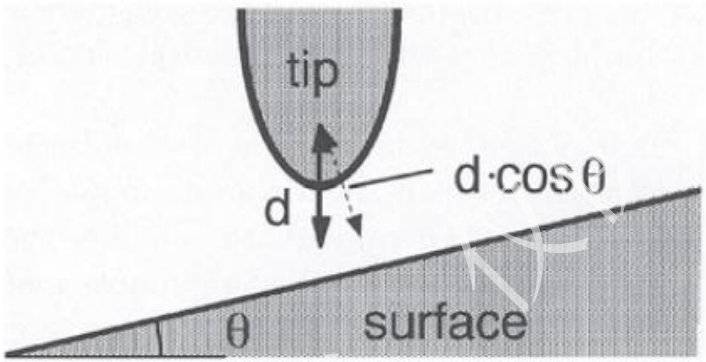

Fig. 7.13. Topographic effect in work function measurements using STM. When the surface is tilted with respect to the direction of the z-axis piezo, the modulation amplitude in the gap distance is reduced to $d\cos\theta$. As a result, the measured work function is reduced apparently by a factor of $\cos^2\theta$

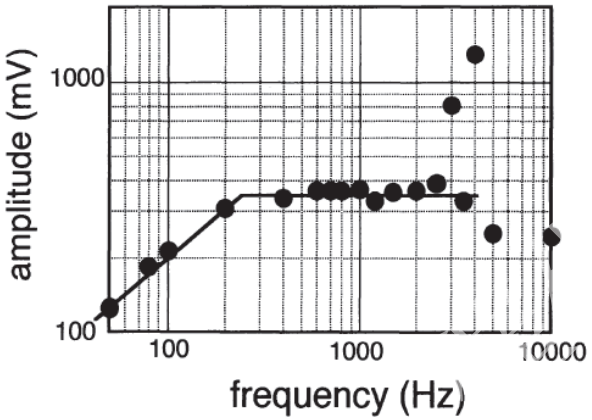

Fig. 7.10. Amplitude of detected tunneling current modulation when a modulated wave is applied on the z-axis piezo, measured as a function of modulation frequency. When the frequency is low, the feedback circuit responds to the modulation, negating its effect. At high frequency, a current amplifier used in this experiment cannot follow because of its limited response. A peak observed around 3–4 kHz is due to resonance of the current amplifier

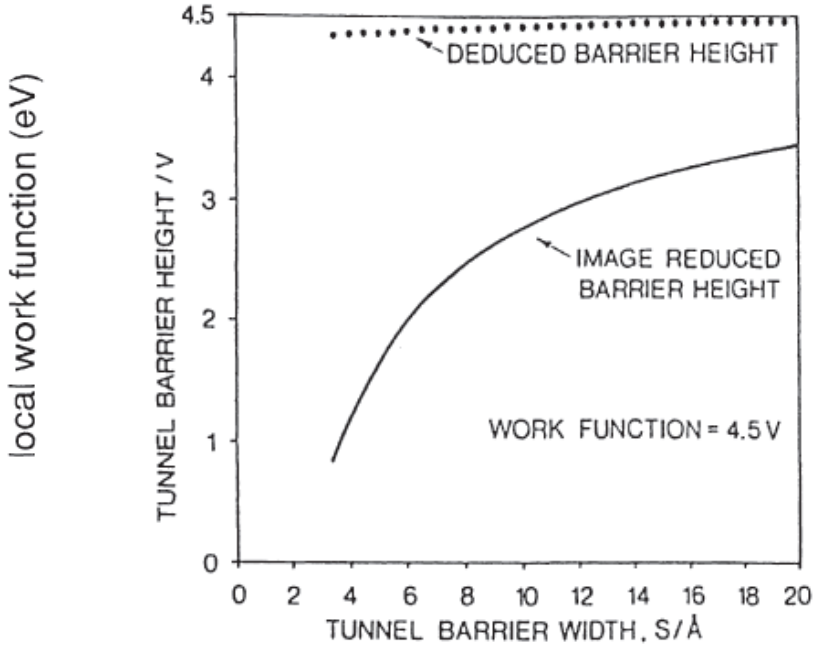

Hasegawa, Y.; Jia, J. F.; Sakurai, T.; Li, Z. Q.; Ohno, K.; Kawazoe, Y., Advances in Scanning Probe Microscopy 2000, 167-191.

局域功函数测量：dI/dV or dz/dV

Image Potential States (IPS)

- An electron brought near a conducting surface polarizes the surface.

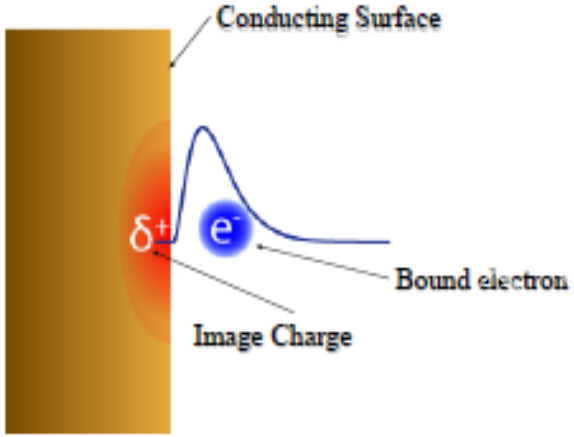

- This allows for the electron to be bound in a potential well for a short period of time.

- Quantum mechanically, an electron bound near the surface can be described by discrete energy levels called ***Image Potential States***[1].

[1] P.M. Echenique et al., Surf. Sci. Reports 52, 219 (2004).

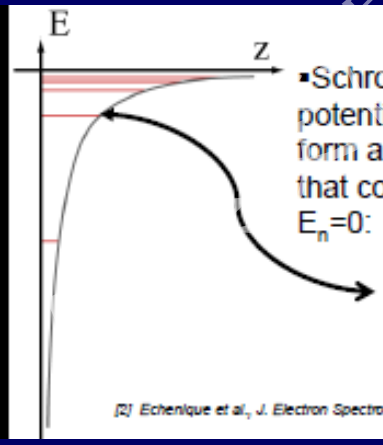

- Schrodinger's equation with the potential above produces energies that form a Rydberg Series, hydrogen-like, that converges to vacuum level energy, E_n=0:

$$E_n^{[2]} = \frac{-0.84eV}{(n+a)^2}$$

[2] Echenique et al., J. Electron Spectrosc. Relat. Phenom. 126, 163 (2002)

IPS in Scanning Tunneling Spectroscopy

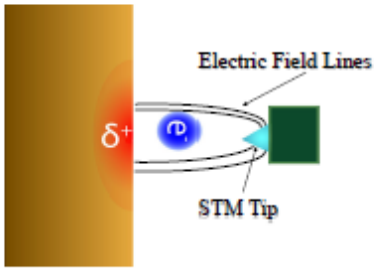

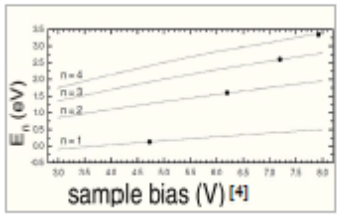

- Scanning Tunneling Microscope (STM) tip's interaction with the surface leads to an higher image potential energy level, **Stark-Shift**[4].

- The shift in the energy of the image potential state is due to the presence of the electric field between the tip and sample.

[4] Wahl et al., K. Phys. Rev. Lett. 2003, 91, 106802

局域功函数测量

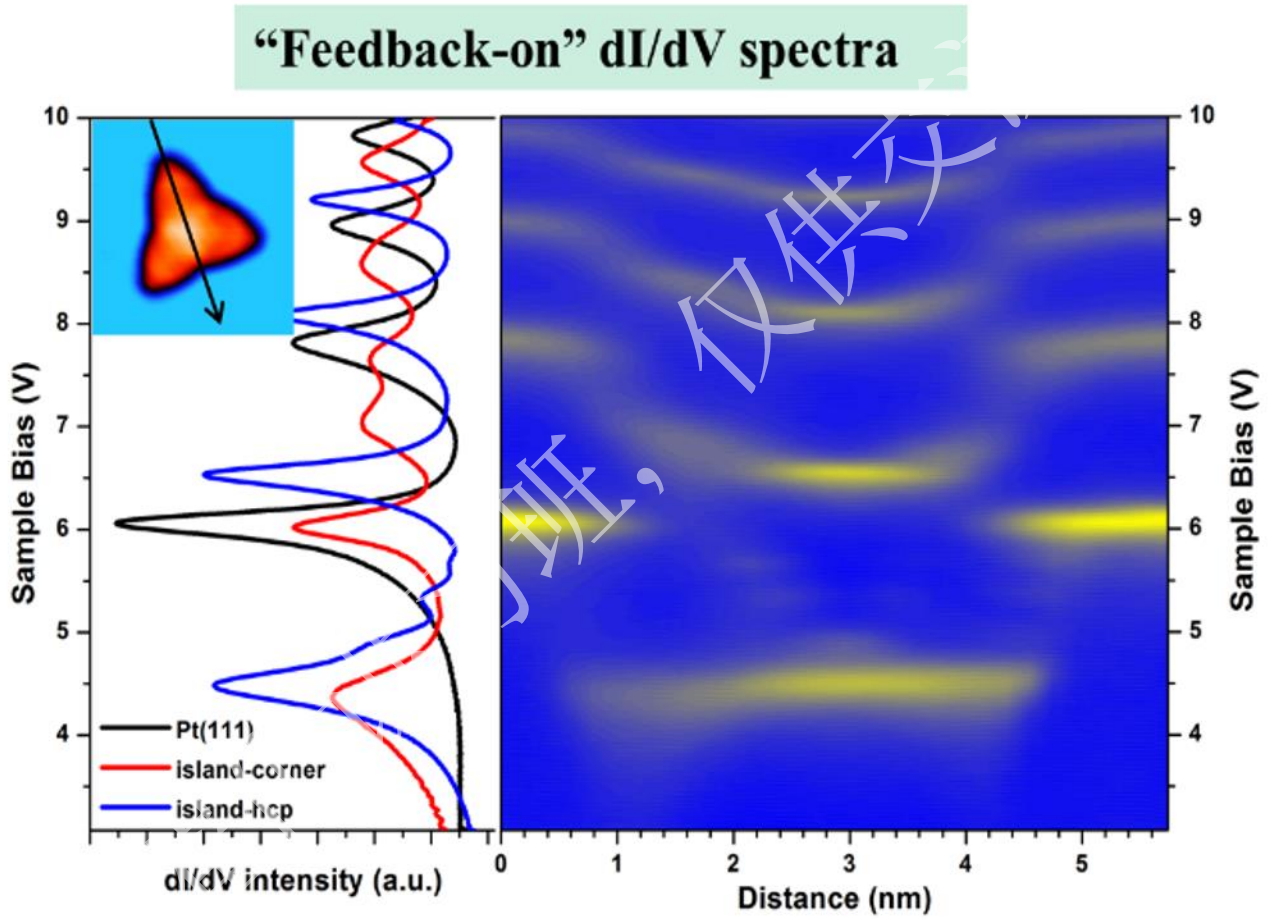

Image potential states: Comparable shifts of n=1 state were attributed to a change in the surface work function.

Theory of (IETS) Inelastic electron tunneling spectroscopy

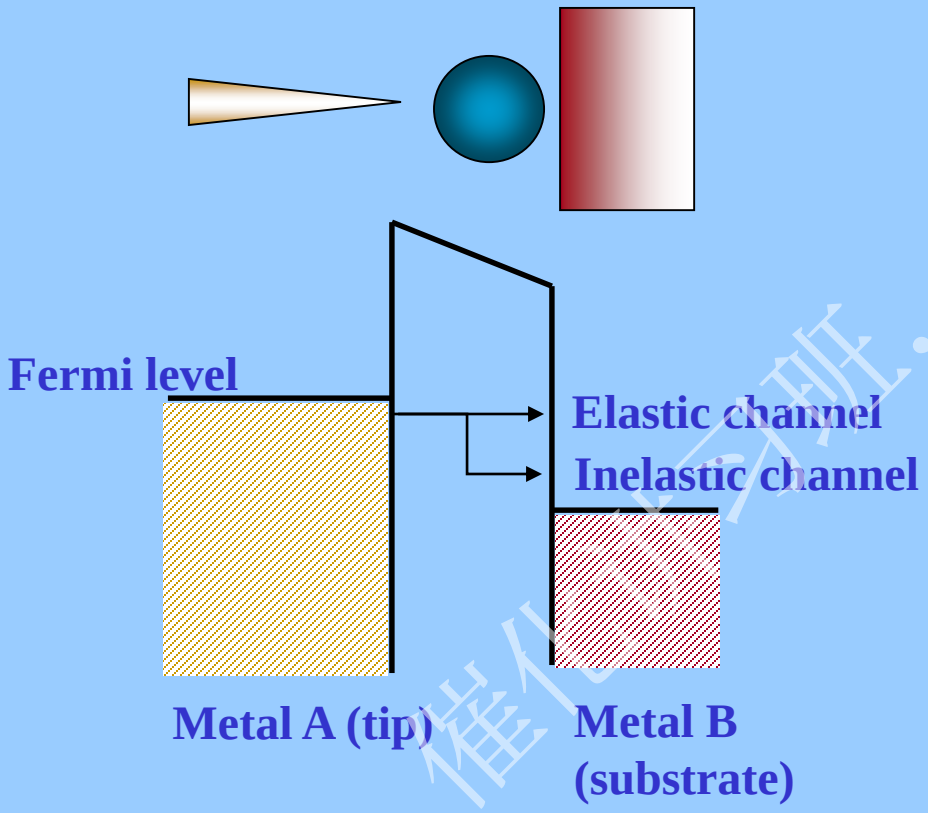

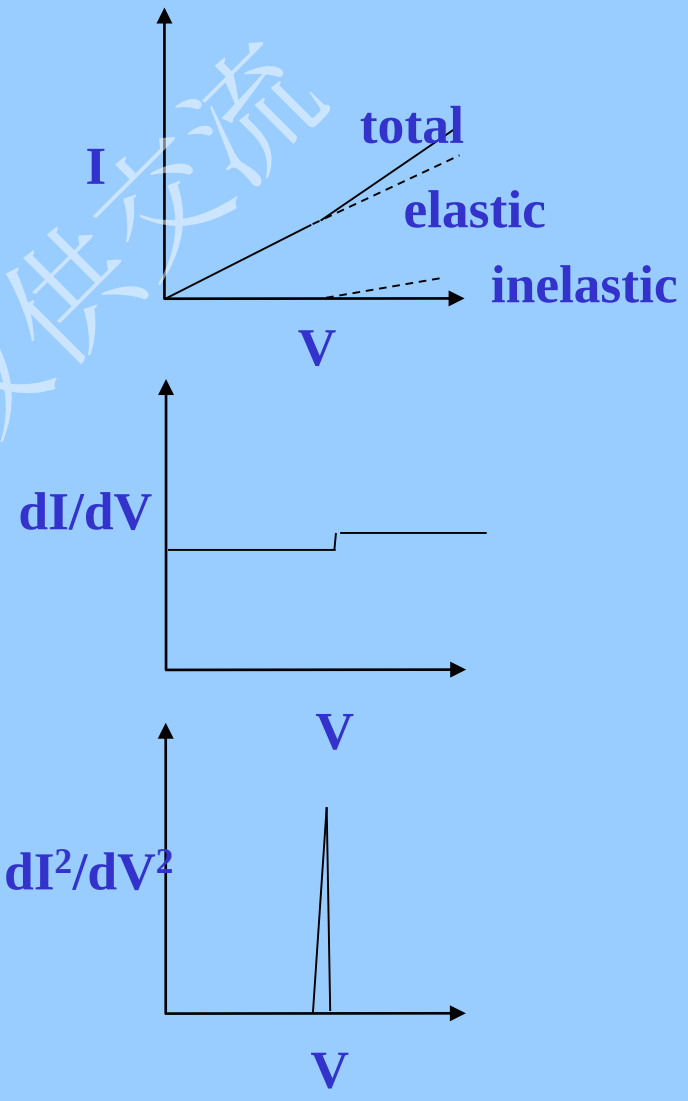

From: "Scanning Probe Microsocpy and Spectroscopy", R. Wiesendanger, Cambridge, 1994

非弹性电子隧穿谱(IETS)

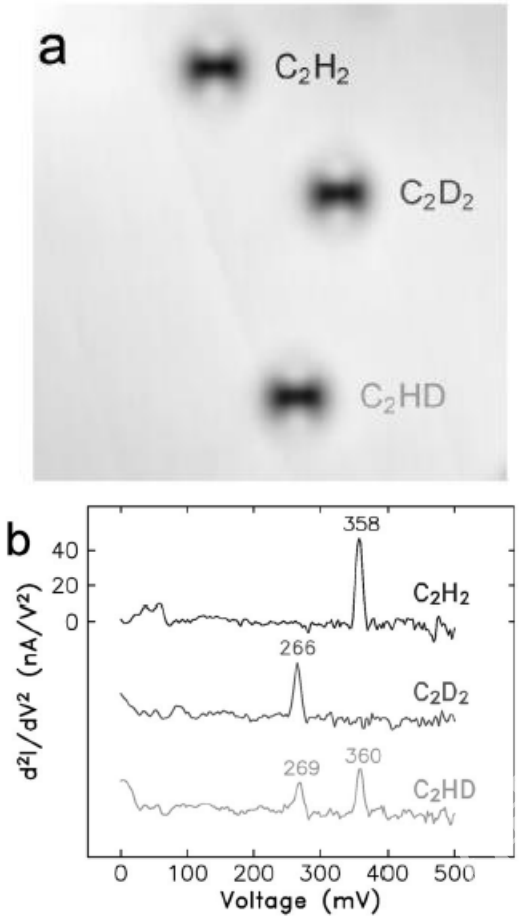

Inelastic electron tunneling spectra for isolated C_2H_2 molecule adsorbed on the copper(100) surface.

The curves are recorded with the STM tip directly over the center of molecule

There is a peak at bias voltages of 358mV, it was assigned to the C-H stretch vibration

B. C. Stipe, M. A. Rezaei, W. Ho , Science, Vol. 280,1732(1998)

3.1 分子吸附/活化

Pt(111)表面上的CO吸附

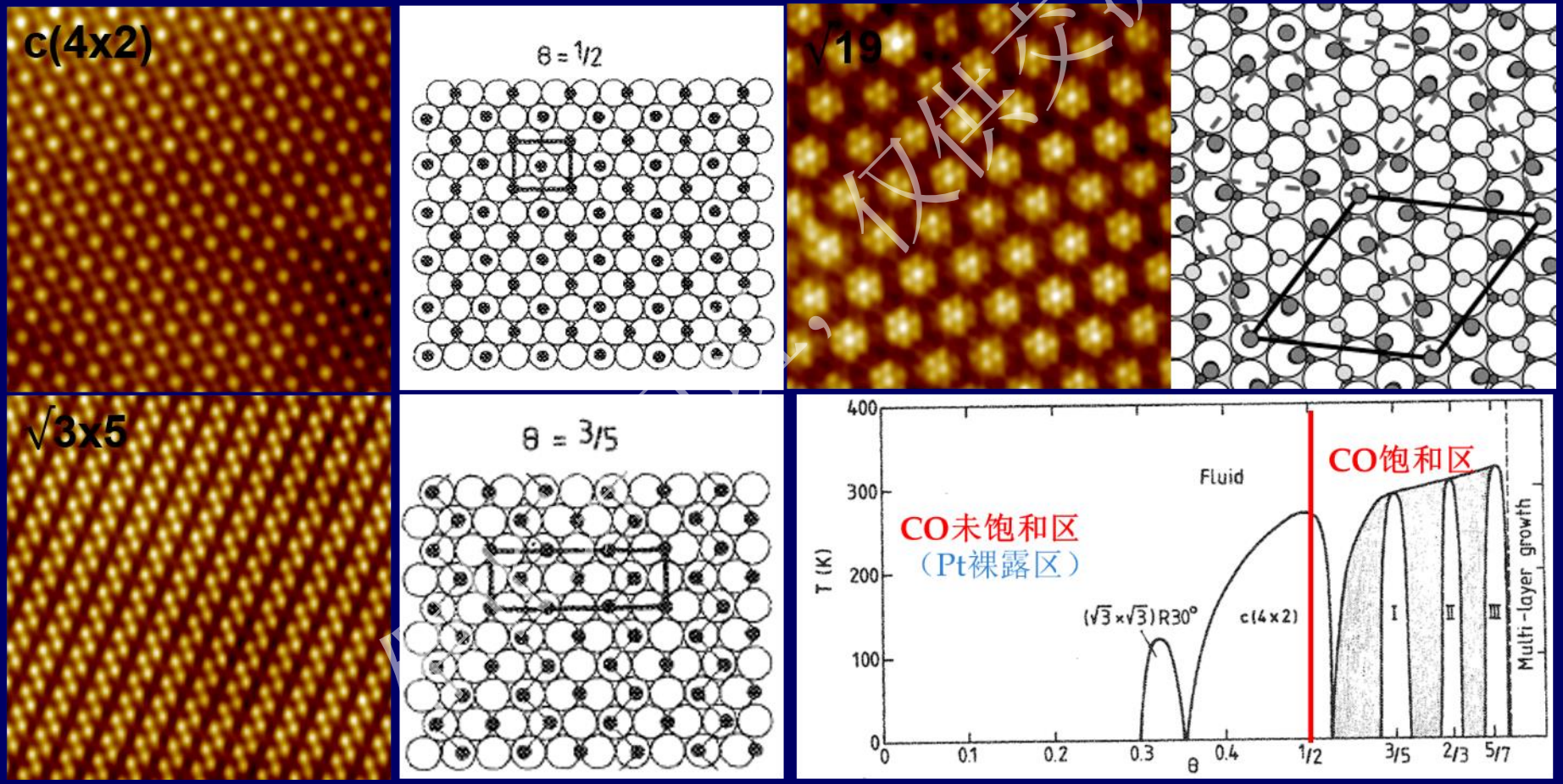

Persson, B. N. J.; Tushaus, M.; Bradshaw, A. M.; *J. Chem. Phys.* 1990, *92*, 5034.

CO adsorption on FeO/Pt(111)

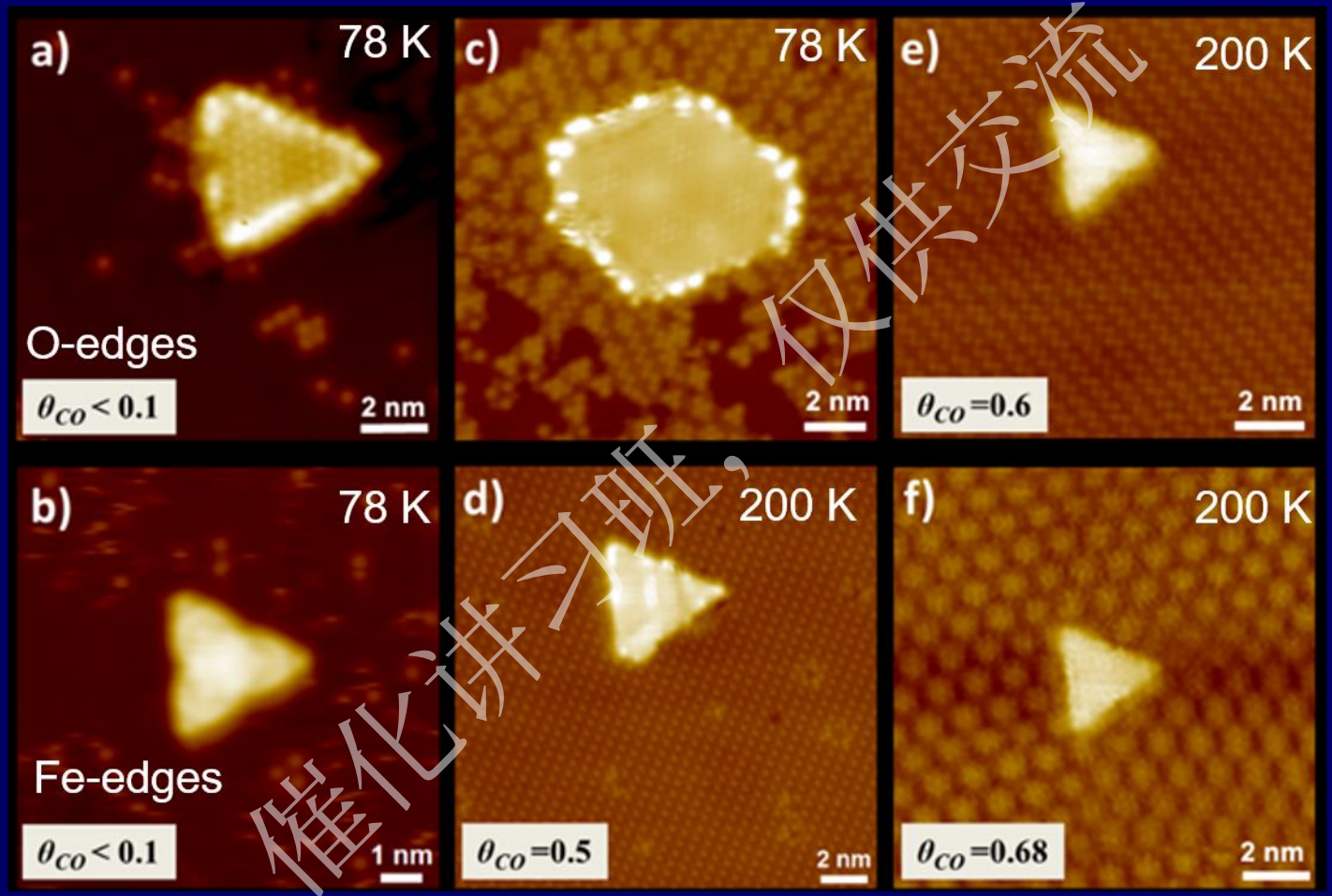

Ertl, G., Neumann, M. & Streit, K. M. (1977). *Surface Science*. **64**, 393–410.
Biberian, J. P. & Van Hove, M. A. (1984). *Surface Science*. **138**, 361–389.
Persson, B. N. J., Tüshaus, M. & Bradshaw, A. M. (1990). *The Journal of Chemical Physics*. **92**, 5034–5046.
Yang, H. J., Minato, T., Kawai, M. & Kim, Y. (2013). *J. Phys. Chem. C*. **117**, 16429–16437.

CO structures on the FeOx/Pt(111) surface

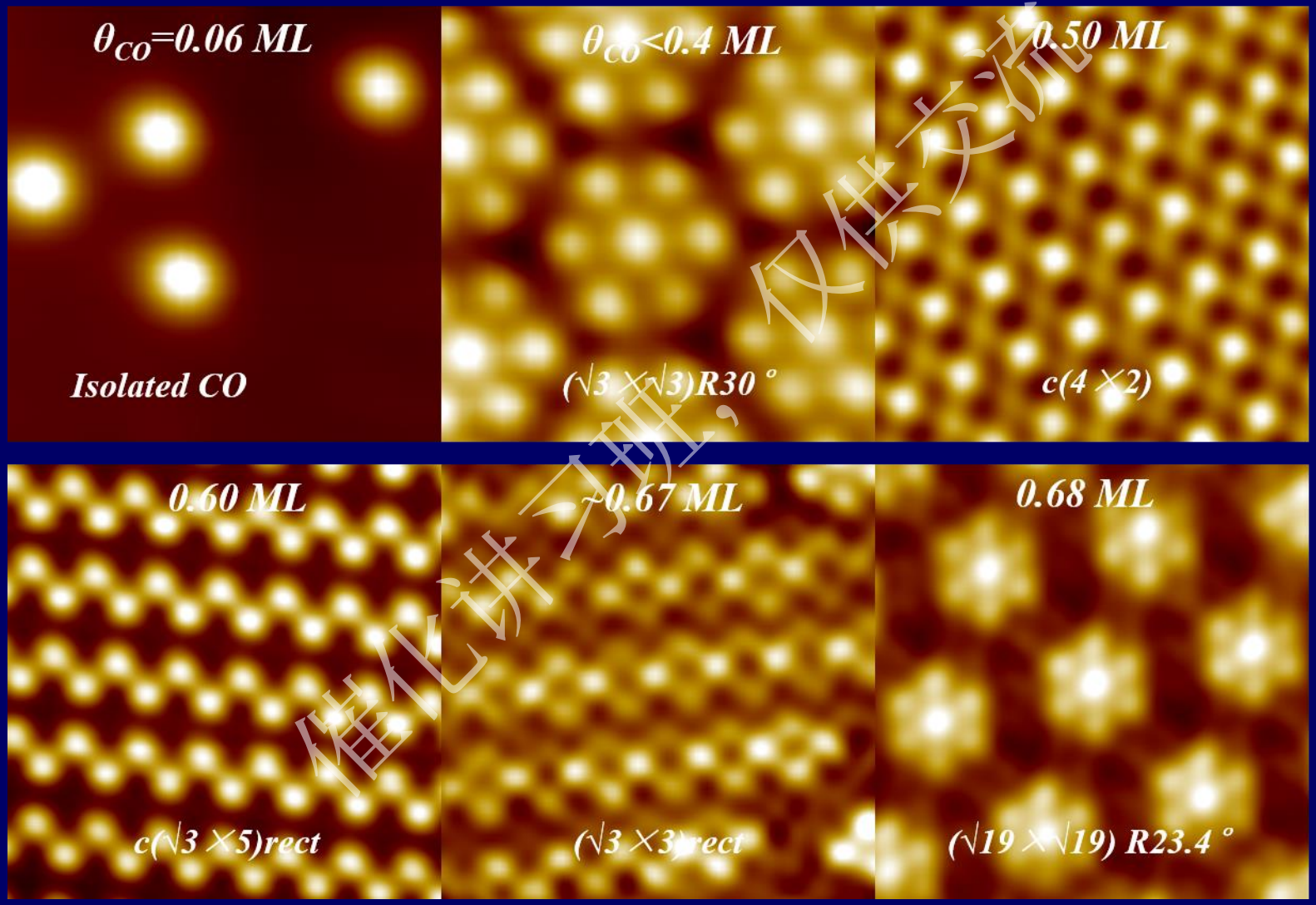

The interaction between CeO_x/Au(111) and CO_2

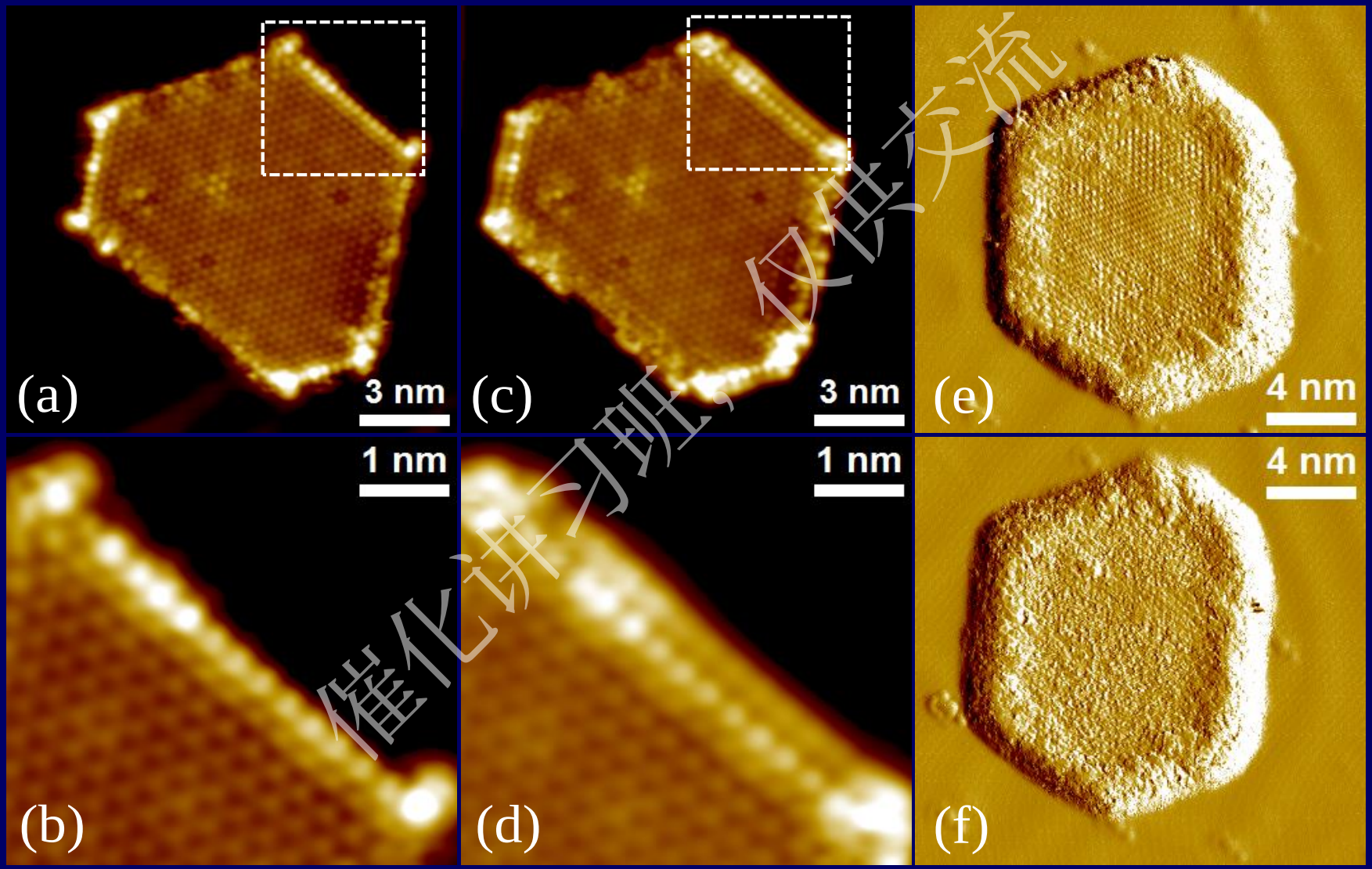

F. Yang, G. X. Wang, X. H. Bao, et al. J. Am. Chem. Soc. 2017, 139 (16), 5652-5655.

The interaction between CeO_x/Au(111) and CO_2

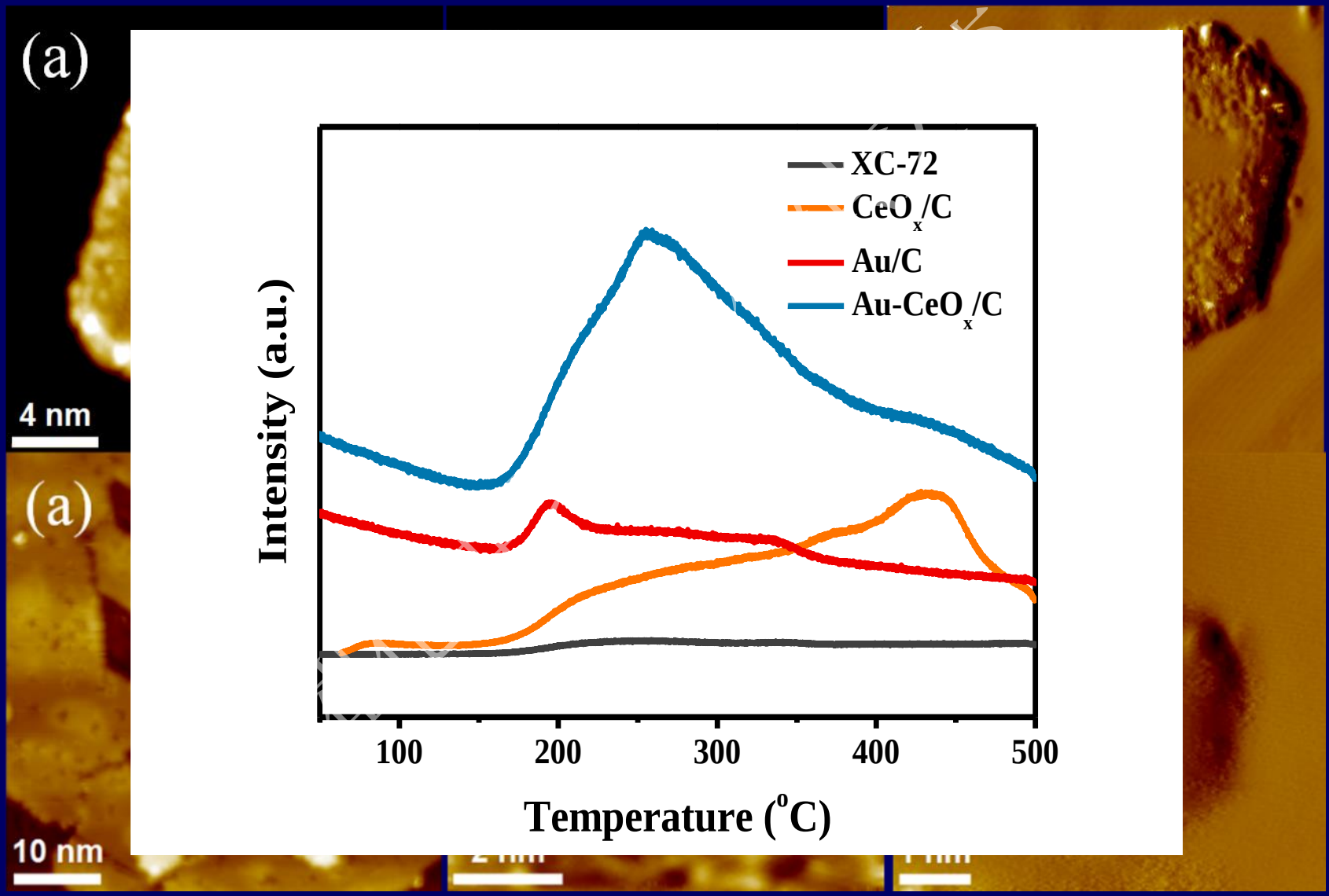

F. Yang, G. X. Wang, X. H. Bao, et al. J. Am. Chem. Soc. 2017, 139 (16), 5652-5655.

Interface Effect on Selective Oxidation of Primary Alcohols

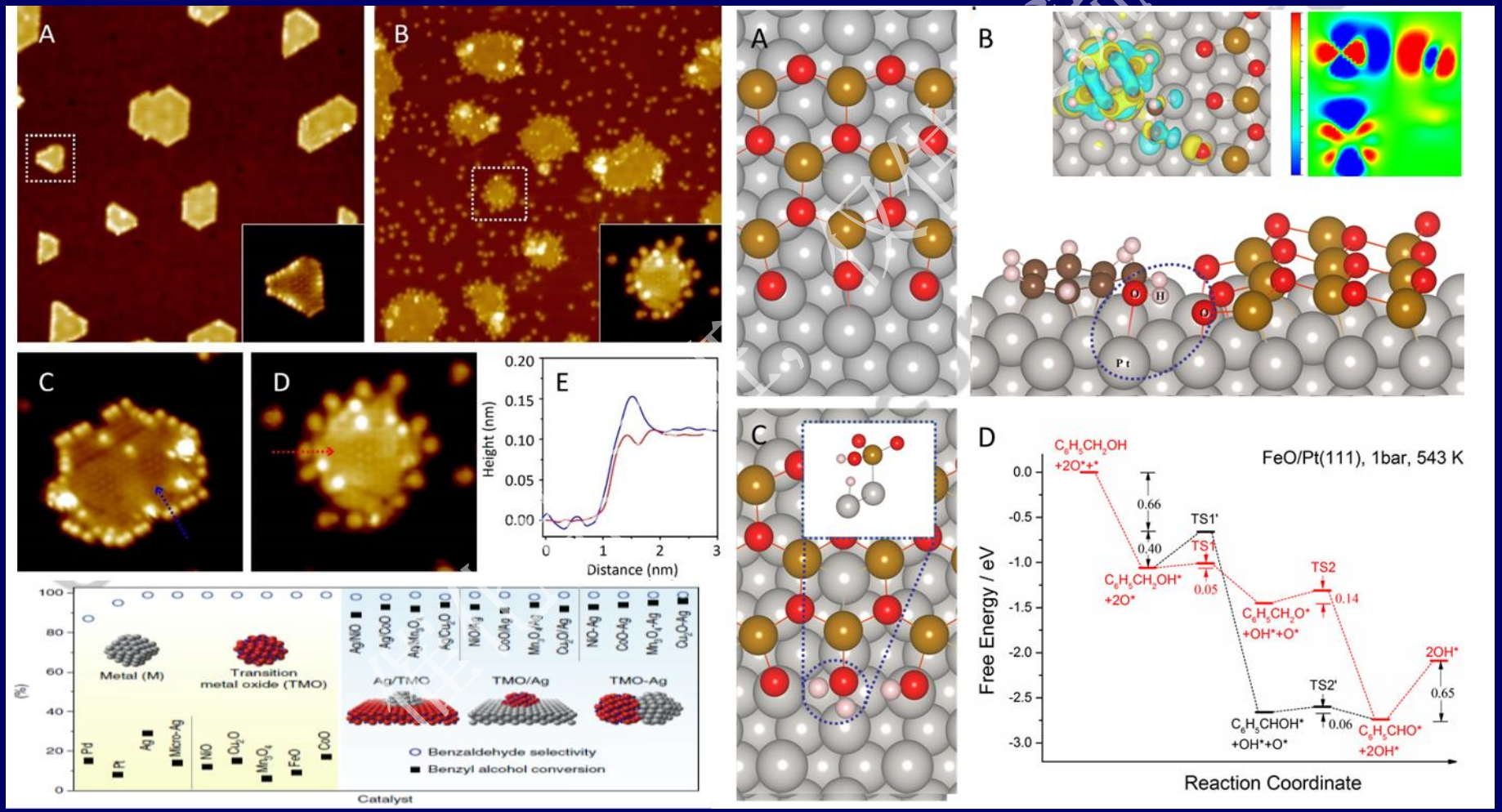

G. Zhao, F. Yang, Z. Chen, P. Hu, X. H. Bao, Y. D. Li et al., Nat. Commun., 2017

Interface Effect on the Selective Oxidation of Primary Alcohols

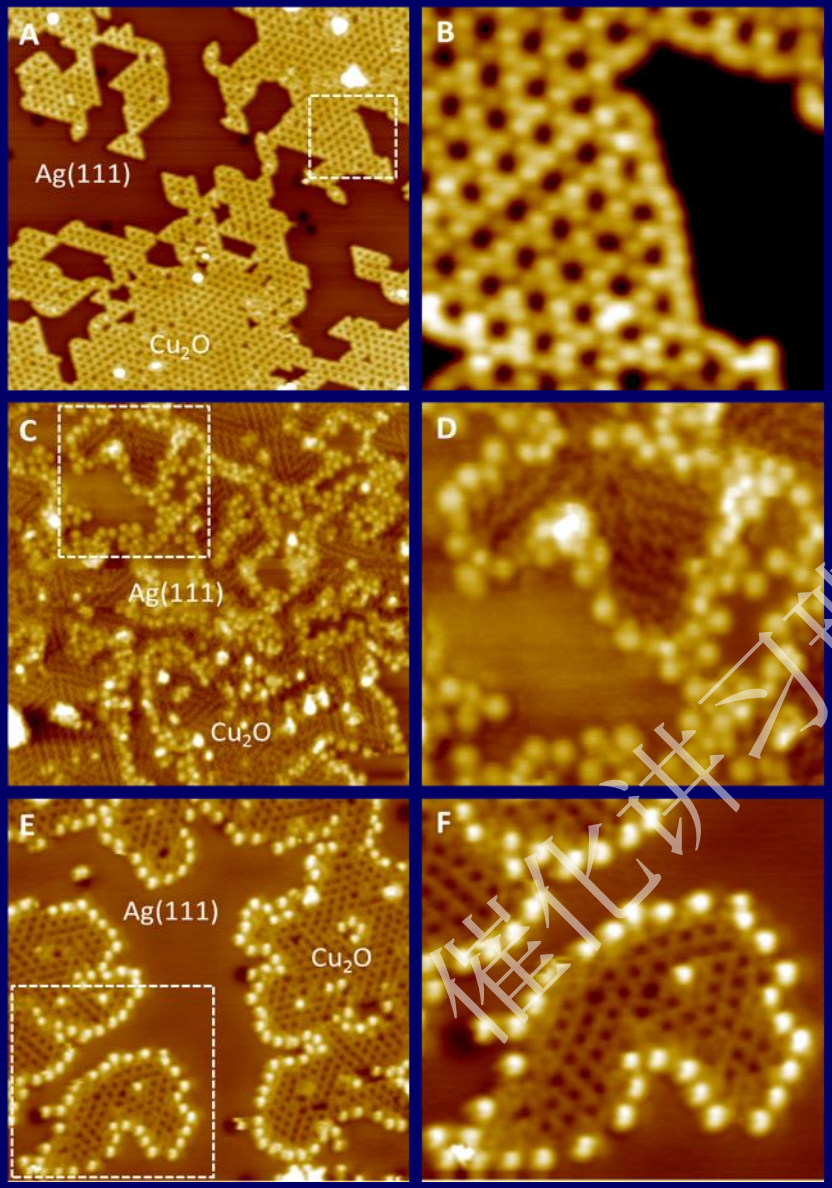

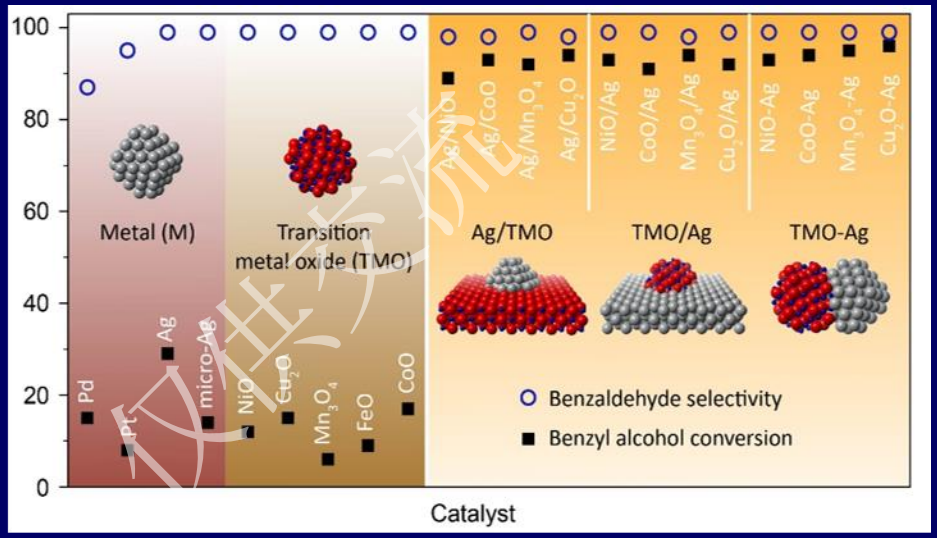

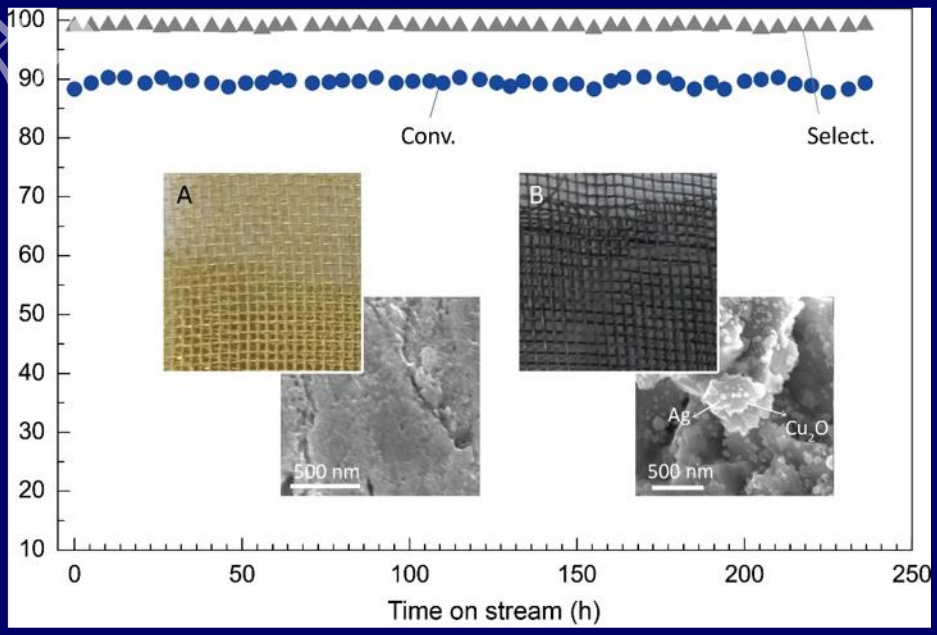

G. Zhao, F. Yang, Z. Chen, P. Hu, X. H. Bao, Y. D. Li et al., Nat. Commun., 2017

3.2 表面催化反应观测

Langmuir Isotherm
Langmuir-Hinshelwood mechanism

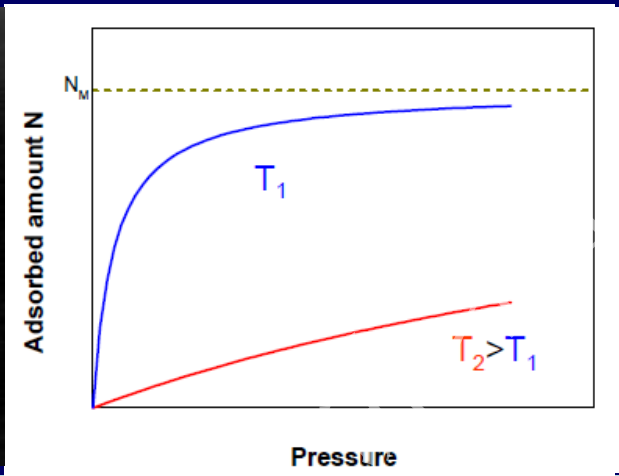

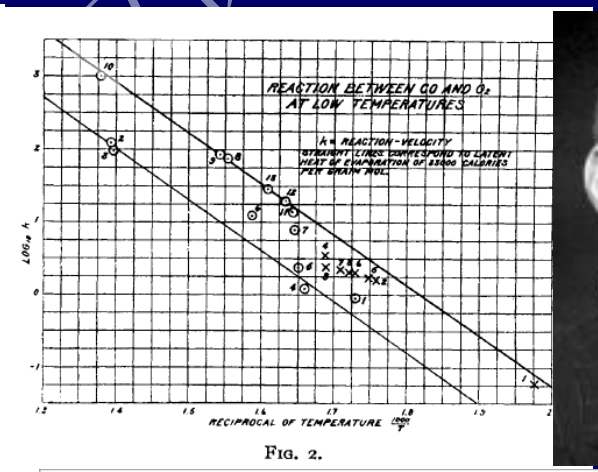

FIG. 2.

$$N = \frac{N_M p}{b + p}$$

Langmuir isotherm

THE MECHANISM OF THE CATALYTIC ACTION OF PLATINUM IN THE REACTIONS $2CO + O_2 = 2CO_2$ and $2H_2 + O_2 = 2H_2O$.

BY IRVING LANGMUIR.

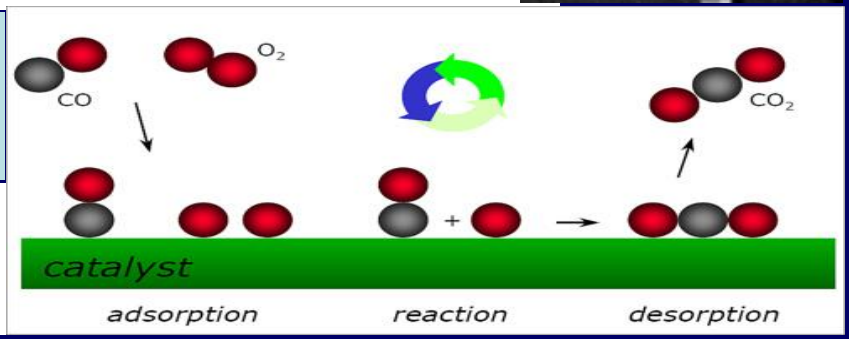

Pressure Gap in low temperature CO oxidation

JACS
JOURNAL OF THE AMERICAN CHEMICAL SOCIETY
ARTICLE
pubs.acs.org/JACS

Chemisorption of CO and Mechanism of CO Oxidation on Supported Platinum Nanoclusters

Ayman D. Allian,[‡,#] Kazuhiro Takanabe,[‡,¶] Kyle L. Fujdala,[*,§,⊗] Xianghong Hao,[§] Timothy J. Truex,[§,†] Juan Cai,[§,▽] Corneliu Buda,[∥] Matthew Neurock,[*,∥] and Enrique Iglesia[*,‡,⊥]

"At low temperatures, CO oxidation occurs on surfaces nearly saturated with chemisorbed CO, making conclusions from previously reported model experimental and theoretical studies in the literature, which were carried out on sparsely covered flat surfaces, difficult to extend to catalytic reactions on small clusters saturated with chemisorbed CO."

文献中的模型实验和理论研究都在未被CO毒化的表面进行，导致其结论难以拓展到实际催化反应下被CO饱和的粒子表面。

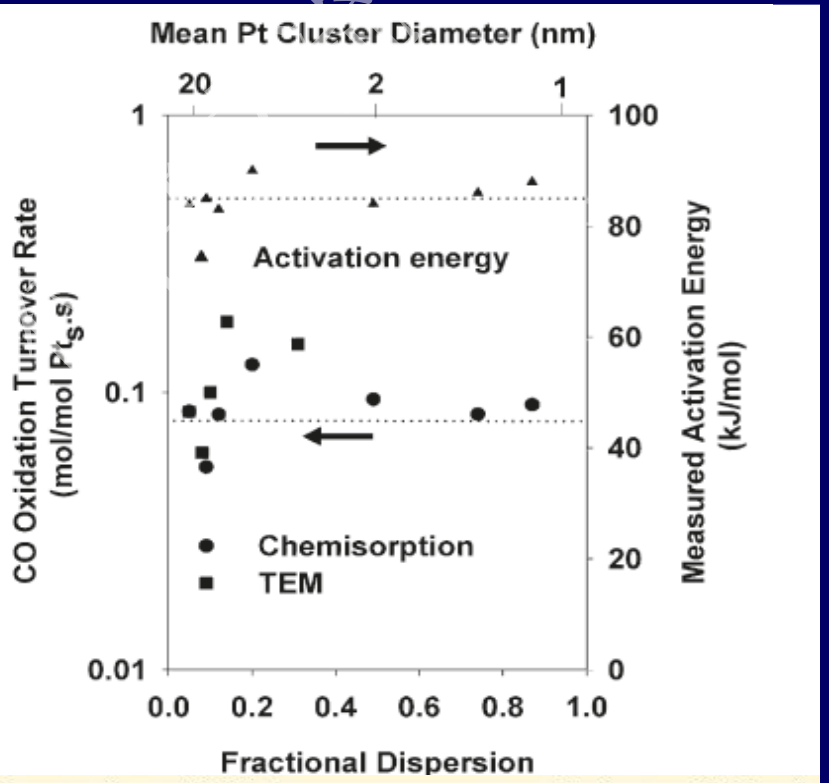

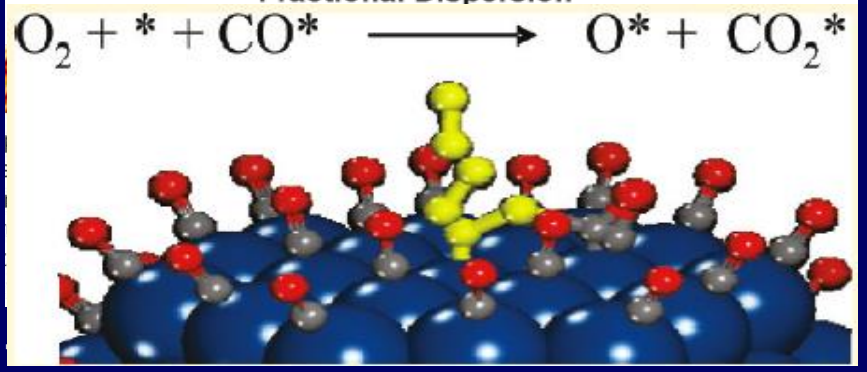

Low temperature CO oxidation

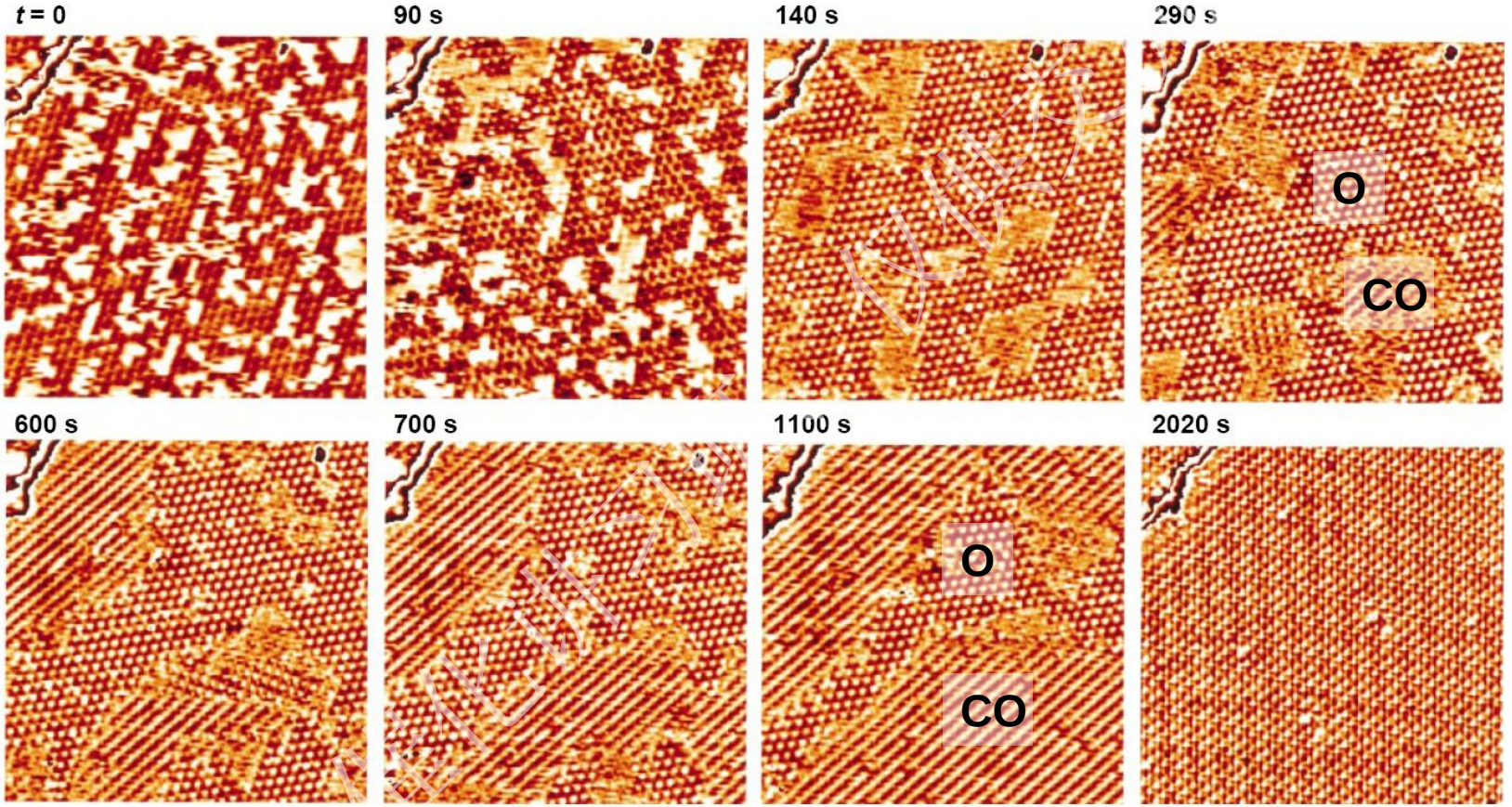

Fig. 1. Series of STM images, recorded during reaction of adsorbed oxygen atoms with co-adsorbed CO molecules at 247 K, all from the same area of a Pt(111) crystal. Before the experiment, a submonolayer of oxygen atoms was prepared (by an exposure of 3 Langmuirs O_2 at 96 K, a short annealing to 298 K, and cooling to 247 K), and CO was continuously supplied from the gas phase ($P_{CO} = 5 \times 10^{-8}$ mbar). At this pressure, the impingement rate of CO molecules is about 1 monolayer per 100 s, where the zero-coverage sticking coefficient on the empty and oxygen-covered surface is about 0.7 (8); the times refer to the start of the CO exposure. The structure at the upper left corner is an atomic step of the Pt surface. Image sizes, 180 Å by 170 Å; tunneling voltage (with respect to the sample), +0.5 V; tunneling current, 0.8 nA.

J. Wintterlin, S. Volkening, T. V. W. Janssens, T. Zambelli, G. Ertl, Science, 278, 1931 (1997)

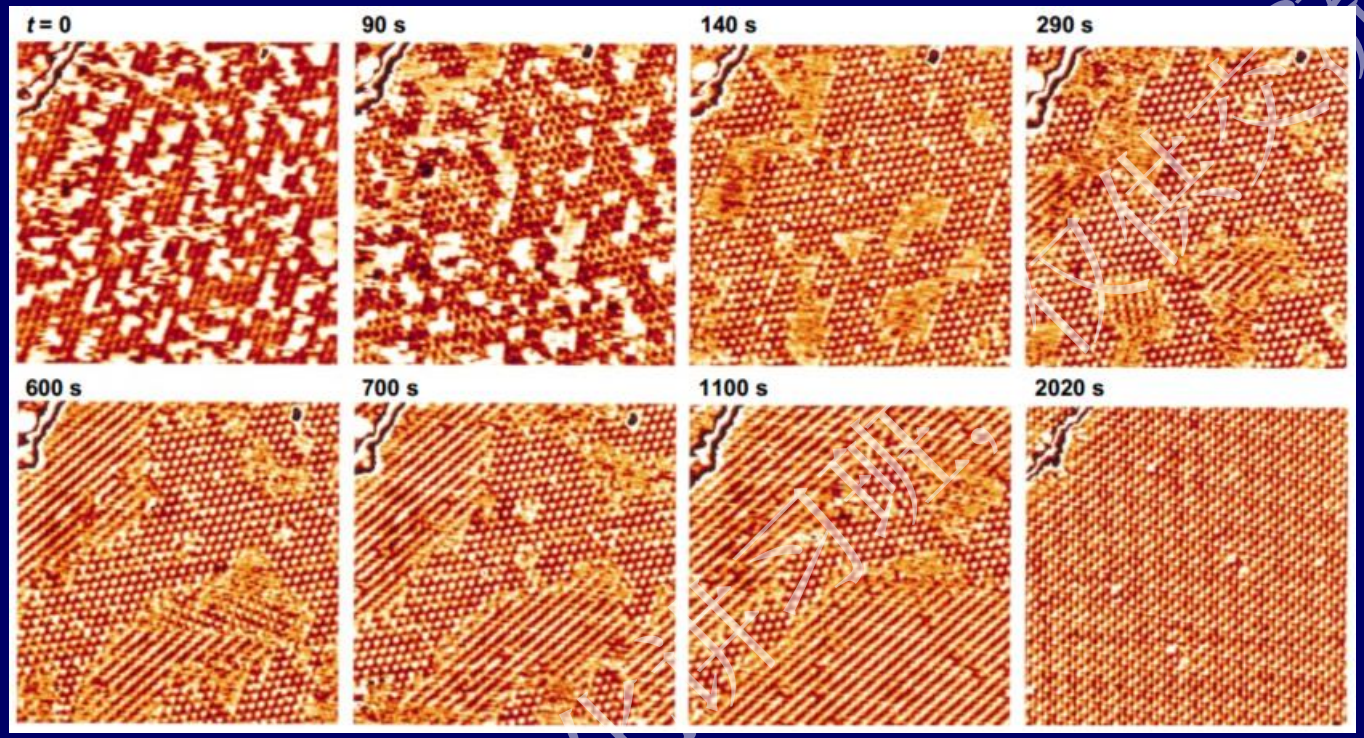

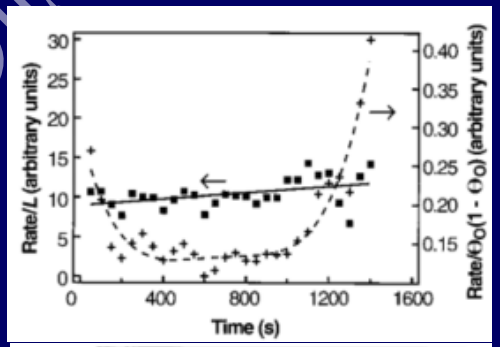

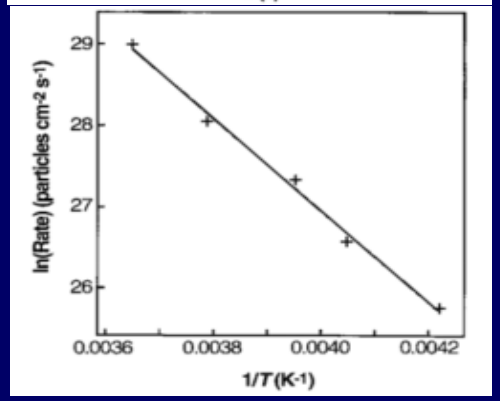

Pt(111): $CO_{ad}+O_{ad} \rightarrow CO_2(g)$ L-H机理的直接确认

J. Wintterlin, G. Ertl et al. (1997). *Science*. **278**, 1931–1934.

3.3 催化剂熟化/失活

CO-induced mobility of one Pd adatom

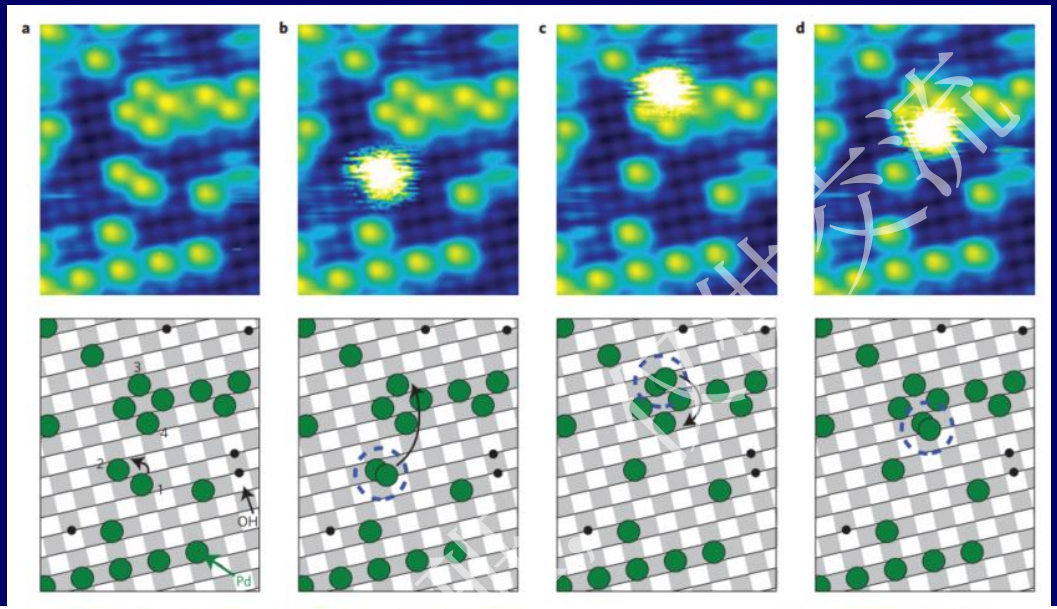

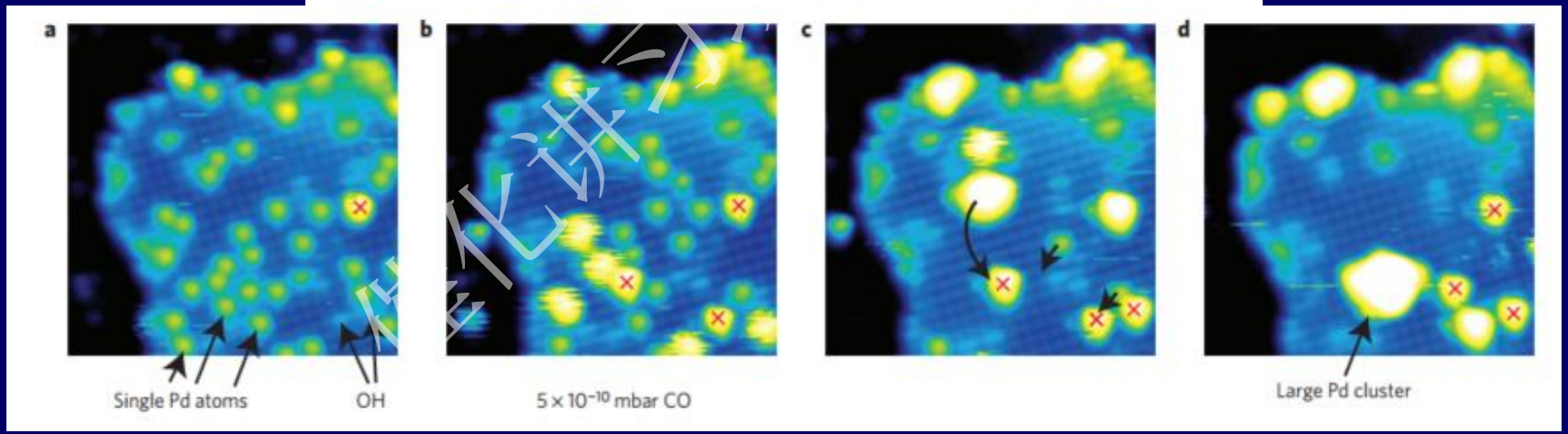

Formation of a stable Pd adatom at a surface hydroxy

Parkinson, G. S& Diebold, U. (2013). *Nature Materials*. **12**, 724–728.

电化学原位STM：Pt表面的电化学CO氧化

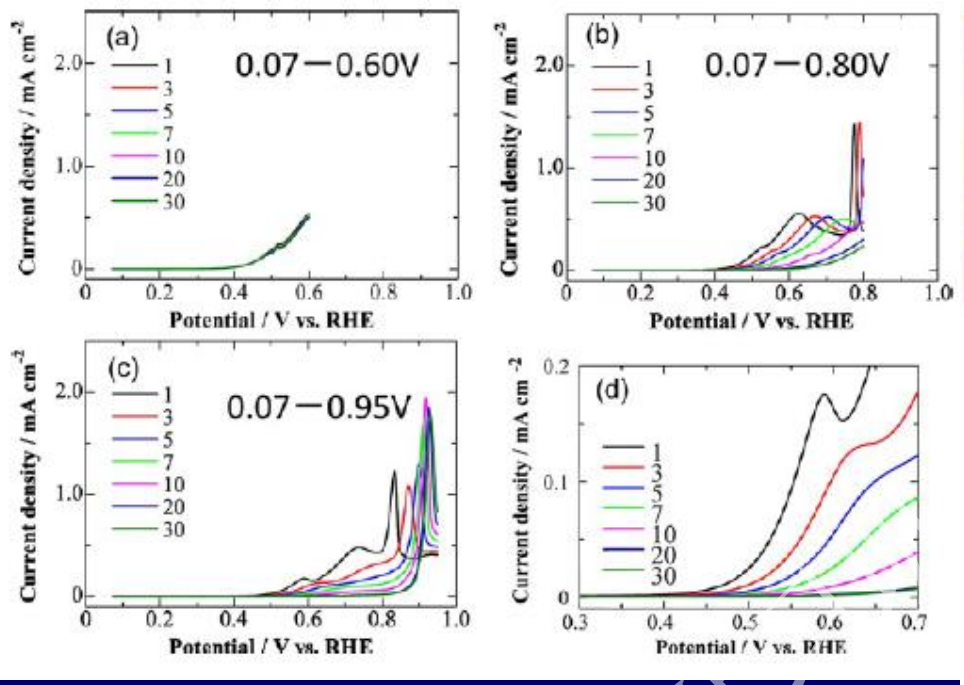

0.1M $HClO_4$， Scan rate:50mV/s

Pt(111)表面CO电化学氧化CV曲线图

随着循环次数的增加，CO氧化起始电位往高电势移动，同时增加其循环的极限电位，起始电位峰将减小更快。

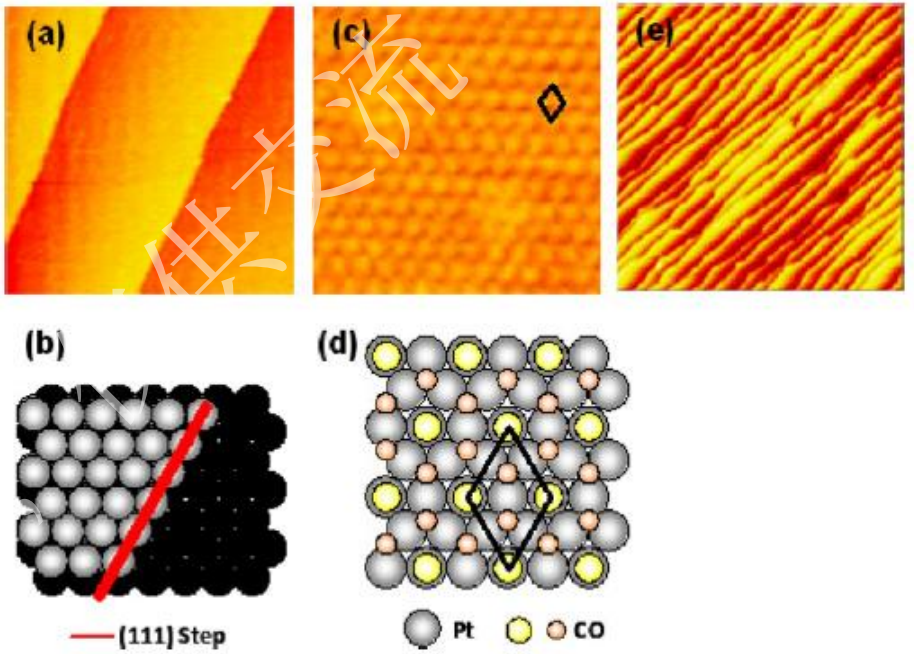

Figure 4. (a) STM image on Pt(111) covered with CO in 0.1 M $HClO_4$ obtained at 0.1 V (200 nm × 200 nm). (b) Structural model of the (111) step. (c) STM image on Pt(111) in CO-saturated 0.1 M $HClO_4$ obtained at 0.60 V (6 nm × 6 nm). Unit cell is shown by the rhombus. (d) Structural model for the (2 × 2) structure of a CO adlayer. (e) STM image on Pt(10 10 9) covered with CO in 0.1 M $HClO_4$ obtained at 0.1 V (100 nm × 100 nm).

Pt(111)表面覆盖CO的STM图

J. J. Inukai, D. A. Tryk, H. Uchida, M. Watanabe. *J. Am. Chem. Soc.* **2013**, 135, 1476-1490.

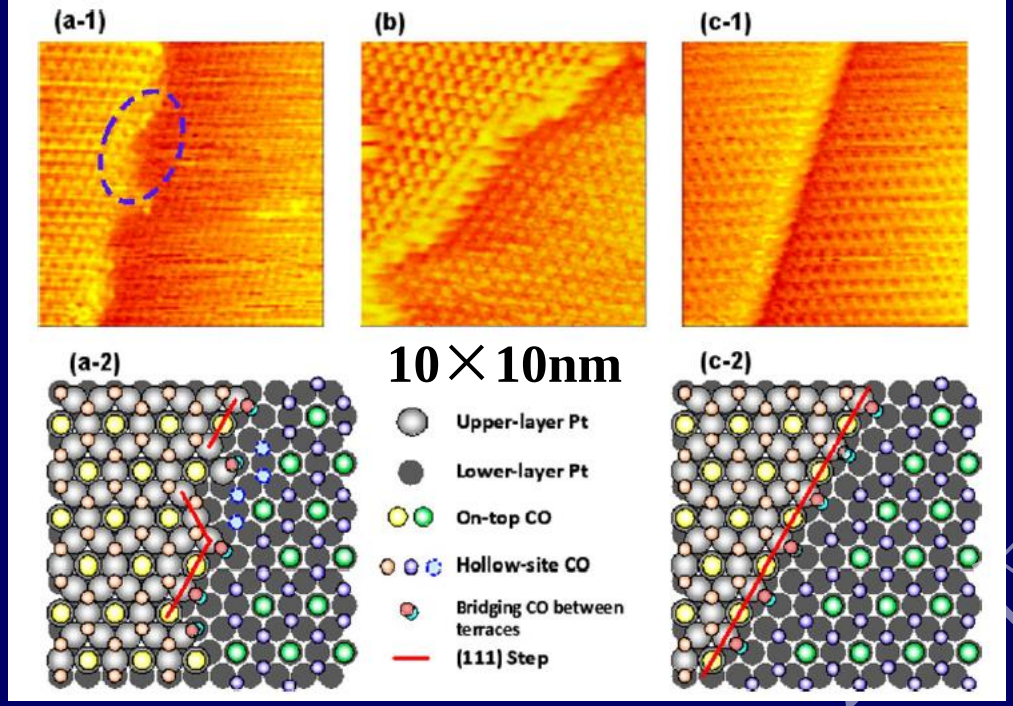

Pt(111)-(111) Steps

(a-1)循环之前;
(b)循环5次后;
(c-1)循环30次后。

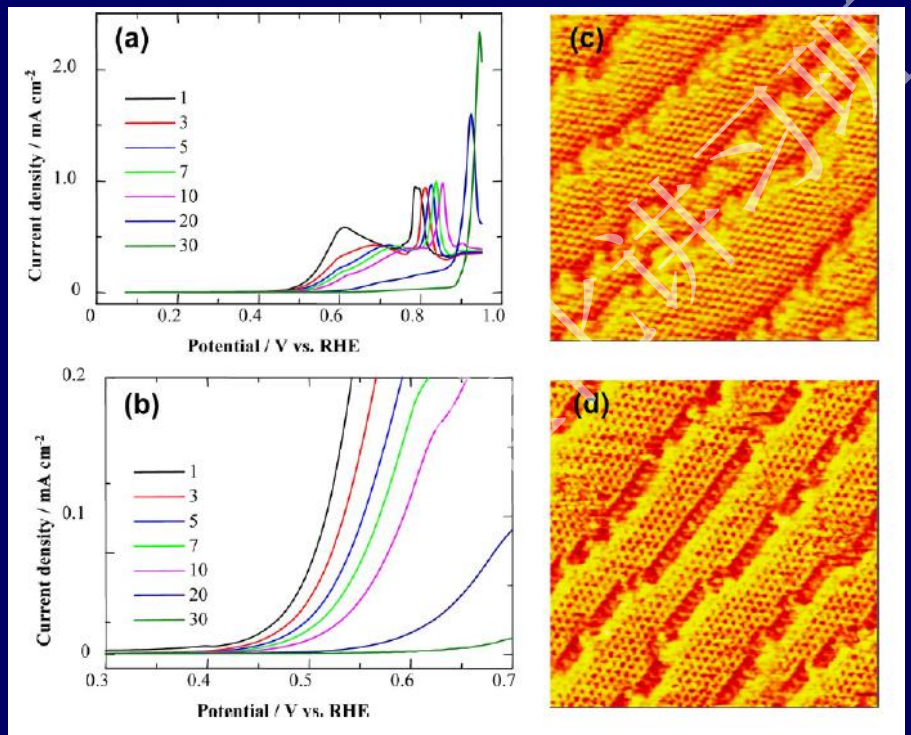

Pt(10 10 9)-(111) Steps

(c)循环前
(d)循环5次后

CO电化学氧化的活性与台阶数目无关，而与其形貌变化有关

Size-dependent oxidation kinetics of FeO islands

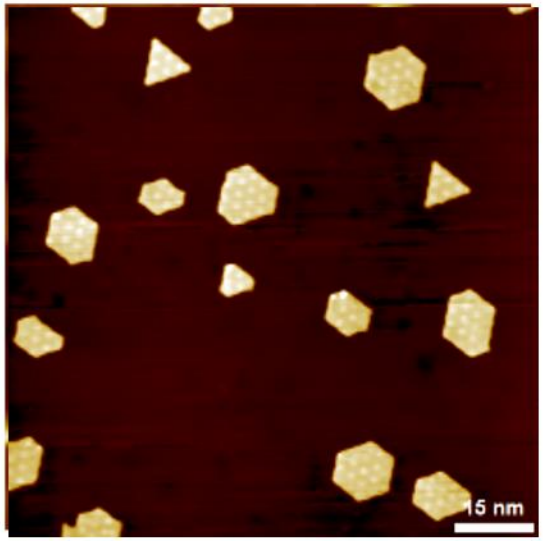

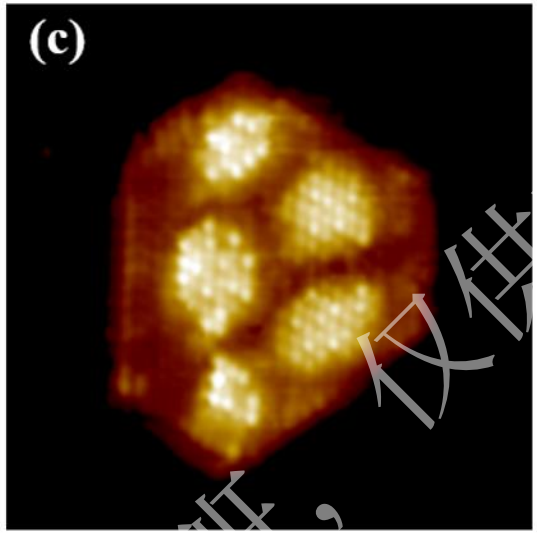

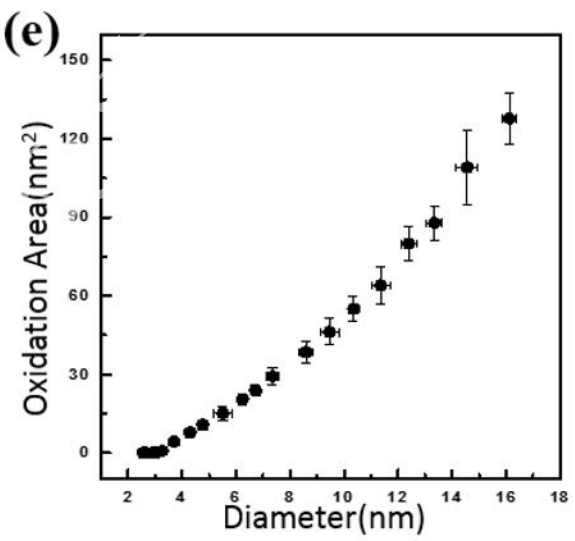

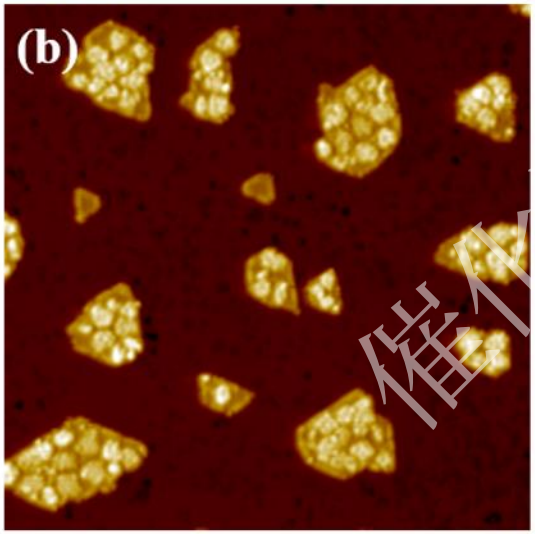

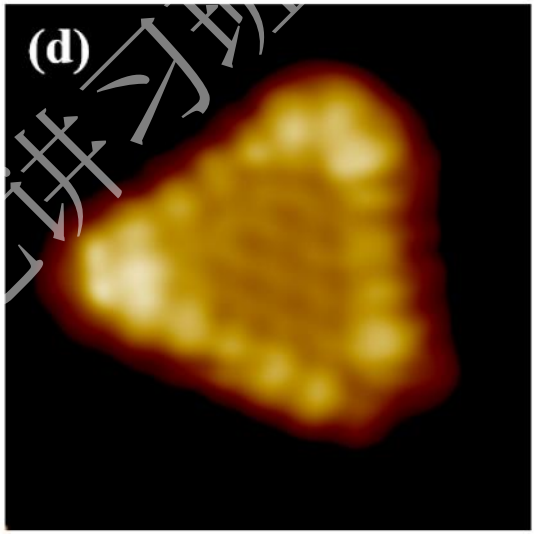

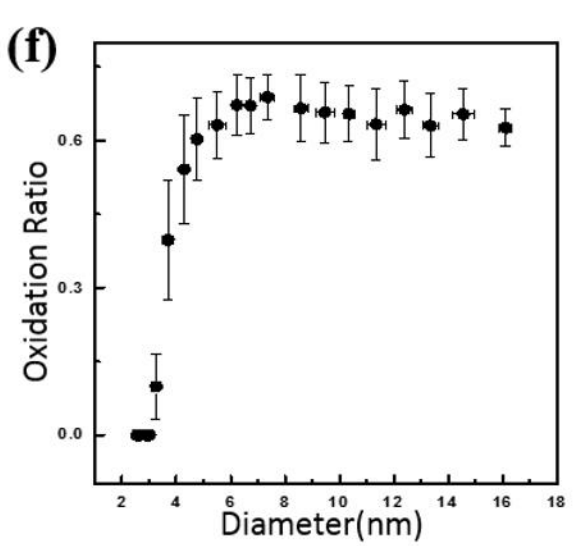

Y. Liu, F. Yang, X. H. Bao, et al., Nat. Commun., 2017

Dynamic Size Effect: complete reconstruction of FeO

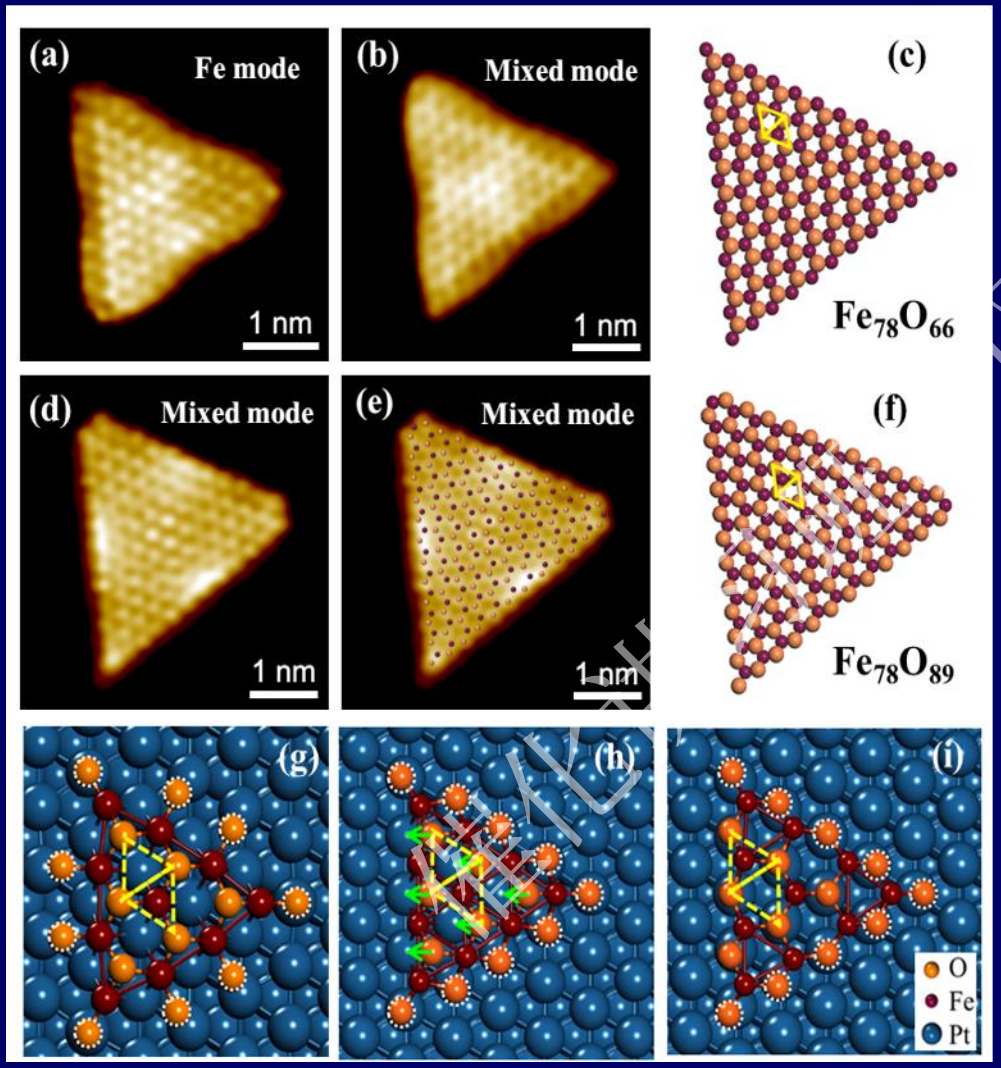

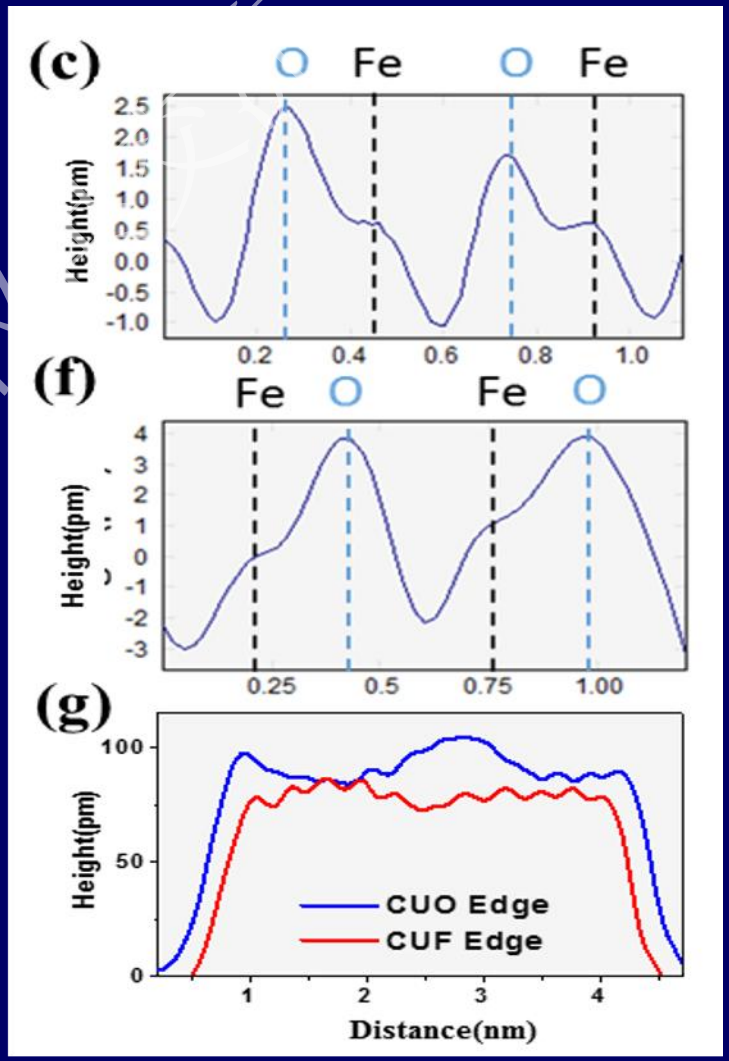

Y. Liu, F. Yang, X. H. Bao, et al., Nat. Commun., 2017

Dynamic Size Effect: partial reconstruction of FeO

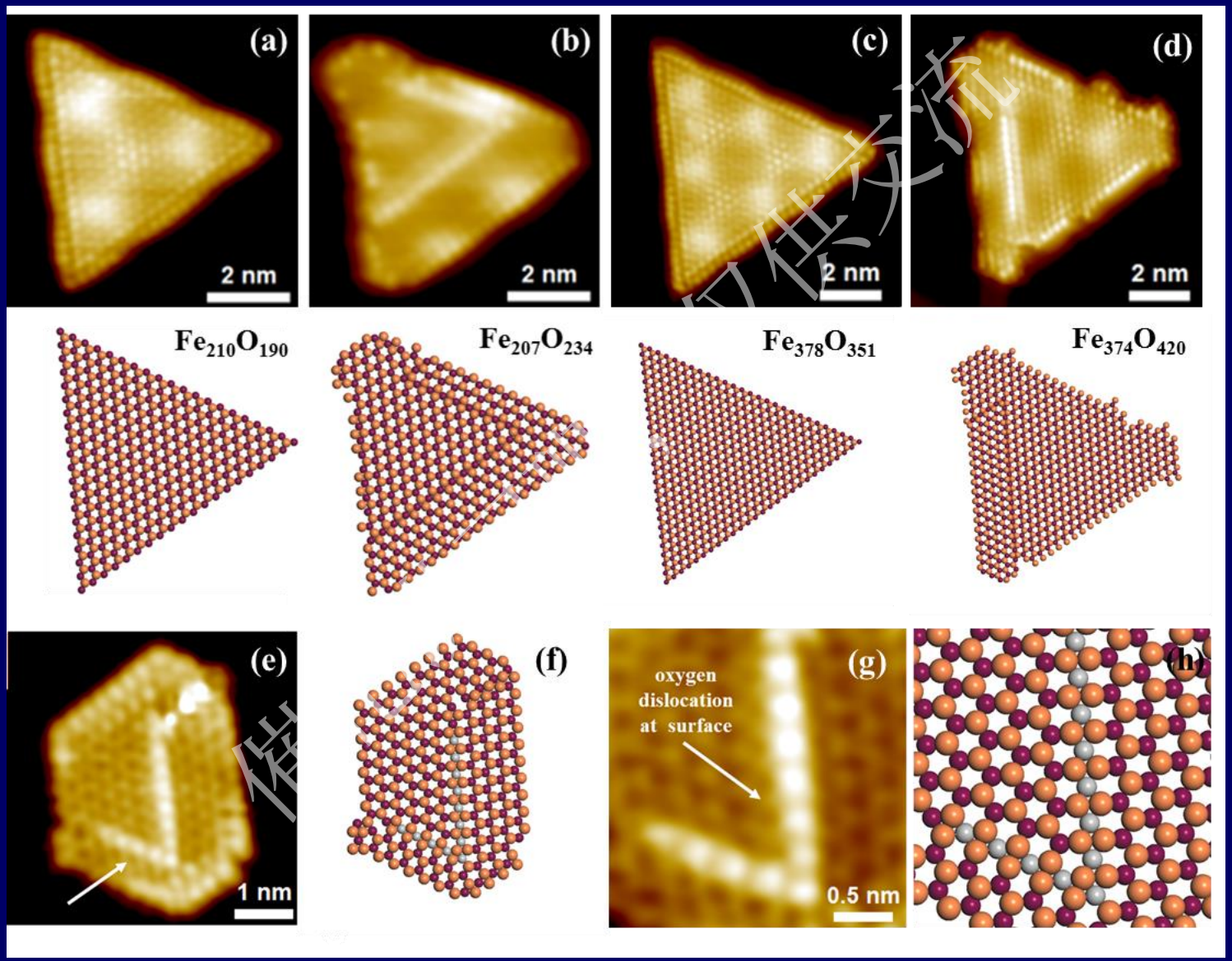

Y. Liu, F. Yang, X. H. Bao, et al., Nat. Commun., 2017

Edge Structures and Oxidation

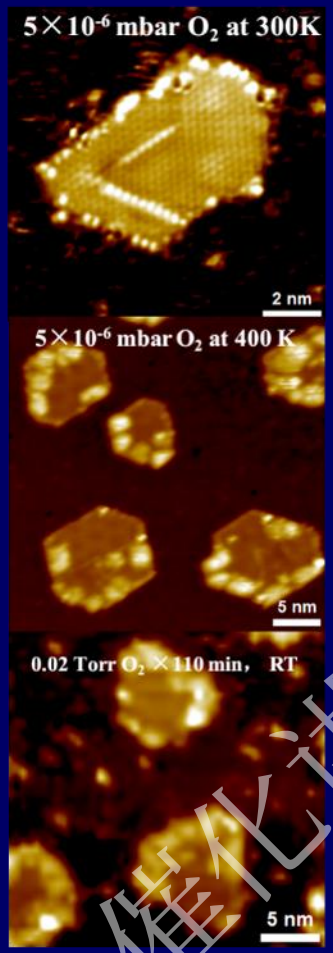

Edge-dependent oxidation rates

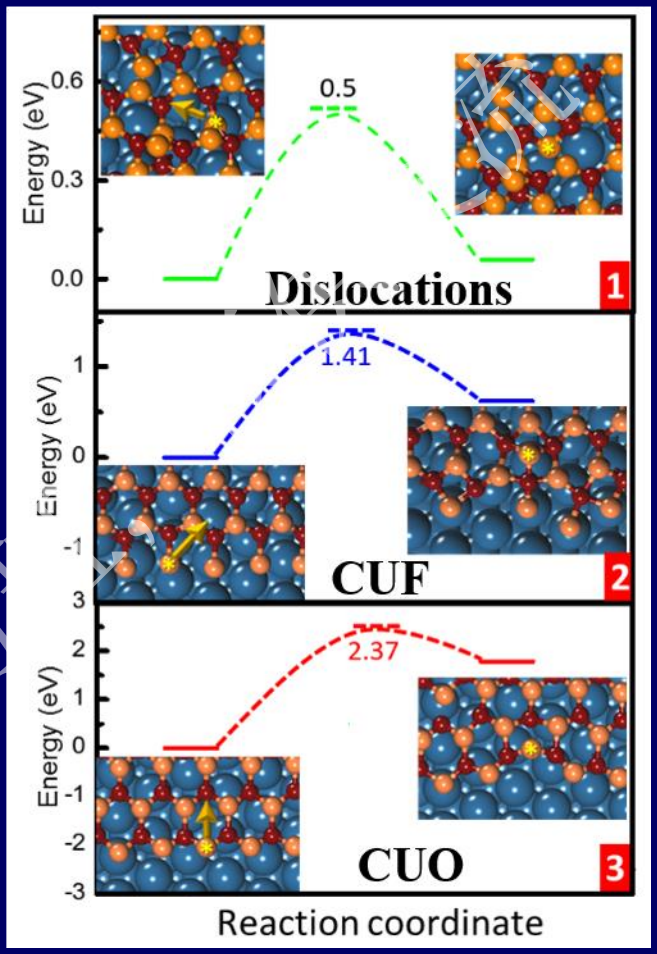

Energy barriers for different O-rich structures

FeO <3 nm: reconstructed into CUO edges completely, and increased oxidation resistance;
FeO >3 nm: dislocations and CUF edges are prone to be oxidized.

The Origin of Dynamic Size Effect

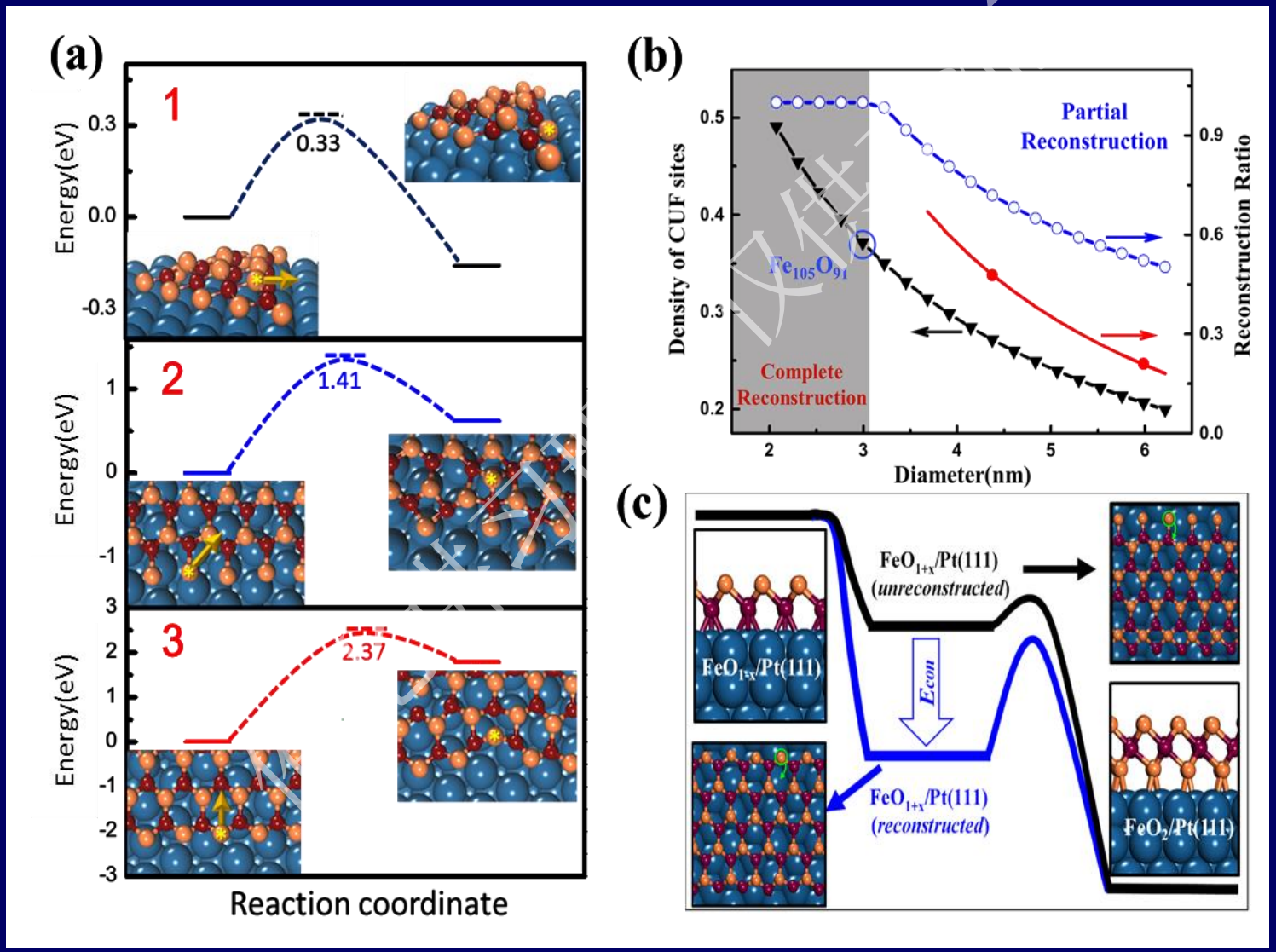

Y. Liu, F. Yang, X. H. Bao, et al., Nat. Commun., 2017

Dynamic Size Effect controlling oxidation kinetics of CoO

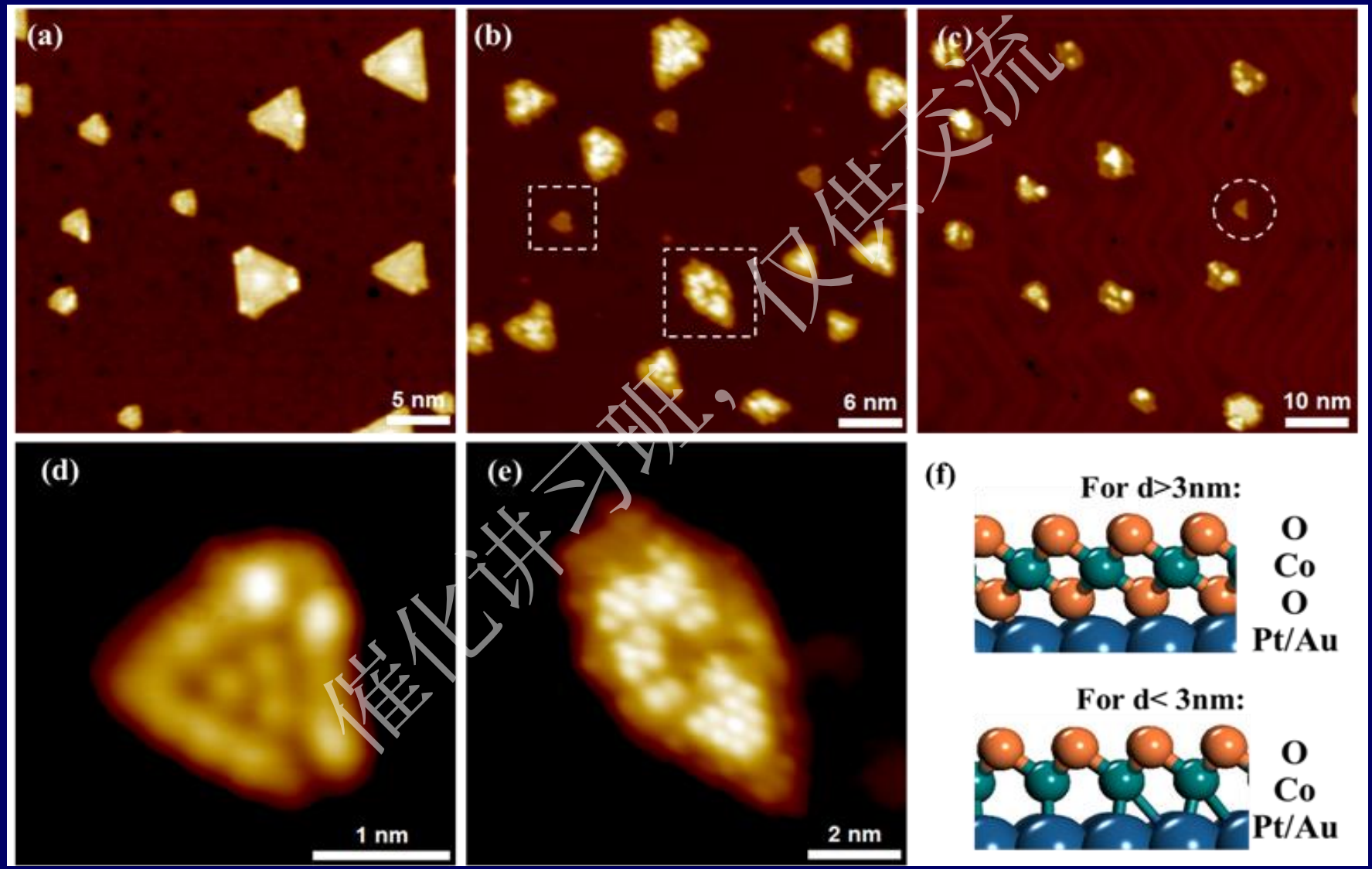

Y. Liu, F. Yang, X. H. Bao, et al., Nat. Commun., 2017

Q1： STM应用于催化研究的优点与不足

Q2：结合实例，谈谈你对STM应用于催化机理研究的理解

Q3：结合具体（你的）研究方向，你设想STM还可以从哪方面入手，增进催化机理的认识

Next：选键催化？

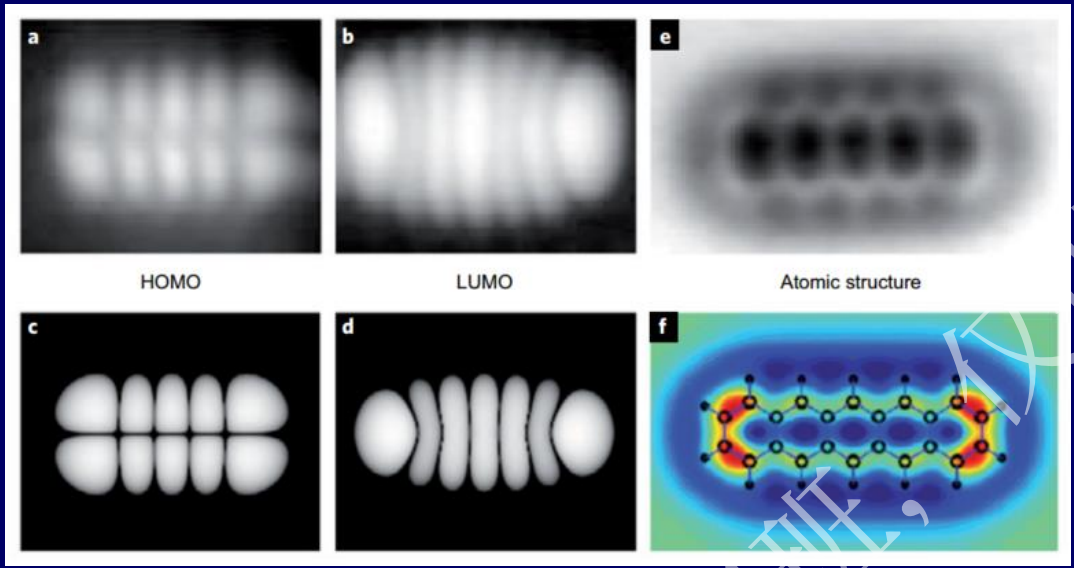

Pentacene imaged with STM and NC-AFM

Gross, L. (2011). *Nat Chem*. **3**, 273–278.

Q-Plus型AFM：

- 分子轨道成像
- 化学键级分辨率

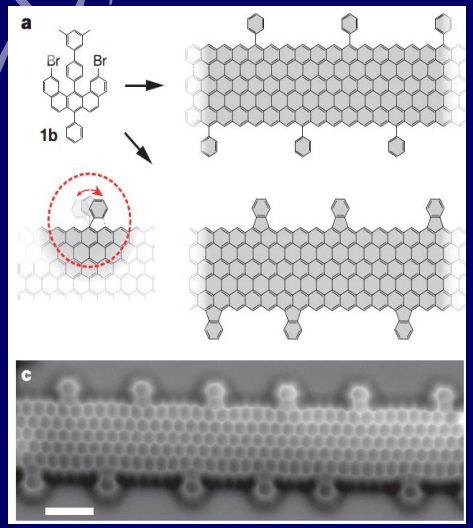

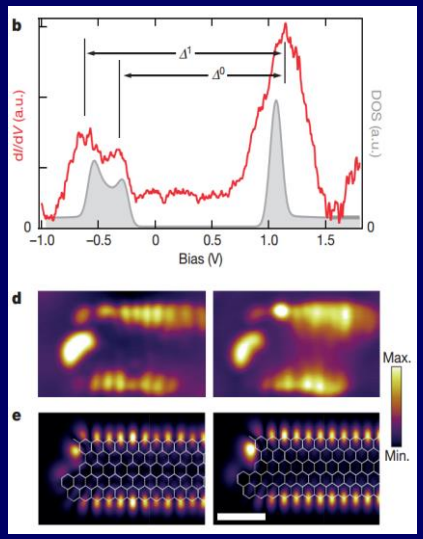

(2016). *Nature*. **531**, 489–492.

Next：催化反应的时间和空间尺度

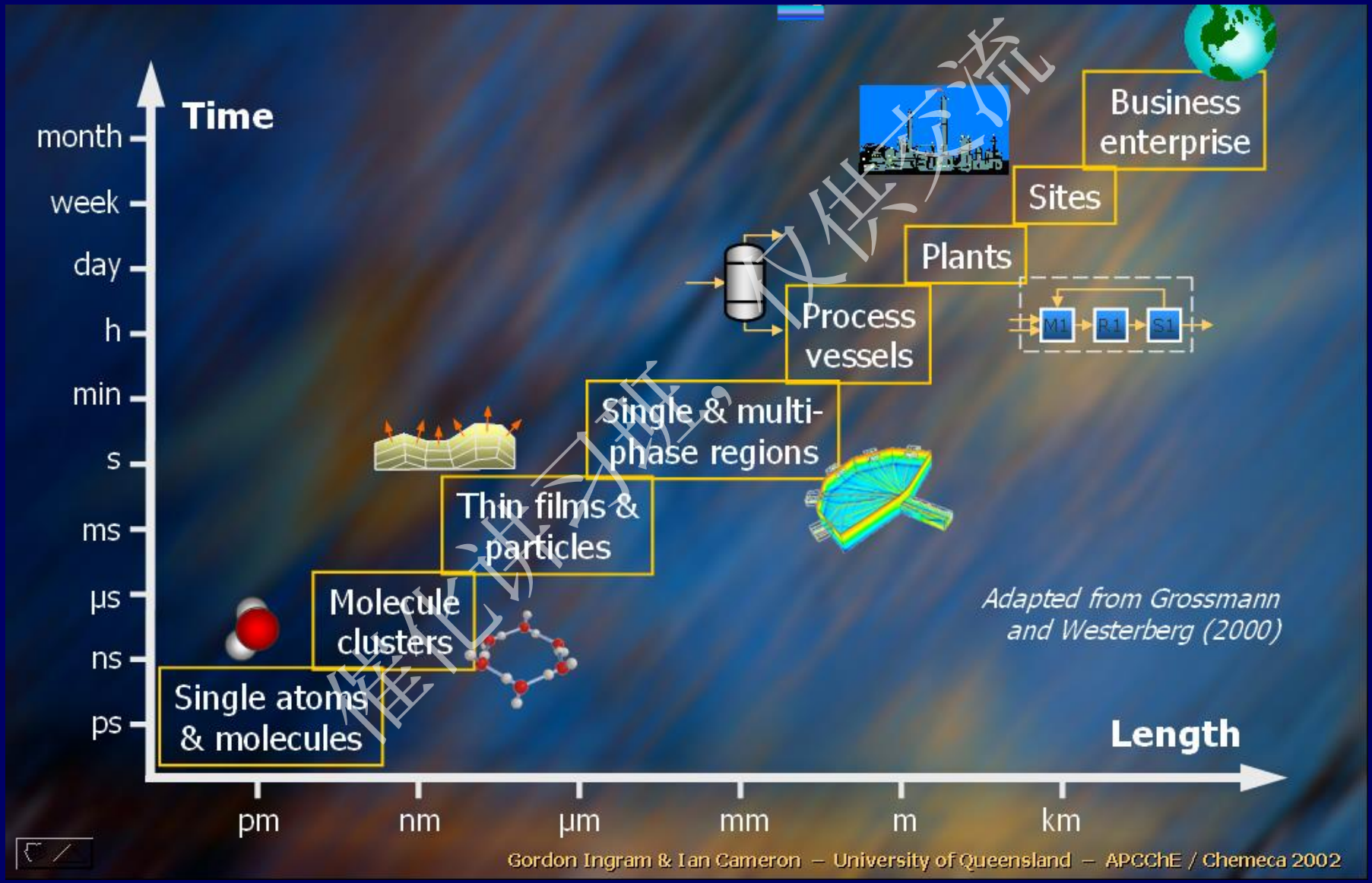

To be continued…

History of Microscope

17th century
A. Leeuwenhoech (Single lens)
R. Hooke (Compound lens)

1932
E. Ruska
(Transmission election microscope)

1938
M. v. Ardenne
(scanning Election microscope)

1951
E. W. Muller
(Field-ion microscope)

1952
V. E. Cosslett
(X-ray microscope)

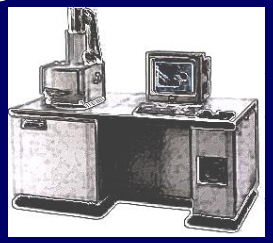

STM
1981
G. Binnig H. Rohrer
(Scanning tunneling microscope)

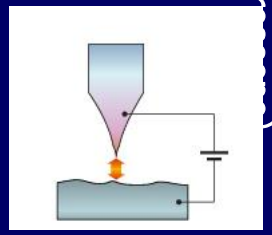

AFM
1986
G. Binnig Quate
(Atomic force microscope)

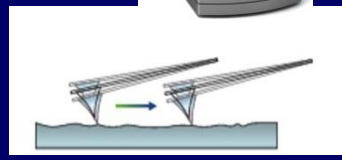

STM: conductors and semi-conductors; UHV;
AFM: including insulating materials; Vacuum, Air, liquid;

Reference: Dr. Kentaro Asakura, 1991

A New Kind of Microscope

Established types of scanning probe microscopy

AFM, atomic force microscopy [1]
- Contact AFM
- Non-contact AFM
- Dynamic contact AFM
- Tapping AFM

BEEM, ballistic electron emission microscopy[2]
CFM, chemical force microscopy
C-AFM, conductive atomic force microscopy[3]
ECSTM electrochemical scanning tunneling microscope[4]
EFM, electrostatic force microscopy[5]
FMM, force modulation microscopy[6]
FOSPM, feature-oriented scanning probe microscopy[7]
KPFM, kelvin probe force microscopy[8]
MFM, magnetic force microscopy[9]
MRFM, magnetic resonance force microscopy[10]
NSOM, near-field scanning optical microscopy (or SNOM, scanning near-field optical microscopy)[11]
PFM, Piezoresponse Force Microscopy[12]
PSTM, photon scanning tunneling microscopy[13]
PTMS, photothermal microspectroscopy/microscopy
SCM, scanning capacitance microscopy[14]
SECM, scanning electrochemical microscopy
SGM, scanning gate microscopy[15]
SHPM, scanning Hall probe microscopy[16]
SICM, scanning ion-conductance microscopy[17]
SPSM spin polarized scanning tunneling microscopy[18]
SSRM, scanning spreading resistance microscopy[19]
SThM, scanning thermal microscopy[20]
STM, scanning tunneling microscopy[21]
STP, scanning tunneling potentiometry[22]
SVM, scanning voltage microscopy[23]
SXSTM, synchrotron x-ray scanning tunneling microscopy[24]

Of these techniques AFM and STM are the most commonly used for roughness measurements.

http://en.wikipedia.org/wiki/Scanning_probe_microscopy

Atomic Force Microscopy

原子力显微镜（AFM）简介

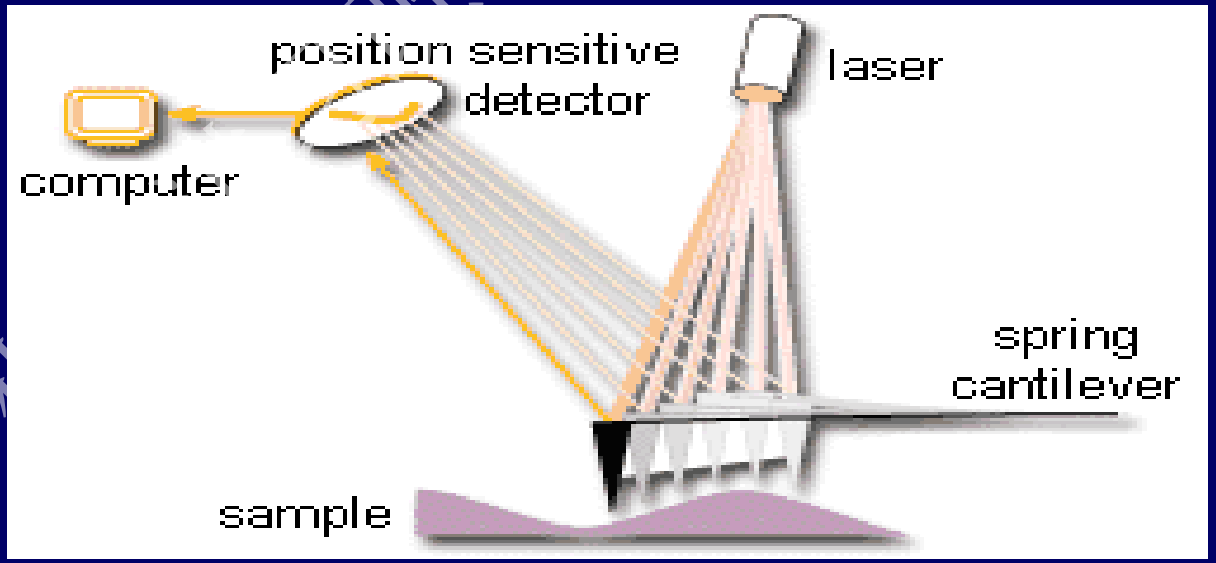

Force Effects in STM

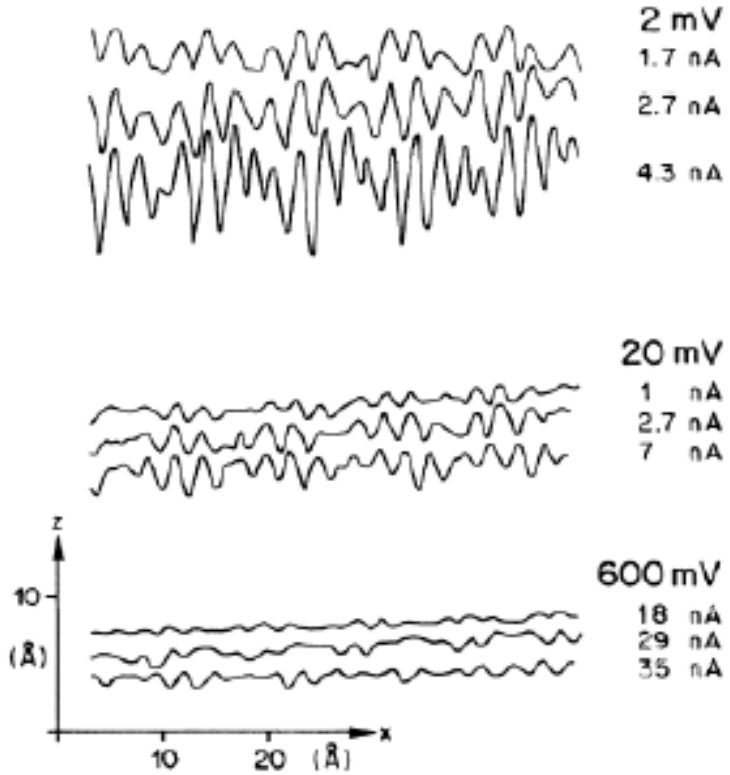

FIG. 1. Graphite STM traces obtained at ambient-air pressure and room temperature with a "pocket-size" STM (Ref. 14) with scanning speeds between 1 and 5 sec per scan. The varying corrugation within a scan is due to the mismatch between crystallographic and scanning directions (Ref. 3); plateaus in the traces indicate the saddle points in the LDOS (Refs. 3 and 11).

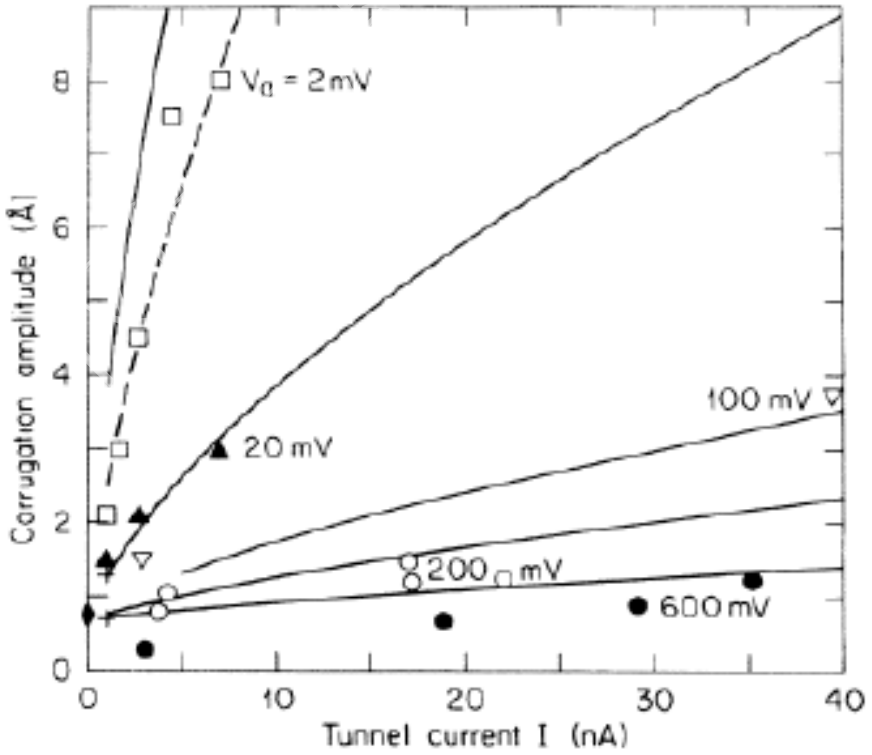

FIG. 4. Measured (symbols) and calculated (solid lines) corrugations as a function of tunneling current and voltage. The dashed line was obtained with $d^* = 0.4$ Å. The two crosses at 1 nA correspond to the measured corrugations at 50 and 400 mV, respectively, of Ref. 3; the diamond at zero current indicates the corrugation of the LDOS at the Fermi level (Ref. 11).

Soler et al. PRL57 444 (1987)
RV. Colemann et al. Adv. Phys 37 559 (1988)

原子力的基本原理

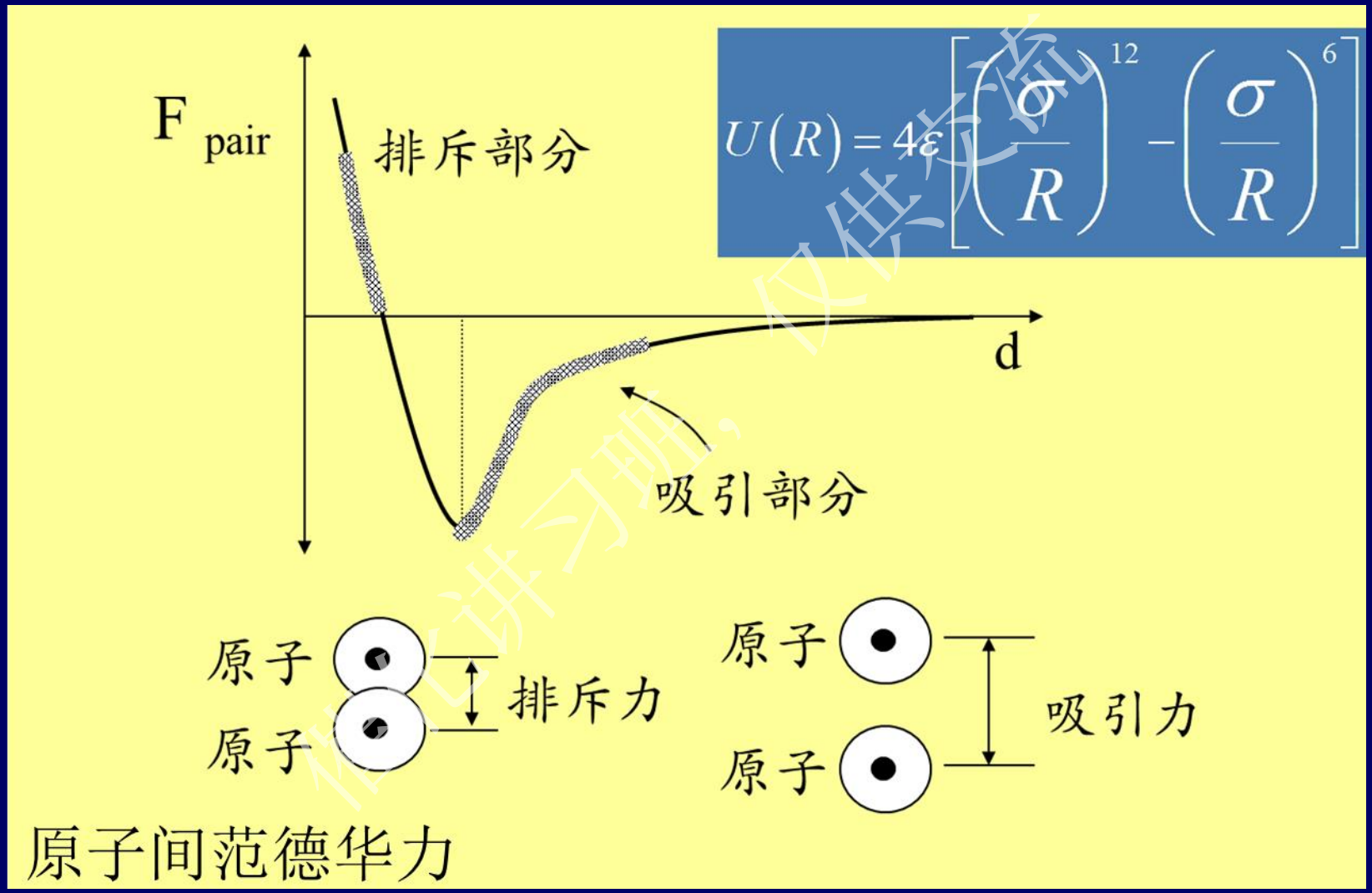

Other forces…

Electrostatic:

$$F_{elec} = -\frac{1}{2}(\Delta V)^2 \frac{\partial C}{\partial z}$$

Magnetic:

$$F_{magnetic} = \mu_o (q + m \bullet \nabla) B$$

In general force detection is limited to ~ 10^{-12} N due to thermal vibrations in the detector.

Typical forces between atoms:

- Quantum mechanical (covalent, metallic bonds): 1-3 nN
- Coulomb (dipole, ionic): 0.1-5 nN
- Polarization (induced dipoles): 0.02-0.1 nN

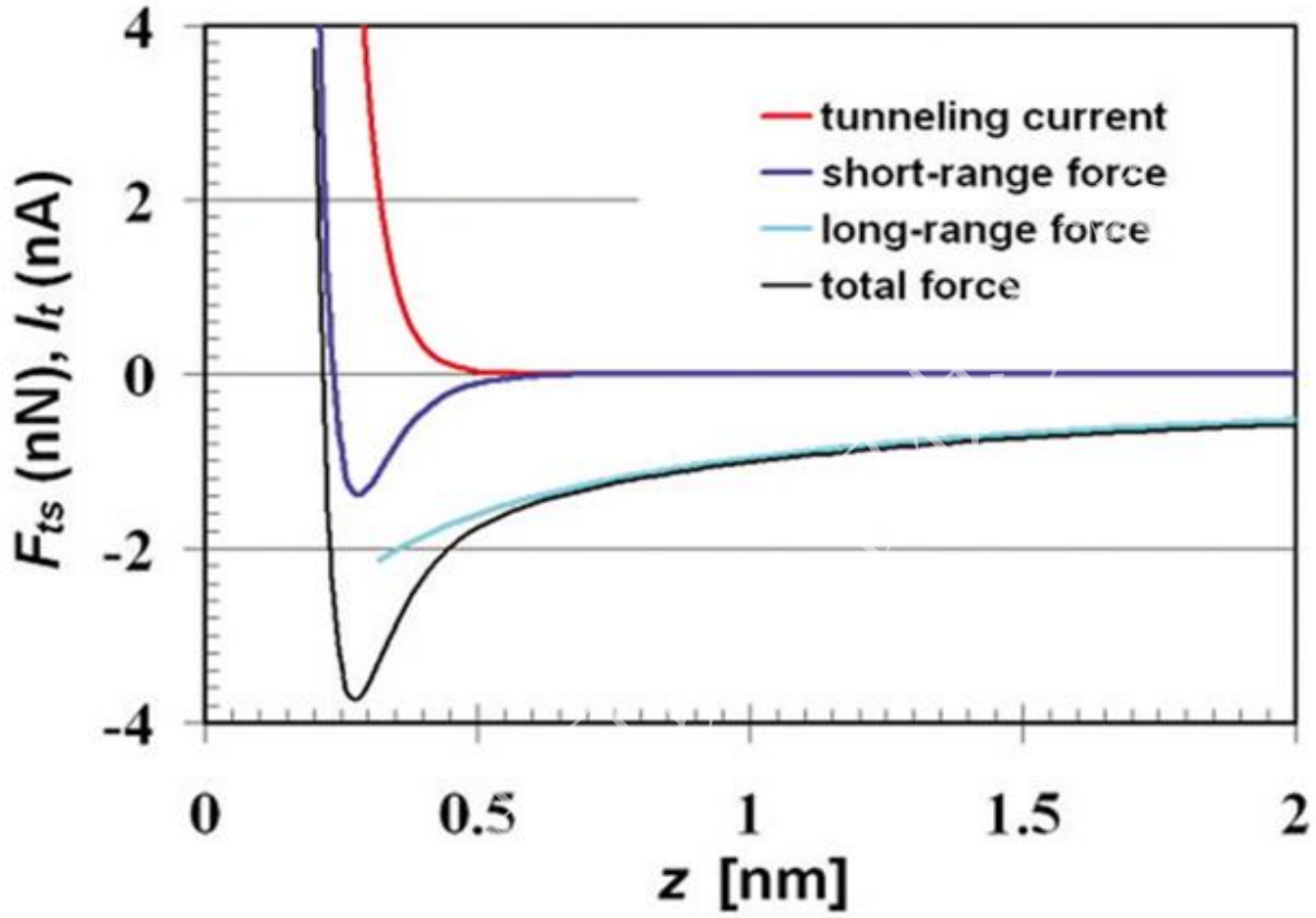

隧道电流，长程、短程作用力与针尖—样品距离的定量关系。隧道电流随着距离的减小而单调增加。而针尖—样品作用力会达到最小值，在成键距离以下再增加。从图中可以看出，较之于STM，AFM若能稳定地探测到短程力作用，将会使得针尖在离样品更近的距离下操作，从而获得比STM更好的分辨。

AFM 的构造与工作原理

The First AFM by G. Binnig, C. Quate and Ch. Gerber (1986)

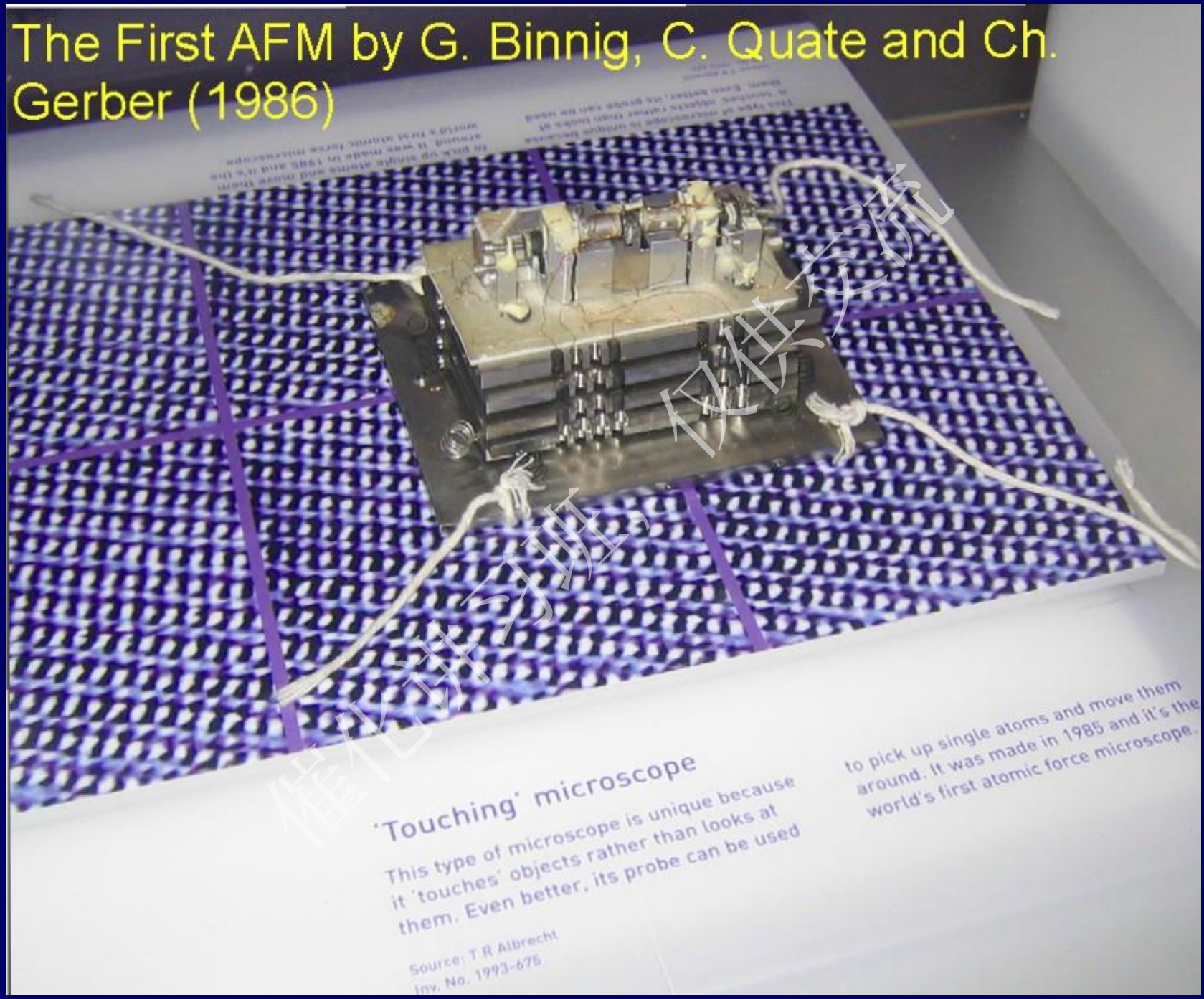

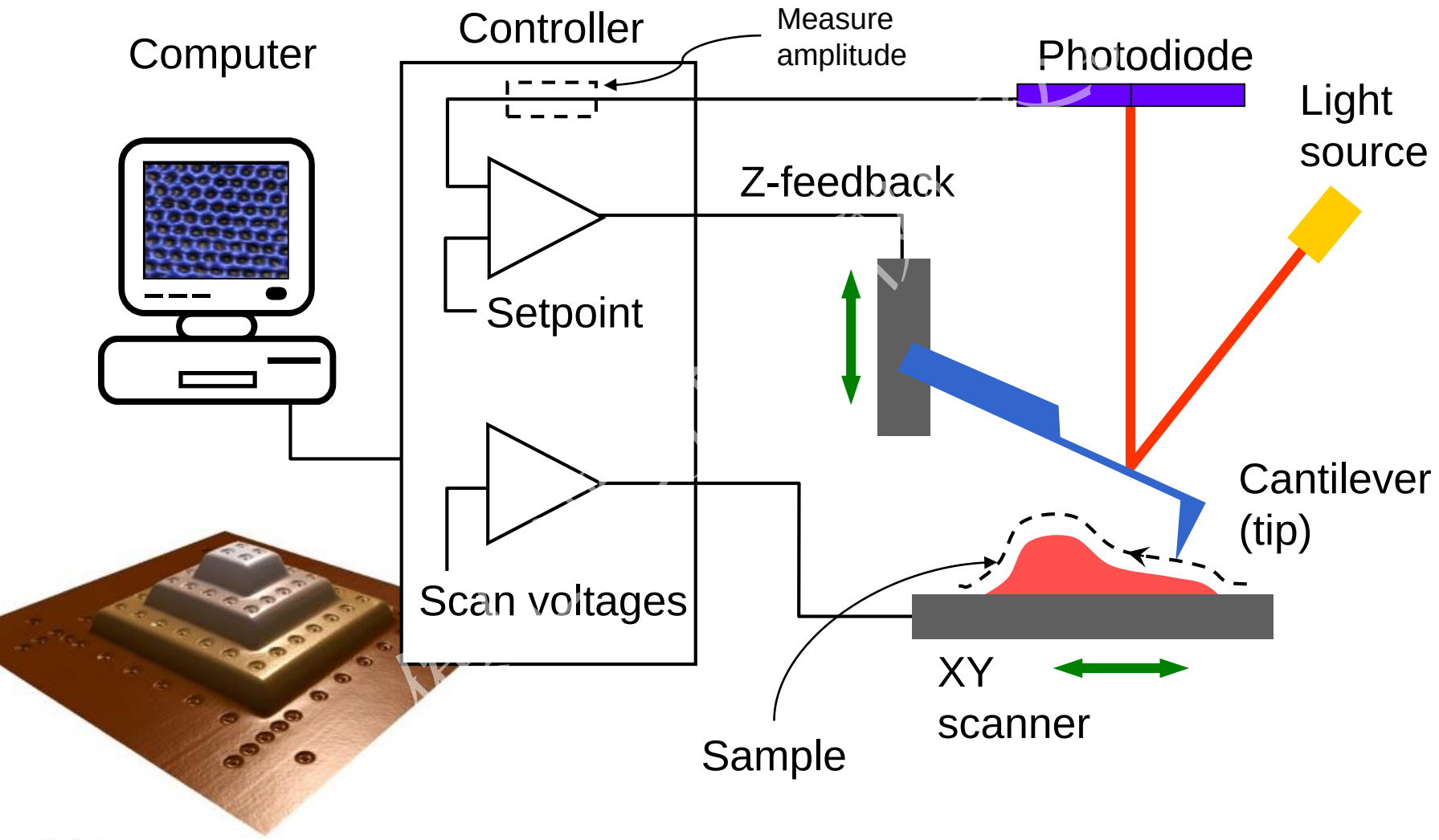

AFM探针

探针的指标主要分三个部分，分别对应了基片，微悬臂梁，和针尖三个部分。

大气和液相AFM的针尖常用材质有：Si， Si_3N_4

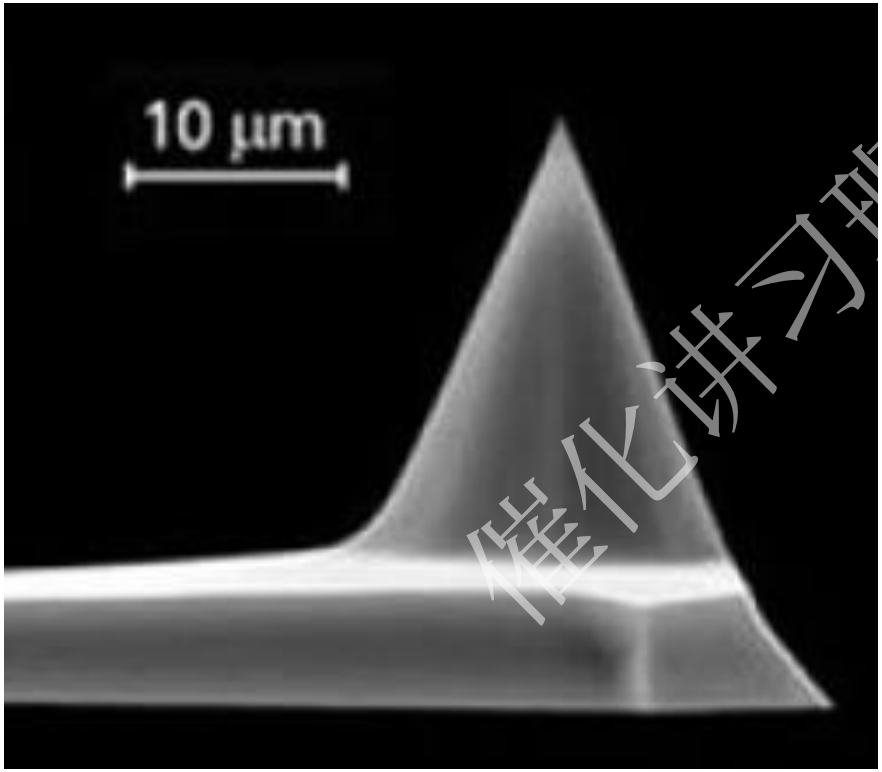

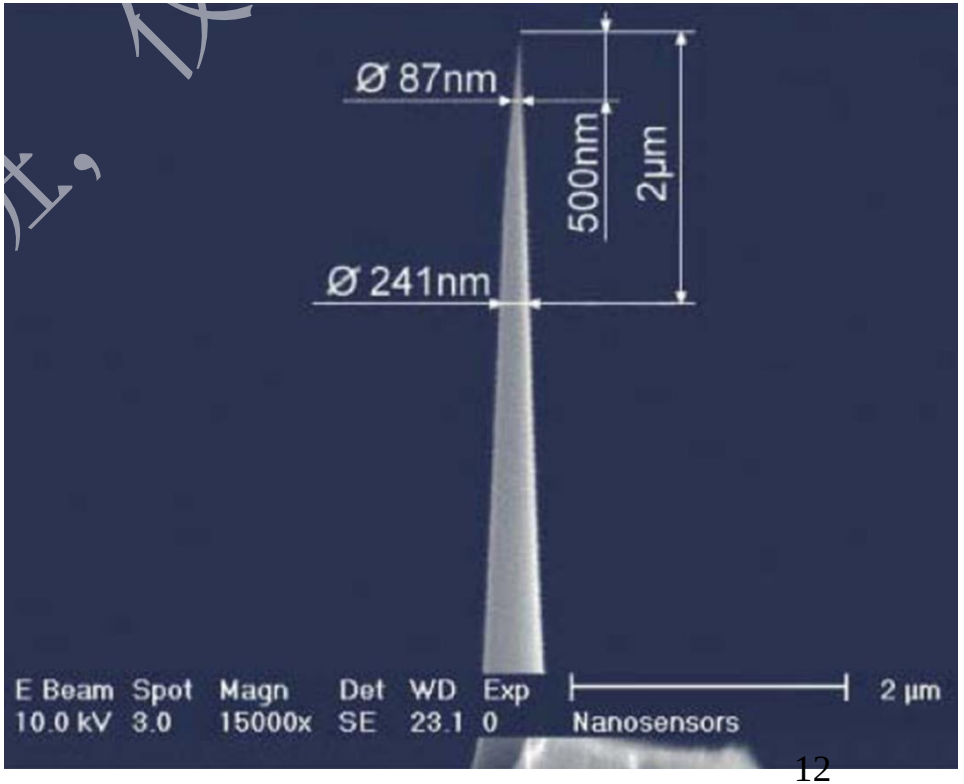

Force Sensors - Cantilevers

There are some simple criteria to be considered, when cantilevers are fabricated:

- resonance frequency f_R > 100Hz (building vibrations), > 10kHz (sound waves)
- high force sensitivity requires low spring constants (MFM:, 0.1 N/m, mRFM: 0.001 N/m)
- atomic resolution requires spring constant to be in range of atomic spring constants > 10N/m
- thermal vibrations of the cantilever < 0.1nm, i.e. k>0.4N/m @ 300K

It can be shown that only cantilevers of dimensions in the micrometer range fulfil these design criteria. Generally, higher resonance frequencies require smaller cantilevers.

single cristalline silicon cantilevers

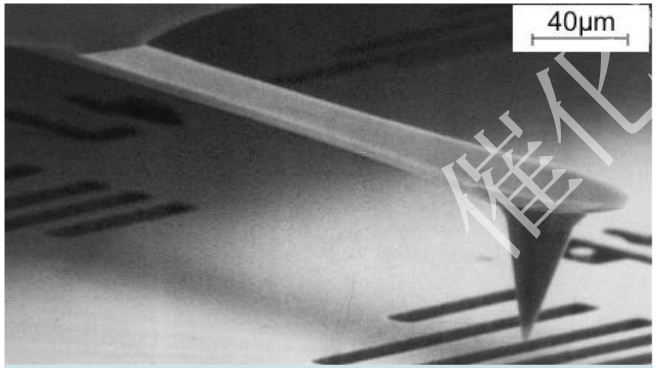

force constant: 0.01 – 100 N/m
resonance frequency: 5 – 500 kHz

high-aspect ratio tips

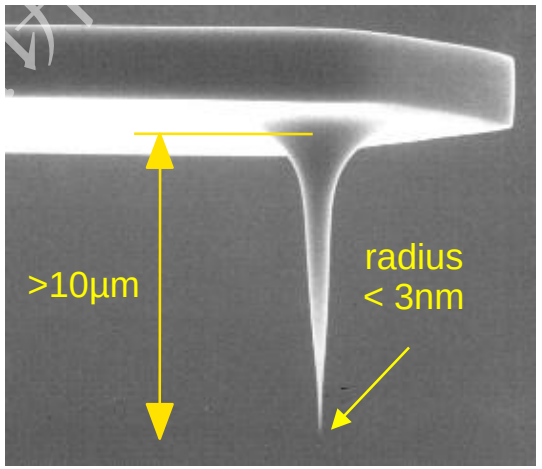

ultrasharp tip

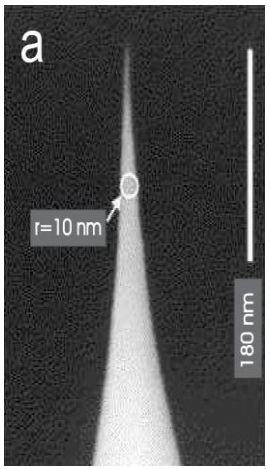

tuning fork sensor

Deflection Sensors

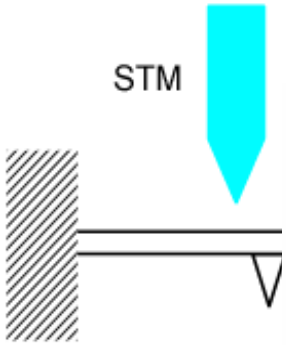

Electron Tunneling

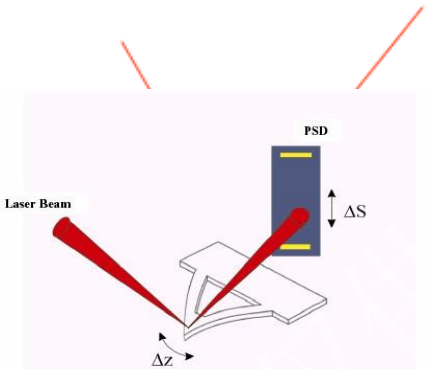

Meyer and Amer, APL53, 1045 (1988)

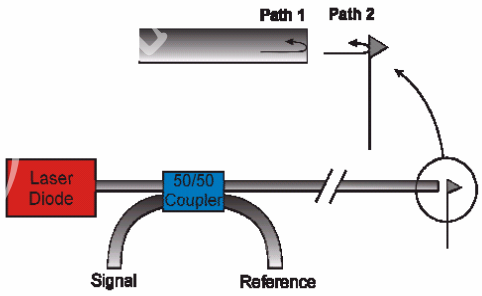

Interferometry

Rugar et al., APL **55**, 2588 (1989)

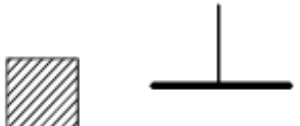

Capacitance

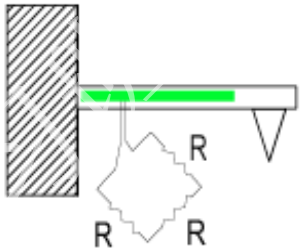

Piezoresistance

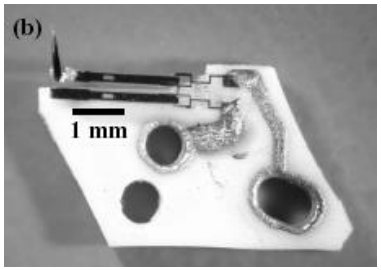

Piezoelectric

Giessibl, APL **73**, 3956 (1998)

Electron Tunneling: original concept, potentially sensitive, practically problematic
Beam Deflection: most widely used, robust, high sensitivity, not directly quantitative, requires calibration
Interferometry: best sensitivity, quantitative, uses limited space, complicated
Capacitance: sensor can be microfabricated, strong force from sensor, limited sensitivity
Piezoresistance: ideal for microfabrication & integration, limited sensitivity, heating of cantilever
Piezoelectric: mostly quartz tuning forks, good for true atomic resolution, limited sensitivity

Beam Deflection

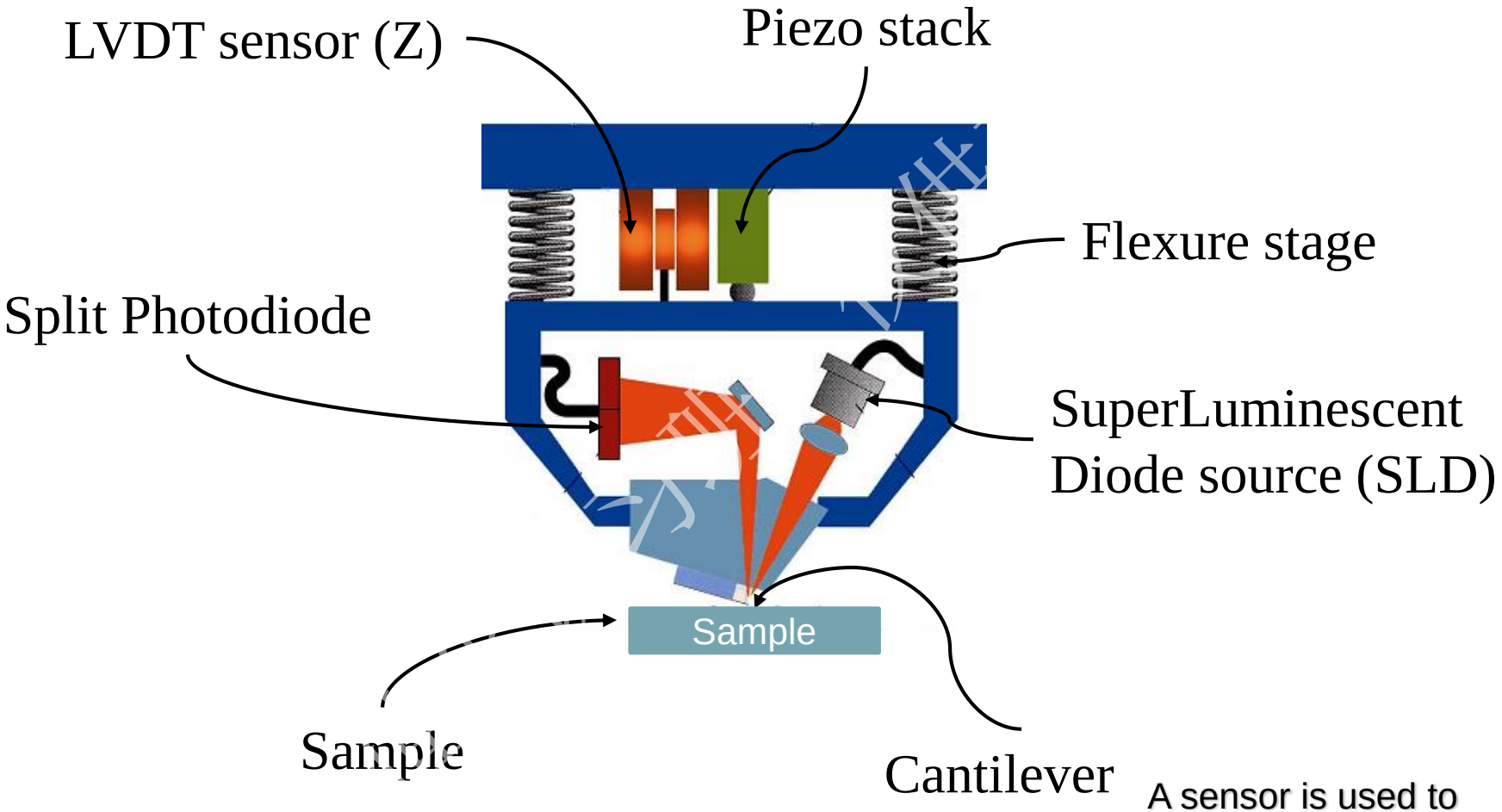

A sensor is used to measure the deflection of the cantilever

Beam Deflection Principle

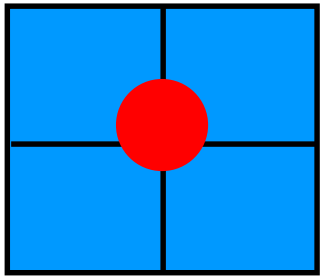

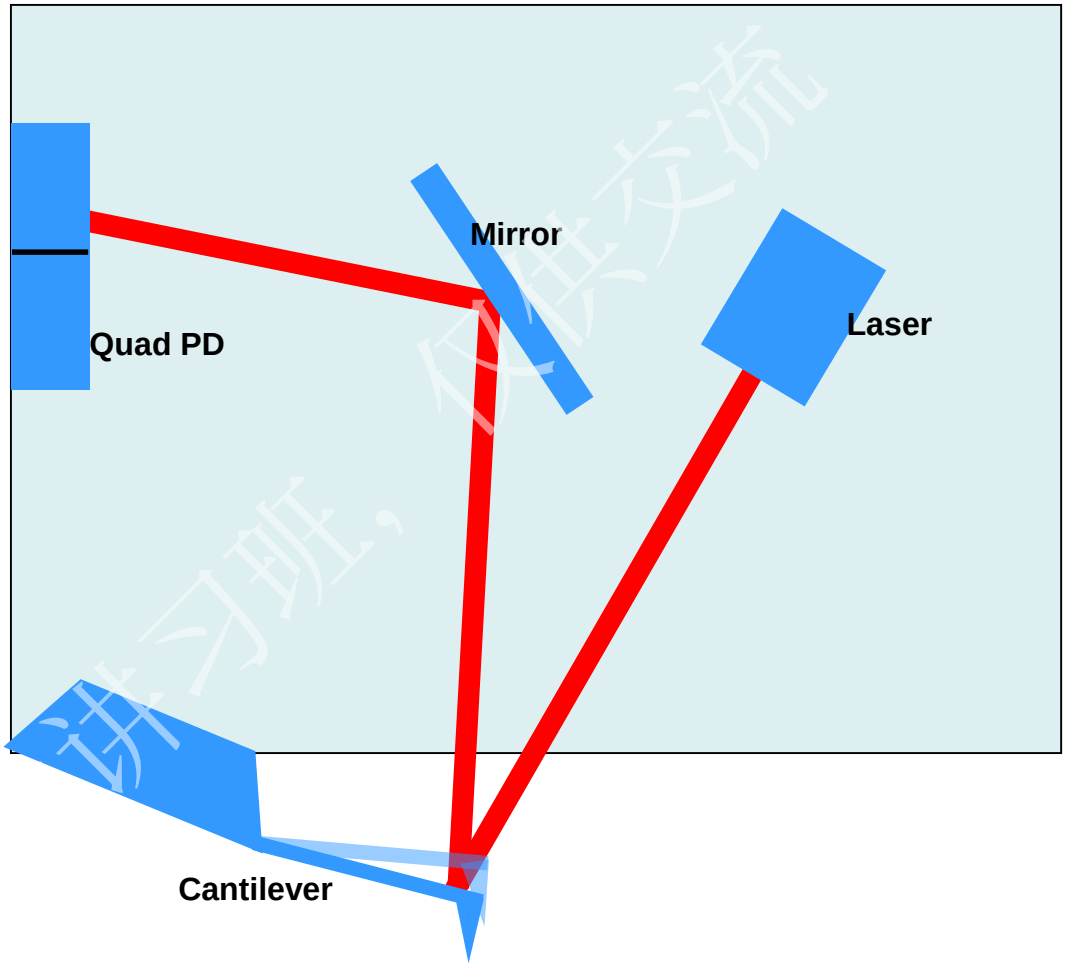

Beam Deflection Principle

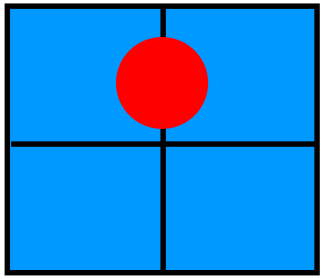

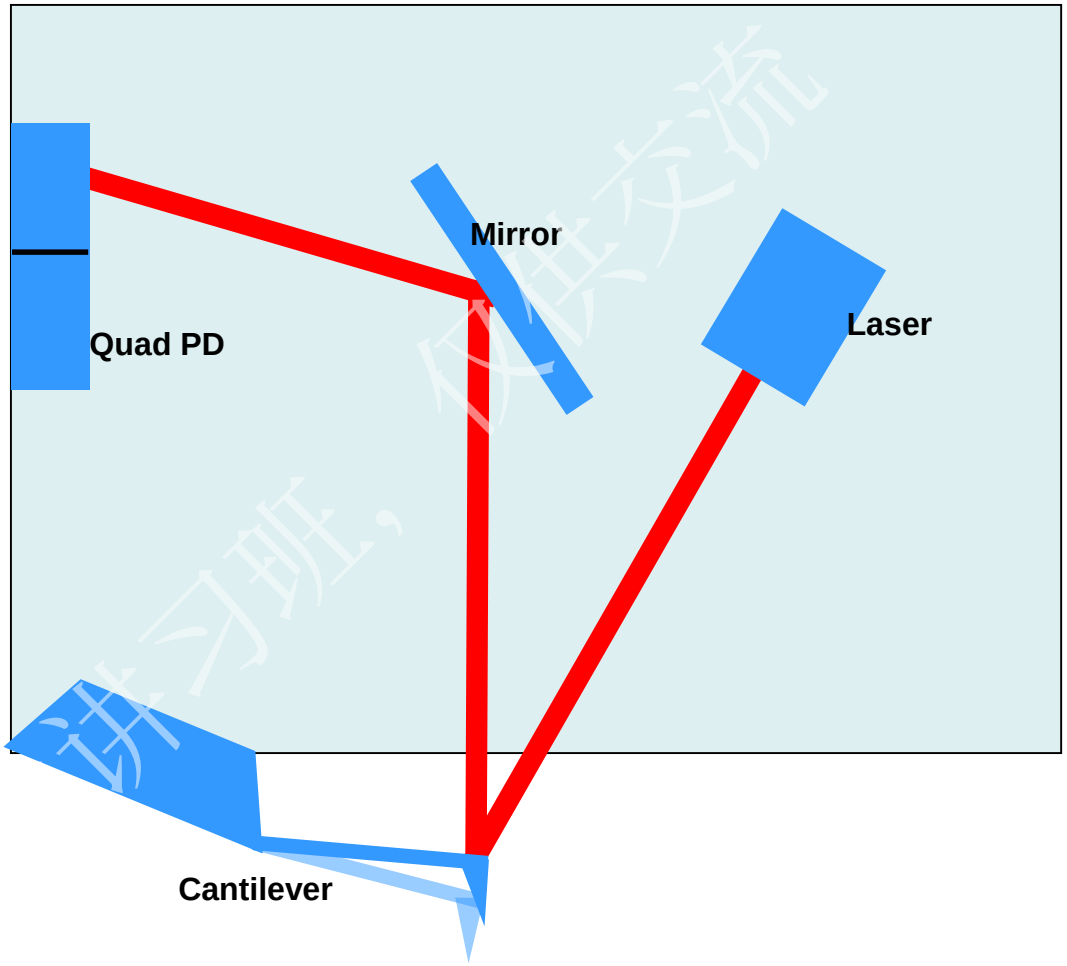

AFM构造图

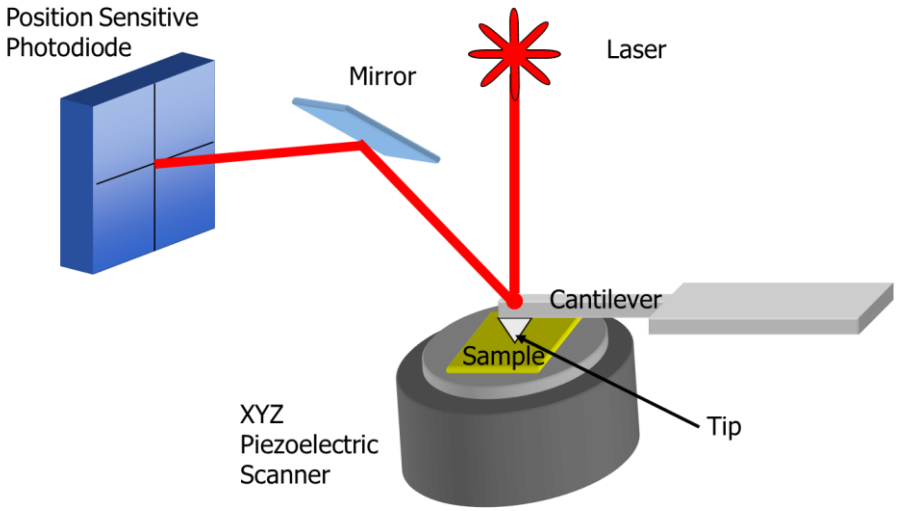

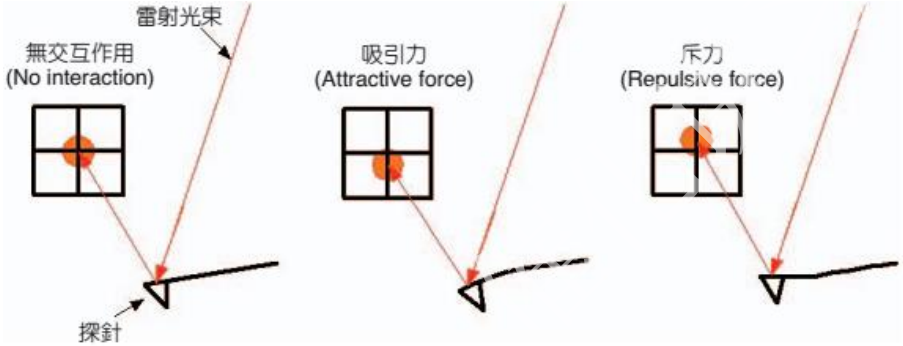

扫描管控制探针在样品表面上方精确地按照预设的轨迹运动，当探针遇到表面形貌的变 化时，由于探针和样品间的相互作用变化了，导致探测信号改变，因此与阈值产生一个差值， 叫做误差信号（Error Signal）。AFM 使用 Z 向反馈来保证探针能够精确跟踪表面形貌的起伏。 Z 向反馈回路连续不断地将探测信号和阈值相比较，如果两者不等，则在扫描管上施加一定的电压来增大或减小探针与样品之间的距离，使误差信号归零。同时，软件系统利用所施加 的电压信号来生成 AFM 图像。

AFM的工作原理

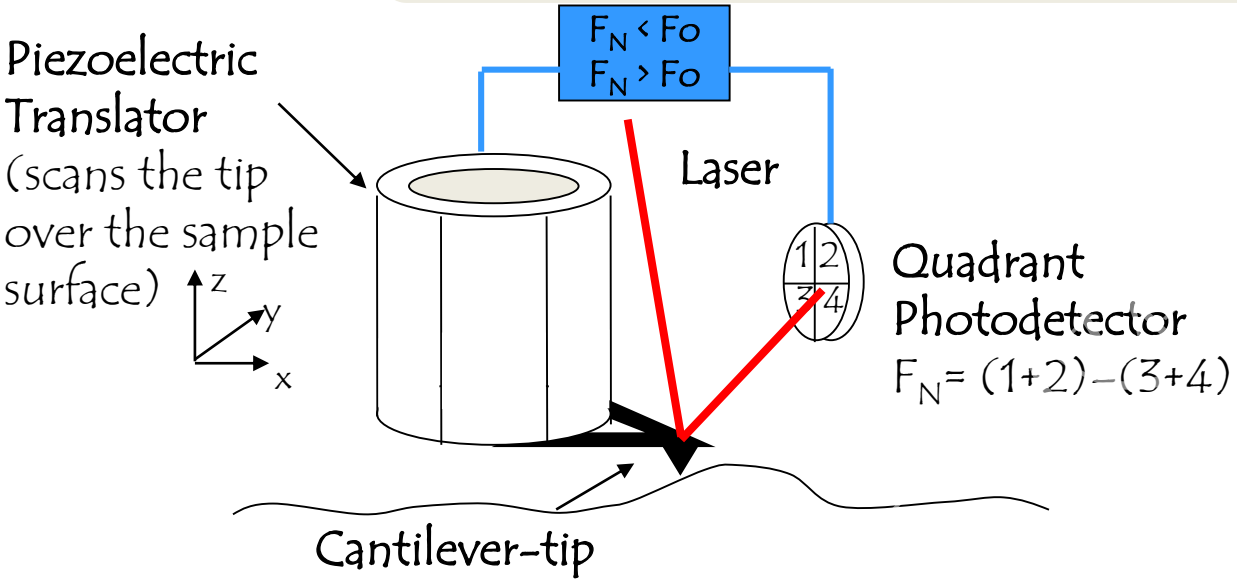

Lever:

$\delta F = -k\delta x$

If you know k you know the force.

Scanning in Contact: Tip follows the profile of the surface maintaining a constant lever deflection (constant force).

AFM Model

Thermal limit on displacement: $(\Delta z)_{rms} = \sqrt{\frac{kT}{m\omega_0^2}}$

1 J = 1 kgm^2s^{-2} $m_{lever} \sim 10^{-13}$ kg $\omega_0 \sim 30$ kHz

Forces acting on the tip provide the signal:

van der Waals; electrostatic, etc.

Sensitivity to intermolecular forces of $\sim 10^{-12}$ N.

工作模式

- 接触模式（Contact mode）
- 非接触模式（Non-contact mode）
- 轻敲模式（Tapping mode）
- 峰值力模式（Peakforce）模式

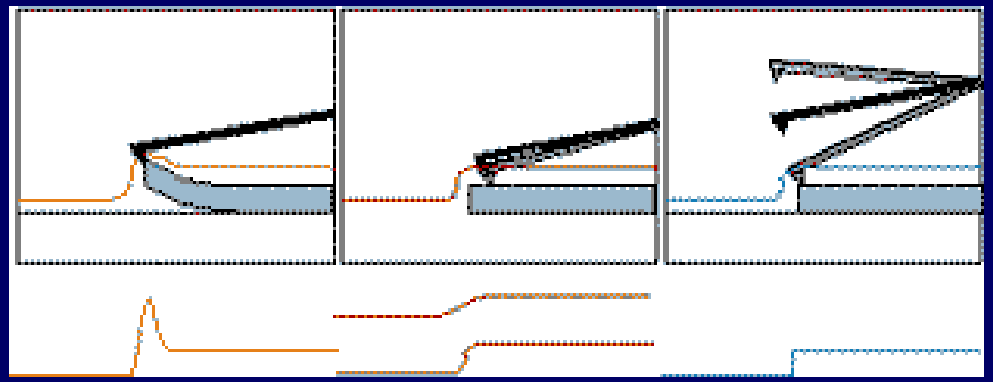

接触模式（Contact Mode）

原理：微悬臂探针紧压样品表面，检测时与样品保持接触，作用力（斥力）通过悬臂梁的变形进行测量

优点：扫描速度快，是唯一能够获得“原子分辨率”图像的AFM。对于垂直方向上有明显变化的质硬样品，有时更适于Contact Mode扫描成像；

缺点：横向力影响图像质量。在空气中，因为样品表面吸附液层的毛细作用，使针尖与样品之间的粘着力很大。横向力与粘着力的合力导致图像空间分辨率降低，而且针尖刮擦样品会损坏软质样品（如生物样品，聚合体等）。因此，这种模式不适用于研究生物大分子、低弹性模量样品以及容易移动和变形的样品

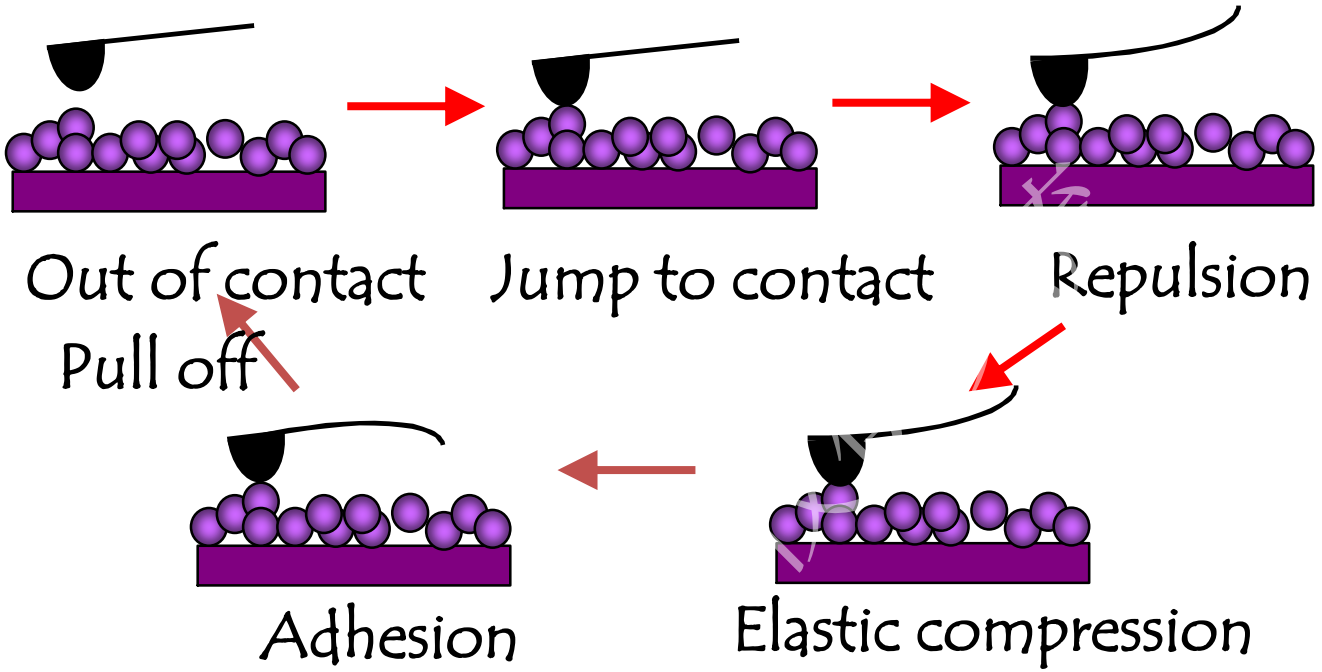

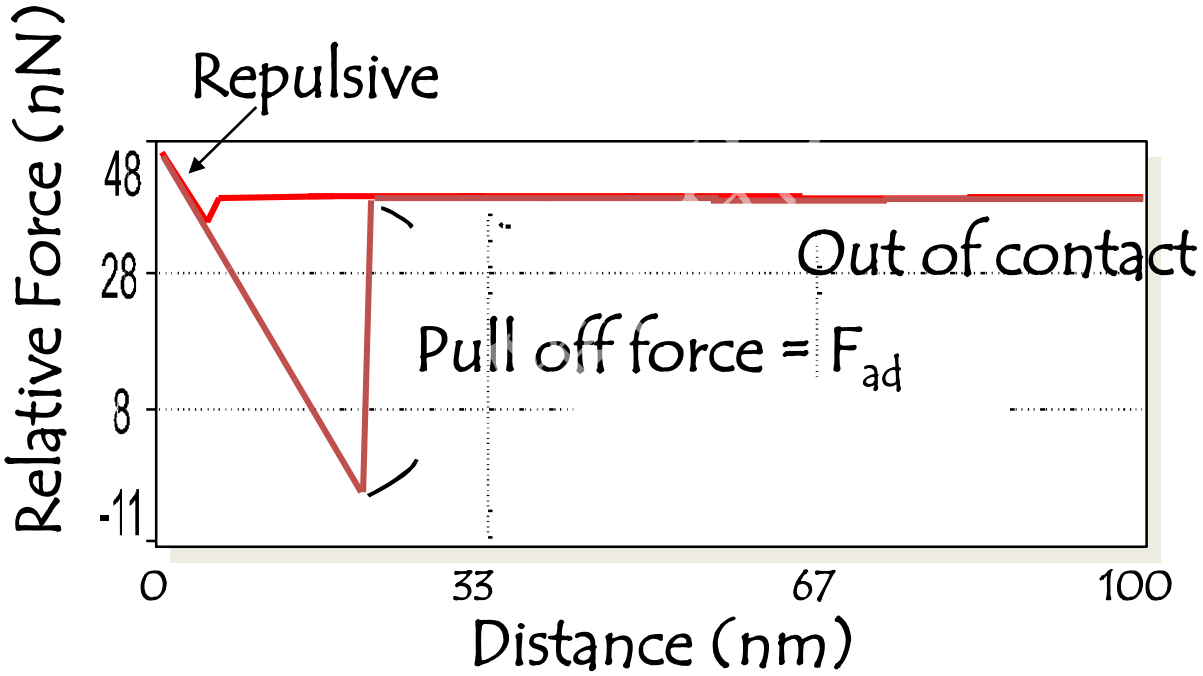

Force-distance spectroscopy

Force versus Distance Curves

Long-range contributions have force gradients like dF/dz » 1-10 N/m.

Spring constants of k ≈0.01-1 N/m provokes “jump-into-contact” when k < dF/dz.

Adhesion causes hysteresis in force vs. distance curves.

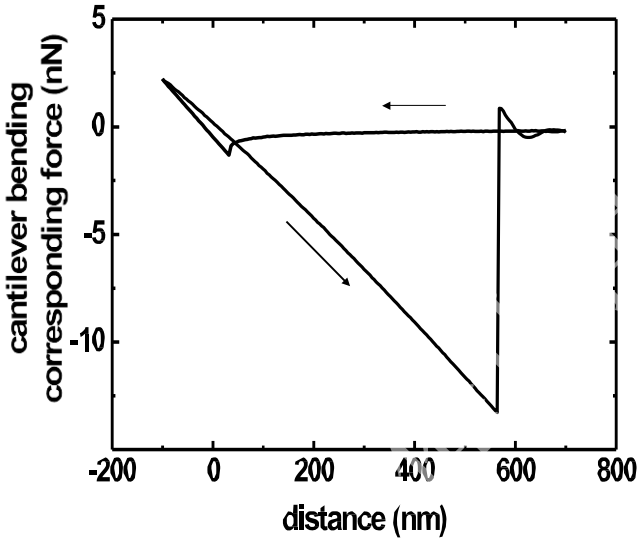

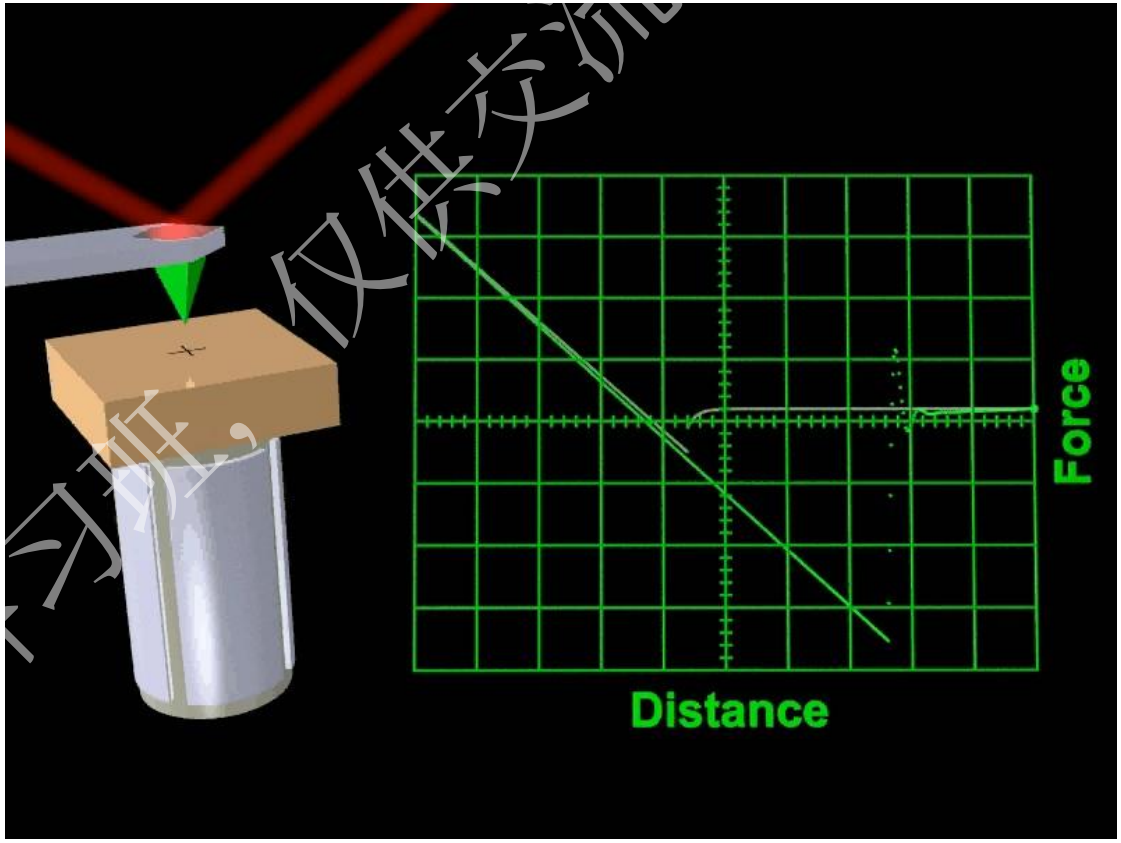

Use Force Distance Curves to obtain Chemical Specificity

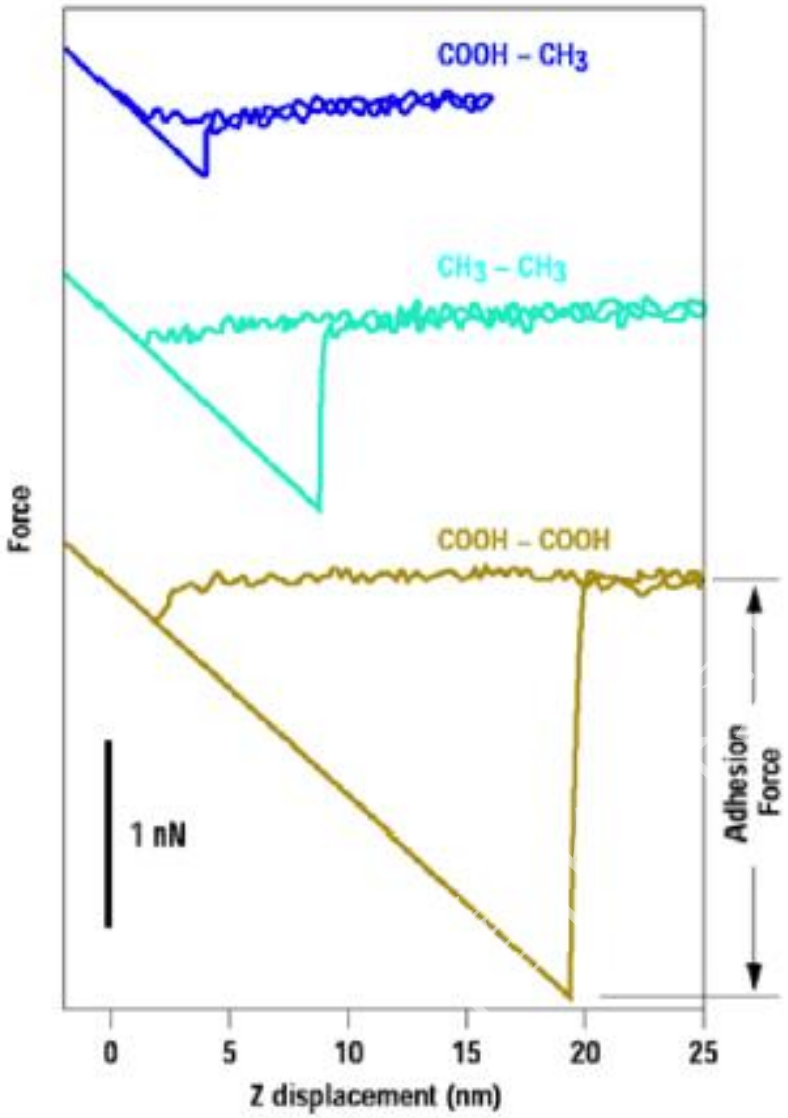

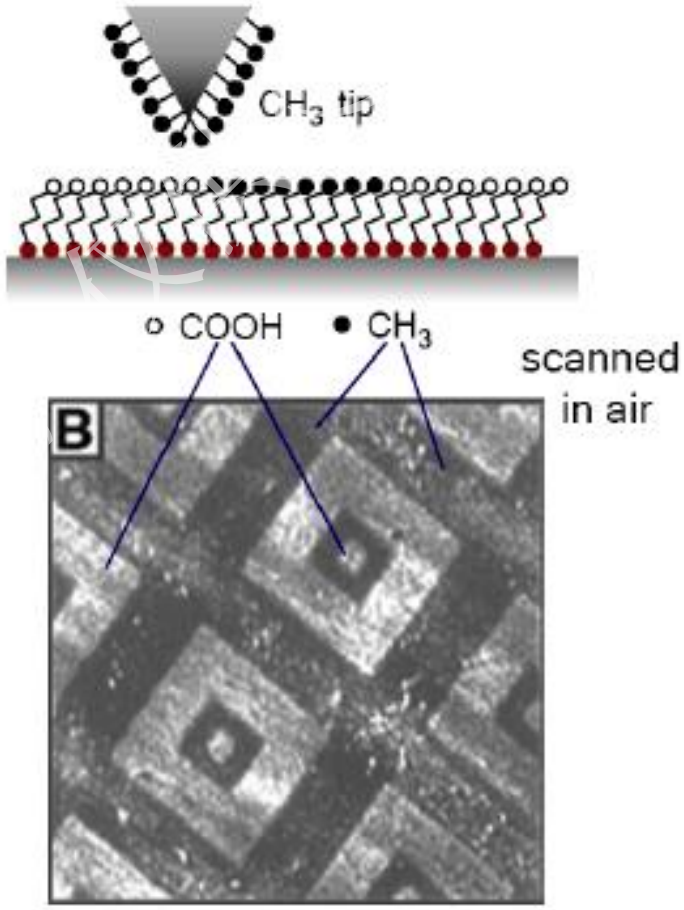

Noy et al., J. Am. Chem. Soc. 117 (1995) 7943.

Pseudo Atomic Resolution

- contact AFM on NaF(001)
- observation of atomic lattice (Moirée-effect)
- step width approximately 1nm indication of tip radius
- single atoms or atomic defects not visible

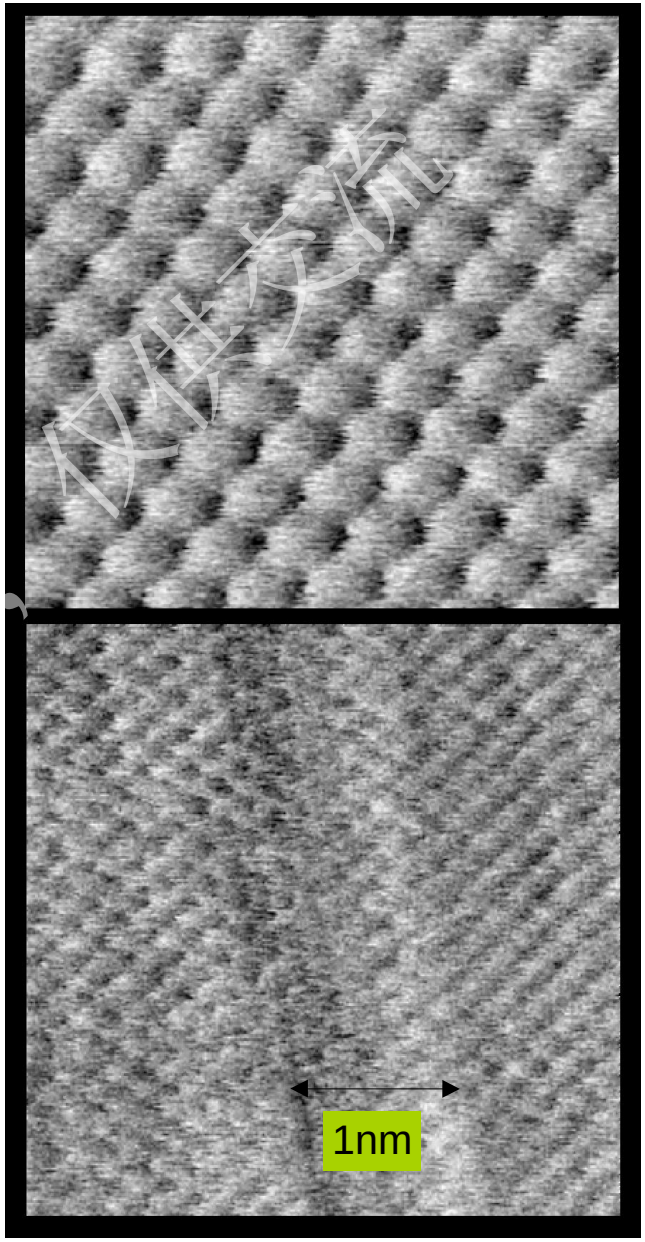

Non-contact Imaging

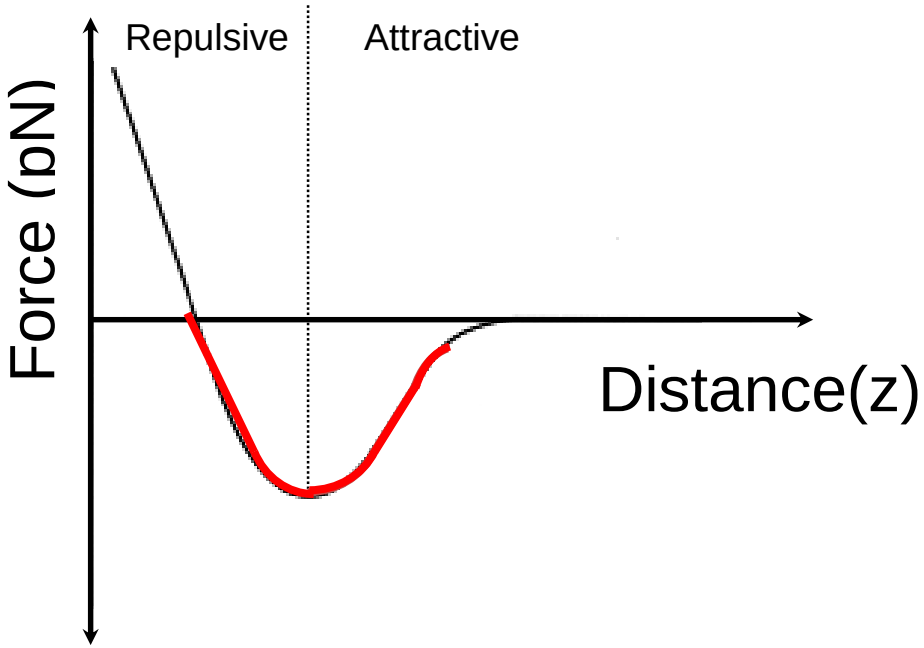

- Purpose: To limit surface and tip damage
- Treat cantilever-tip as a damped oscillator.
- Maintain a constant dF/dz for feedback.

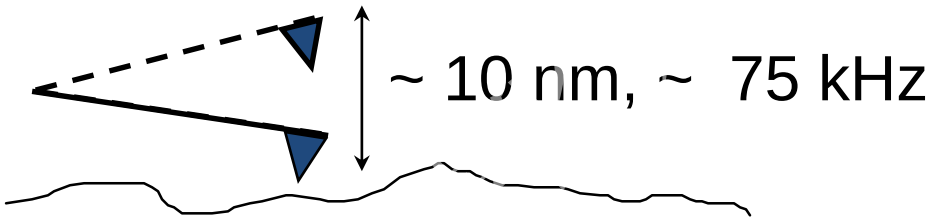

Intermittent-contact

Tips spends time in contact and out of contact with the surface.

$$F_0 = k_0 A_0 cos(w_0 t + \Phi)$$

非接触模式

悬臂在距离试样表面上方5～10 nm 的距离处振荡，作用力（引力）通过悬臂梁的变形进行测量。这种操作模式的不利之处在于要在室温大气环境下实现这种模式十分困难。因为样品表面不可避免地会积聚薄薄的一层水，它会在样品与针尖之间搭起一小小的毛细桥，将针尖与表面吸在一起，从而增加尖端对表面的压力

优点：没有力作用于样品表面，样品不会被破坏，而且针尖也不会被污染，特别适合于研究柔嫩物体的表面。

缺点：由于针尖与样品分离，横向分辨率低；为了避免接触吸附层而导致针尖胶粘，其扫描速度低于Tapping Mode和Contact Mode 模式。通常仅用于非常怕水的样品，吸附液层必须薄，如果太厚，针尖会陷入液层，引起反馈不稳，刮擦样品。由于上述缺点，此模式的使用受到限制

非接触模式基本概念：dynamic modes

frequency modulation: changes in the oscillation frequency provide information about tip-sample interactions. Frequency can be measured with very high sensitivity and thus the frequency modulation mode allows for the use of very stiff cantilevers. Stiff cantilevers provide stability very close to the surface and, as a result, this technique was the first AFM technique to provide true atomic resolution in ultra-high vacuum conditions (Giessibl).

amplitude modulation: changes in the oscillation amplitude or phase provide the feedback signal for imaging. In amplitude modulation, changes in the phase of oscillation can be used to discriminate between different types of materials on the surface. Amplitude modulation can be operated either in the non-contact or in the intermittent contact regime. In ambient conditions, most samples develop a liquid meniscus layer. Because of this, keeping the probe tip close enough to the sample for short-range forces to become detectable while preventing the tip from sticking to the surface presents a major hurdle for the non-contact dynamic mode in ambient conditions. Dynamic contact mode (also called intermittent contact or tapping mode) was developed to bypass this problem. In dynamic contact mode, the cantilever is oscillated such that it comes in contact with the sample with each cycle, and then enough restoring force is provided by the cantilever spring to detach the tip from the sample.

Driven Damped Oscillator

Amplitude of Cantilever

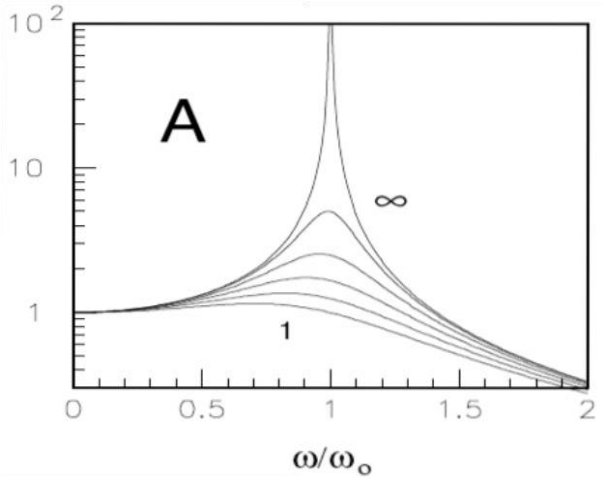

$$A(\omega) = \frac{F_0}{k} \frac{1}{\sqrt{\left(1 - \frac{\omega^2}{\omega_o^2}\right)^2 + \frac{\omega^2}{Q^2\omega_o^2}}}$$

Phase Loss of Cantilever relative to Excitation

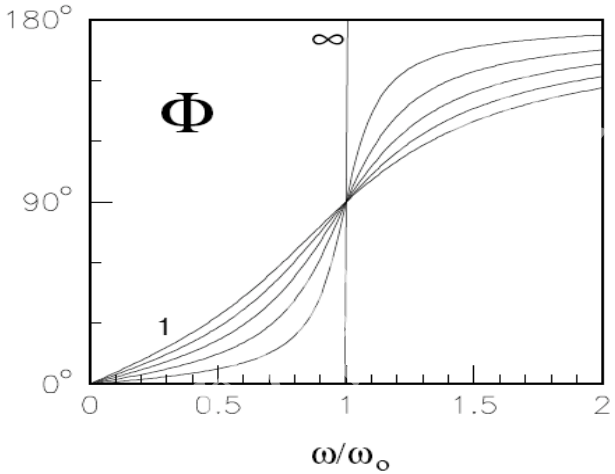

$$\Phi(\omega) = \arctan\left(\frac{\omega_o\omega}{Q(\omega_o^2 - \omega^2)}\right)$$

on resonance the cantilever lags 90° behind the excitation

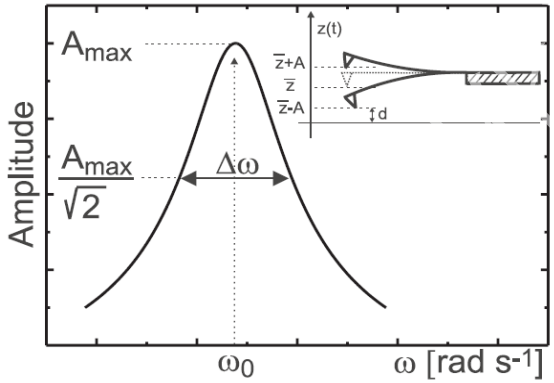

$$Q = A_{max}/A_{exc} = \omega_0/\ \Delta\omega$$

Dynamic Operation Mode

cantilever resonance

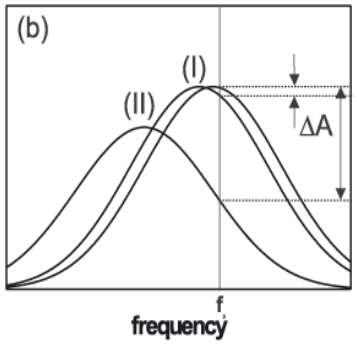

in air
-> low quality factor of cantilever
-> excitation with fixed frequency
-> lock-in amplifier

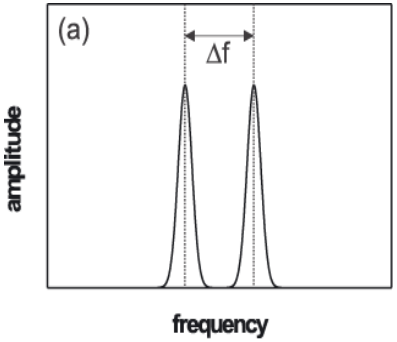

in vacuum
-> high quality factor
-> excitation on resonance
-> requires phase locked loop

low Q, wide resonance: lock-in amplifier

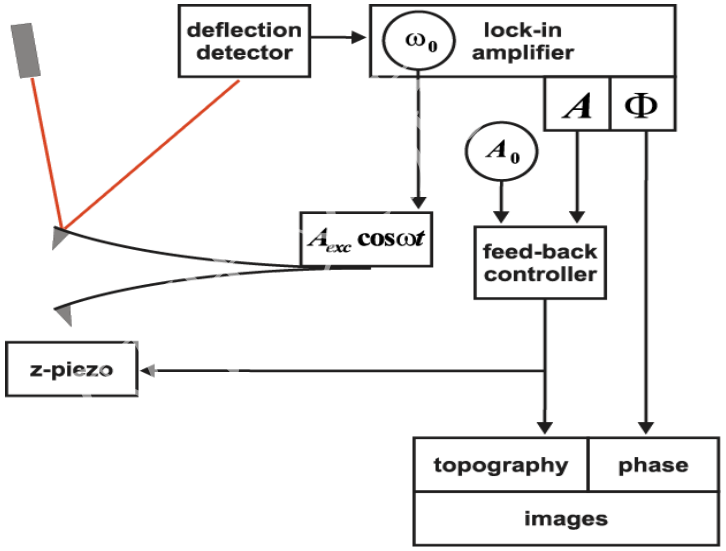

high Q, narrow resonance: PLL

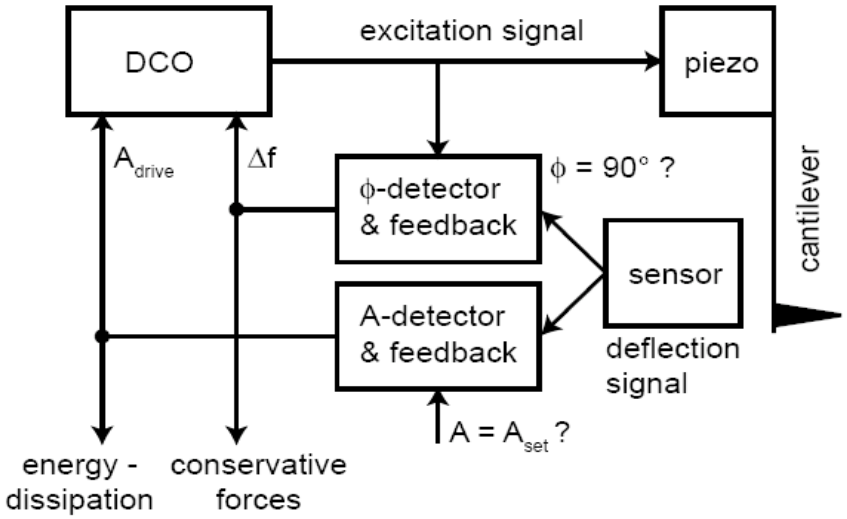

轻敲模式AFM

轻敲式AFM的基本原理

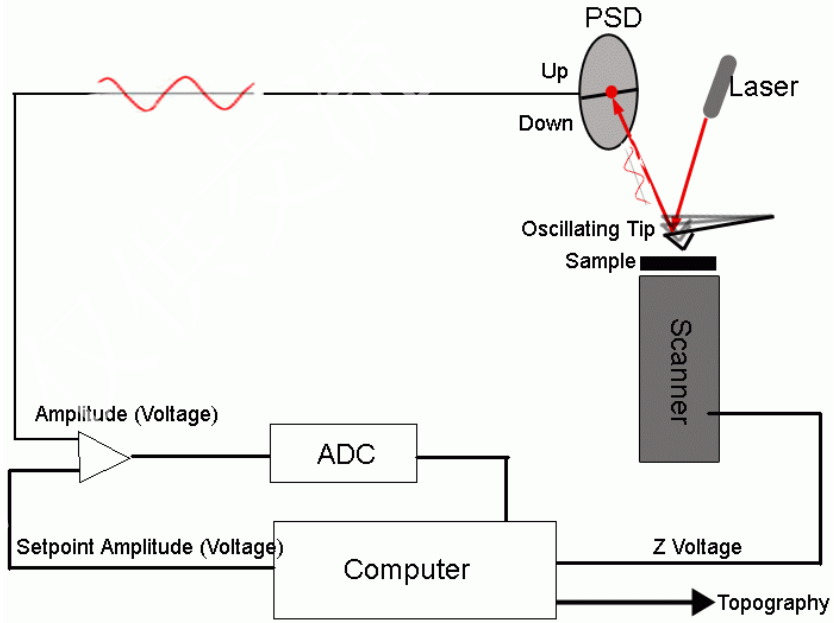

用处于共振状态、上下振荡的微悬臂探针对样品表面进行扫描，样品表面起伏使微悬臂探针的振幅产生相应变化，从而得到样品的表面形貌。该模式下，针尖对样品进行“敲击”，两者间只有瞬间接触，能有效克服接触模式下针尖引起的相互损伤，适合于柔软或吸附样品的检测。

Modes of Operation – AC (tapping) mode

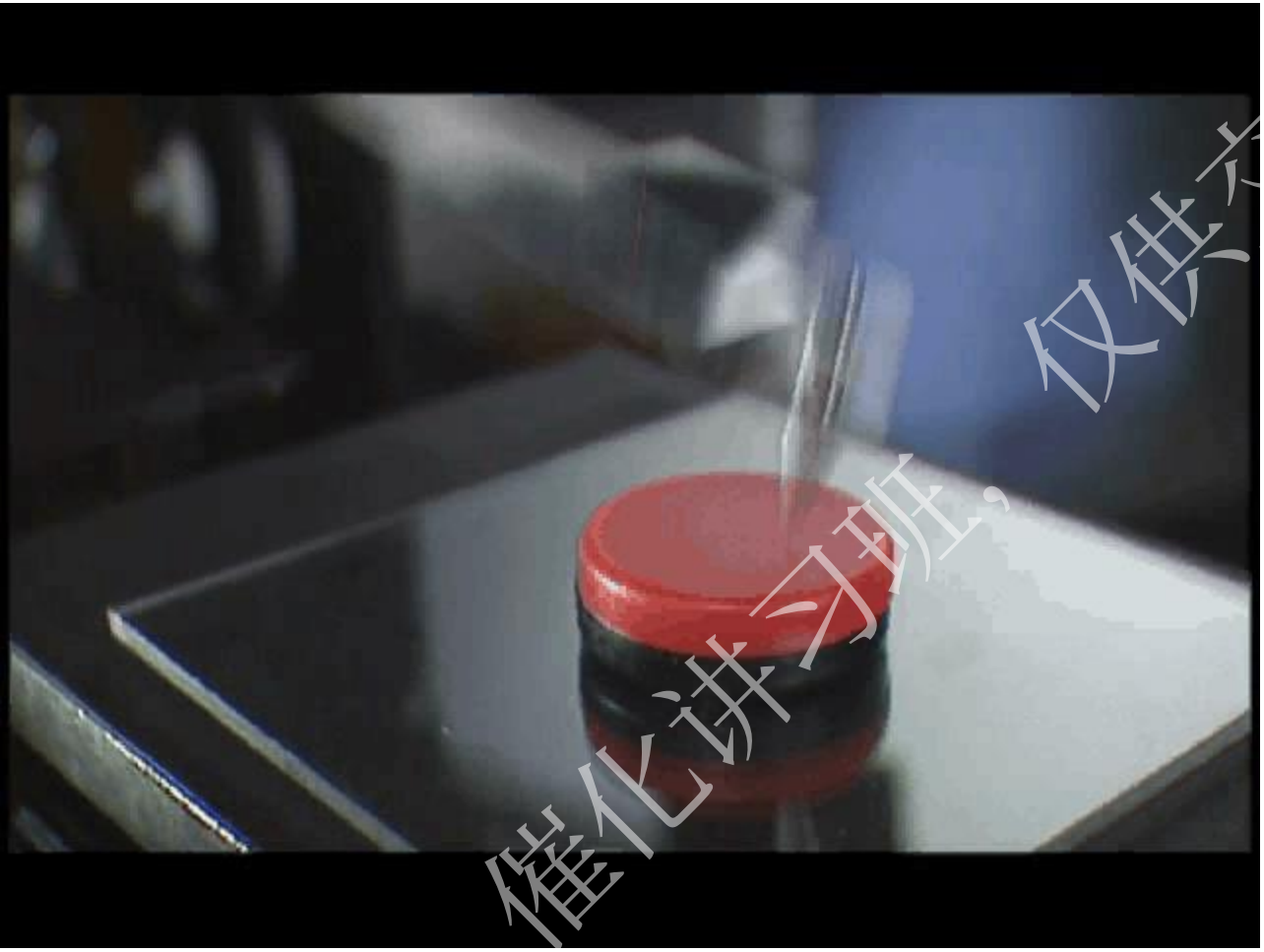

Changes in cantilever height while scanning are displayed on the computer as topography

轻敲模式AFM的优缺点

Tapping mode is good for

- works best in air (not vacuum)
- measurement of topography on soft samples
- measurement of loose particles adsorbed on surfaces
- topography measurement on samples with high friction
- topography on samples with vertical features

is easy to use and robust !

but:

- the cantilever oscillation can be strongly non-harmonic, i.e. bent resonance curves with instabilities
- stable operation is obtained at high amplitudes and with hard cantilevers
- but the highest phase contast is obtained close to the critical points

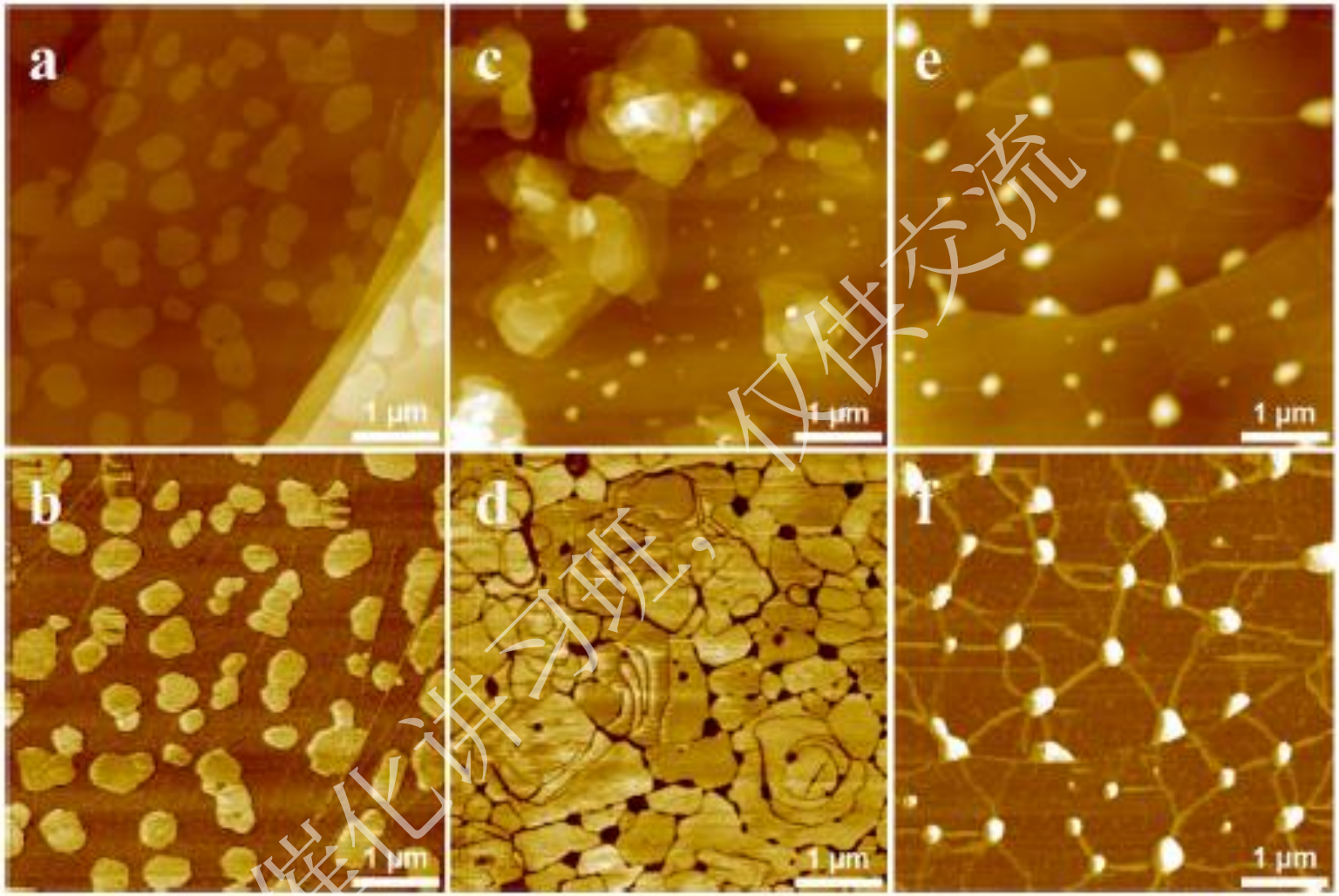

Fig. 3. Surface morphology of the drop-casted Fe-N-C catalyst on HOPG as a function of deposition amount. The corresponding surfaces of HOPG after the deposition of petroleum ether solution, containing Fe-N-C catalysts, were characterized by tapping mode AFM. (a), (c) and (e) display height images of the surfaces casted with 12 μL, 24 μL or 60 μL solution. (b), (d) and (f) show the corresponding phase images of (a), (c) and (e), respectively. All images have the same size at 5 μm × 5 μm. Graphene nanosheets (GNs) tend to disperse homogeneously on HOPG at the initial stage of deposition. The HOPG substrate is almost covered by the stacks of GNs in (c) and fully covered by multilayers of GNs in (e).

Tapping Mode Phase reveals Local Stiffness

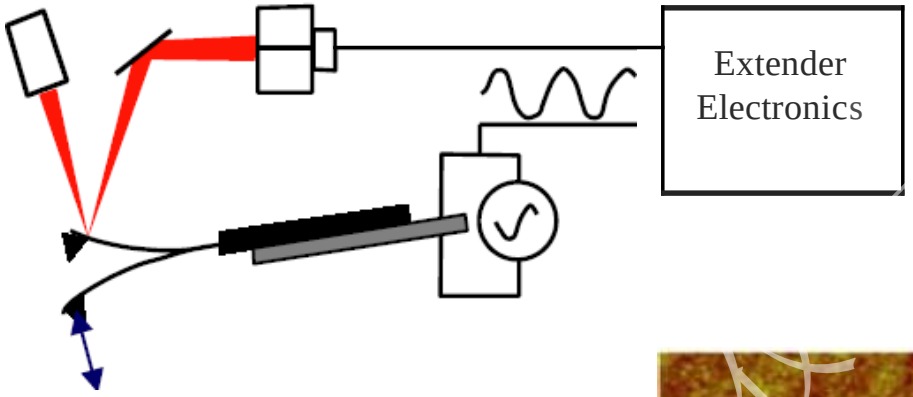

amplitude

phase

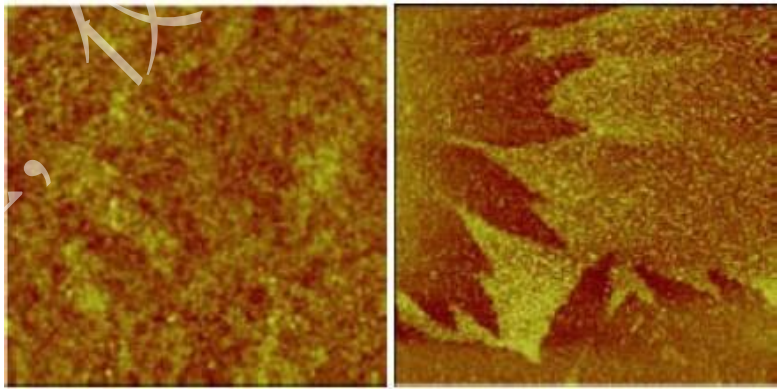

Two-phase structure of a semi-crystalline polyn1er

left:
topography

right:
phase image

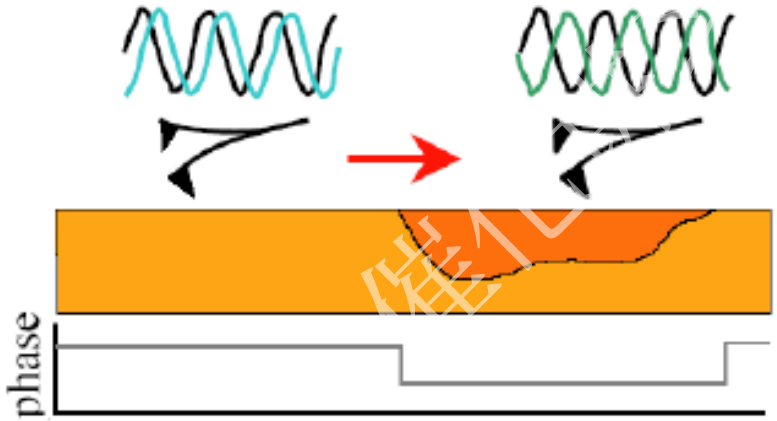

Phase channel gives the ‘lag’ or delay between the sinusoidal drive signal and the response signal at the photodetector

The probe is a simple harmonic oscillator driven at or near resonance

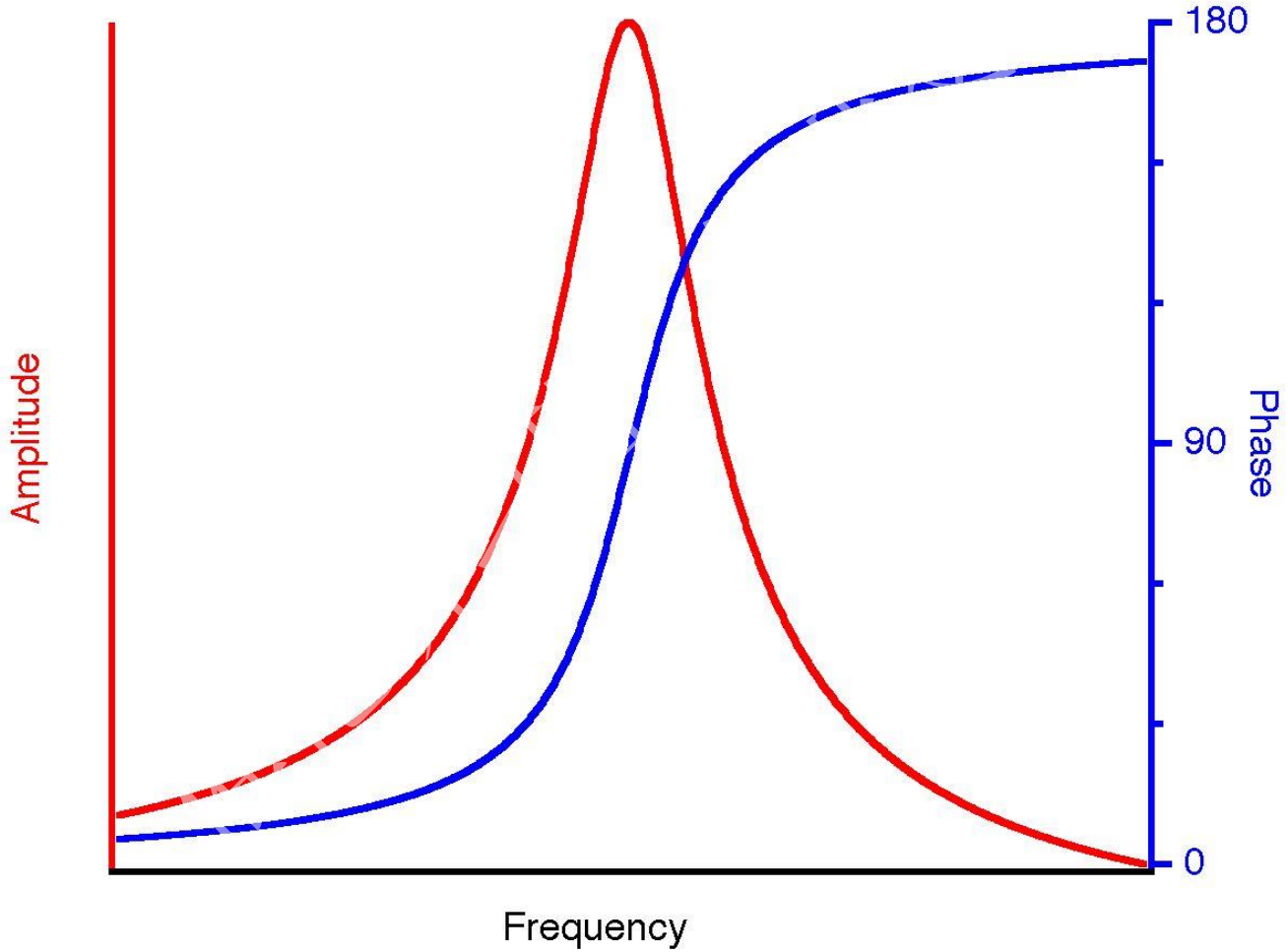

Phase Shift

$$U_{total} = \frac{1}{2}kx^2 + U_{sample}$$

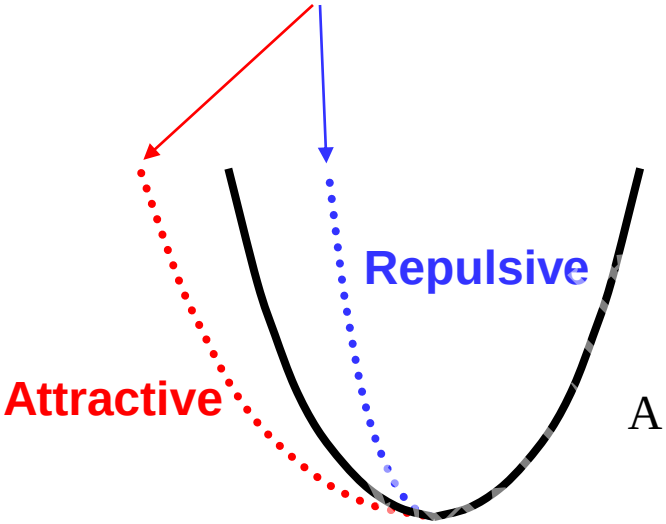

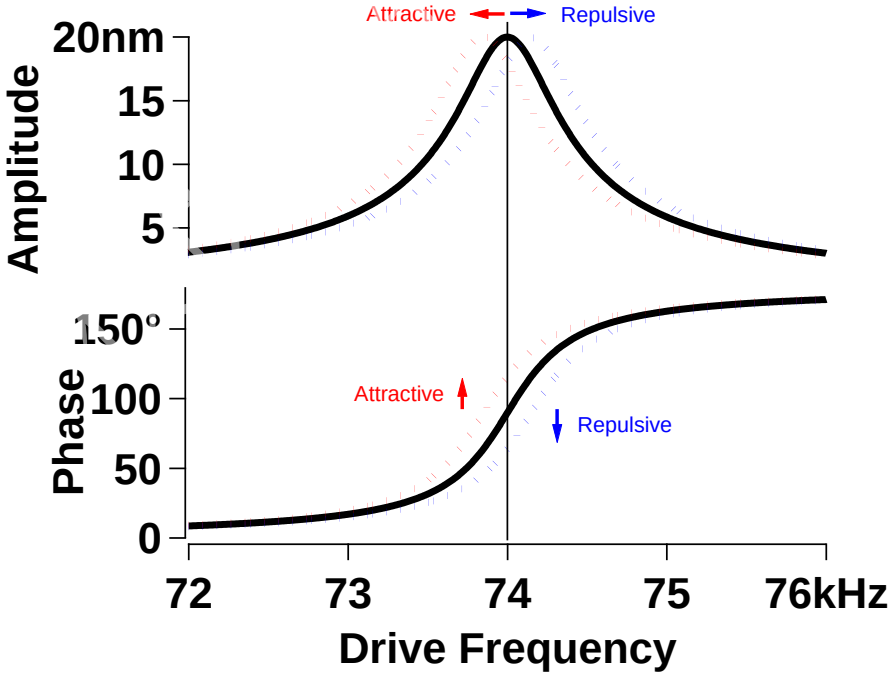

A potential well (tip sample interaction)

Attractive – Softens the potential well – Positive Phase shift

Repulsive – Sharpens the potential well – Negative Phase Shift

PeakForce Mode

- Based on PeakForce Tapping mode
- Every tap on the surface produces additionally a force curve, which is extracted
- Force-curves are acquired more than 1000x faster than in standard force distance spectroscopy
- Obtain quantitative material properties by force curve analysis at every pixel.

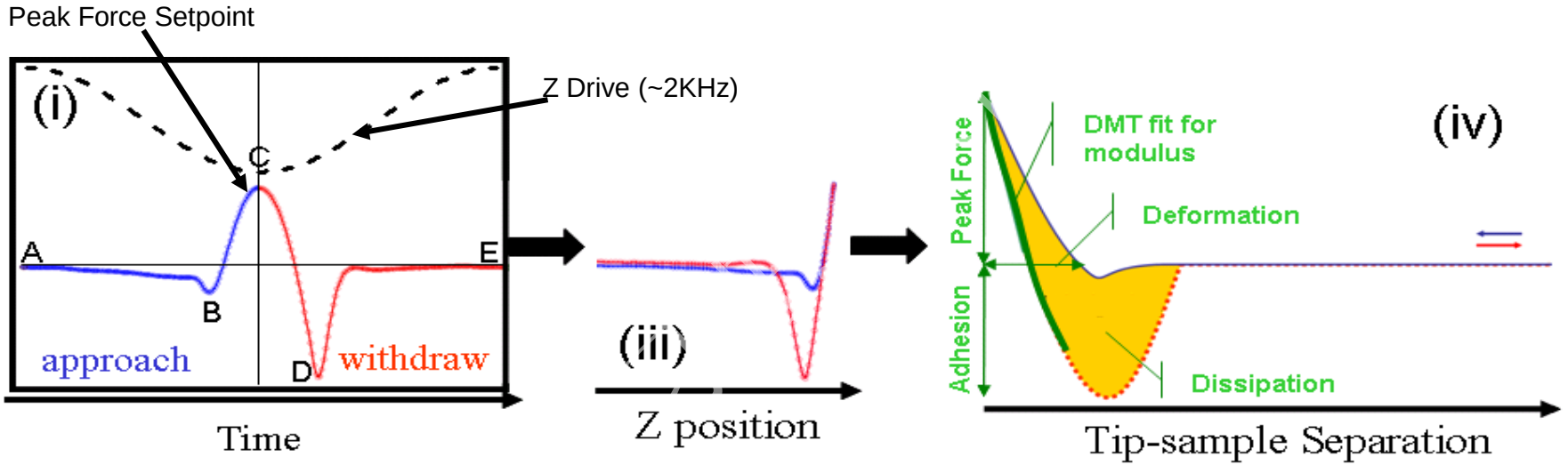

Derjaguin-Muller-Toporov (DMT) model

$$F_{tip} = \boxed{\frac{4}{3} E^* \sqrt{R}\, d^{3/2}} + F_{adh},$$

in contact:
Hertz Theory

$$\frac{1}{E^*} = \frac{1-\nu_1^2}{E_1} + \frac{1-\nu_2^2}{E_2}$$

and E_1, E_2 are the elastic moduli and ν_1, ν_2 the Poisson's ratios associated with each body.

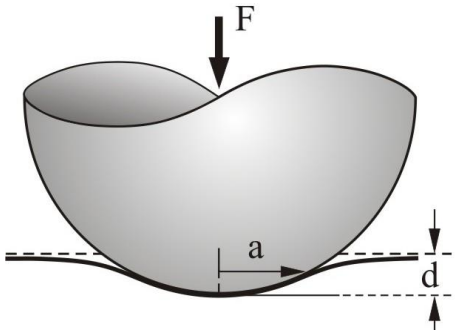

峰值力模式（Peakforce）模式

在传统接触模式成像过程中探针与样品之间存在剪切作用，容易造成样品的损坏；在传统轻敲成像模式中，由于是基于对快速振动的探针的微悬臂振幅值监测来对探针针尖与样品作用力进行反馈控制，因而探针针尖与样品间的作用力难以精确控制，仍有可能导致待测样品严重变形或破坏。

峰值力模式是用正弦波代替传统三角波的方式来驱动压电陶瓷扫描管Z方向上的运动；在该模式中，探针受压电陶瓷扫描管在Z方向上的作用而受迫振动

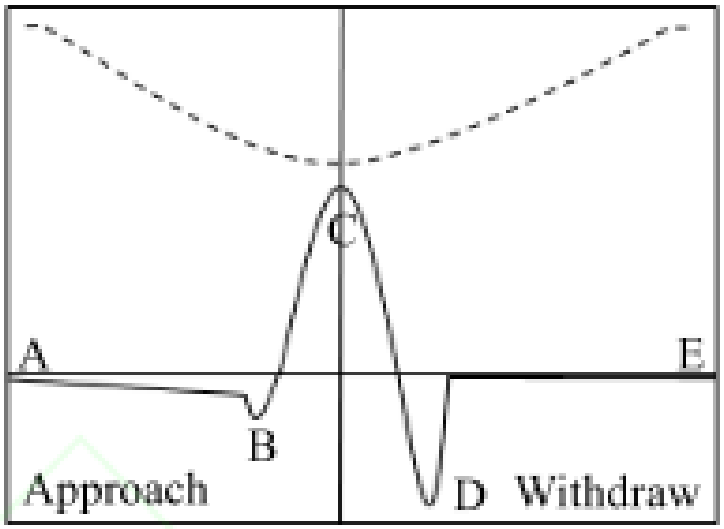

图 3　峰值力测量模式

峰值力模式（Peakforce）模式

该操作模式的优点是：越接近样品表面，探针相对样品的运动速度越慢，因此避免了因系统响应的延迟而导致探针的不必要的移动，可以更精确的控制探针和样品之间的相互作用力。

不同的物理量用于AFM的反馈系统时对应的成像模式

用于反馈的物理量P	基本成像模式
悬臂振幅A	轻敲模式AFM（Tapping Mode AFM）
悬臂弯曲量D	接触模式AFM（Contact Mode AFM）
悬臂弯曲量D	非接触模式AFM（NC mode AFM）
探针-样品相互作用 F	峰值力 AFM（PeakForce Tapping AFM）

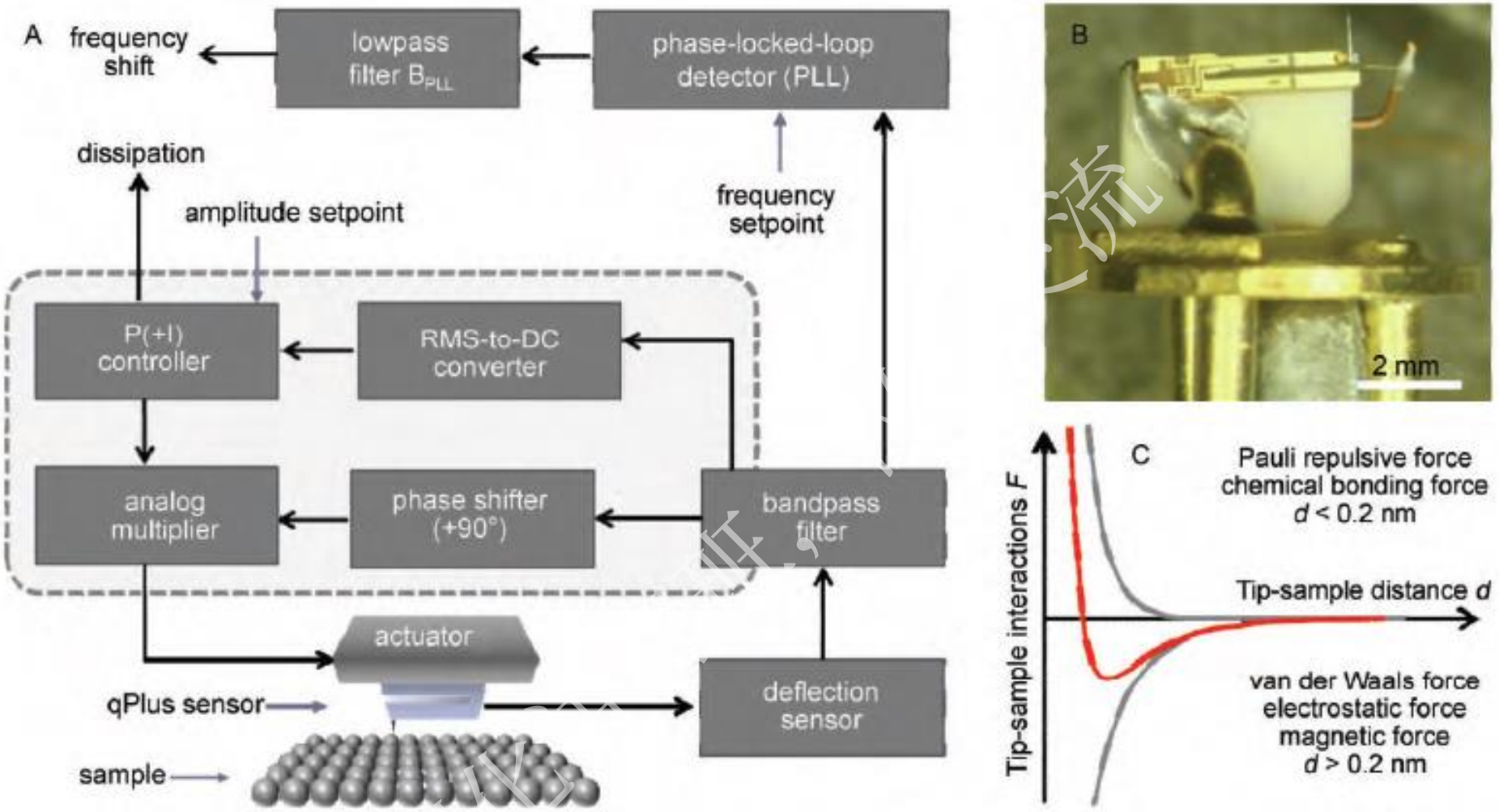

图1　非接触原子力显微镜的工作原理[6]

Fig.1　Working principle of non-contact atomic force microscopy (NC-AFM)[6]

(A) block diagram of the NC-AFM feedback loop for constant amplitude control and frequency-shift measurement; (B) qPlus sensor; (C) total interaction force between tip and sample

频率调制 FM-AFM

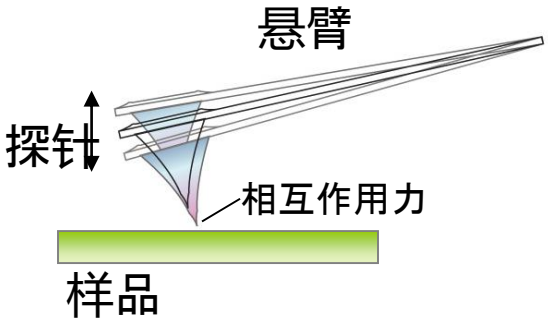

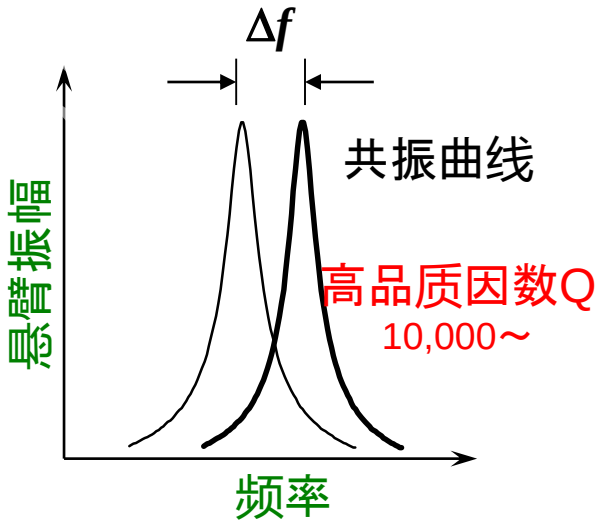

高品质因数Q=10,000～ (UHV)时高灵敏度

低品质因数Q时,

Q=100 (大气中)

Q=1～10 (液体中)

→灵敏度降低

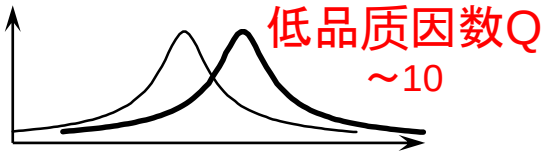

目标

用FM-AFM在低品质因数的环境里实现原子级分辨率和物理特性的测量

Principle of Dynamic Force Microscopy with Atomic Resolution

First demonstration of true atomic resolution:

For small amplitudes, the frequency shift is a very simple function of the tip-sample forces:

- it is proportional to the tip-sample force gradient k_{ts} .
- for large amplitudes, the frequency shift is given by the rather complicated equations (see above).
- with integration by parts, the complicated formula transform into a very simple expression

oscillation ~ 9.5 nm

$$\Delta f(z) = f_0 \frac{\langle k_{ts}(z) \rangle}{2k} \quad \text{with} \quad \langle k_{ts}(z) \rangle = \frac{1}{\frac{\pi}{2} A^2} \int_{-A}^{A} k_{ts}(z - q') \sqrt{A^2 - q'^2}\, dq'$$

, L1086 (1995)

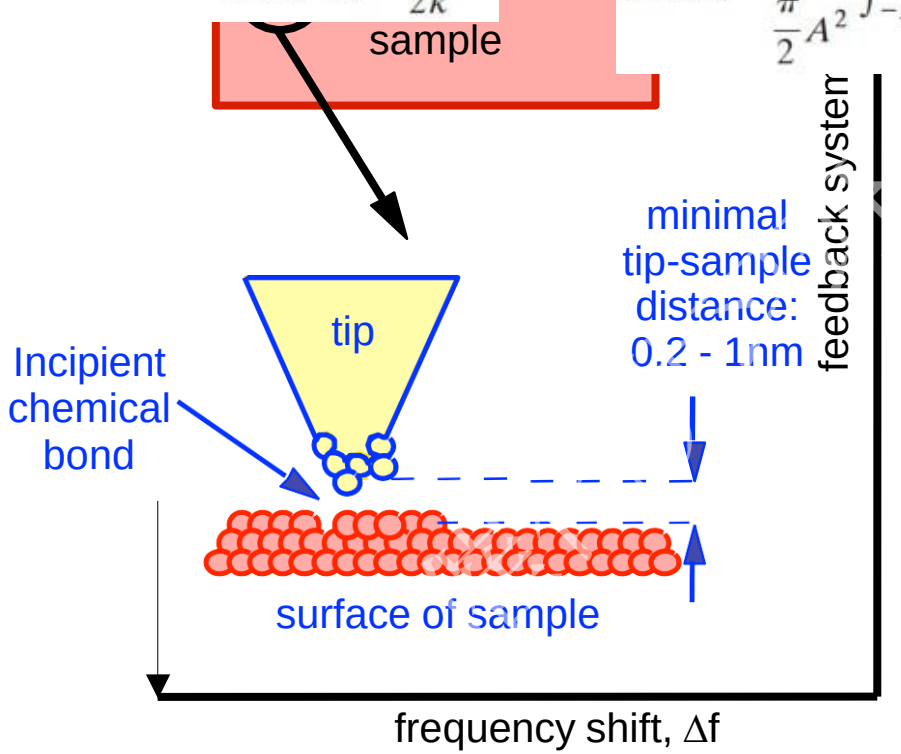

FM Detection:

T.R. Albrecht et al., J. Appl. Phys. 69, 668 (1991) describe an FM demondulation technique for fast measurement of frequency shift.

U.Dürig et al., J. Appl. Phys. 82, 3641 (1997), Ch. Loppacher et al., Appl. Phys. A66, 215 (1998)

- adjust frequency of oscillation circuit to keep phase between excitation and cantilever oscillation constant (phase locked loop)
- keep cantilever oscillation amplitude constant, i.e. cantilever excitation signal is proportional to energy dissipation
- conservative and non-conservative interactions can be separated

Large vs. small oscillation amplitude

large thermal noise

low detection sensitivity

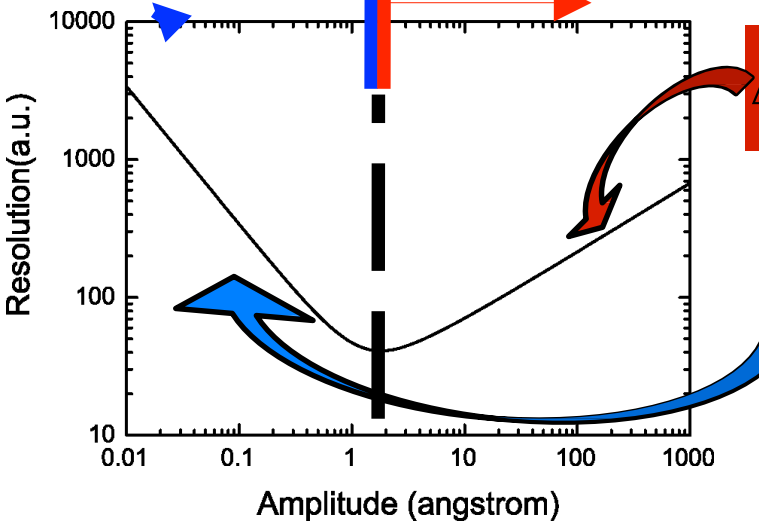

Detection sensitivity

$$\Delta f(z) = -\frac{f_0^2}{kA}\int_0^{1/f_0} F_{ts}\left(z + A + A\cos(2\pi f_0 t)\right)\times\cos(2\pi f_0 t)\,dt$$

Thermal noise

$$\partial f_{th} = \frac{1}{A}\sqrt{\frac{2k_B T f_0 B}{\pi k Q}}$$

Amplitude comparable to range of interaction is optimal!

Absolute value of resolution depends on:

- probe specifications (f_o, k, Q)
- detector sensitivity

Example: k=2000N/m,
f_o= 1.6MHz, Q=100 000
A_{th}= 1440fm @300K
A_{th}= 170fm @4.2K
Required sensitivity of detector @1kHz BW:
A_{noise}< 50fm @300K
A_{noise}< 6fm @4.2K

S. Kawai and H. Kawakatsu. APL **88**, 133103 (2006)

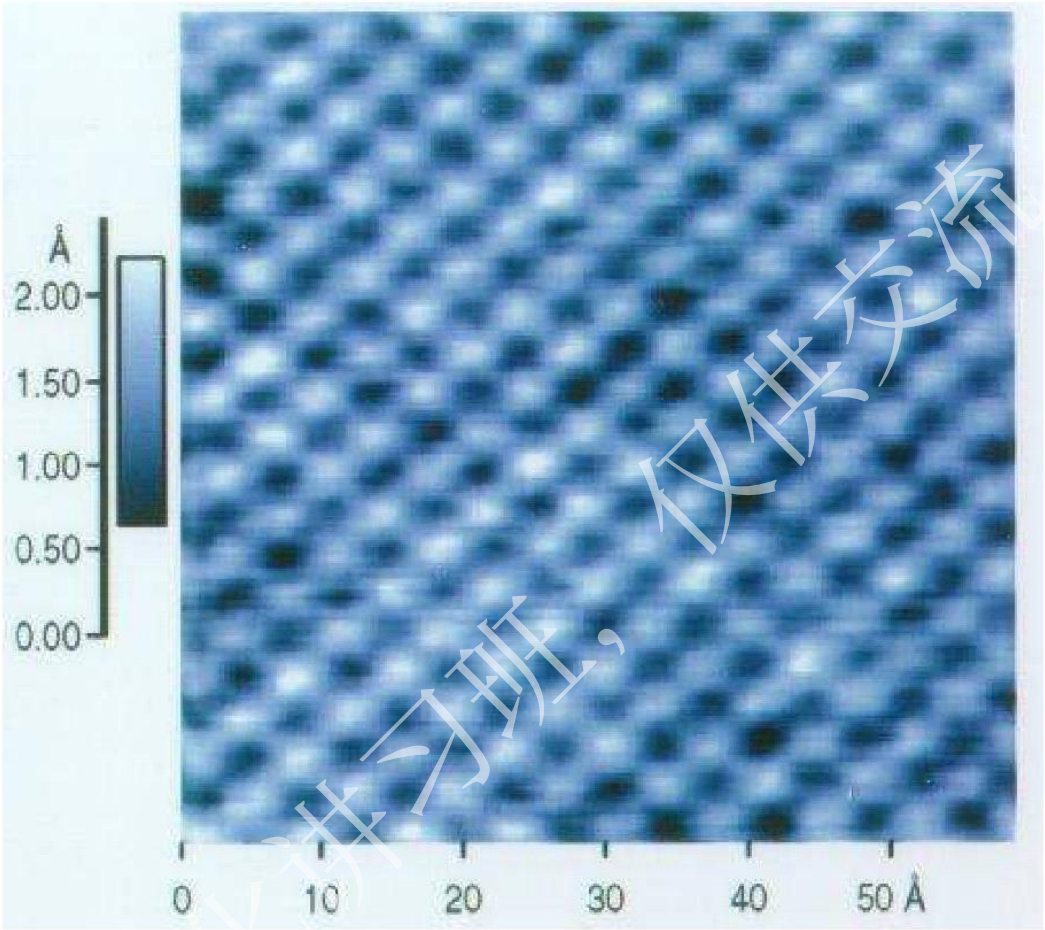

First FM-AFM image of an insulator (KCl) with true atomic resolution.

AFM 在催化中的应用

Atomic Resolution on Si(111)-7x7

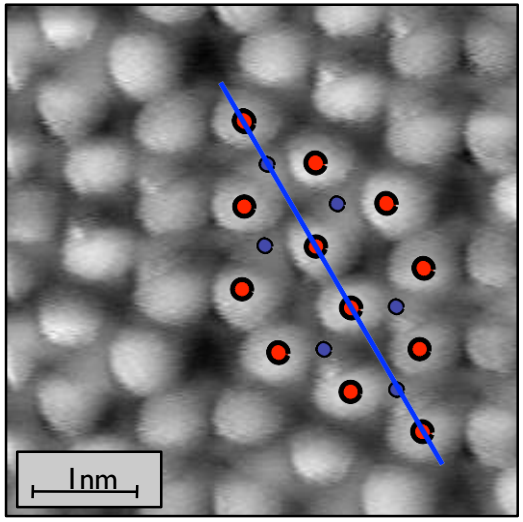

measurement parameters
Δf = -31Hz, scan speed 0.6nm/s
Cantilever: c_L = 28.6 N/m,
f_0 = 155 719.3 Hz, Q = 370‘000
temperature: 7.2K

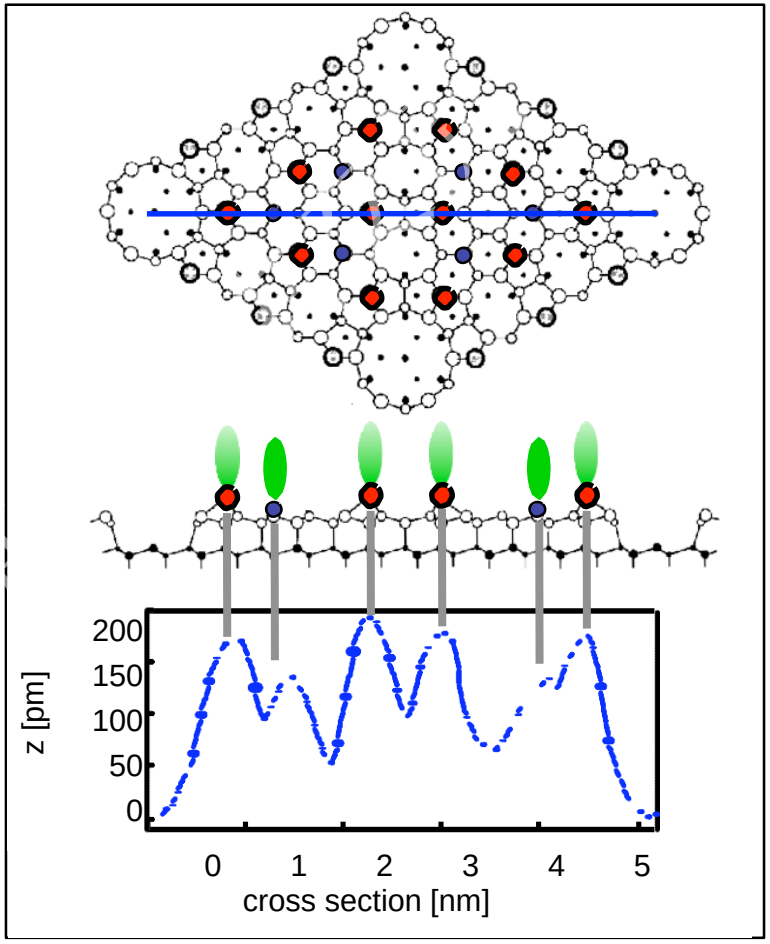

- height difference between inequivalent adatoms due to small differences in reactivity

M. A. Lantz and H.J. Hug et al., Phys. Rev. Lett. 84, 2642 (2000)
K. D. Brommer, et al., Phys. Rev. Lett. 68, 1355 (1992) **&**
I. Stich, et al., Phys. Rev. Lett. 68, 1351 (1992).

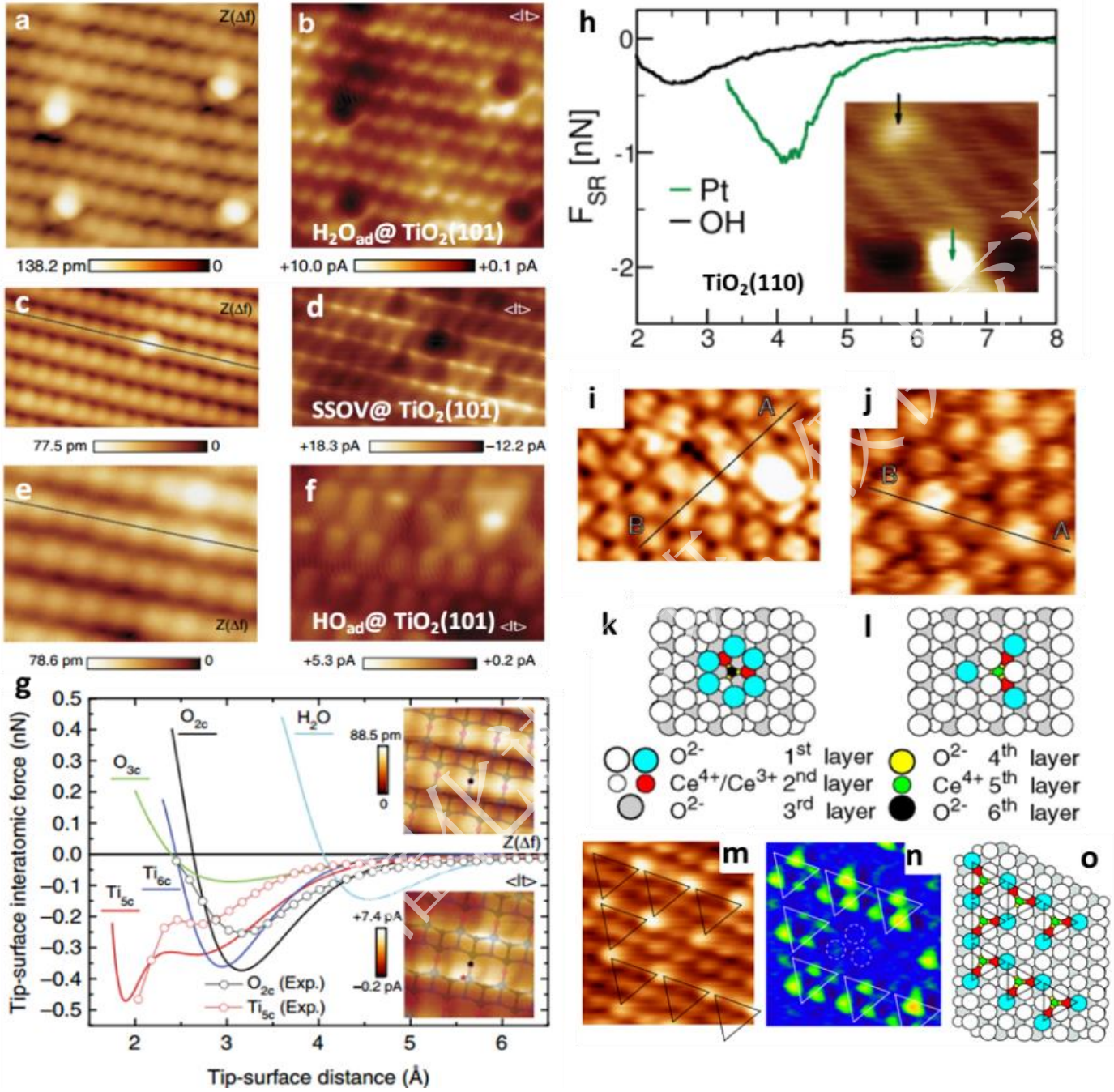

(a~g) STM/AFM联合表征锐钛矿型TiO_2(101)表面。水分子(H_2O_{ad})，次表层氧缺陷(Subsurface Oxygen Vacany, SSOV)和表面羟基(HO_{ad})的AFM(a, c, e)和STM(b, d, f)图像。(g) DFT和实验取得的不同表面位点力学曲线。(h) 金红石型TiO_2(110)表面上表面羟基和Pt原子的力学谱判别(i~o)CeO_2(111)表面的氧缺陷和次表层缺陷观测。(i~j) CeO_2(111)表面氧缺陷(i)和次表层氧缺陷(j)的AFM图。次表层缺陷的有序排列的AFM形貌图(m)，能量损耗信号(n)以及结构模型(o)。

Chemical identification of individual surface atoms

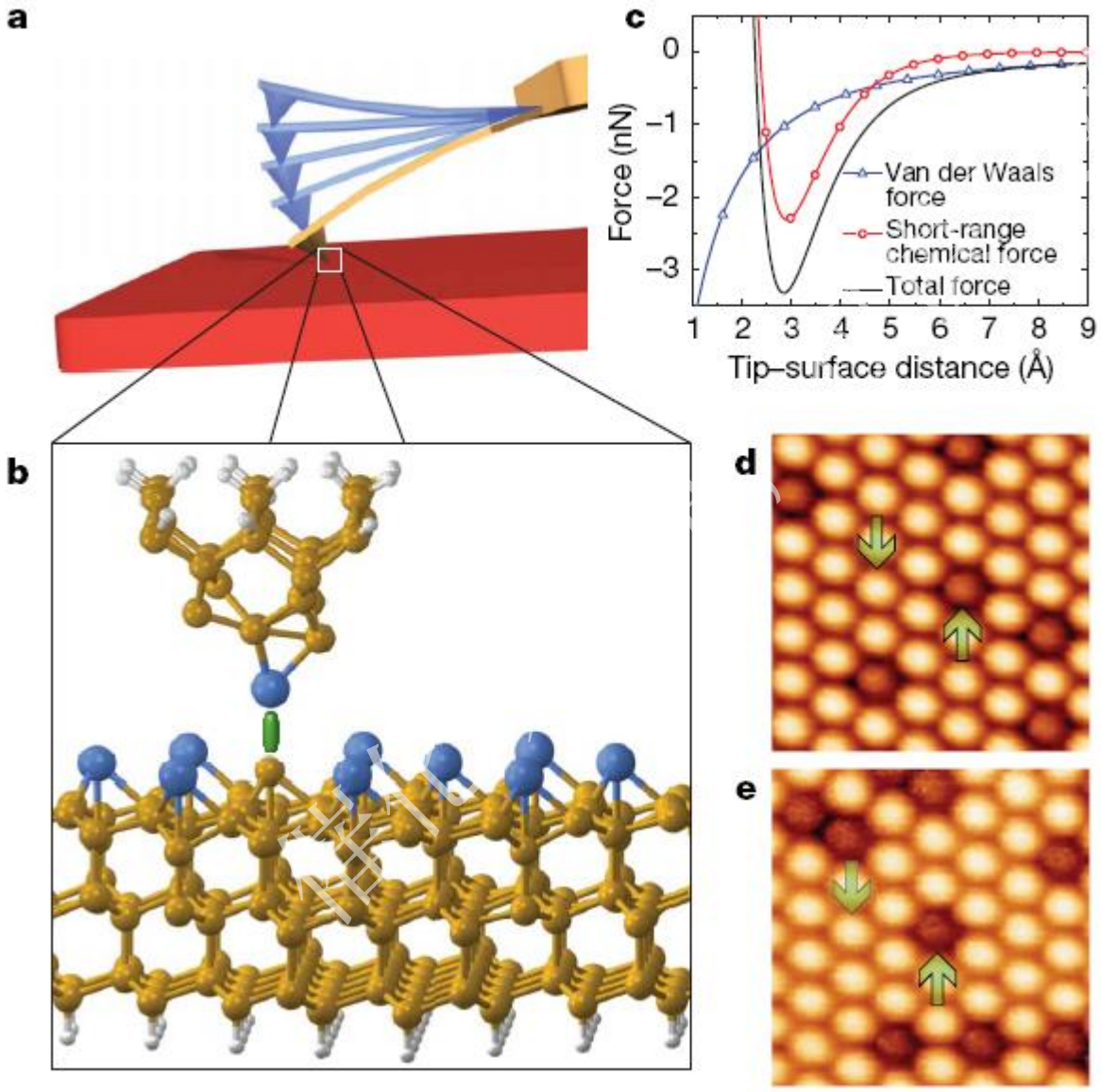

Nature, 446, 64 (2007)

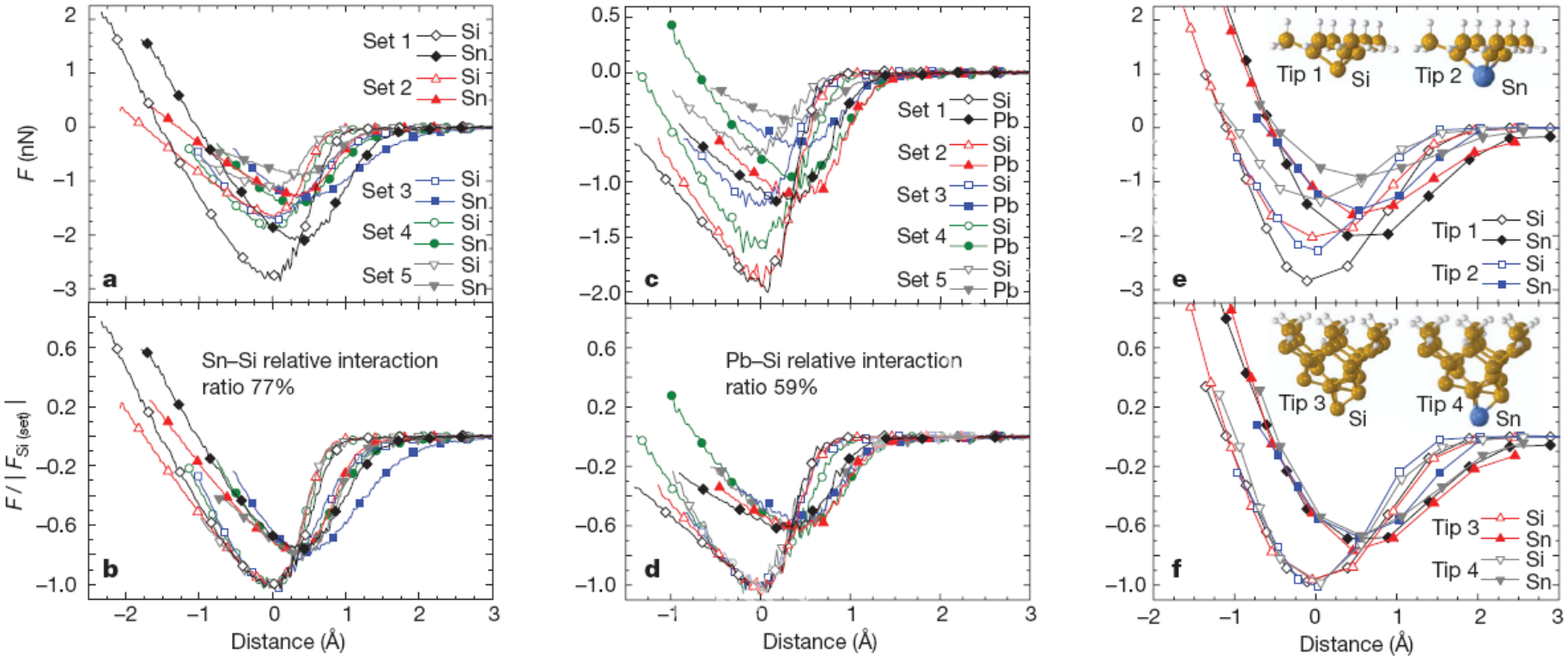

A meaningful comparison of measured short-range forces requires some data processing to reduce the variability caused by the use of tips with different terminations. We have found that the relative interaction ratio, that is, the ratio of the maximum attractive short-range forces of the two curves within a set of measurements over Si and Sn (acquired using a tip that had the same apex termination), remains nearly constant.

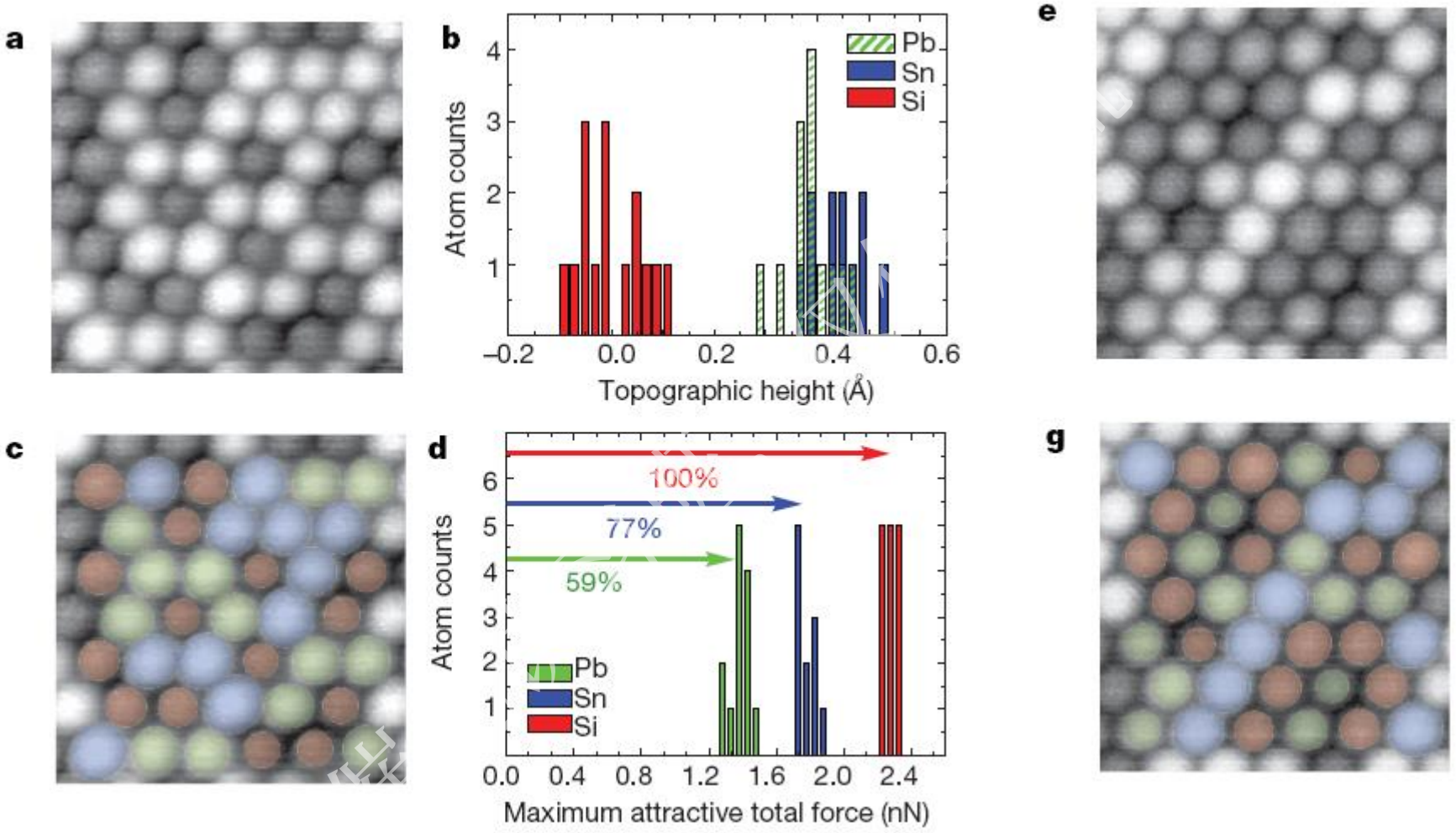

Blue, green, and red atoms correspond to Sn, Pb and Si, respectively

Imaging Molecules

Figure 1. Model of a CO-modified tip (C gray, O red) above a pentacene molecule (C gray; the colored surface represents experimental data.

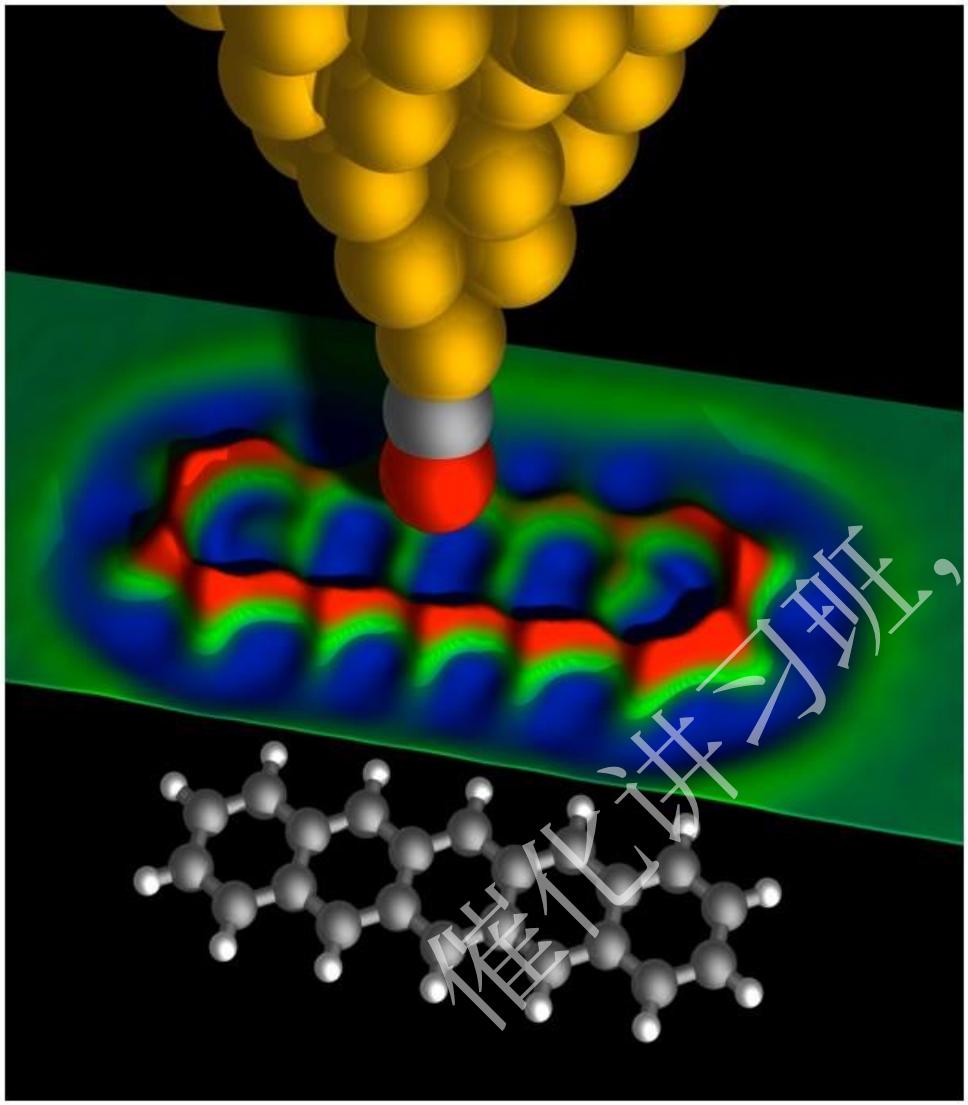

Imaging the chemical structure of molecules with atomic resolution was achieved by probing the short-range chemical forces via noncontact atomic force microscopy (NC-AFM). Our low-temperature STM/AFM is based on a qPlus sensor design [1] and is operated in an ultrahigh vacuum at a temperature of 5 K.

The key step to achieving atomic resolution on molecules is the functionalization of the microscope's tip apex with suitable, atomically well-defined terminations, such as CO molecules (see schematic image). In this case, atomic manipulation techniques are essential for the controlled buildup of the tip used for AFM imaging.

Density functional theory (DFT) calculations are performed to elucidate the physical origin of the observed atomic contrast. The calculations reveal that the Pauli repulsion is the source of the atomic resolution, whereas van der Waals and electrostatic forces only add a diffuse attractive background [2].

References
[1] F. J. Giessibl, Appl. Phys. Lett. 76, 1470 (2000).
[2] L. Gross, F. Mohn, N. Moll, P. Liljeroth, G. Meyer, Science 325, 1110 (2009).

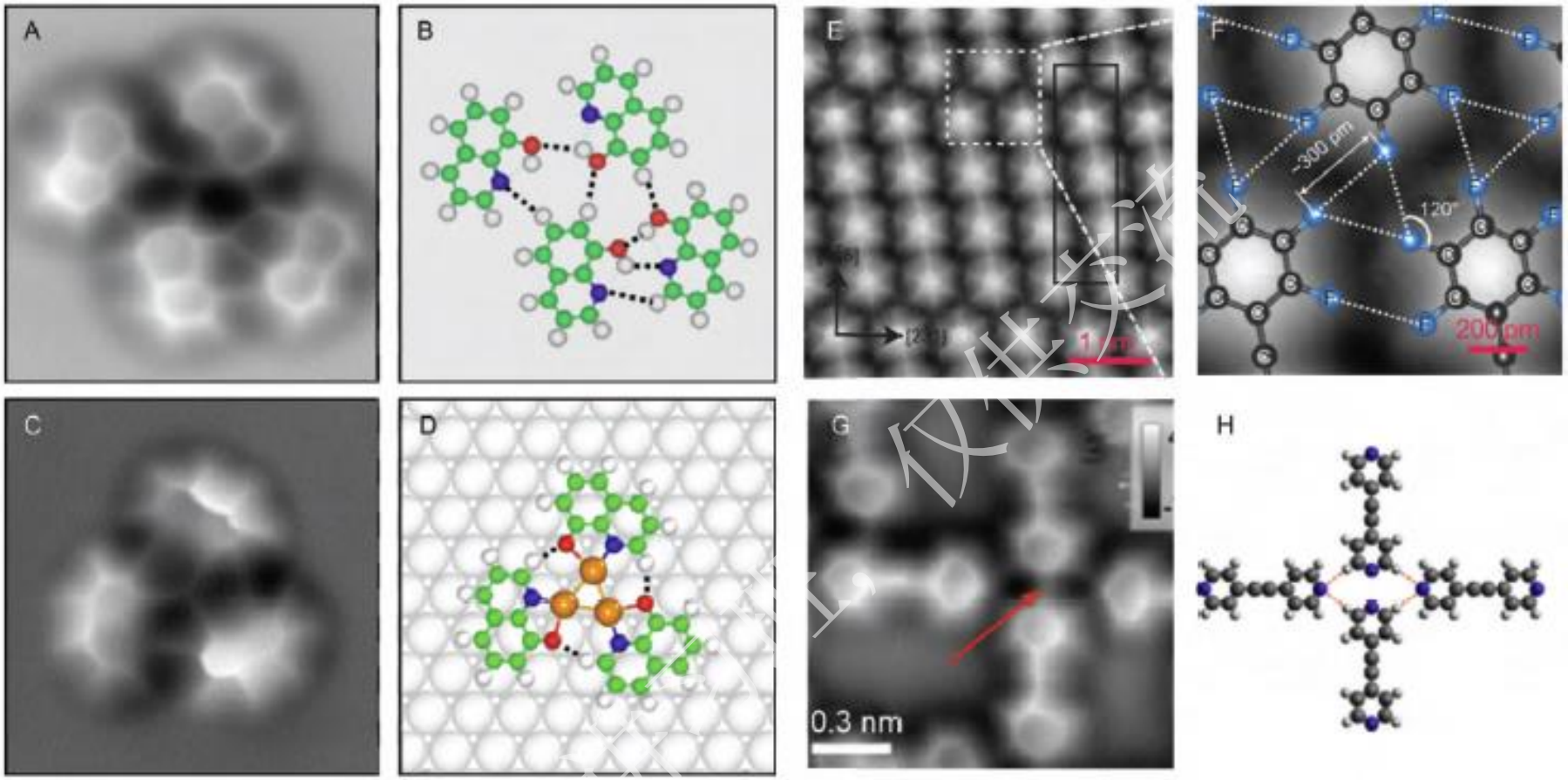

图3　分子间化学键高分辨成像

Fig.3　High resolution imaging of the intermolecular chemical bonds

(A, B) constant-height NC-AFM image of typical 8-hydroxyquinoline (8-hq) molecule-assembled clusters (CO-tip) and the corresponding structure model; (C, D) constant-height NC-AFM image (CO-tip) and the corresponding density functional theory (DFT) calculated structure models of trimer (Cu3q3) complexes (q, dehydrogenated 8-hq)[18]; (E) constant-height NC-AFM image of the self-assembly fluoro-substituted phenyleneethynylene (BPEPE-F18), taken with a CO-terminated tip. The unit cell is shown by a black rectangle; (F) magnified NC-AFM image with a superimposed stick-and-ball drawing of the molecules[19]; (G) AFM image of the bis(para-pyridyl)acetylene (BPPA) tetramer taken with a CO terminated tip showing apparent intermolecular bonds; (H) schematic of the BPPA tetramer[21]

金属团簇的原子分辨

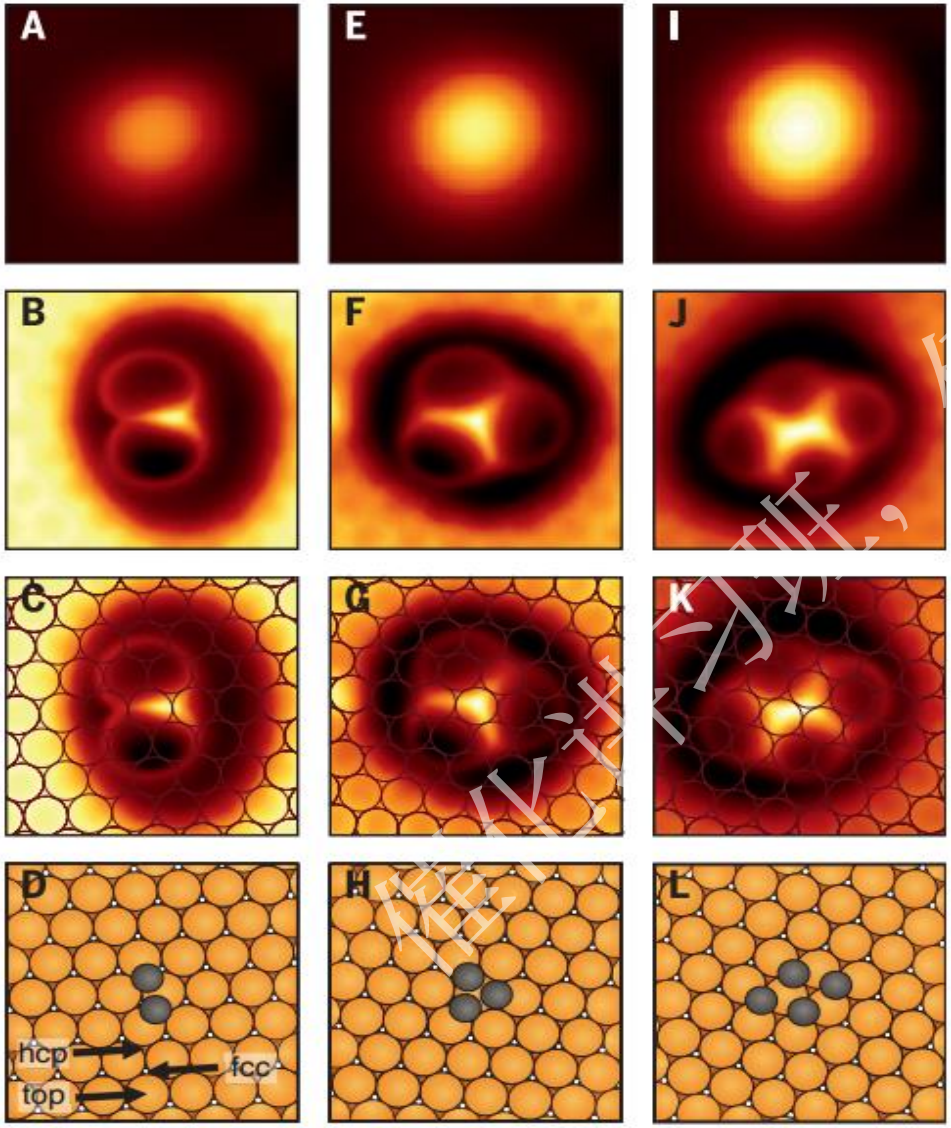

铁原子的双聚体，三聚体和四聚体的图像以及计算的吸附位点。(A),(E)和(I)是恒流STM图像。(B),(F)和(J)是AFM的频率偏移图像。(C),(G)和(K)中用黑色圆圈显示表面Cu原子的信号。最后一排(D),(H)和(L)给出了吸附位点，对于二聚体吸附于两个相邻的桥位。三聚体也吸附于桥位附近，中心为顶位。四聚体吸附在fcc位点[29]。

反应中间体的识别

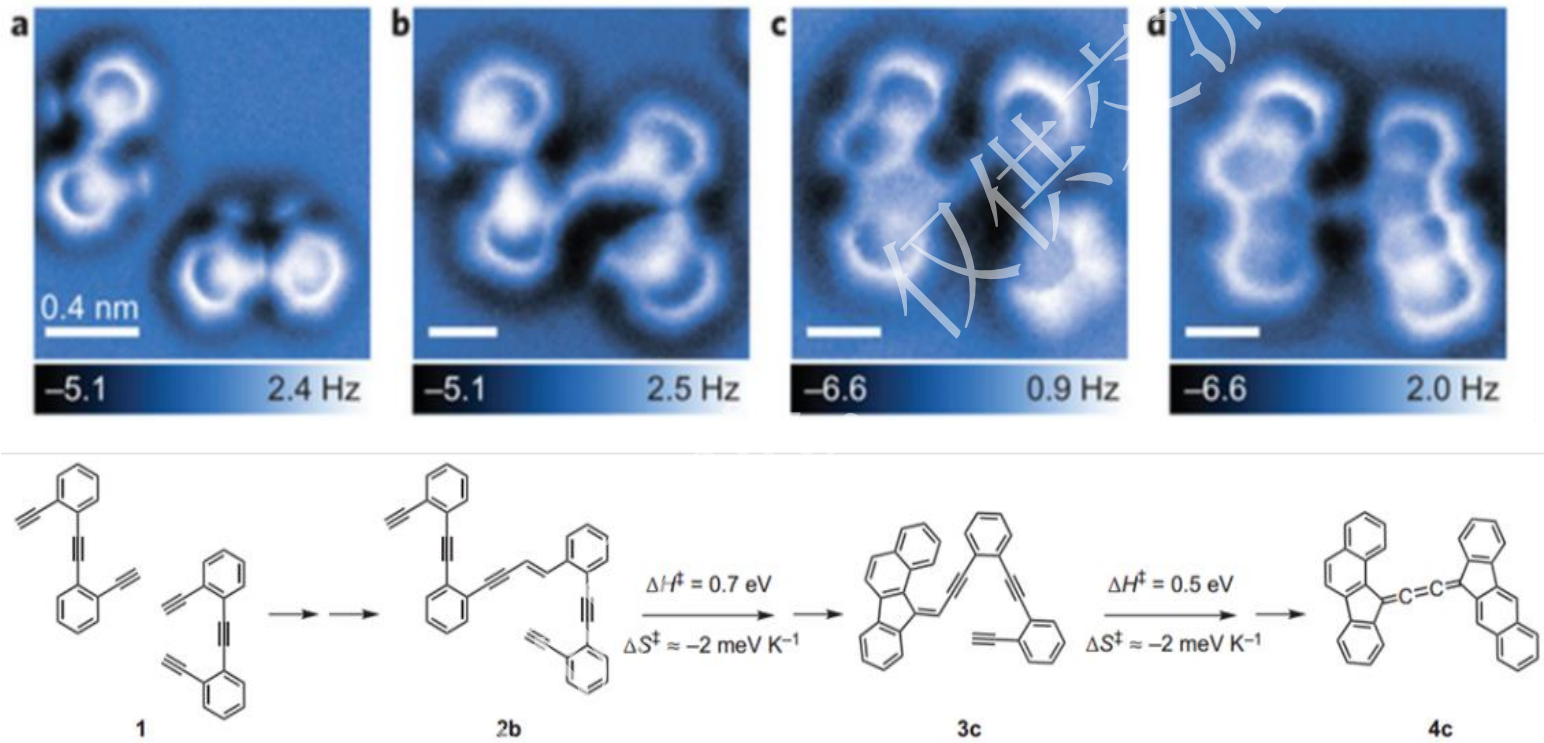

双分子烯二炔偶联和环化反应的逐步过渡中间态的实验观测。a-d，恒高nc-AFM图像，显示从1到4c的反应路径。相应的化学结构示于图像的下方。图中还给出了理论计算得到的反应焓变和活化熵值。

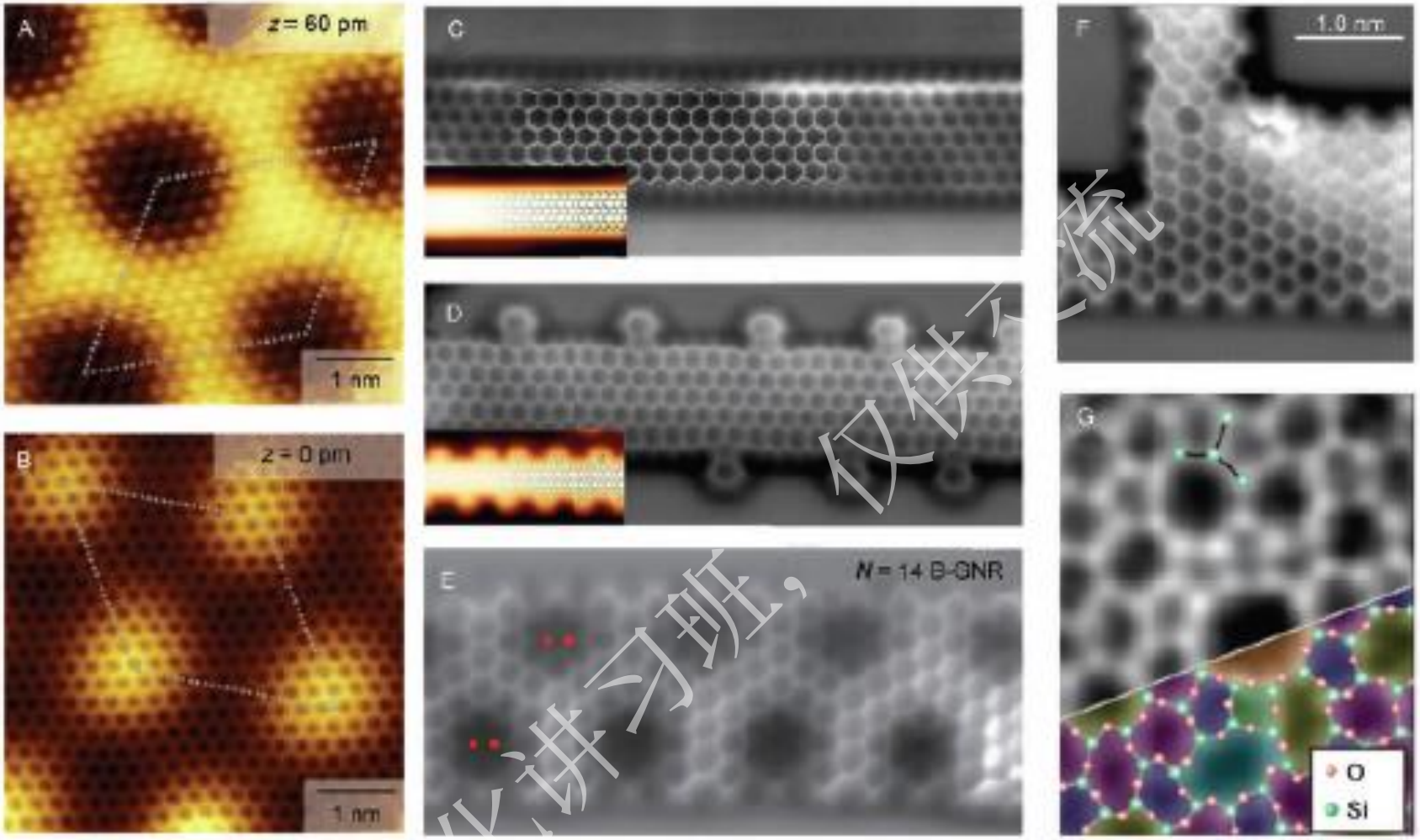

图6　qPlus NC-AFM 在低维纳米材料中的应用

Fig.6　Applications of qPlus NC-AFM in low dimentional nanomaterials

(A, B) constant-height NC-AFM images of epitaxial graphene on Ir(111) with a metallic tip and CO tip, respectively[62]. (C) constant-height NC-AFM image taken with a CO tip. Intra-ribbon resolution shows the formation of 6-zigzag graphene nanoribbons (6-ZGNRs) with atomically precise CH edges. (D) constant-height NC-AFM image of edge-modified ZGNR[62]. (E) constant-height NC-AFM image of fused n = 14 B-GNR[63]. (F) constant-height NC-AFM image of the junction between two 7-armchair graphene nanoribbons (7-AGNRs) and one 14-AGNR[64]. (G) NC-AFM image representing a single atomically resolved constant-height measurement of two-dimensional silica[65]

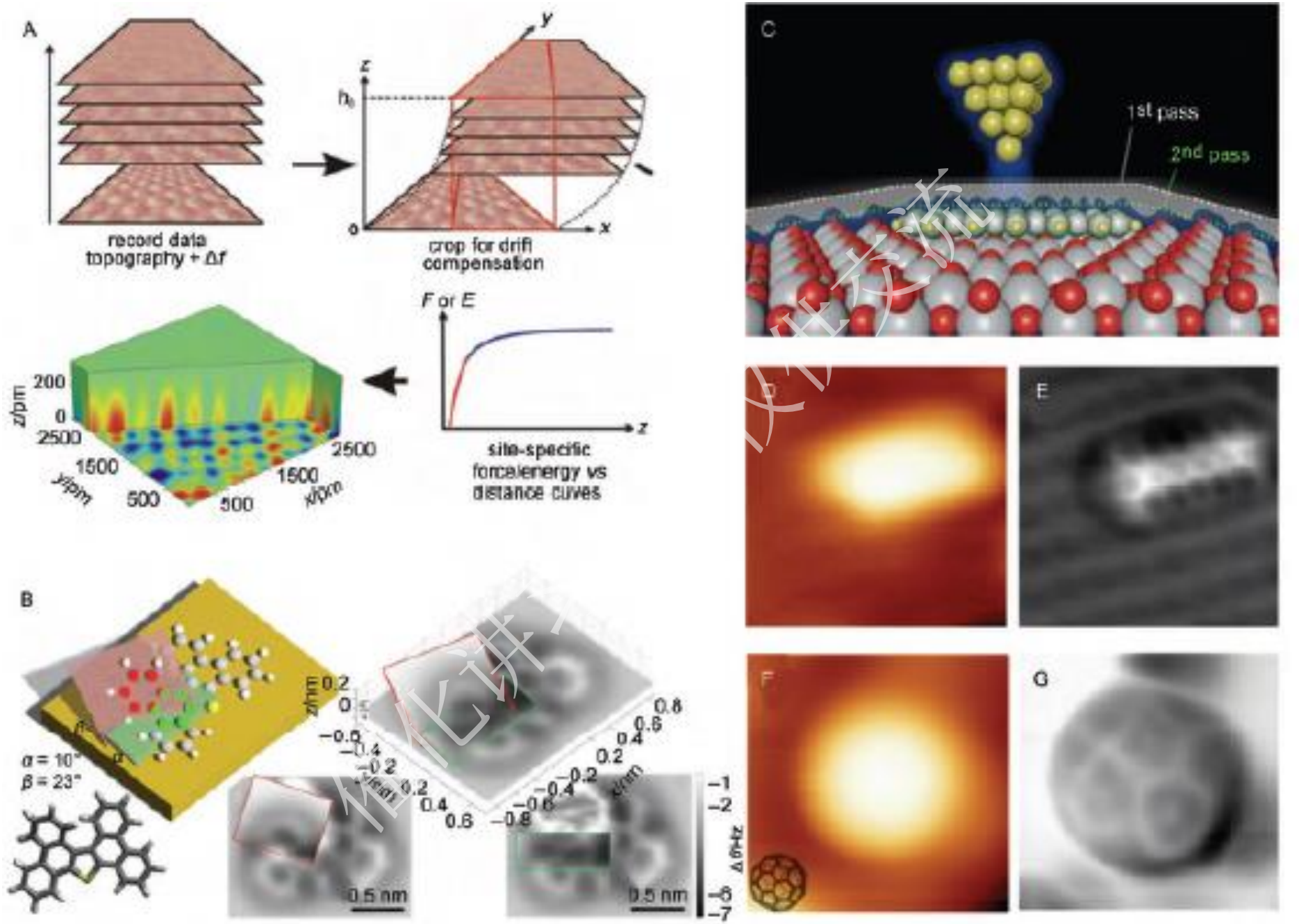

图8　qPlus NC-AFM的三维成像

Fig.8　3D imaging of qPlus NC-AFM

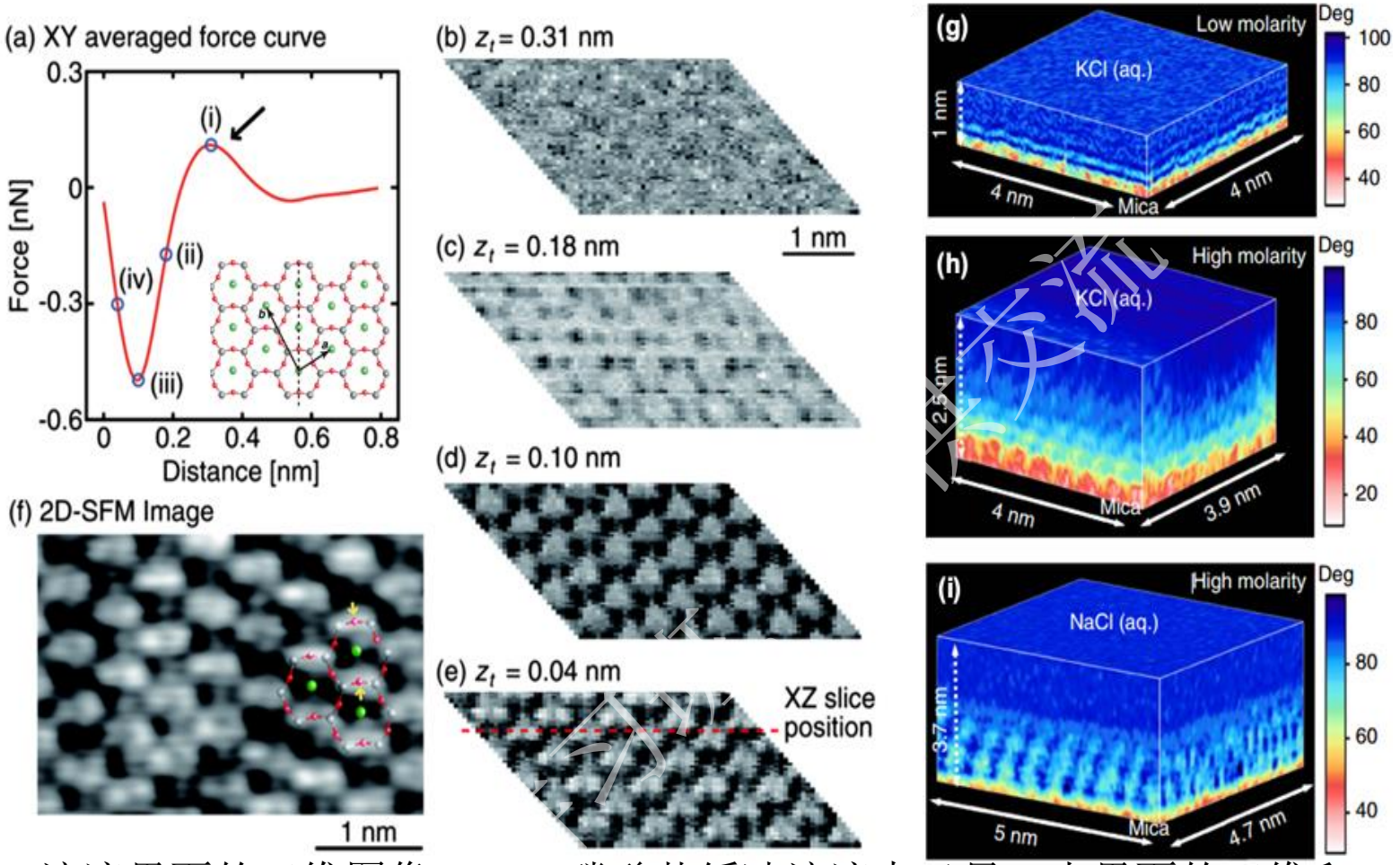

云母—溶液界面的三维图像。(a~e)磷酸盐缓冲溶液中云母—水界面的三维和二维原子力图像。(a)XY 方向平均的力学曲线，插图为云母表面的。(b~e)三维AFM图像中不同高度(0.31nm, 0.18nm,0.10nm和0.04nm)的XY平面的截面图，分别对应于(a)中曲线的(i)~(iv)点。(e)中虚线显示XZ方向界面图分析的位置(见文中)。(f)另一针尖获得的二维图像。（g）0.2M KCl水溶液三维AFM图像。图中显示了表面吸附的K^+离子单层(红色),其顶端有两层水合层(带状条纹)。水合层约0.3nm厚，随表面起伏而排列。(h) 4M KCl水溶液,云母—水的界面。此界面层分为两个区域，表面的2nm厚的有序液相层和体相溶液层。（i）原子级有序的云母—NaCl溶液界面[35]。

Contact Potential

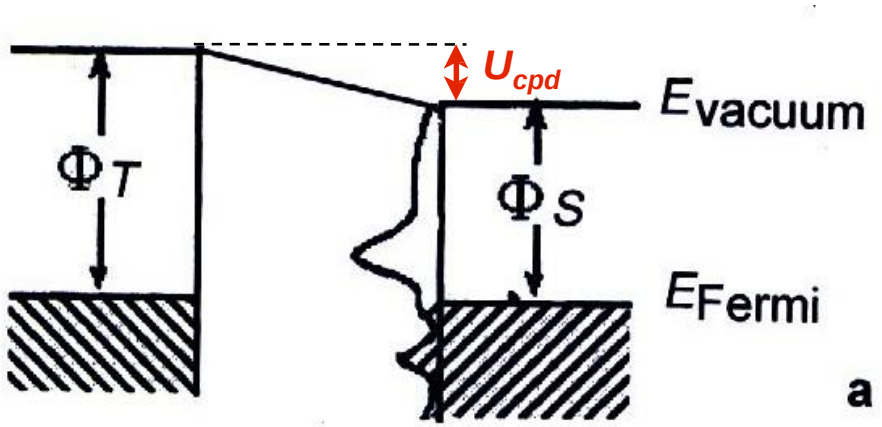

Band alignment under zero sample bias.

The Fermi levels match, no net tunnel or contact current is flowing.

A contact potential U_{cpd} is established

Quadratic dependence of measured force or here frequency shift on tip-sample bias

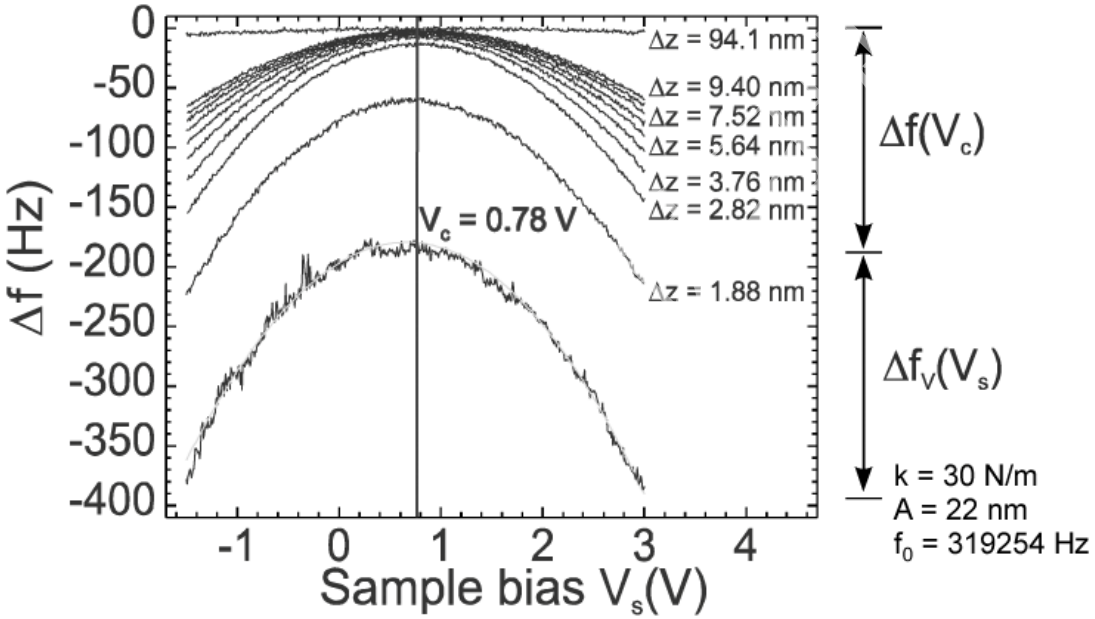

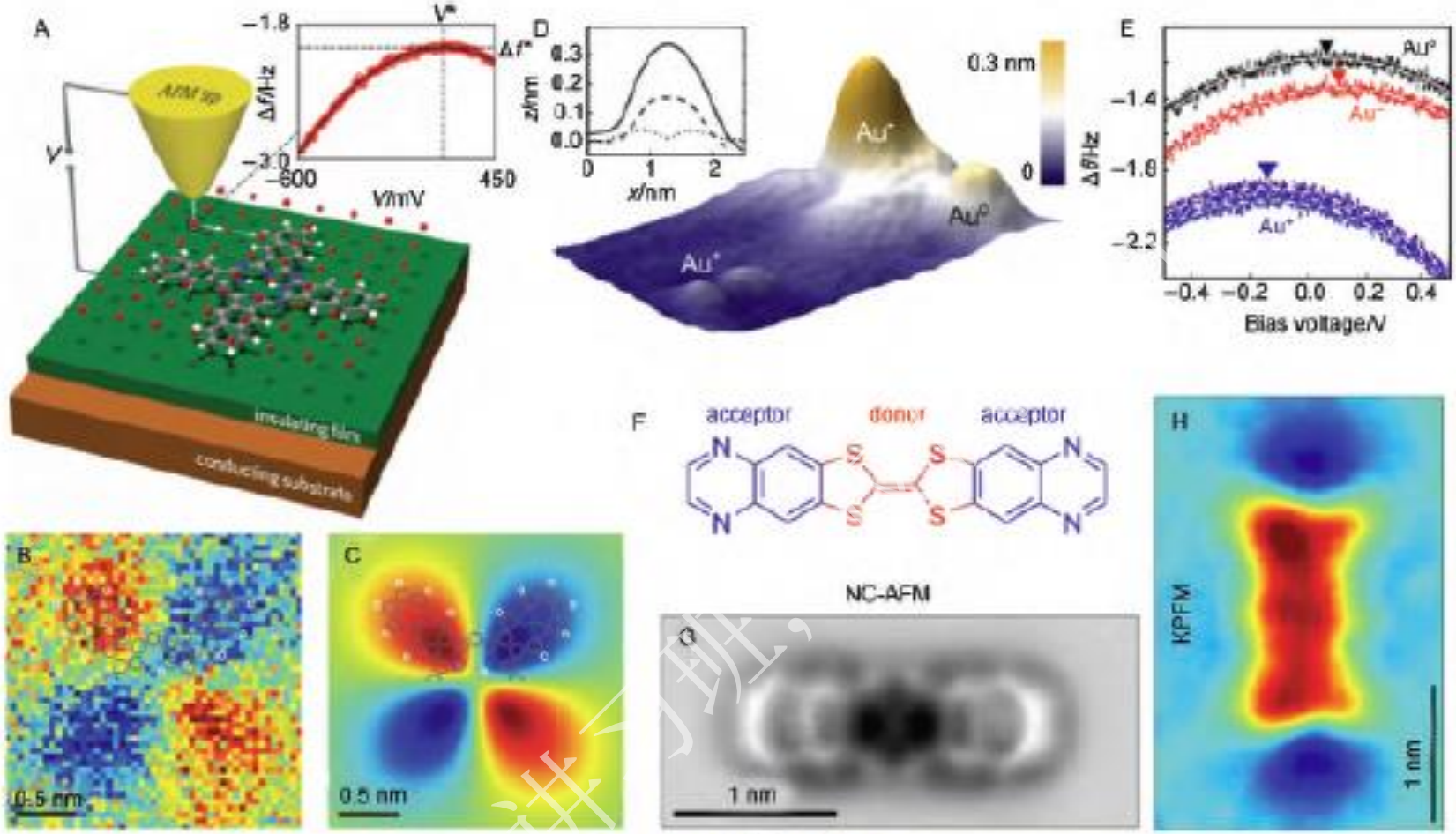

图9　表面电荷分布测量

Fig.9　Measurements of the surface charge distribution

(A) schematic of the measurement principle. At each tip position, the Δf is recorded as a function of the sample bias voltage (inset, red circles). The maximum of the fitted parabola (inset, solid black line) yields V* and Δf* for that position. The images were recorded with a copper-terminated tip on a 64 × 64 lateral grid at constant height; (B) local contact potential difference (LCPD) images of naphthalocyanine on NaCl(2 ML)/Cu(111); (C) DFT-calculated asymmetry of the *z*-component of the electric field above a free naphthalocyanine molecule at a distance d = 0.5 nm from the molecular plane[45]. (D) 3D constant-height NC-AFM image of three Au adatoms on a NaCl(10 ML)/Cu(111) film with charge states neutral, positively. charged, and negatively charged. Height profiles are shown in the inset figure (solid line: Au^-, dashed line: Au^0, dotted line: Au^+). (E) charge-state readout by recording Δf(V) spectra (dots) and determining the LCPD (triangles) from fitted parabolas (dashed lines)[47]. (F) model of tetrathiafulvalene-pyrazine$_2$ (TTF-PYZ_2) with the donor part in red and the acceptor part in blue; (G) constant-height NC-AFM image of TTF-PYZ_2 in the "down" conformation with a CO tip. (H) LCPD (V*) maps of TTF-PYZ_2 in the "down" conformation with a CO tip[48]; color online

扫描探针与光谱的结合

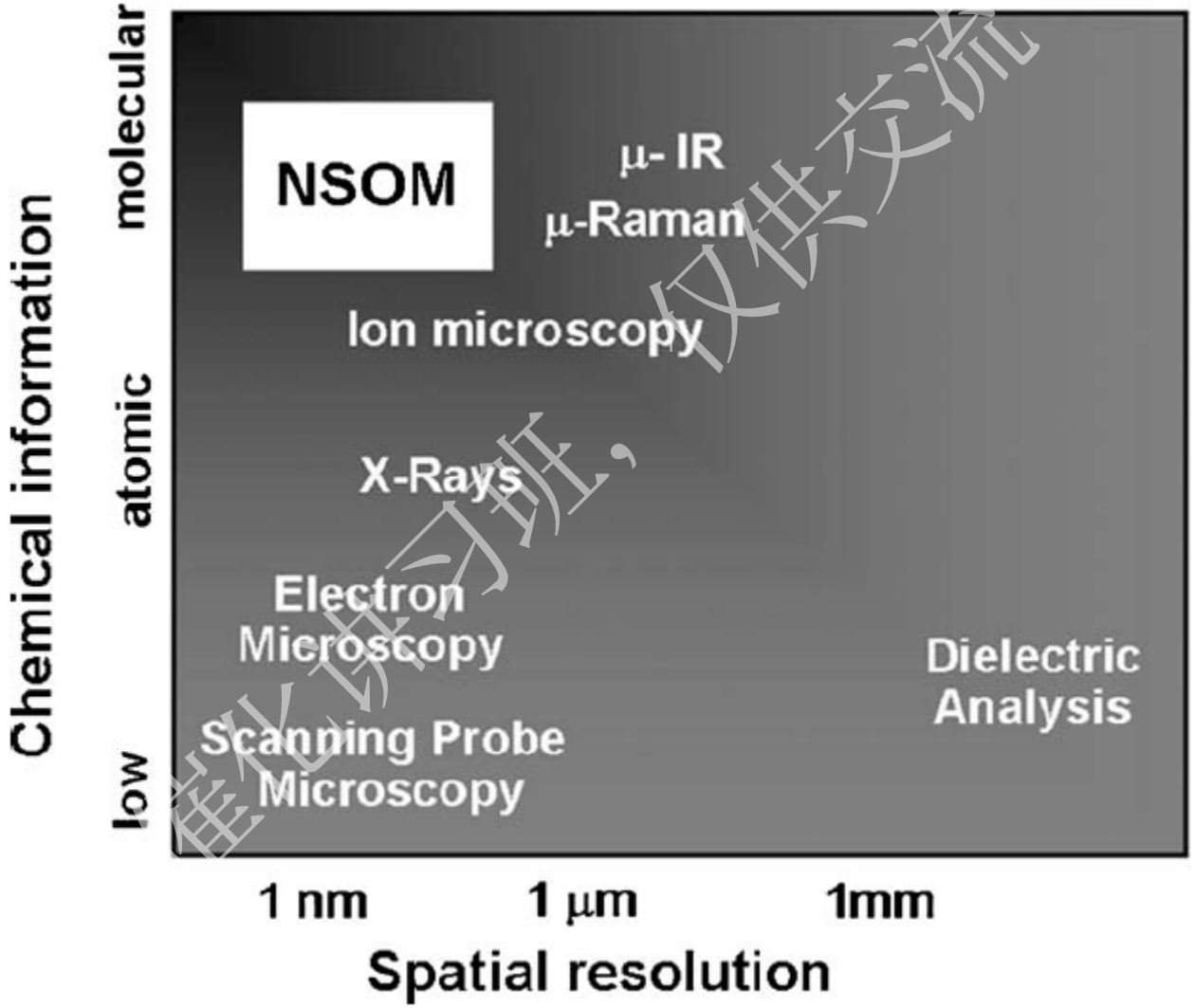

Stranick, NIST

光学衍射极限

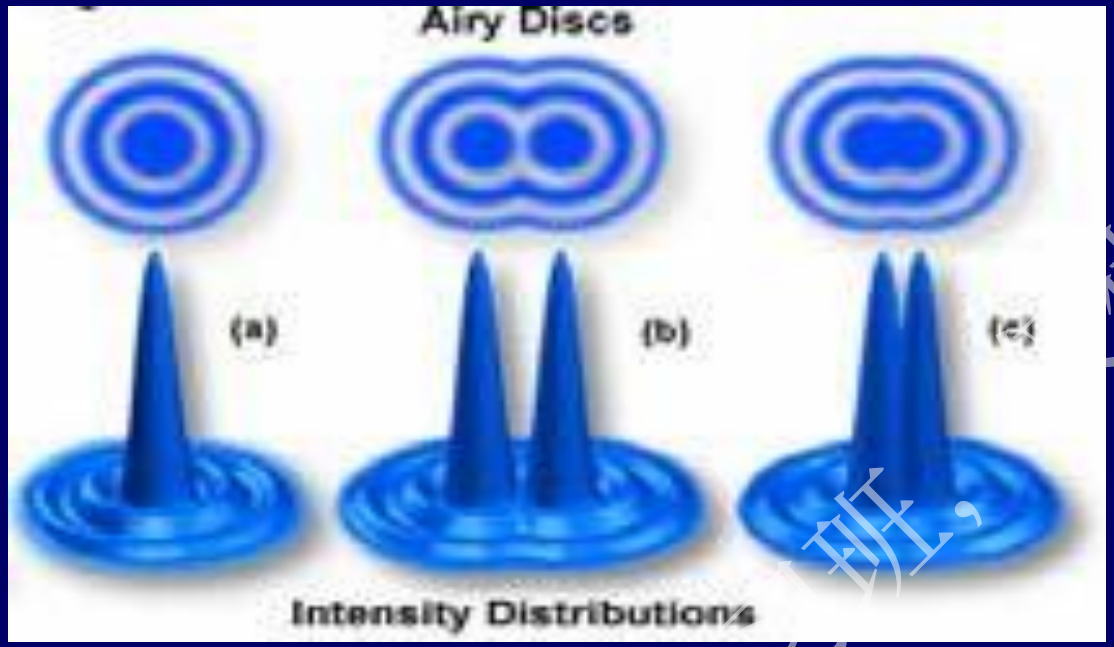

点光源衍射斑（*Airy*斑）的空间分辨：

(a) 单个点光源夫琅和费衍射形成的照度分布
(b) 两个相互接近的相同点光源形成的总照度分布
(c) 两点光源像恰好分辨时，照度中心极小值为最大值的74%（*Rayleigh*判据）

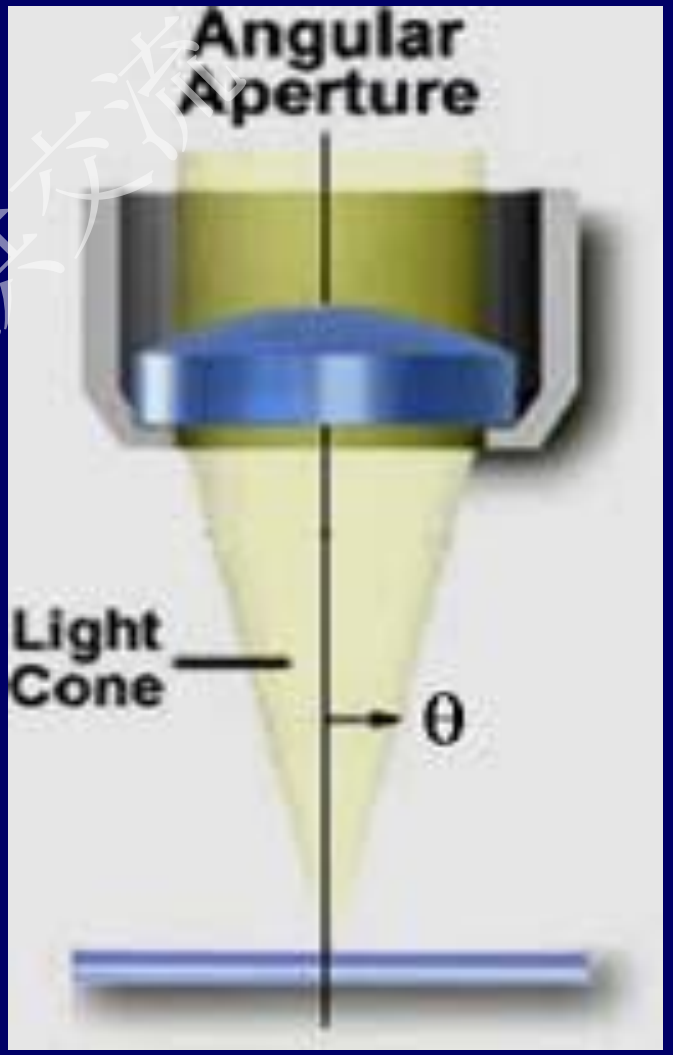

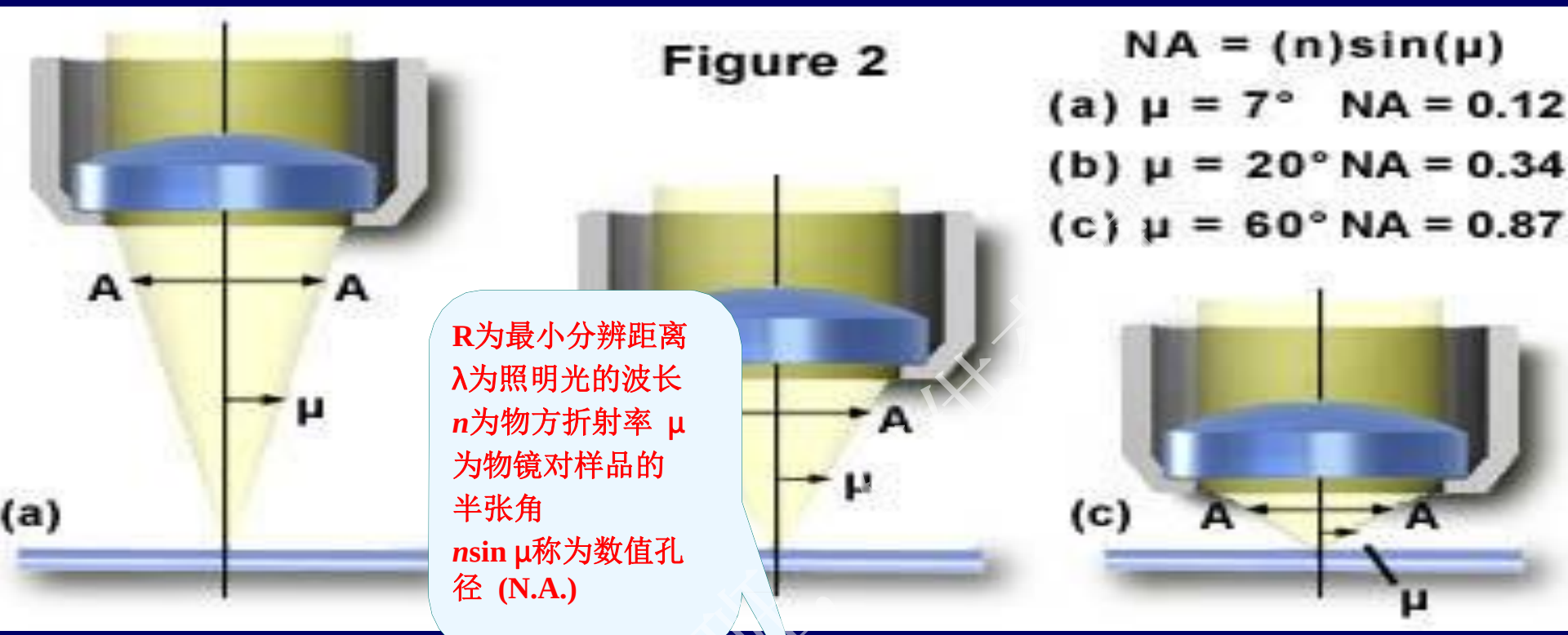

R为最小分辨距离
λ为照明光的波长
*n*为物方折射率 μ为物镜对样品的半张角
*n*sin μ称为数值孔径 (N.A.)

光学显微的分辨本领

Numerical Aperture

$R = 0.61\lambda / NA \quad (NA = n\sin\mu)$

提高常规光学显微镜的分辨本领：

（1）减小照明光波长λ　　（2）增大数值孔径N.A.

若N.A.为1.2，入射波长 为500nm，则分辨率 250nm

提高光学显微镜的分辨本领：减小照明光波长λ，或增大数值孔径N.A.。最好的油浸式显微镜的N.A.也不过1.5左右。
假如使用500nm的入射波长，仅可以得到200nm的分辨率。

共焦光学显微镜的空间分辨率也只能达到约0.15 μm

电子：
波长(0.0037nm -- 100Kev) 远小于光波长，成像分辨率达到10^{-1}nm的量级

电子显微镜需要高真空，不能用来观察处于 空气和液体中的样品。并且，电子显微镜亦不能用于样品光学性质的研究，其高能电子束也会对有活性的生物样品造成损伤。

- 1928年，Synge提出用亚波长的小孔在样品表面扫描，可 以获得亚波长的分辨率。
- 1972年，Ash和Nicholls首先在微波波段实现了λ/60的分辨率。

1928年	**Sir Synge**	用一个比衍射极限小的孔紧贴物体表面指出有可能得到比衍射极限分辨率高的光学图象，　困难在于：小孔的制造和弱光的检测
1972年	**Ash & Nichols**	λ=　3cm 的微波得到λ/60 的分辨率
1980年	**D.W.Pohl IBM Zurich)**	STM技术镀上金属的石英针尖 得到了近场光学图象
1986年	**A.Harootunian (Cornell University)**	用光纤拉制探光小孔
1991年	**Betzig AT&T Bell Lab**	镀上金属铝的光纤针尖得到 λ/20 的光学分辨率，　突破了光学显微镜的衍射极限

近场光学的发展历史

- **1984** 光纤式**SNOMs**成像技术 （光学信息）
- **1999** 散射式近场光学**s-SNOM**成像技术 （光学信息）
- **2010** 纳米红外**PTIR**技术**---**成像和光谱 （化学信息）
- **2012** 散射式**s-SNOM**光谱技术 **(**化学信息）

Scanning Near-Field Optical Microscopy (SNOM)

- An SPM technique that examines the *near-field* or *evanescent* light reflecting off a surface.
- The Rayleigh criterion that limits standard *far-field* or *propagating* optical microscopy does not apply to evanescent light.
- Evanescent light is confined close to the surface.
  - Imaginary wave vector; it cannot propagate through space like far-field light.
  - Intensity falls off exponentially with distance from emitter.
  - Often thought as ‘photon tunnelling’.

How to Detect Evanescent Light

- Firstly, surface has to be illuminated.
- In order to detect the evanescent waves, a ‘nano-probe’ needs to be brought into the evanescent field.
- The atoms in the probe absorb evanescent photons and re-radiate propagating photons.
- These photons can be collected conventionally using a lens or CCD, etc.
- The diagram summarises this:

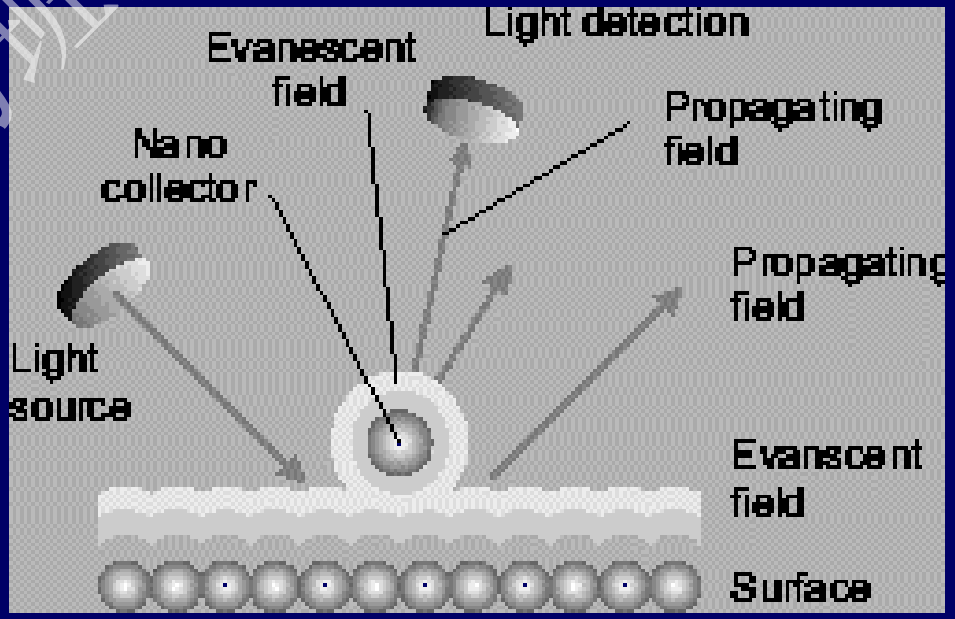

Different types of nano-probe: 1

- There are two main types of nano-probe used to convert the evanescent light
- Type 1: Standard STM tungsten tip
  - Known as the *'aperture**less**'* method.
  - Tip is excited by evanescent light.
  - Tip then re-radiates propagating light that can be detected away from the tip.
  - Good in principle, but it is hard to separate the return signal amongst other light that is reflected from the surface.

Different types of nano-probe: 2

- Type 2: Optical fibre tip
  - Known as the *'aperture'* technique.
  - The tip ends in a sub-wavelength sized aperture.
  - Laser light passed down optical fibre illuminates the sample with evanescent light.
  - Same aperture picks up the reflecting evanescent light and converts it into propagating light.
  - Return signal carried up fibre to detector.
  - Better method: picks up return signal close to the surface.

近场光学技术的发展

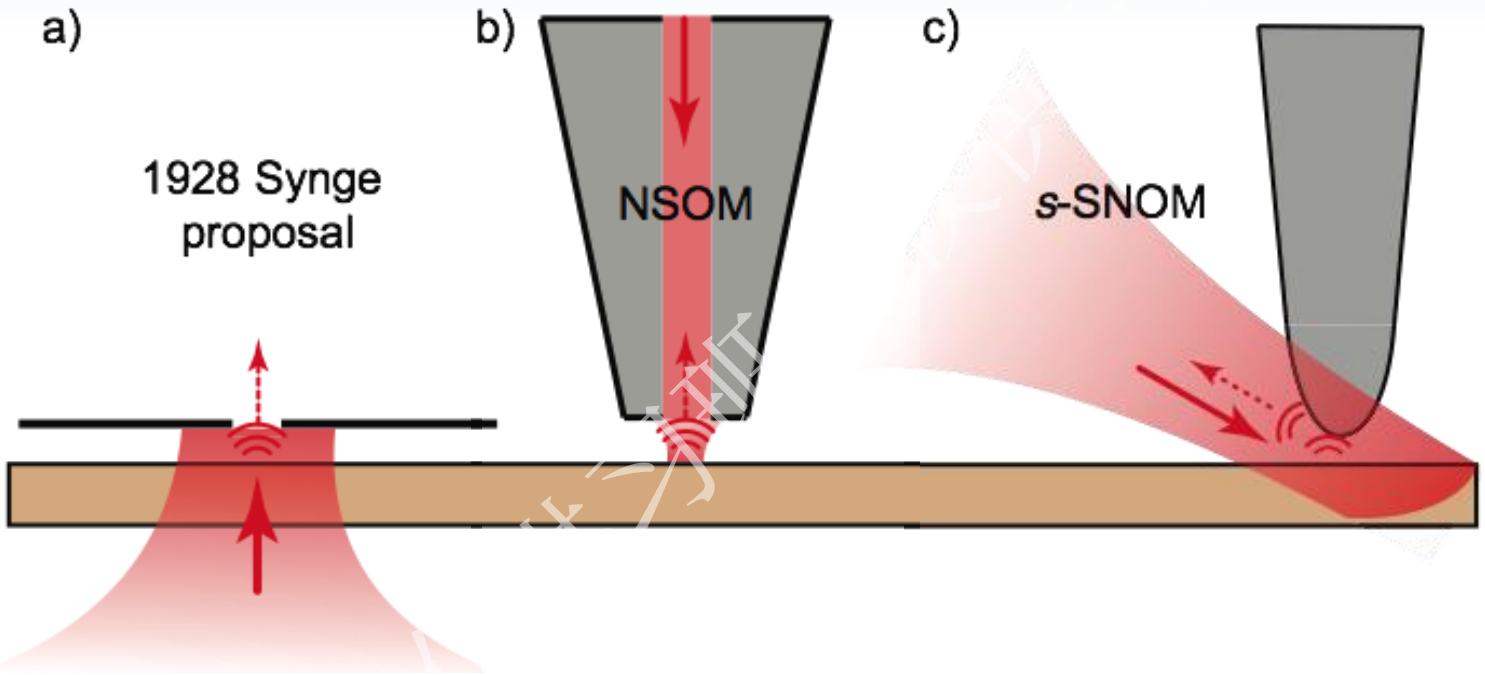

scattering scanning near-field optical microscopy: *s*-SNOM

tip-enhanced microscopy
(tip-enhanced Raman scattering, TERS)

[Pohl, Betzig, Lewis ...]

[Kawata, Hänsch, Novotny, Keilmann, Hillenbrand, Raschke...]

Creating SNOM tips

- STM tip made in conventional way
  - Chemically etched tungsten wire.
- Optic fibre tip: Two methods
  - Either, heat and pull an optic fibre to a sharp point,
  - Or, chemically etch optic fibre to a sharp point.
  - Once a sharpened fibre is produced, it is then coated in a thin layer of aluminium to create a sharply defined aperture.

Pictures of SNOM Aperture Probes

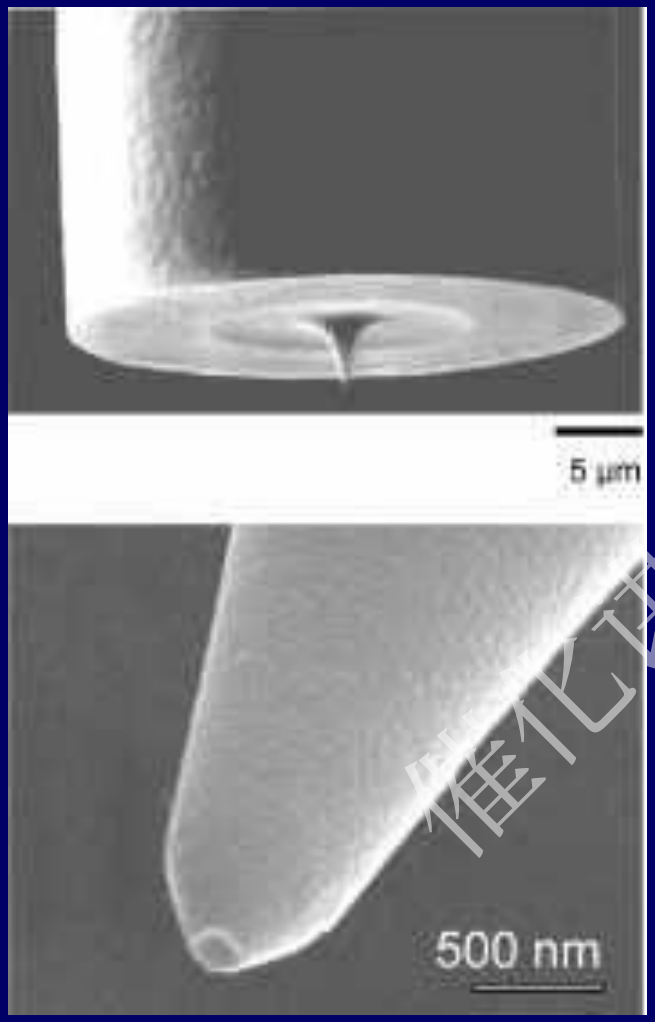

光纤探针的缺点:

50nm的小孔

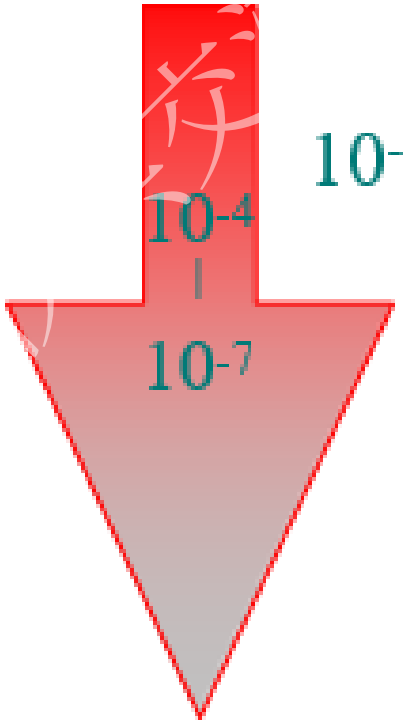

极低的通光量
(low throughput)

低重复性(low reproducibility)

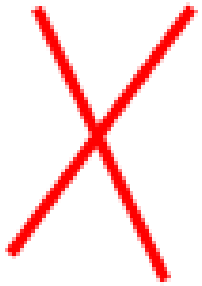

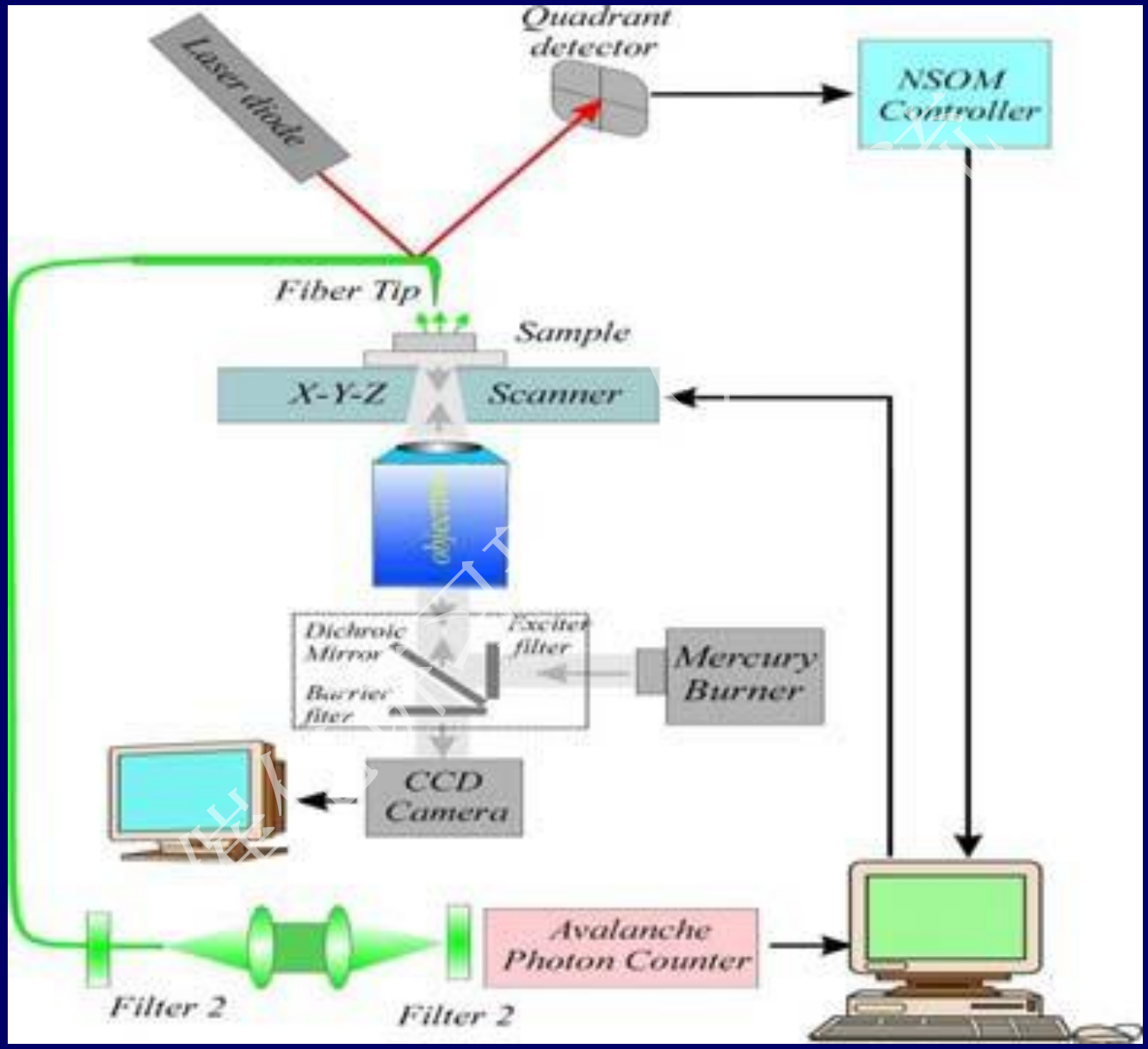
Laser diode
Quadrant detector
NSOM Controller
Fiber Tip
Sample
X-Y-Z
Scanner
Dichroic Mirror
Exciter filter
Barrier filter
Mercury Burner
CCD Camera
Avalanche Photon Counter
Filter 2
Filter 2

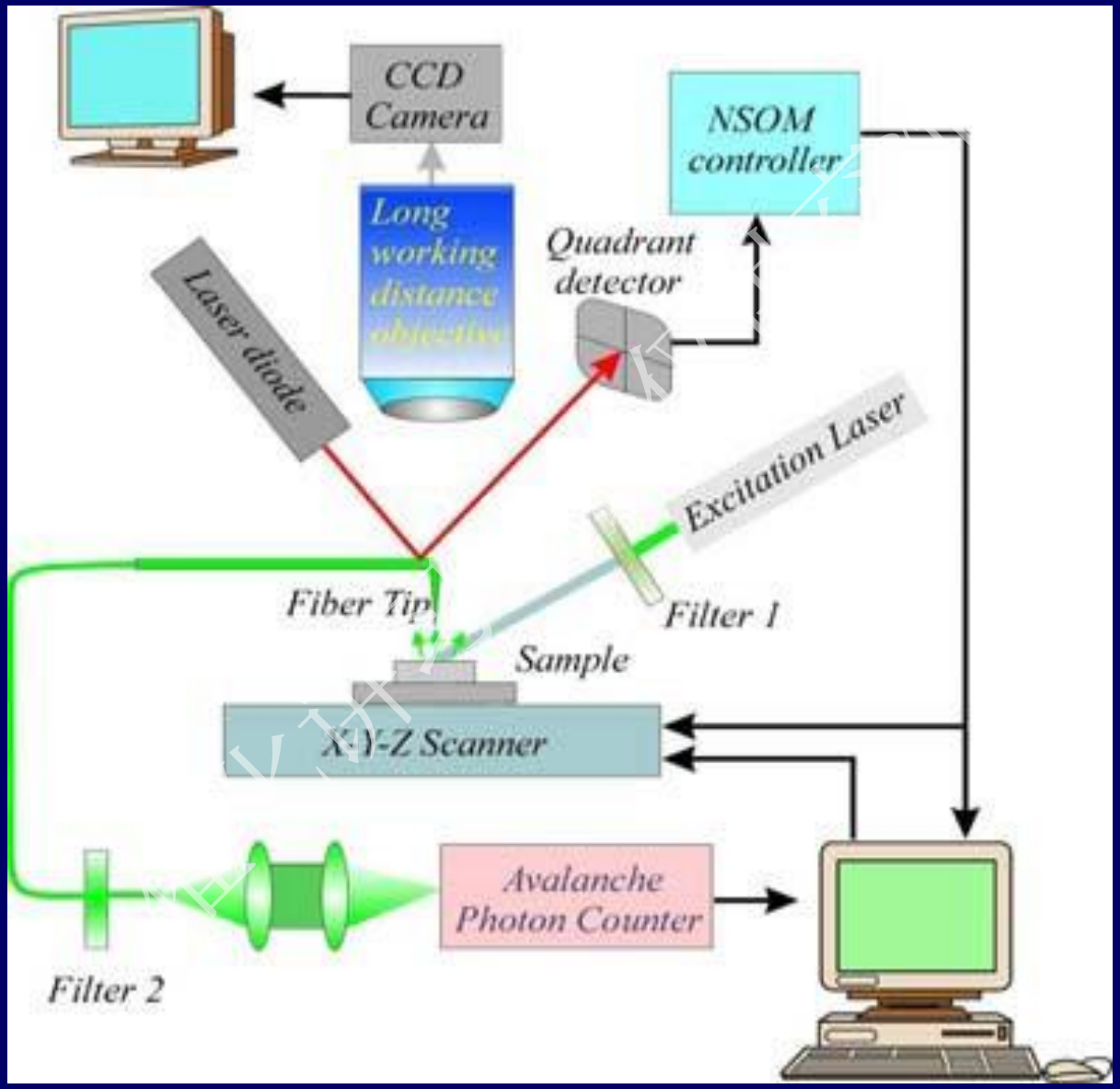
CCD Camera
NSOM controller
Long working distance objective
Quadrant detector
Laser diode
Excitation Laser
Fiber Tip
Filter 1
Sample
X-Y-Z Scanner
Avalanche Photon Counter
Filter 2

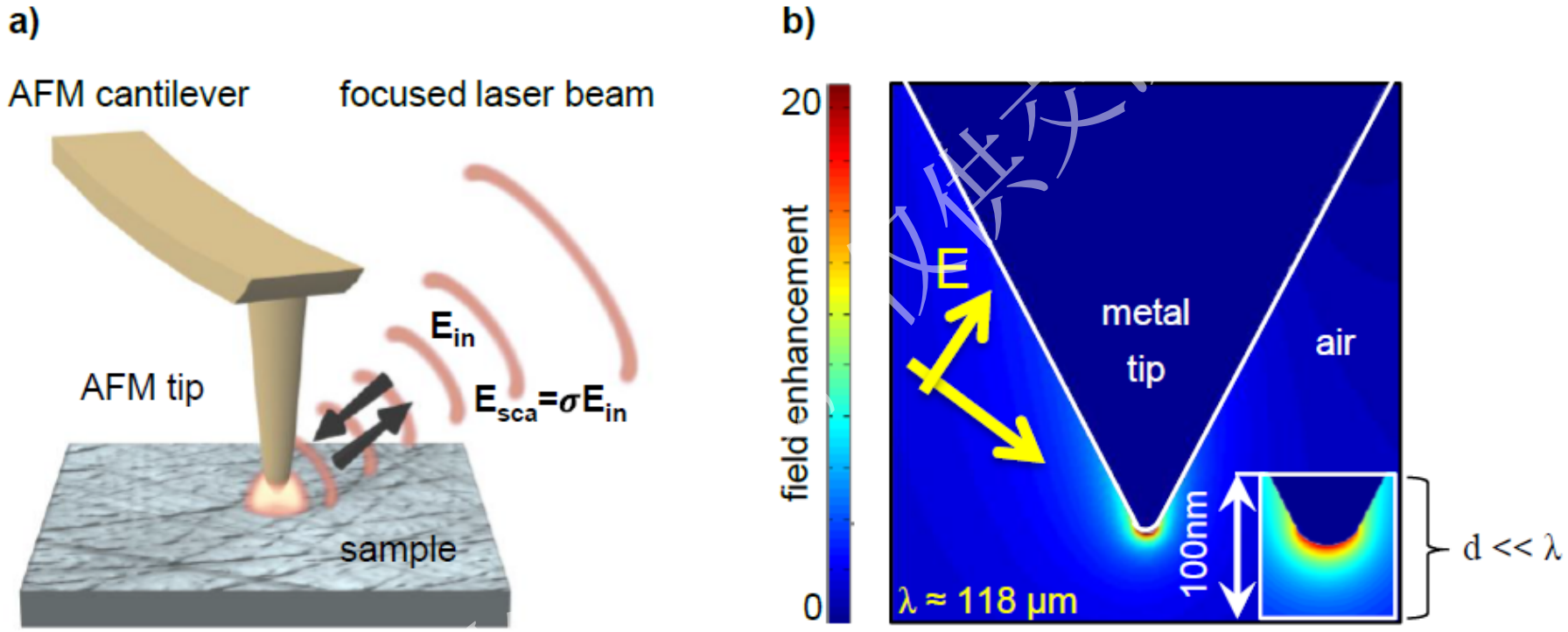

Fig. 4.4 Tip illumination and field enhancement in s-SNOM. **a)** A sharp AFM tip is mounted on a cantilever and illuminated by a focused laser beam. (Image taken from[60]) **b)** Numerical simulation of a metal cone, illuminated by far-infrared light with $\lambda = 118$ µm. (Taken from[8]).

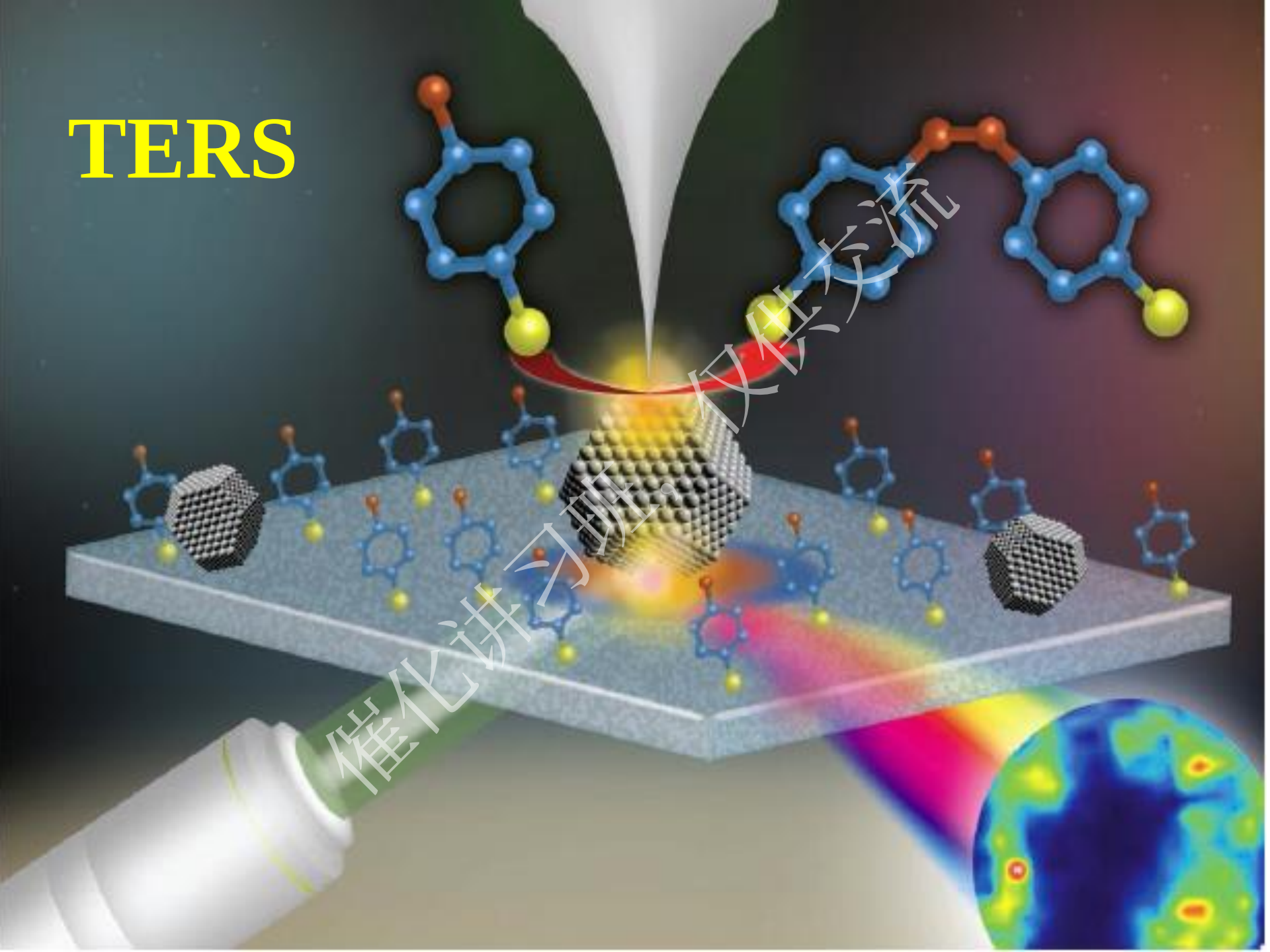

Raman Imaging. . .

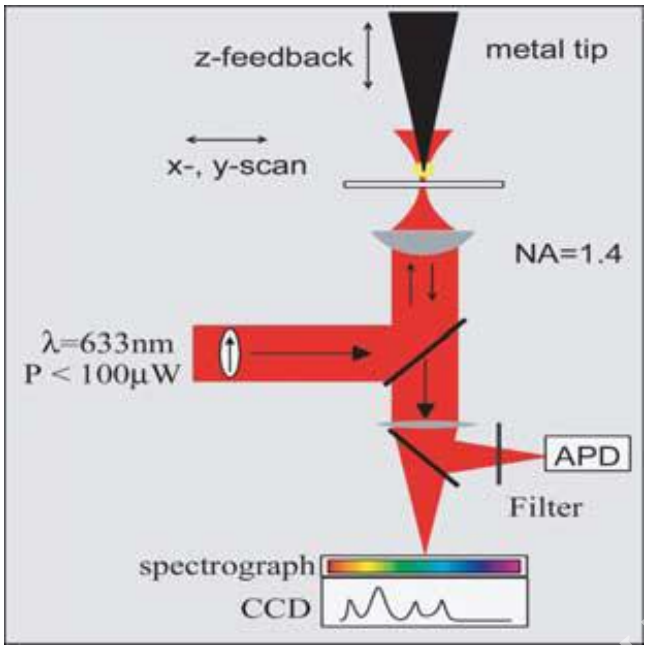

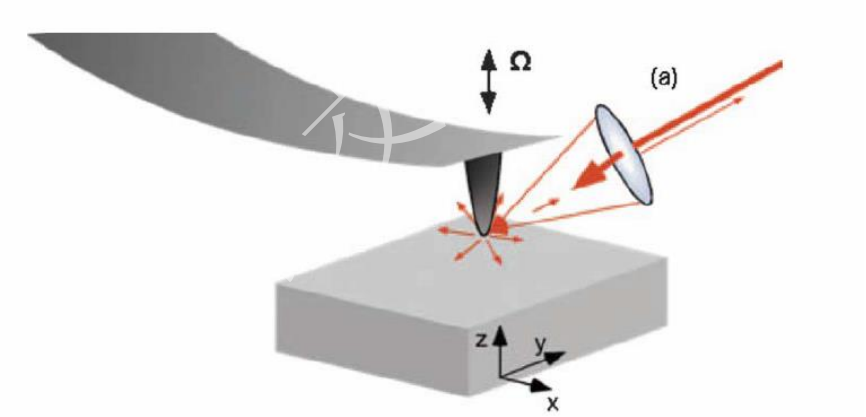

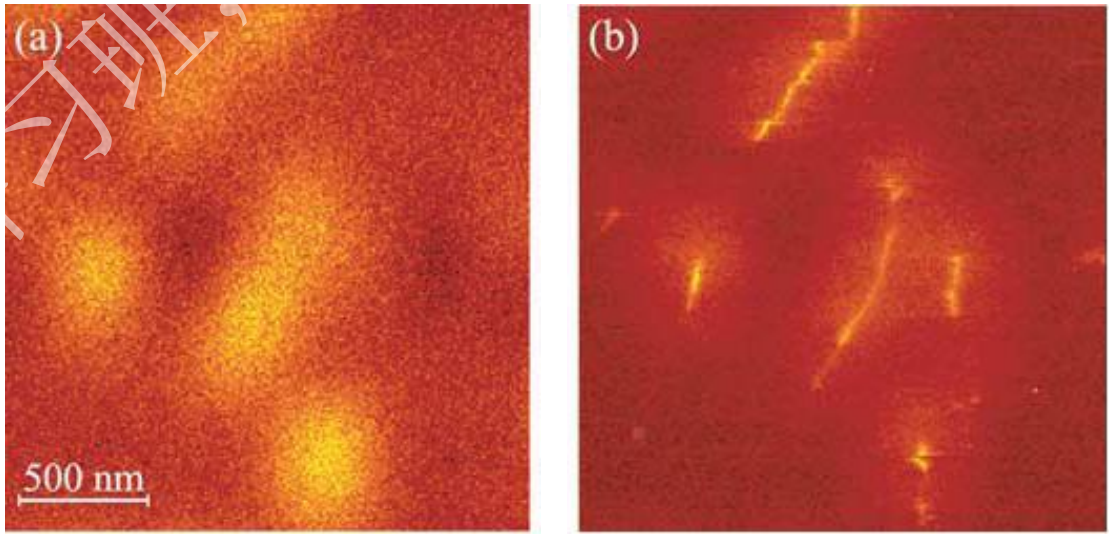

Confocal

Tip enhanced Raman (TERS)

Novotny, U. of Rochester

MWNT's in a polymer film . . .

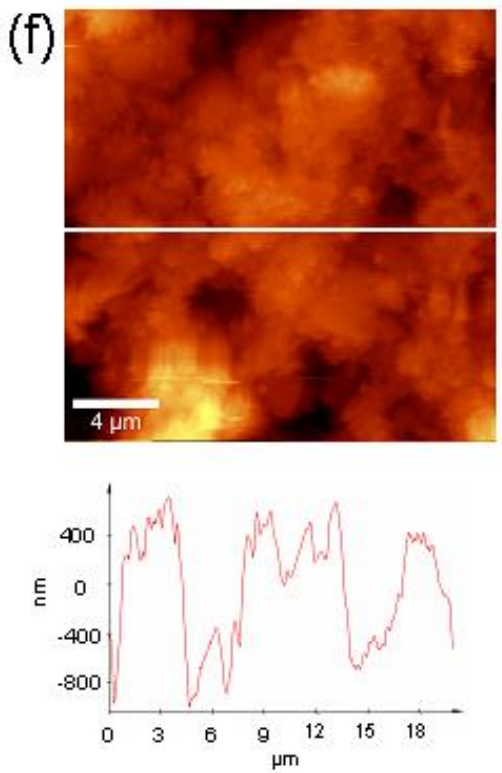

形貌像

20X 0.45 NA

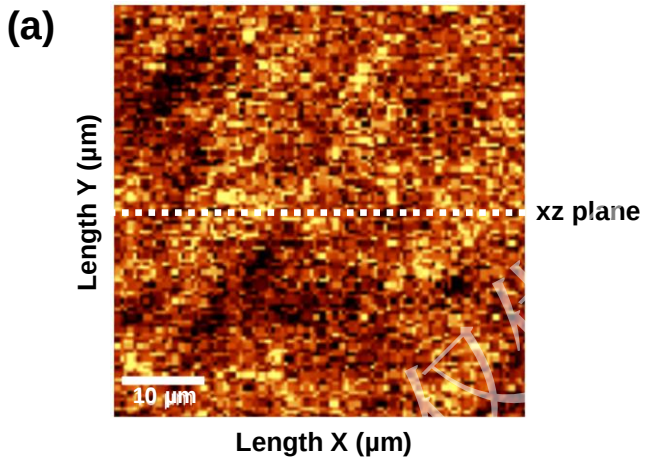

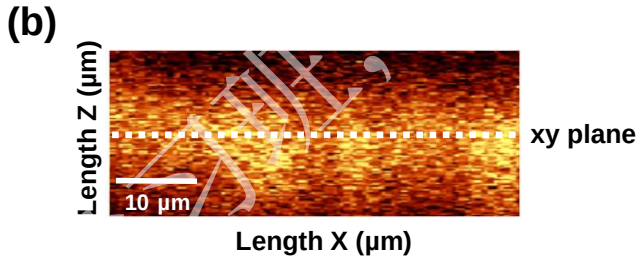

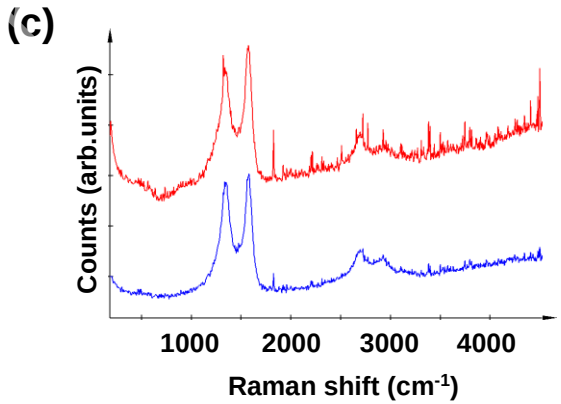

100X 0.9 NA

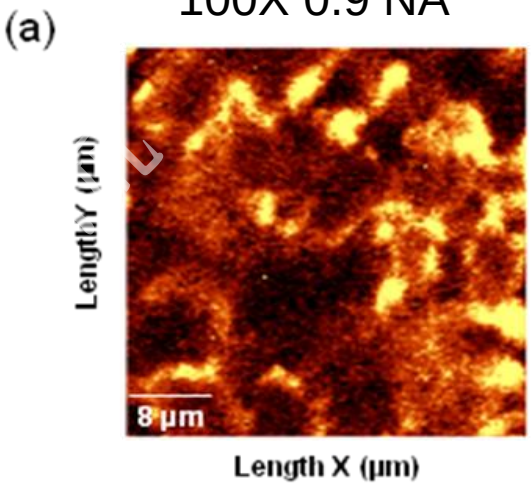

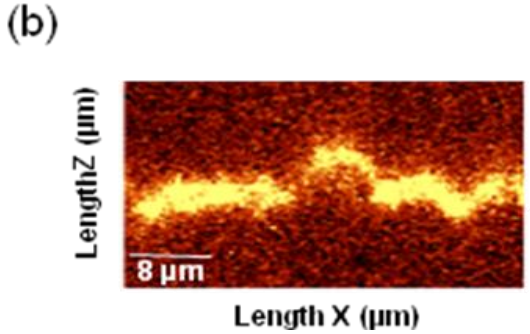

PRL Vol.90, 095503-1 (2003)

nature nanotechnology
LETTERS
PUBLISHED ONLINE: 19 AUGUST 2012 | DOI: 10.1038/NNANO.2012.131

Catalytic processes monitored at the nanoscale with tip-enhanced Raman spectroscopy

Evelien M. van Schrojenstein Lantman[1], Tanja Deckert-Gaudig[2], Arjan J. G. Mank[1,3], Volker Deckert[2,4]* and Bert M. Weckhuysen[1]*

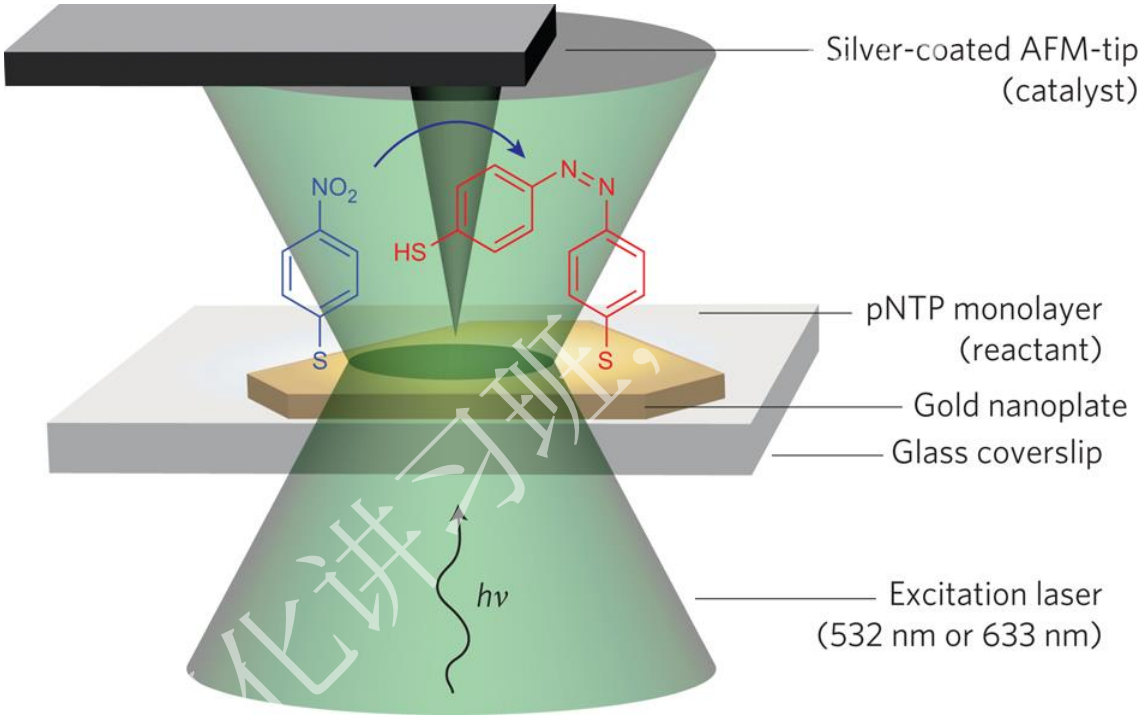

TERS用于催化反应表征示意图。pNTP形成单分子层作为反应物。光激发和光谱收集从底部进行。银涂覆AFM针尖充当催化剂，催化pNTP生成DMAB的光反应；同时也提供了TERS的增强电磁场。

nature nanotechnology

LETTERS

PUBLISHED ONLINE: 19 AUGUST 2012 | DOI: 10.1038/NNANO.2012.131

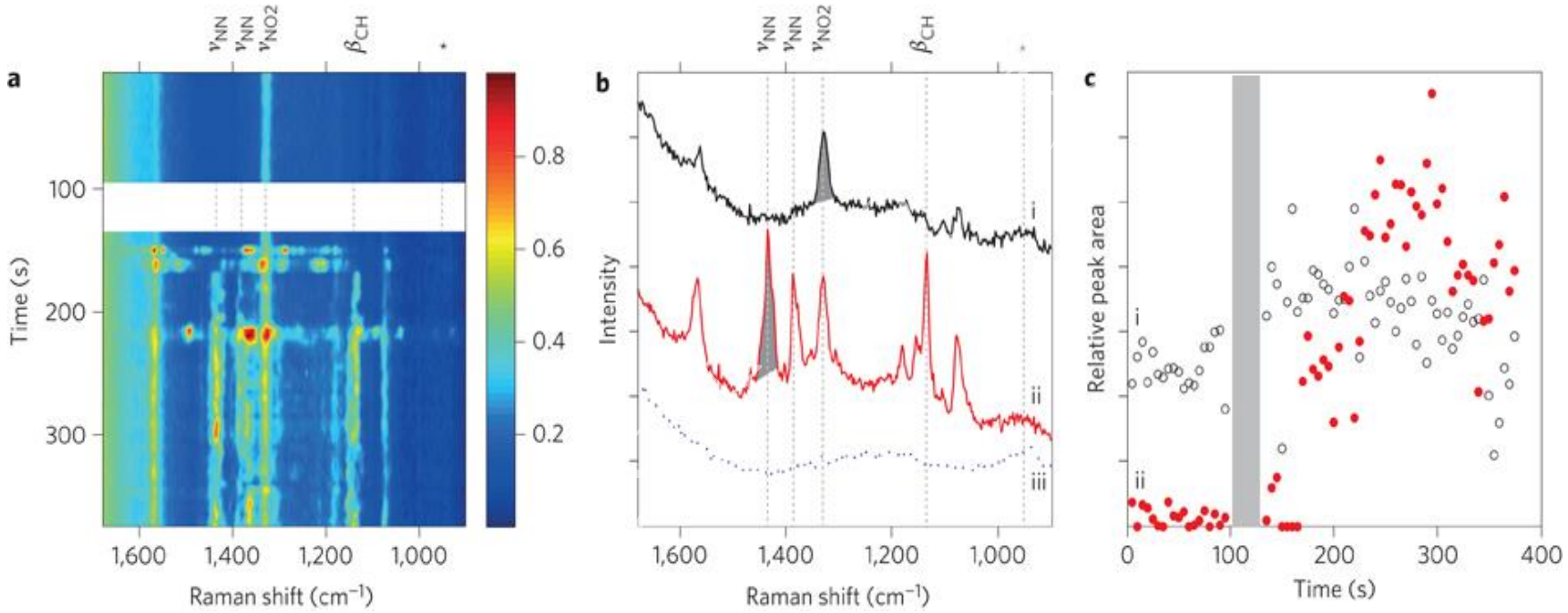

反应前和反应后的TERS测量。a，633 nm激发下的时间分辨TERS光谱，顶部为激光辐照前，底部为辐照后。b，取自a的两条光谱线，i取自90 s，ii取自265 s。光谱iii为参照光谱。c，pNTP分子在1335 cm^{-1}位置，和DMAB分子在1440 cm^{-1}位置的峰面积。 100-130 s的绿光辐照用阴影带示出。

pMA
对巯基
苯胺的
光催化
氧化

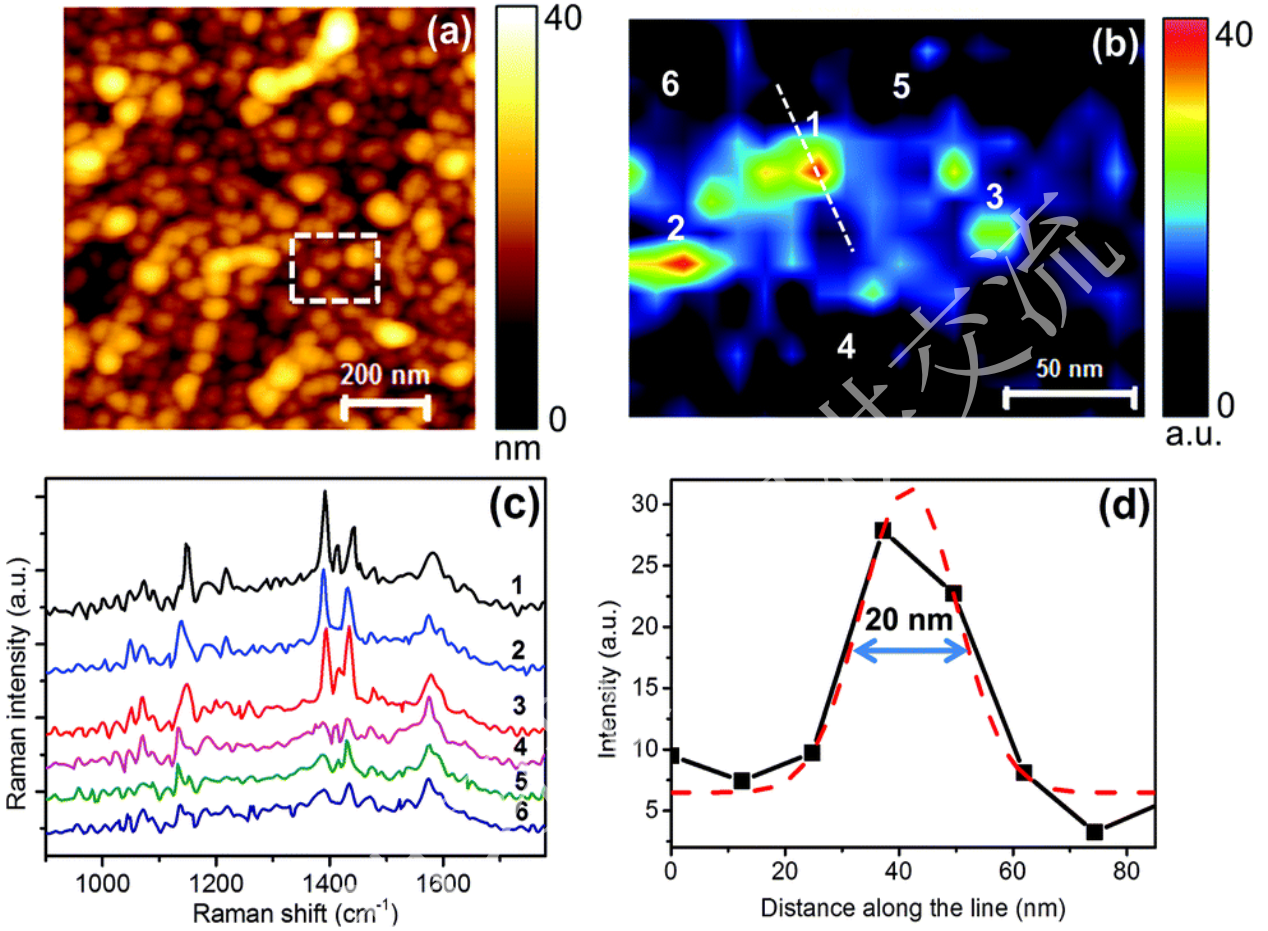

利用TERS在纳米尺度进行催化反应的成像。a，玻璃衬底上Ag纳米粒子的AFM高度图。b，DMAB的1142 cm-1 峰的空间TERS成像，所成像区域为a中虚线方框。c，b中所示1,2,3位点的近场光谱为产物DMAB的Raman峰，而4,5,6位点为反应物pMA的特征峰。d，b中所示直线的强度剖面图，显示出20 nm的空间分辨率。

LETTER

doi:10.1038/nature12151

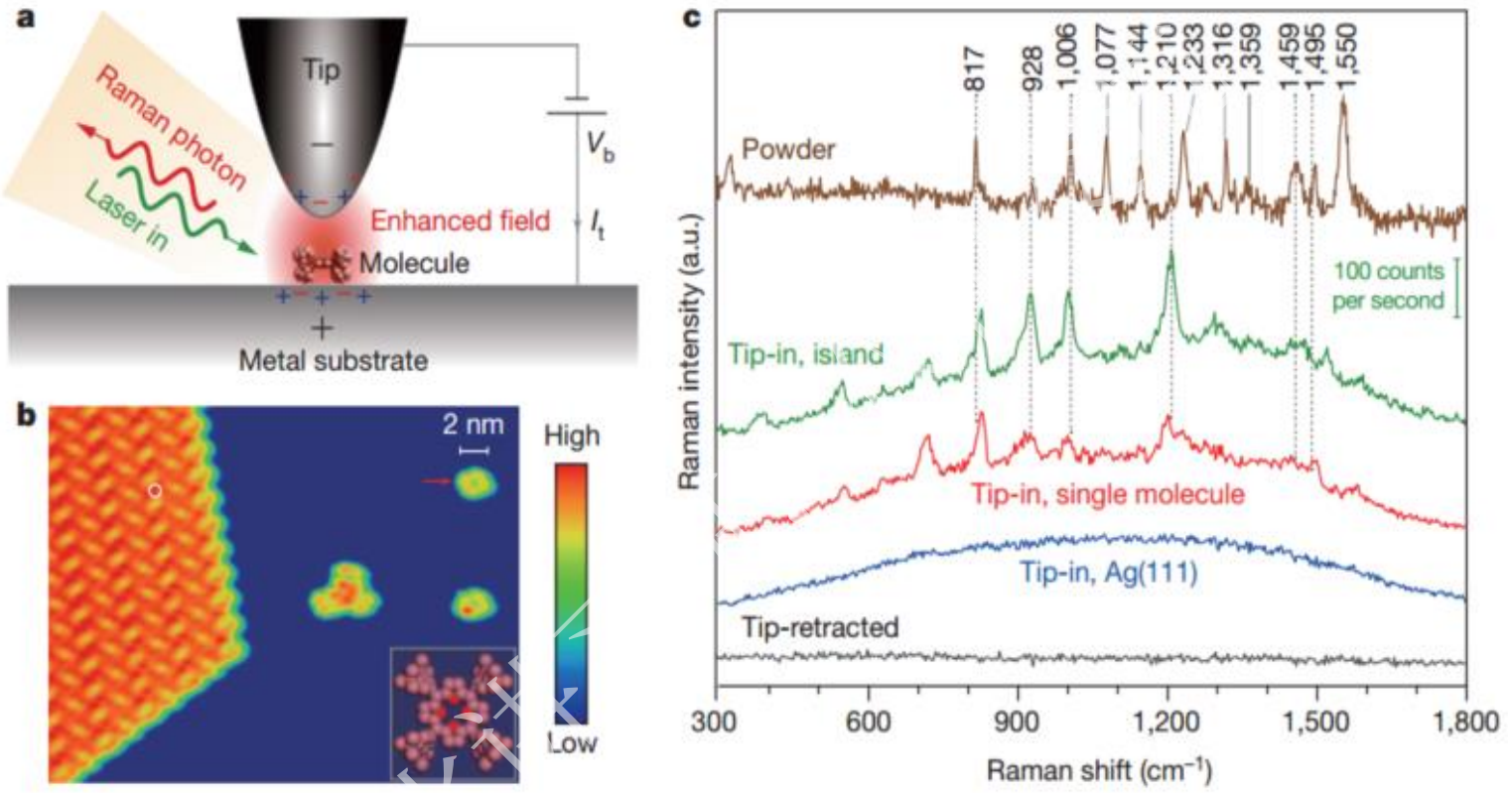

UHV亚纳米分辨TERS谱图。a, 隧穿控制TERS的图示。b, Ag(111)亚单层H_2TBPP分子的STM形貌图。c,不同条件下的TERS光谱。绿色光谱线为分子聚集成岛的Raman光谱。红色线为单个分子的Raman光谱。蓝色线为干净Ag(111)表面的光谱，黑色线为针尖远离表面5 nm的谱线。棕色线为H_2TBPP分子的粉末样品的标准Raman谱图。

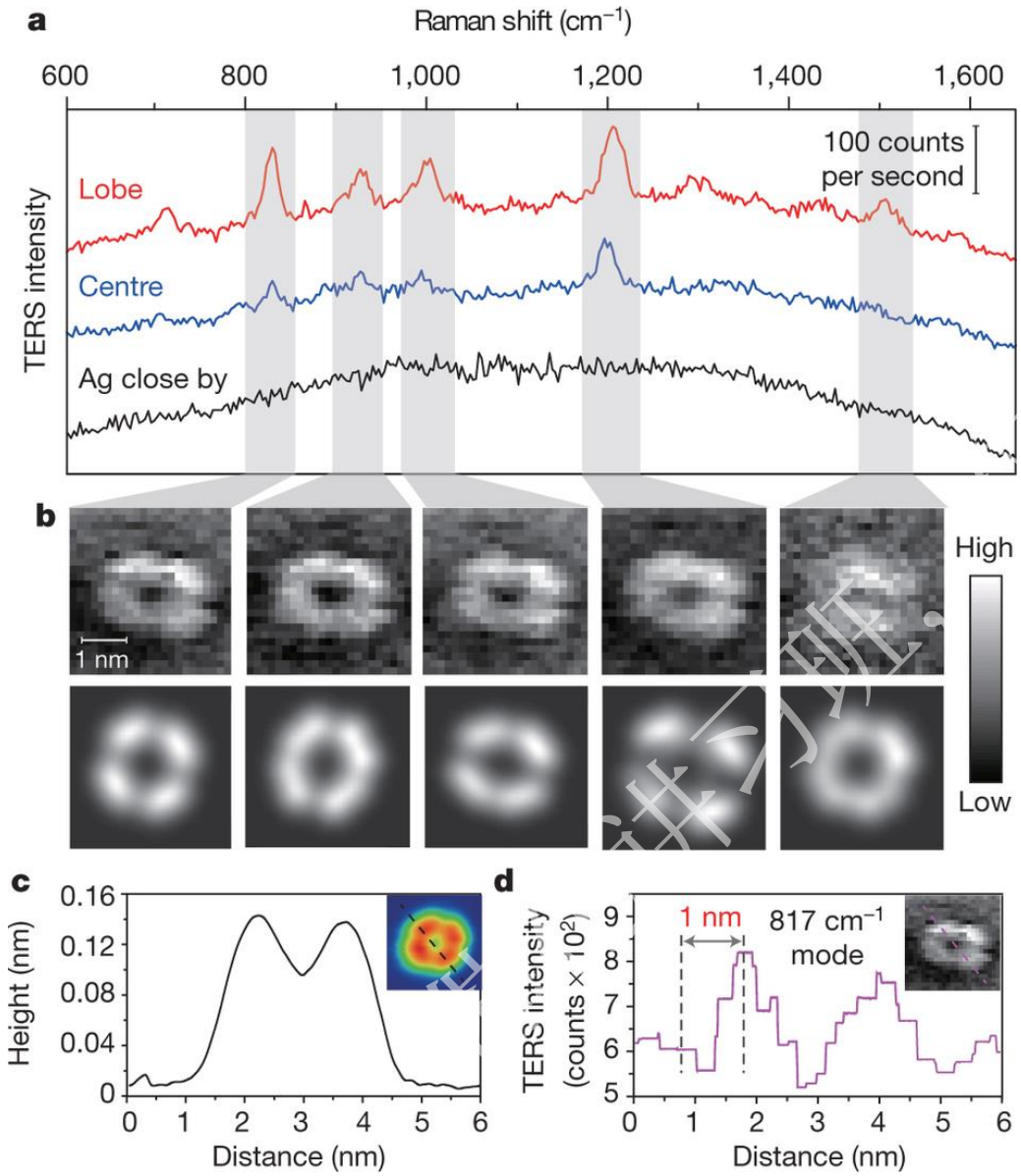

Ag(111) 表面单个H2TBPP分子的TERS空间成像。a,代表性的单分子TERS光谱，红色线为分子的四周叶片处，蓝色为分子中心处，黑色为干净Ag表面处。b, 上部分给出了单个分子的TERS实验空间成像图。下部分为理论模拟的TERS成像。c, 插图所示的STM形貌图的高度轮廓。d, 与c相同位置处的817cm^{-1} Raman峰的TERS成像强度轮廓图。

nature nanotechnology
LETTERS
PUBLISHED ONLINE: 21 NOVEMBER 2016 | DOI: 10.1038/NNANO.2016.241

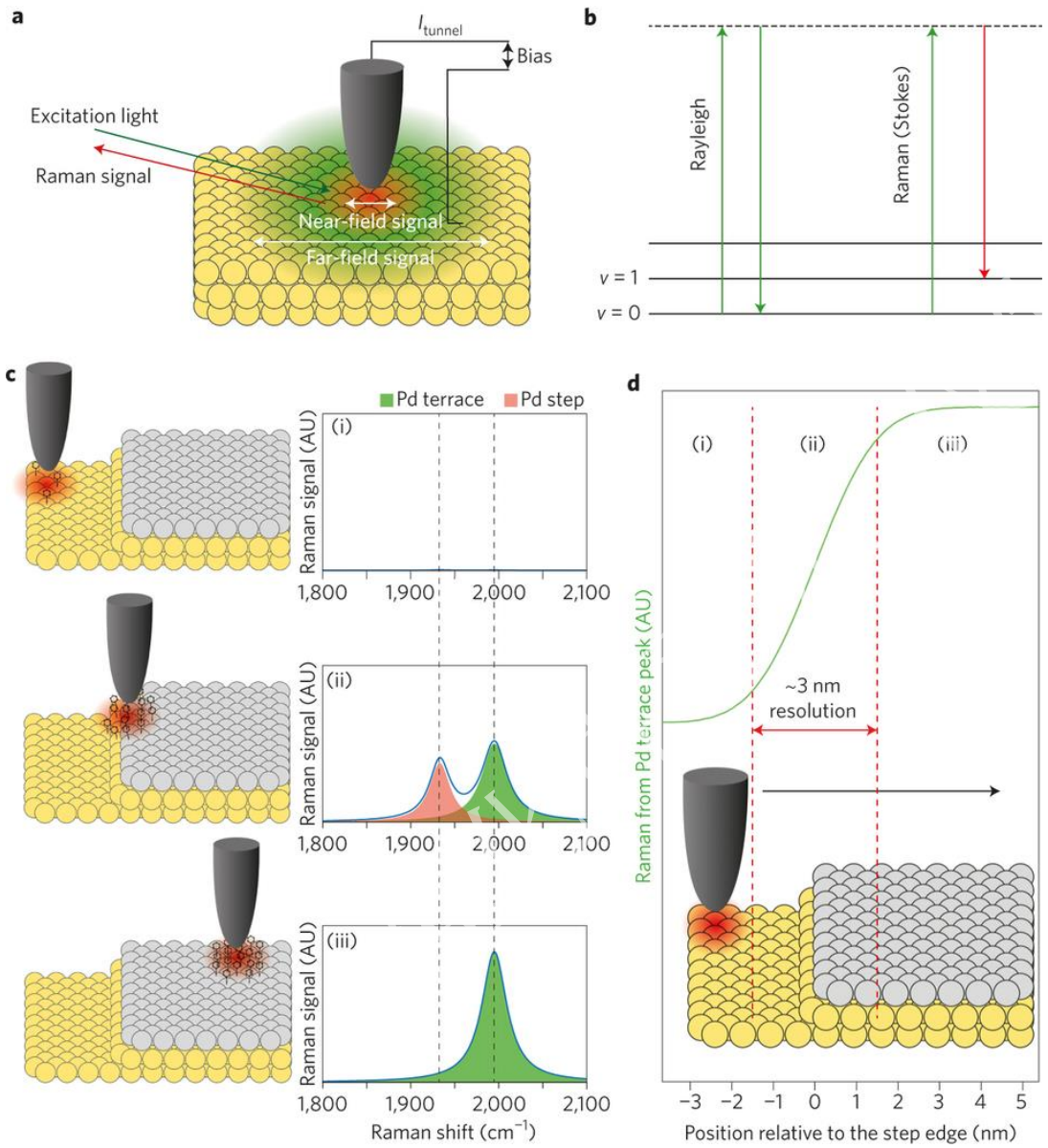

Pd/Au 界面利用Raman光谱实现纳米级分辨。a, 利用STM实现TERS的实验装置。信号主要来自于针尖下端的小部分区域。b, Raman散射的能级示意图显示出波长偏移的Stokes信号。c, Raman光谱可以解析来自不同表面不同吸附结构的振动峰。d, TERS可以在表面不同点获得空间纳米级分辨的化学信息。

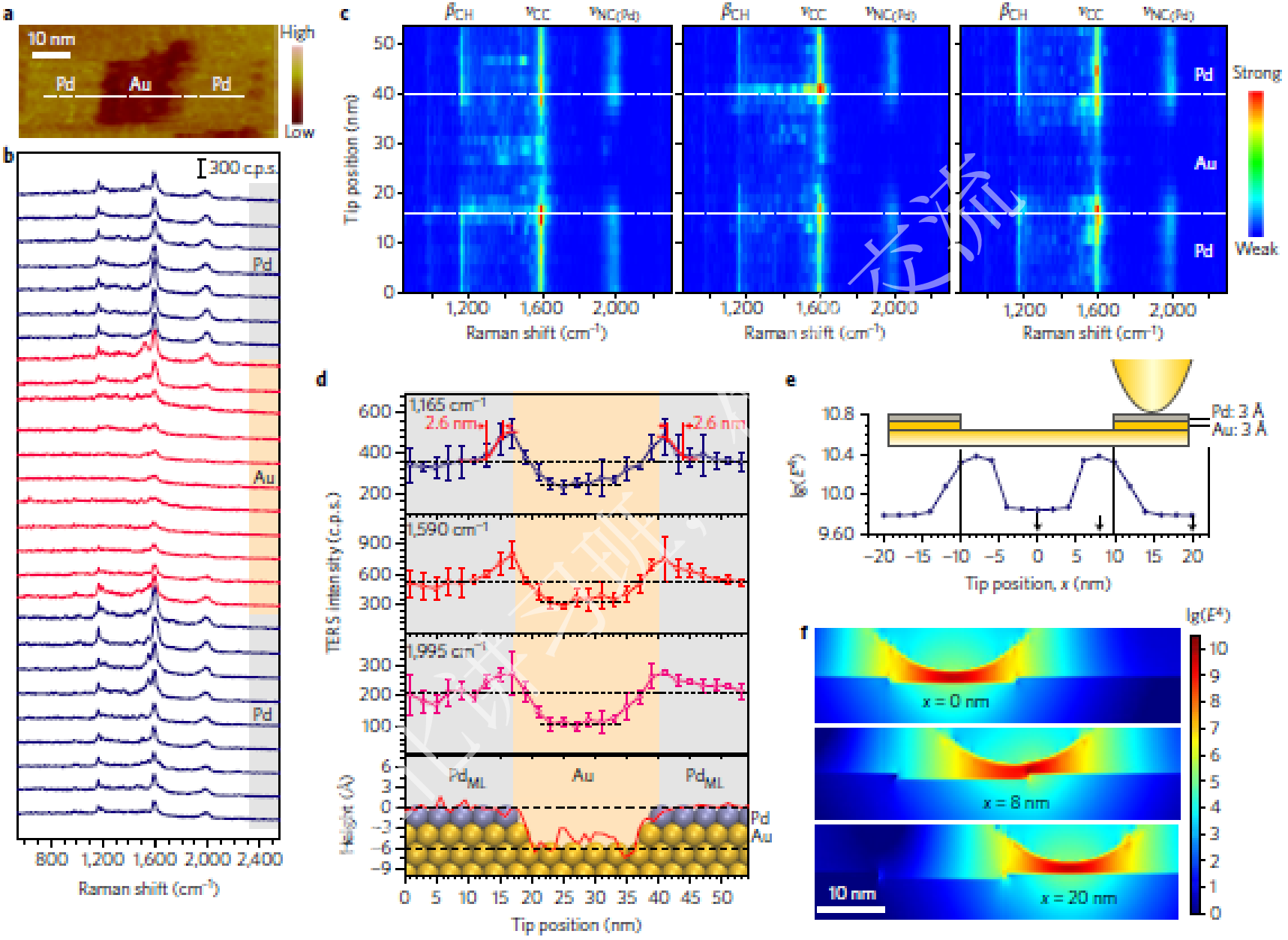
a
10 nm
Pd
Au
Pd
High
Low
b
300 c.p.s.
Pd
Au
Pd
800 1,200 1,600 2,000 2,400
Raman shift (cm⁻¹)
c
βCH
νCC
νNC(Pd)
Tip position (nm)
0 10 20 30 40 50
1,200 1,600 2,000
Raman shift (cm⁻¹)
Pd
Au
Pd
Strong
Weak
d
1,165 cm⁻¹
2.6 nm
2.6 nm
1,590 cm⁻¹
1,995 cm⁻¹
TERS intensity (c.p.s.)
Height (Å)
PdML
Au
PdML
Pd
Au
Tip position (nm)
e
Pd: 3 Å
Au: 3 Å
lg(E⁴)
Tip position, x (nm)
f
lg(E⁴)
x = 0 nm
x = 8 nm
x = 20 nm
10 nm

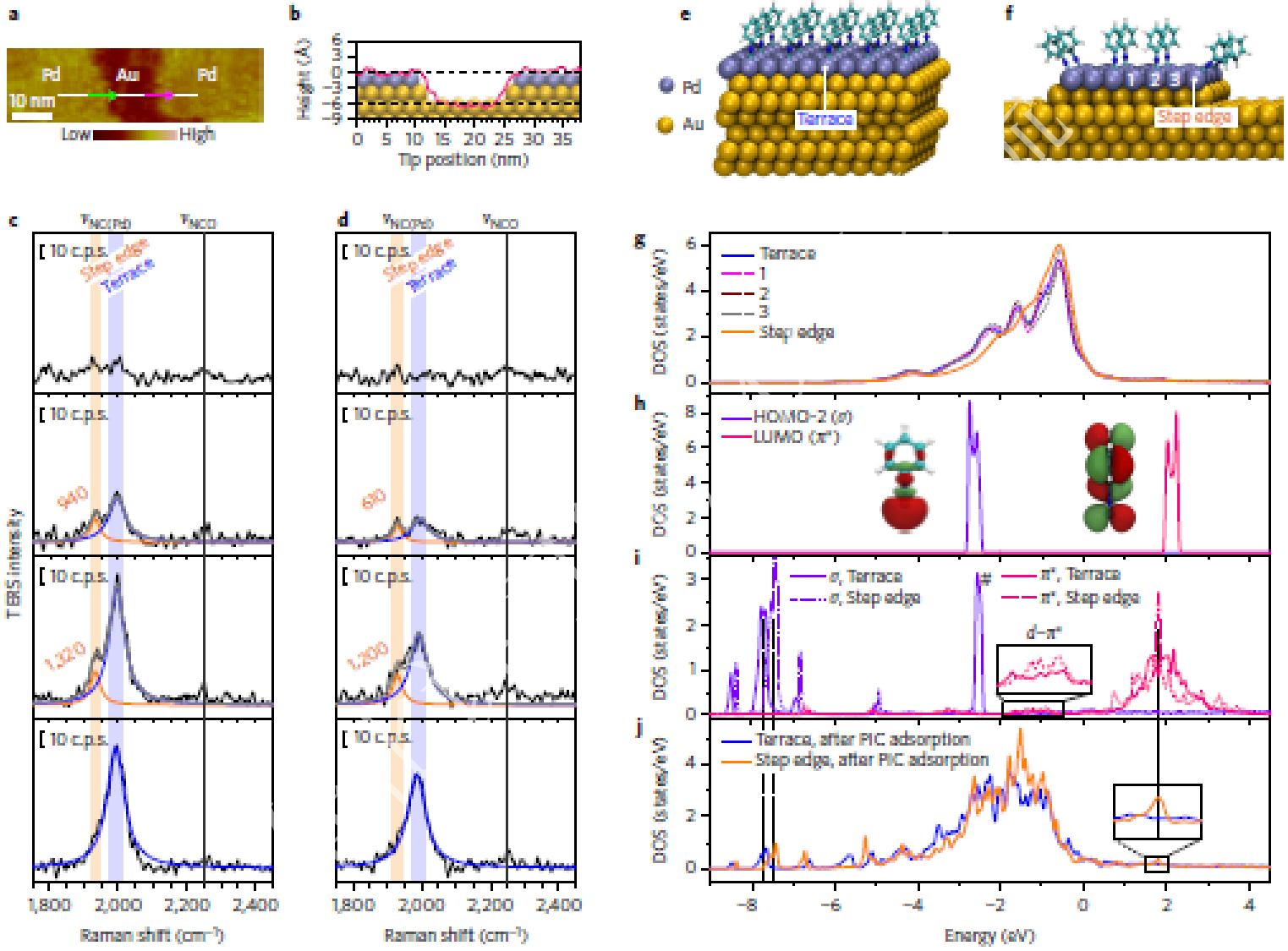
a
Pd
Au
Pd
10 nm
Low
High
b
Height (Å)
0 5 10 15 20 25 30 35
Tip position (nm)
e
Pd
Au
Terrace
f
1 2 3 1
Step edge
c
d
TERS intensity
10 c.p.s.
Step edge
Terrace
940
610
1,320
1,200
1,800 2,000 2,200 2,400
Raman shift (cm⁻¹)
g
DOS (states/eV)
Terrace
1
2
3
Step edge
h
HOMO-2 (σ)
LUMO (π*)
i
σ, Terrace
σ, Step edge
π*, Terrace
π*, Step edge
d–π*
j
Terrace, after PIC adsorption
Step edge, after PIC adsorption
−8 −6 −4 −2 0 2 4
Energy (eV)

IR-SNOM 与 AFM-IR

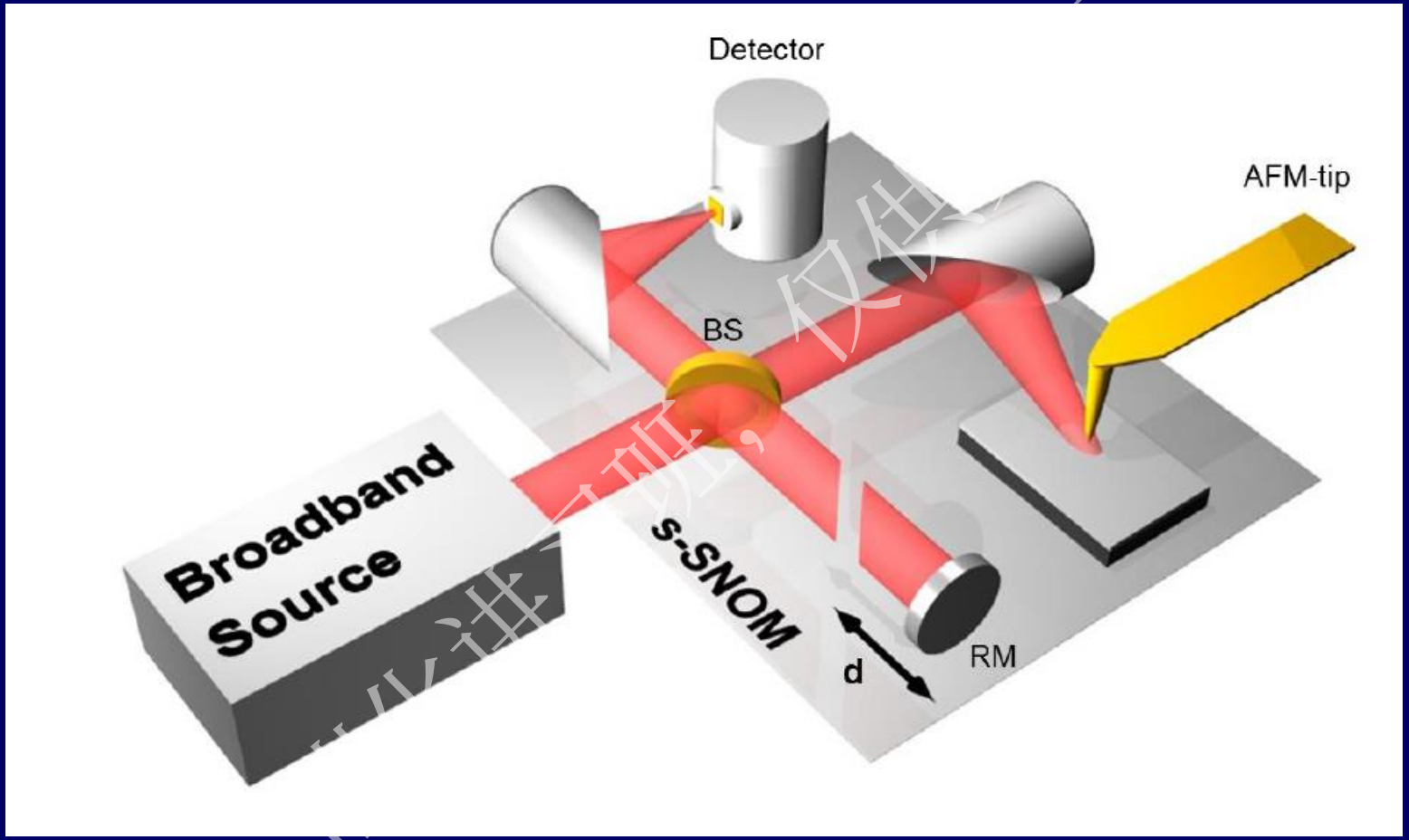

NeaSNOM 组成结构

NeaSNOM System

1 NeaSNOM 显微镜平台

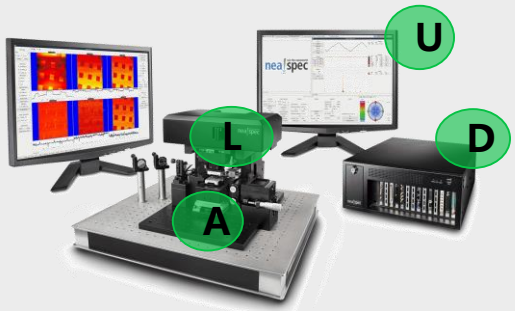

NeaSNOM 显微镜平台包括:

- **A** NeaSNOM 原子力显微镜(AFM)
- **L** 光聚焦和收集单元
- **D** NeaSNOM 数字扫描控制器
- **U** 用户 PC 预装 NeaSCAN software

2 NeaSNOM 信号探测模块

取决于光源类别，至少需要1种探测模块，:

- **C** 单色激光用单色近场探测模块
- **D** 宽波光源用宽波近场探测模块

为表面等离子激元应用提供透射照明模块。

3 Neaspec 认证光源

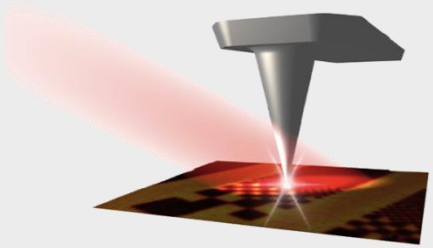

广泛的照明系统已经Neaspec验证，可以应用到NeaSNOM系统上，包括:

- CO_2 IR 激光系统(ca. 9.2–11.2μm)
  - QCL 激光系统(中心波长范围： 3.8–10.8μm)
  -可见/近红外激光系统 (i.e. HeNe-laser)
- 宽带激光系统用于近场光谱应用
  - 中红外光谱区间(ca. 5–15μm)
  - 可见/近红外 (ca. 600-1000nm)
- 同步辐射光源
- 太赫兹光源

NeaSNOM 独特的双光路设计可以提供优越的近场测量环境

Possible configuration:

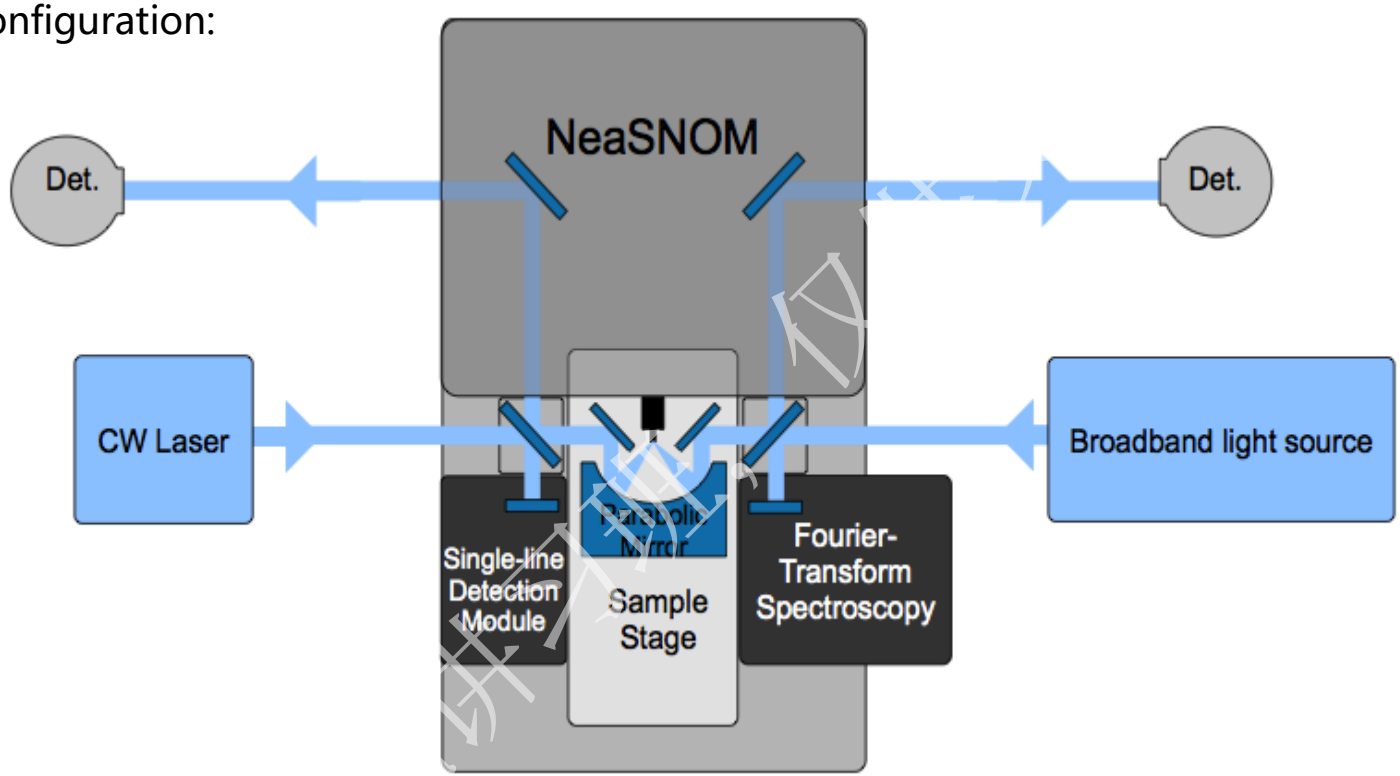

- 抛面镜用于针尖照明和信号收集→ 适用于**宽带光源**
- 两个独立的光路设计用于两个独立的系统设置
- 自由光路Free propagating optical beams
- 专门设计的探测组块，同时测量近场光学的强度和相位。

仪器的基本组成

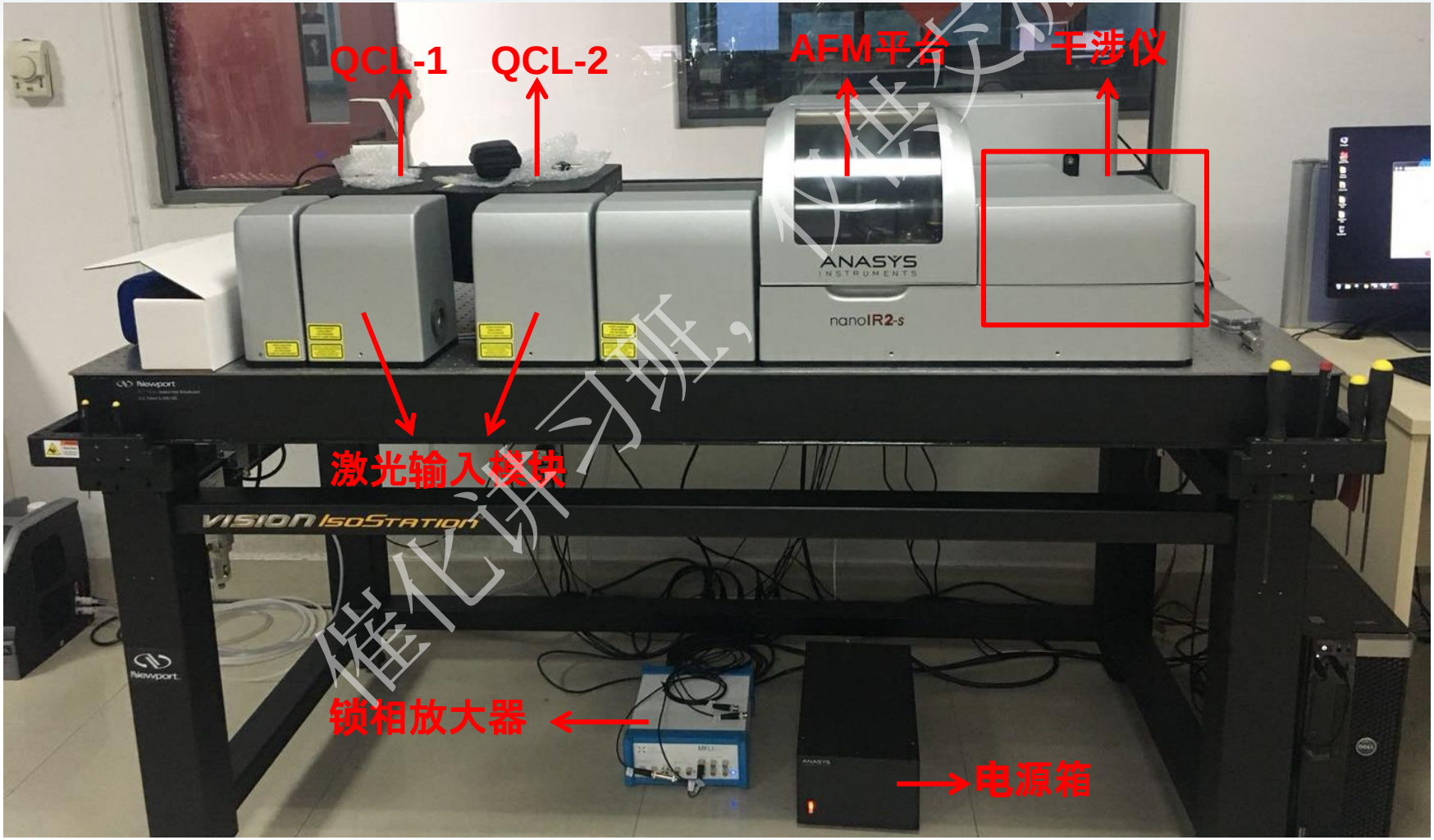
QCL-1
QCL-2
AFM平台
干涉仪
激光输入模块
锁相放大器
电源箱
ANASYS
nanoIR2-s
VISION IsoStation
Newport

nano-FTIR 工作原理

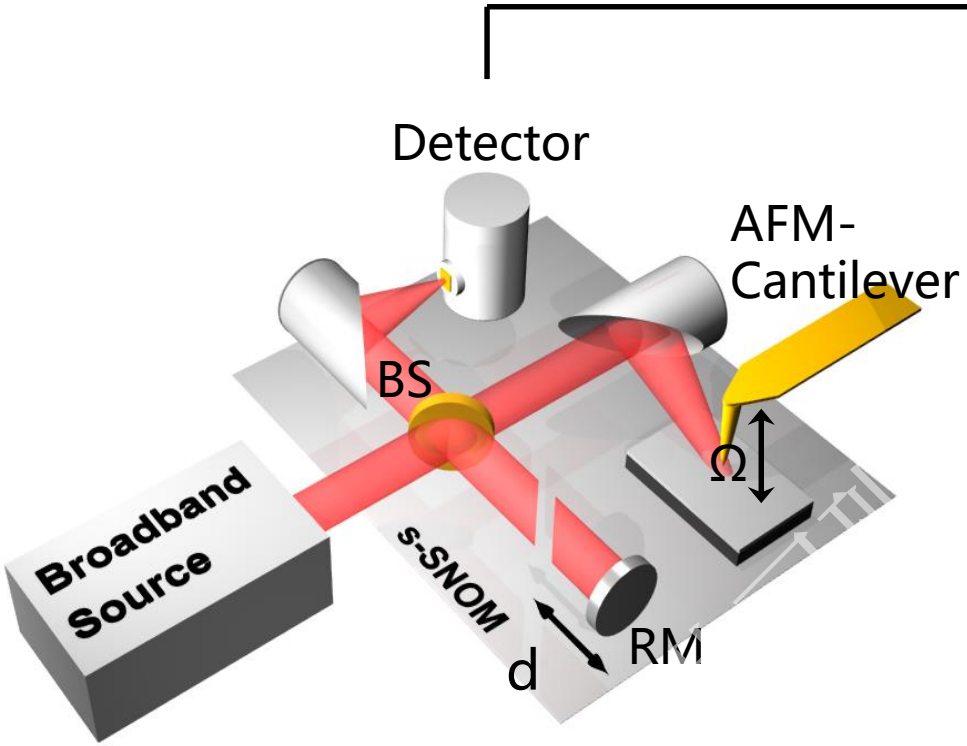

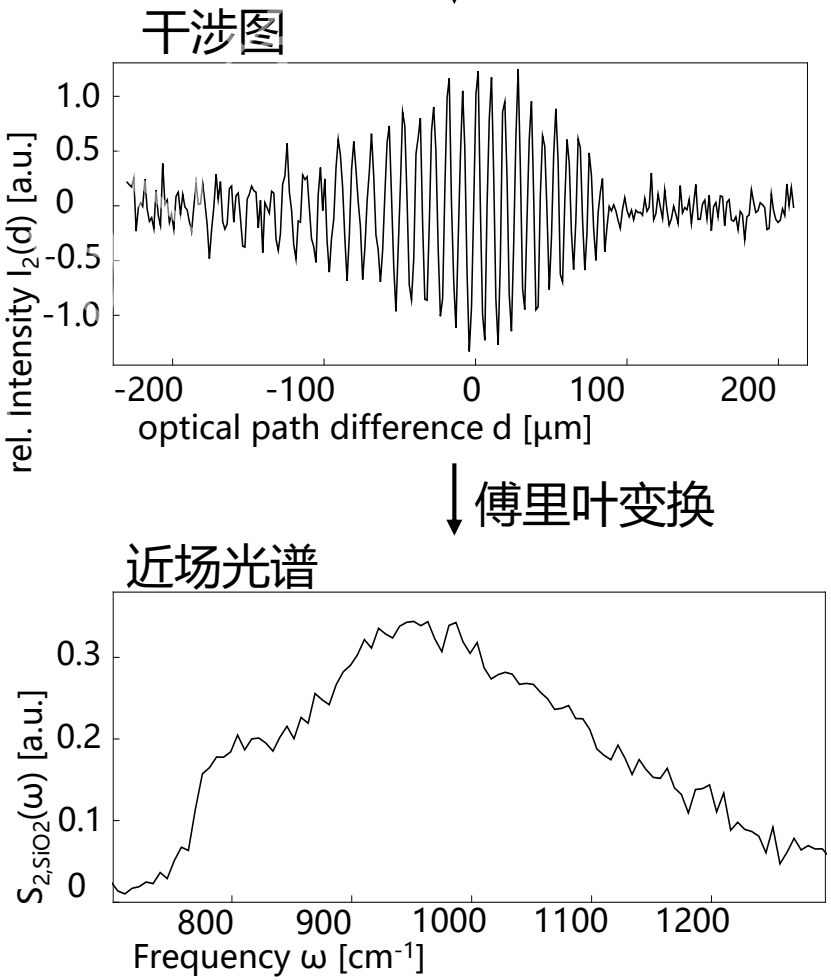

无孔径扫描近场显微镜利用纳米聚焦点成像

同时测量表面形貌和近场光学信号

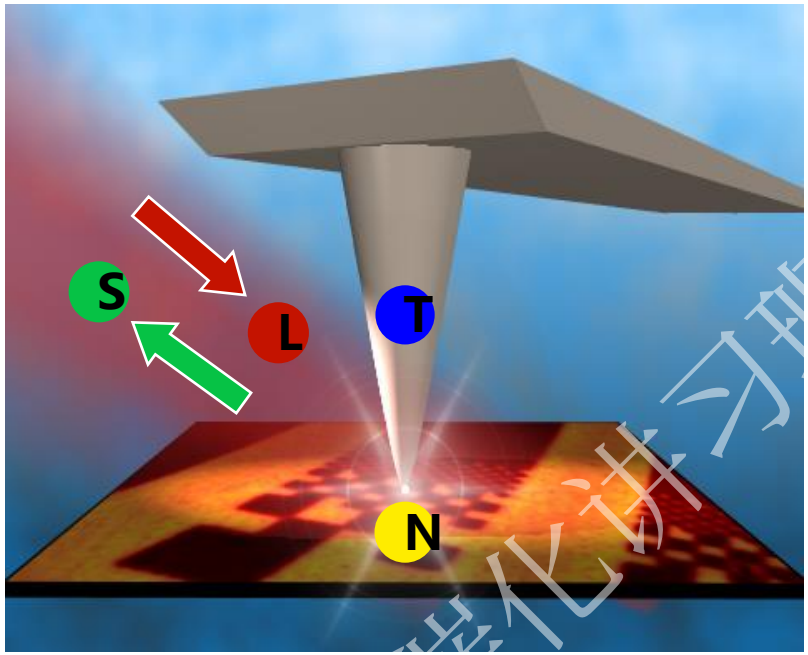

- 将激光束 L 聚焦照明到商用AFM探针上 T
- 针尖被激发出一个nano-focus N，其尺寸与针尖半径相当，大约10 nm（Lightning Rod Effect)
- 针尖与样品间的近场效应改变了弹性散射光 S 的性质。
- 通过扫描样品表面，即可得到10nm分辨率的光学成像。

在可见、红外和太赫兹波段均可获得不受波长影响的10 nm分辨率

无孔径扫描近场光学显微镜需要有效地背景压制技术

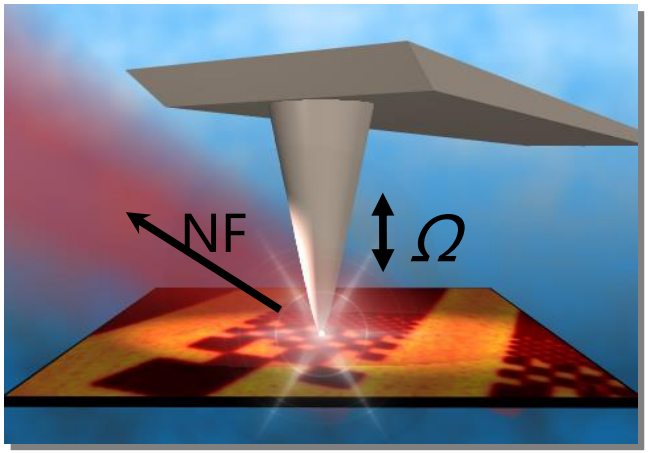

1% 近场信号...

- 由针尖与样品之间的近场互相作用产生
- 高度区域（距离）敏感
- 可以由成熟的数学模型预测提取

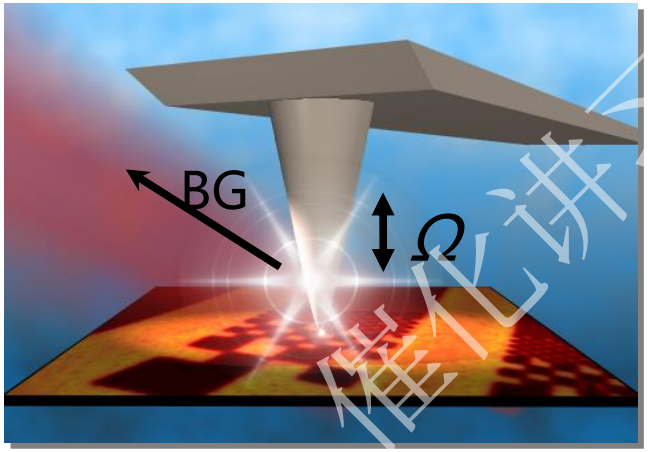

99% 背景信号

- 由样品和针尖散射产生
- 无法有效限制局限
- 因为衍射、样品形貌等原因无法预测

→ 高阶信号解调
Higher order signal demodulation (nΩ) for background suppression

NeaSNOM 信号取决于样品的光学性质

$E_{sca} \propto \alpha_{eff} \cdot E_{loc}$

$E_{sca} \propto \alpha_{eff} \cdot (E_{tip} + E_{sur})$

„Dielectric probing “ ∝ distance Field “Mapping “

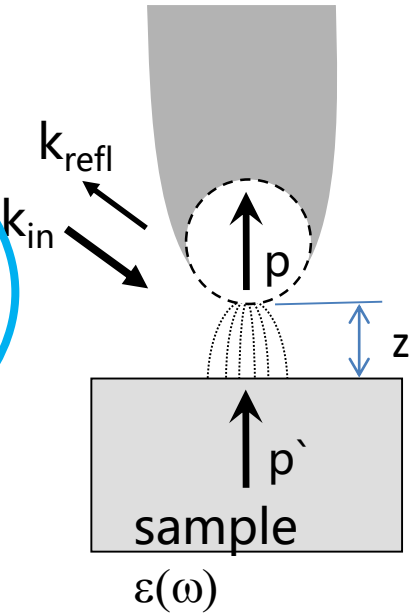

Dipole above surface
(dipole model)

Cvitkovic et al.,
Opt. Exp. 15, p.8550 (2007)

$$\alpha_{\text{eff}} = \frac{\alpha(1+\beta)}{1-\alpha\beta/(16\pi(a+z)^3)}.$$

$$\alpha = 4\pi a^3 \frac{\varepsilon_t - 1}{\varepsilon_t + 2}$$ 针尖介电性质正比

$$\beta = \frac{\varepsilon_s - 1}{\varepsilon_s + 1}$$ 样品介电性质正比

a_{eff} 与样品针尖(α)、表面(β)极化度、，针尖样品间隙(z)，针尖曲率半径（a) 有关。

成像过程中α、z、a不变，因此近场信号的变化首要反映了样品介电性质的变化。

NeaSNOM取决于样品的介电性质ε(ω)

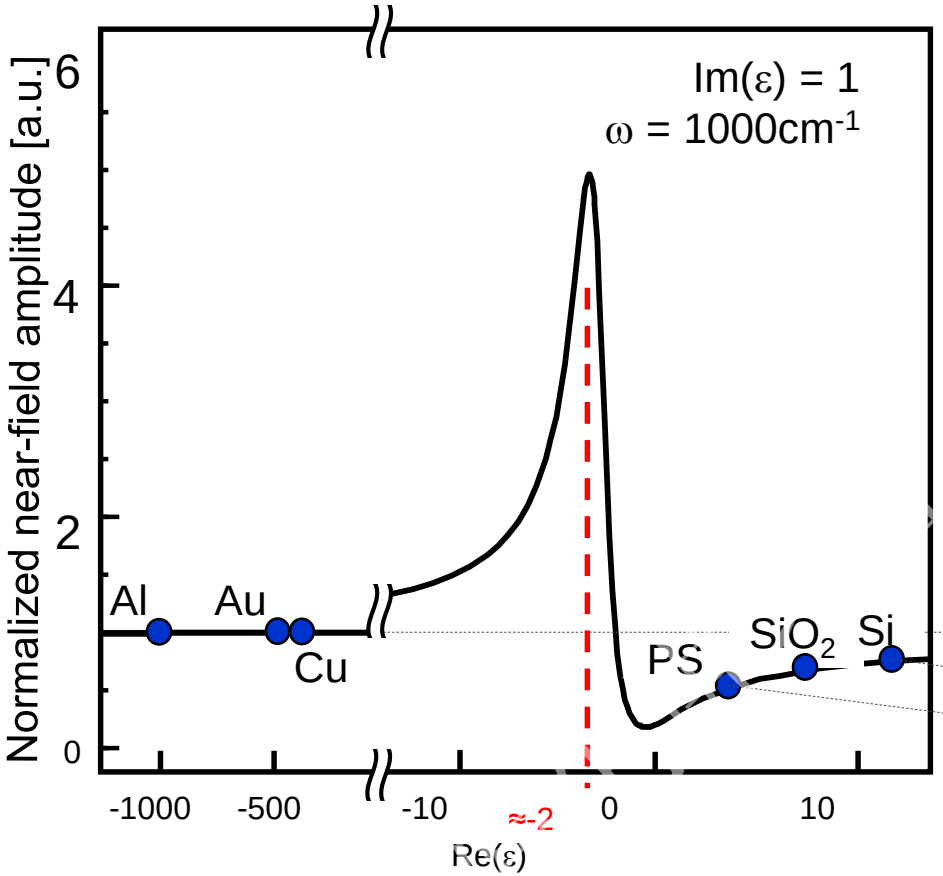

近场信号强度与样品介电常数成正比，且存在一共振频率，不同物质在其共振频率上具有增强的近场信号

Metals

Si (undoped)

Dielectrics

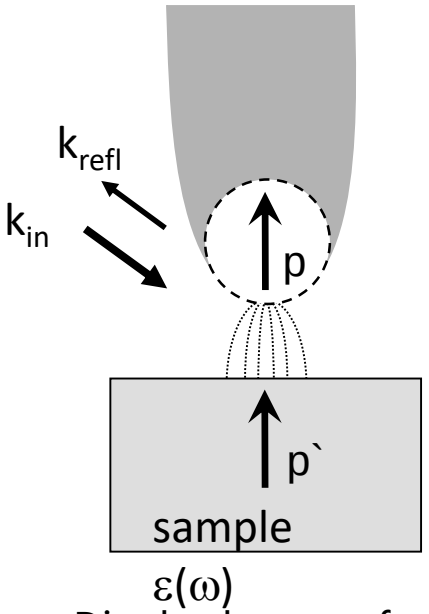

Dipole above surface (dipole model)

Cvitkovic et al., Opt. Exp. 15, p.8550 (2007)

指定物质的近场信号

nature International weekly journal of science

Knoll et. al, Nature 399, p.134 (1999)
Hillenbrand et. al, Nature 418, p.159 (2002)

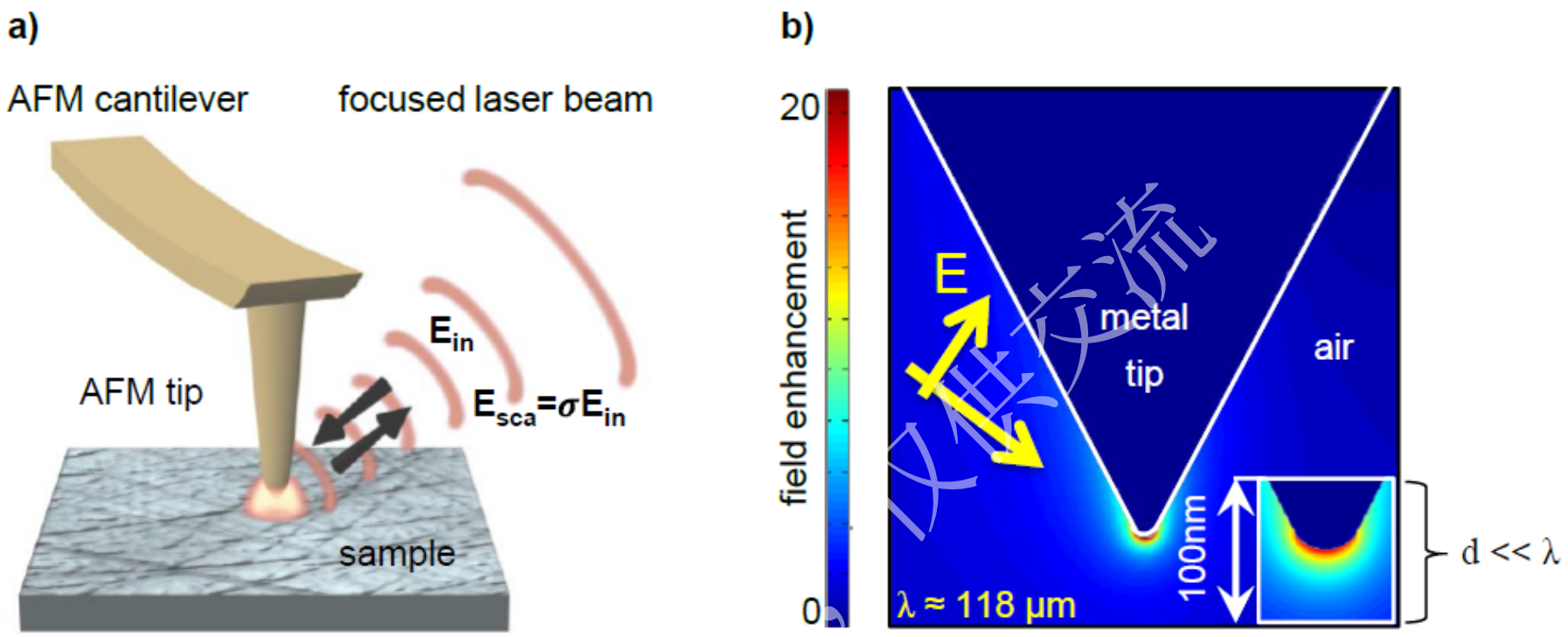

Fig. 4.4 Tip illumination and field enhancement in s-SNOM. **a)** A sharp AFM tip is mounted on a cantilever and illuminated by a focused laser beam. (Image taken from[60]) **b)** Numerical simulation of a metal cone, illuminated by far-infrared light with $\lambda = 118$ µm. (Taken from[8]).

$$I_{\mathrm{det}} \propto I_{\mathrm{sca}} \propto |E_{\mathrm{sca}}|^2 = |E_{\mathrm{nf}} + E_{\mathrm{bg}}|^2 = (E_{\mathrm{nf}} + E_{\mathrm{bg}})(E_{\mathrm{nf}} + E_{\mathrm{bg}})^*$$

$$E_{\mathrm{sca}} = E_{\mathrm{nf}} + E_{\mathrm{bg}} = \sum_{n=0}^{\infty} E_{\mathrm{nf,n}} \cos(\mathrm{n}\Omega t) + \sum_{n=0}^{\infty} E_{\mathrm{bg,n}} \cos(\mathrm{n}\Omega t)$$

where $E_{\mathrm{nf,n}}=\sigma_{\mathrm{nf,n}}E_{\mathrm{in}}=s_{\mathrm{nf,n}}e^{i\varphi\mathrm{nf,n}}E_{\mathrm{in}}$ and $E_{\mathrm{bg,n}}=\sigma_{\mathrm{bg,n}}E_{\mathrm{in}}=s_{\mathrm{bg,n}}ei^{\varphi\mathrm{bg,n}}E_{\mathrm{in}}$ denote the n$^{\mathrm{th}}$ order complex-valued Fourier coefficients of E_{nf} and E_{bg}, respectively.

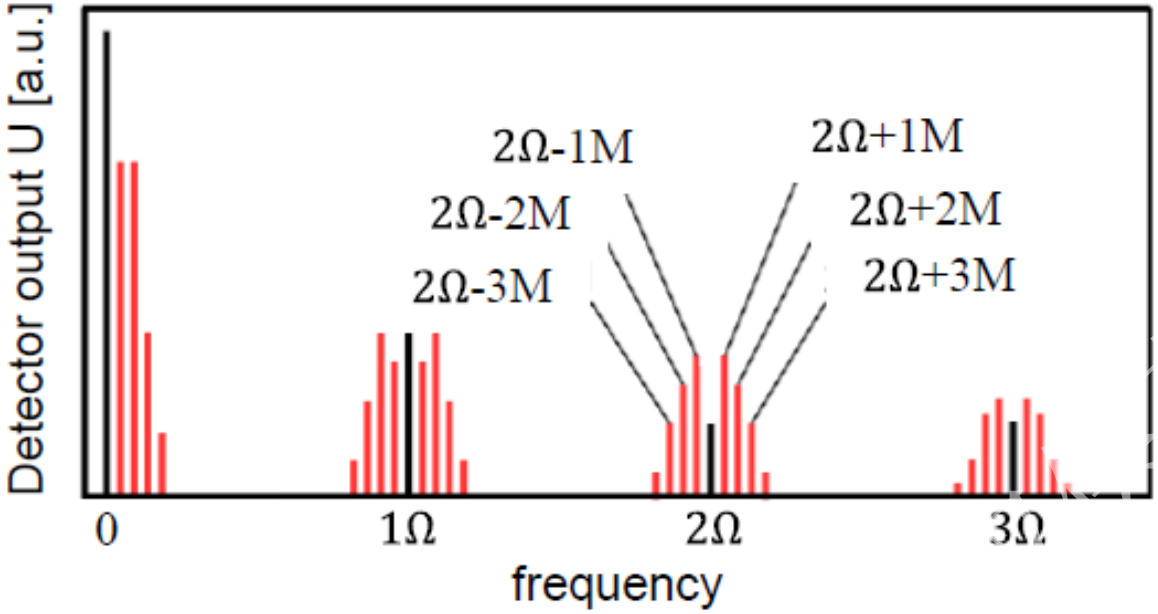

Signal splitting in pseudo-heterodyne detection in s-SNOM. The metallic AFM-tip is oscillating with a frequency Ω, and the reference mirror with a frequency M ($M \ll \Omega$), causing the interferometric signal to split up in sidebands $n\Omega \pm mM$.

Near-field scattering E_{nf} arises is strongly non-linear with the tip-sample distance and creates signal contributions in the higher harmonics nΩ of the tip oscillation frequency Ω. Background scattering E_{bg} can in good approximation be considered to change linear with the tip position. The contribution of the background scattering to the signal is mostly restricted to the oscillation frequency Ω.

By demodulating the detected signal at sufficiently high harmonics nΩ (in the infrared usually for $n \geq 2$) the Fourier coefficients $\sigma_{bg,n}$ are negligible compared to the Fourier coefficients $\sigma_{nf,n}$, i.e. $\sigma_{nf,n} \gg \sigma_{bg,n}$.

$$U_n \propto E_{bg,0} E^*_{nf,n} + E_{nf,n} E^*_{bg,0}$$

doi:10.1038/nature20795

High-spatial-resolution mapping of catalytic reactions on single particles

Chung-Yeh Wu[1,2], William J. Wolf[1,2], Yehonatan Levartovsky[3,4], Hans A. Bechtel[5], Michael C. Martin[5], F. Dean Toste[1,2] & Elad Gross[3,4]

The critical role in surface reactions and heterogeneous catalysis of metal atoms with low coordination numbers, such as found at atomic steps and surface defects, is firmly established[1,2]. But despite the growing availability of tools that enable detailed *in situ* characterization[3], so far it has not been possible to document this role directly. Surface properties can be mapped with high spatial resolution, and catalytic conversion can be tracked with a clear chemical signature; however, the combination of the two, which would enable high-spatial-resolution detection of reactions on catalytic surfaces, has rarely been achieved. Single-molecule fluorescence spectroscopy has been used to image and characterize single turnover sites at catalytic surfaces[4,5], but is restricted to reactions that generate highly fluorescing product molecules. Herein the chemical conversion of N-heterocyclic carbene molecules attached to catalytic particles is mapped using synchrotron-radiation-based infrared nanospectroscopy[6,7] with a spatial resolution of 25 nanometres, which enabled particle regions that differ in reactivity to be distinguished. These observations demonstrate that, compared to the flat regions on top of the particles, the peripheries of the particles—which contain metal atoms with low coordination numbers—are more active in catalysing oxidation and reduction of chemically active groups in surface-anchored N-heterocyclic carbene molecules.

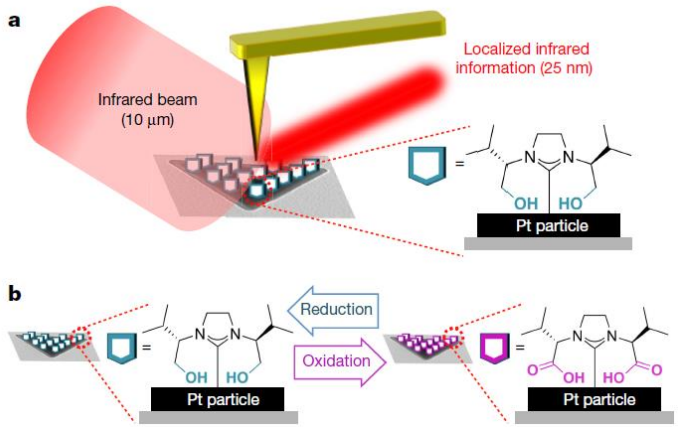

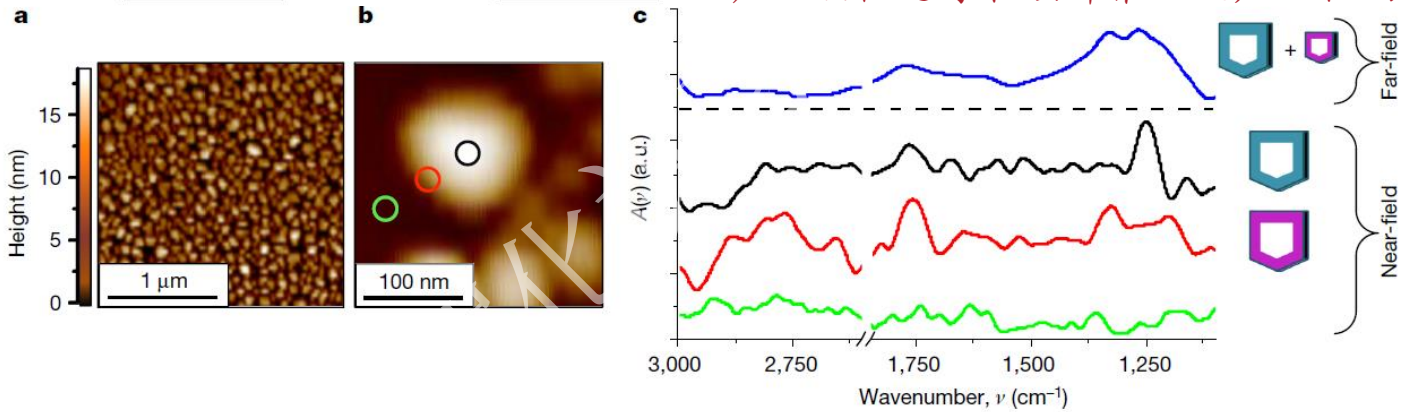

1）25纳米空间分辨率红外光谱

2）Pt颗粒边缘和顶部催化反应活性的不同

3）光谱范围：1000-3000波数

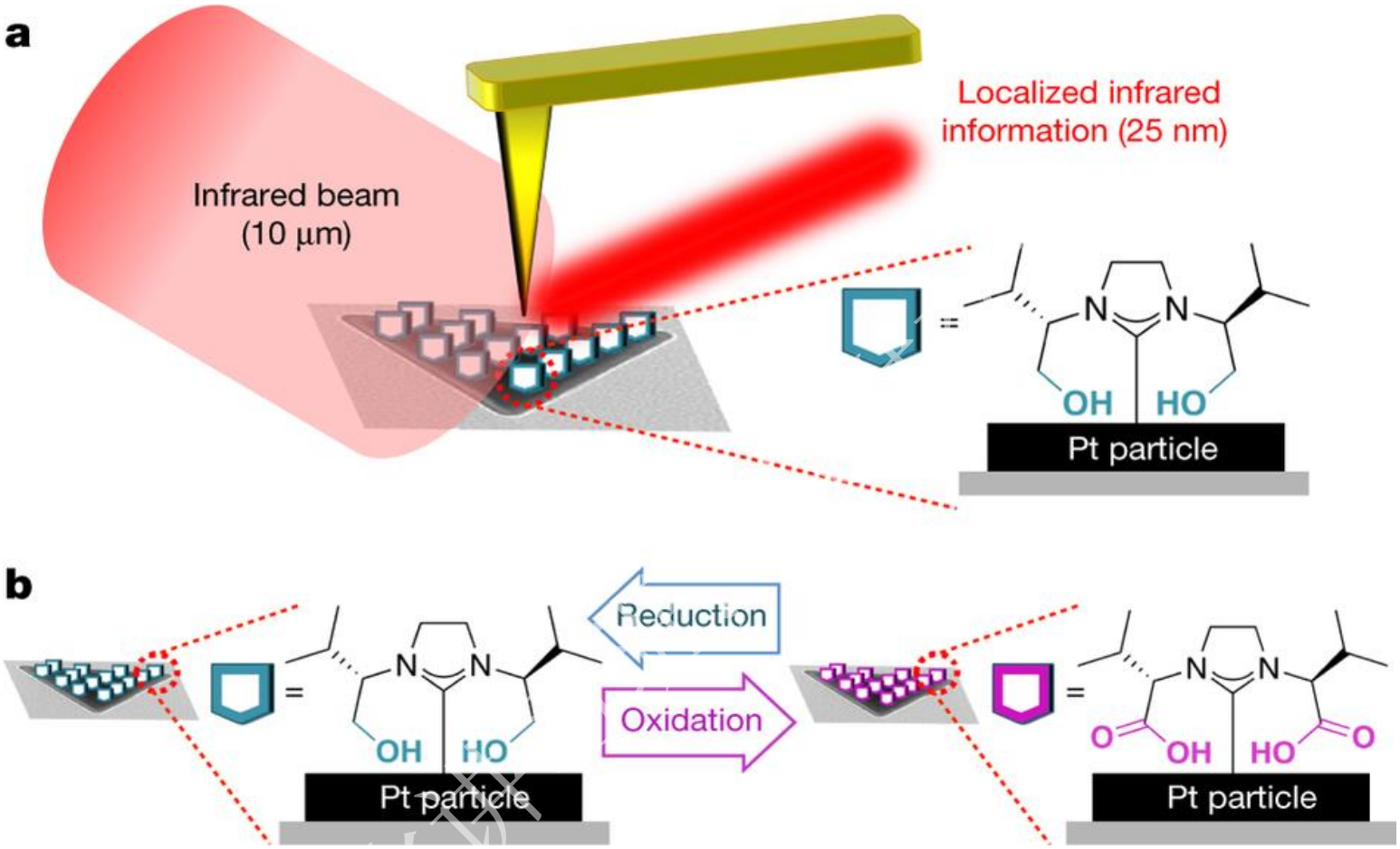

同步辐射红外纳米光谱的实验装置示意图。a, OH官能化的NHC分子(蓝色五边形)锚定于Pt粒子的表面。PtSi AFM针尖充当光学天线，将衍射限制的同步辐射红外光源（光斑为10μm）局域化，诱导出红外散射信号其空间分辨率为25 nm。b, 在氧化条件下，催化活性的Pt纳米粒子将醇羟基氧化成羧基，且此过程可逆。

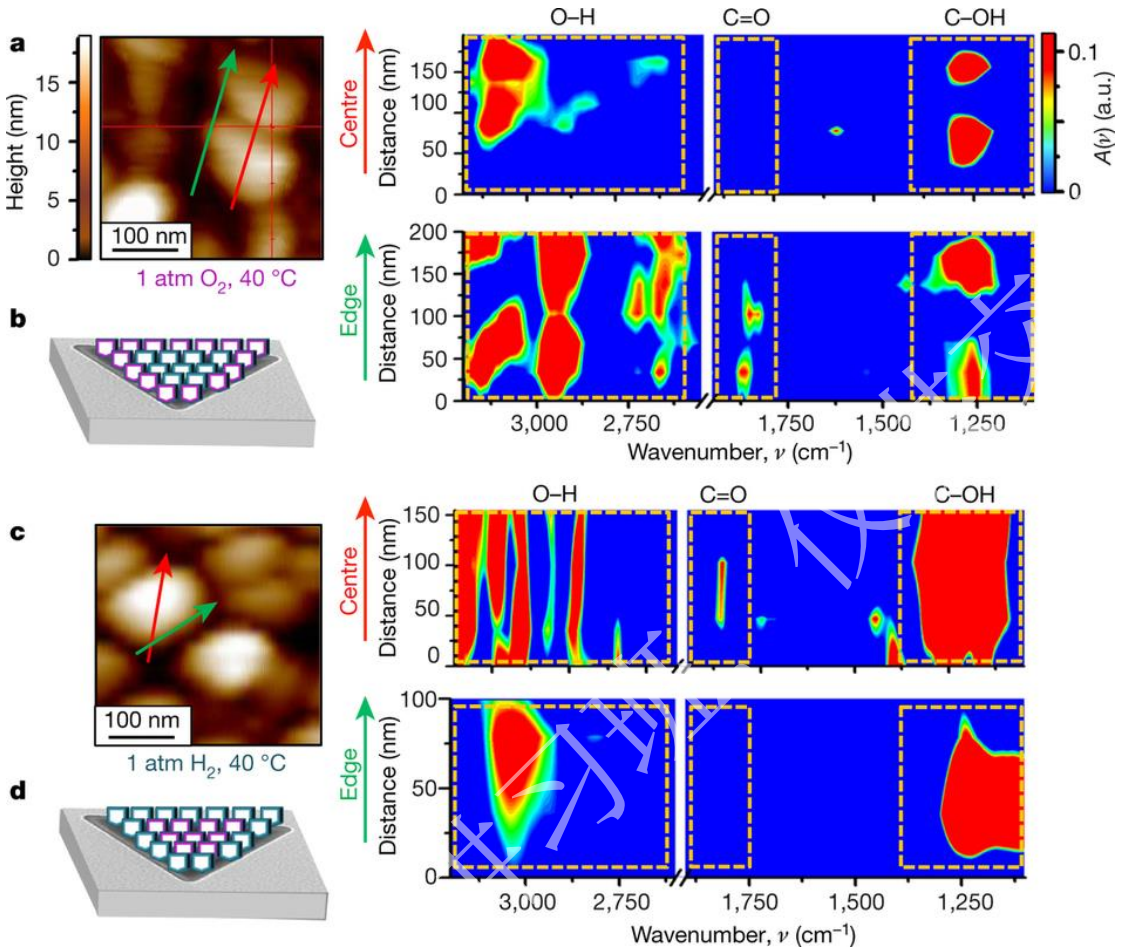

不同反应条件下，SNOM红外光谱在Pt颗粒上的一维分布。波谱范围：1000-3250波数。O-H, C=O, C-OH官能团。光谱是最有说服力的数据：特征官能团在颗粒上不均匀分布

Pt粒子中心和边缘的红外纳米光谱。a，c 红外纳米光谱扫描线穿过NHC包覆Pt纳米粒子的中心（红线）和边缘（绿线），随后将样品暴露于温和的氧化(a)和还原(c)气氛下。虚线方框标识着CO-H，C=O和O-H吸收峰的波数区域。b，d，NHC包覆的Pt粒子在暴露于还原(b)和氧化(d)条件的图示。

工作原理（AFM-IR）

光热诱导共振技术（PTIR，也称AFM-IR）

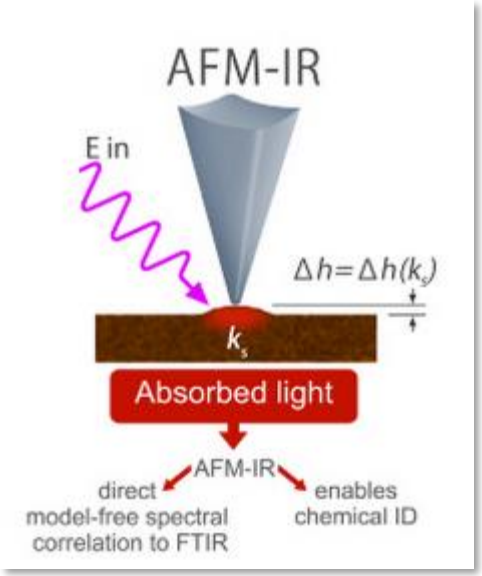

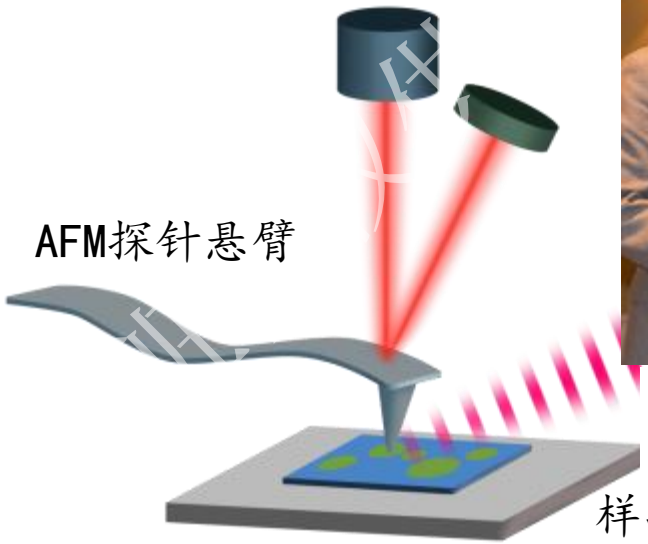

Alexandre Dazzi
2014 Ernst Abbe Award

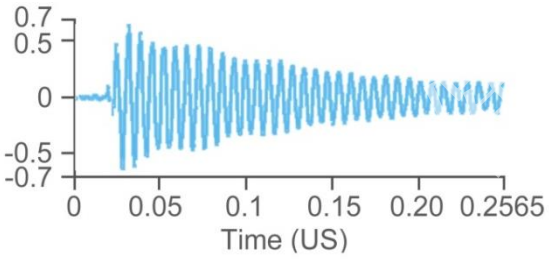

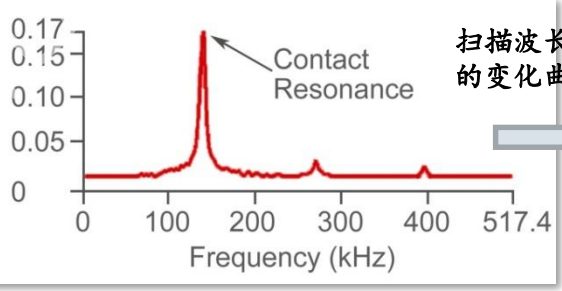

扫描波长，绘制强度随波长的变化曲线即红外光谱

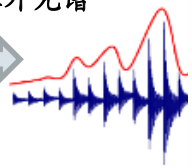

探针的震荡大小~ IR 吸收系数成正比

Tapping AFM-IR Concept

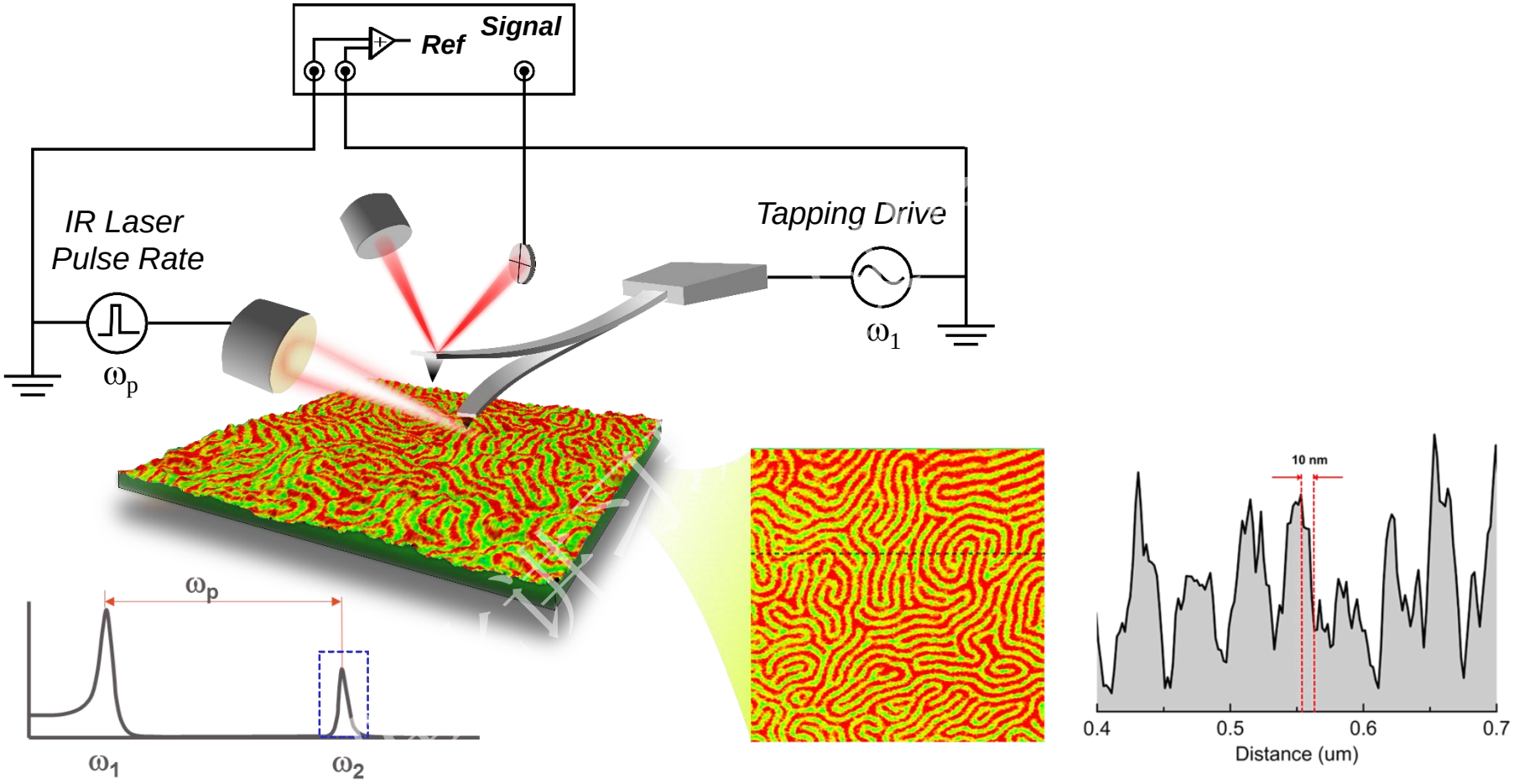

Resonance Condition: $\omega_1 + \omega_p = \omega_2 \rightarrow 2^{nd}$ Harmonic of the Cantilever Oscillation)

原子力和红外光源联用---
目前为止最好的纳米微区光学/化学组分表征方案

- 高分辨-10-20nm
- 比较强的信号
- 光谱速度快
- 使用范围广

1999年

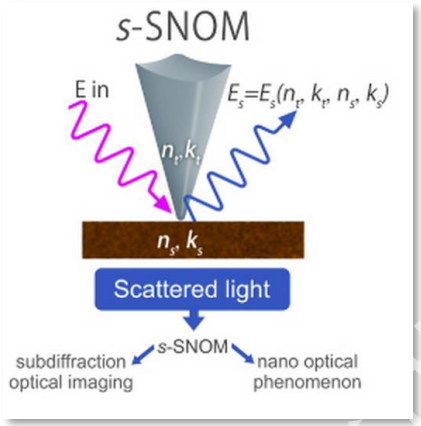

和IR椭偏效应类似

n: 折射率
k: 消光系数

2010年

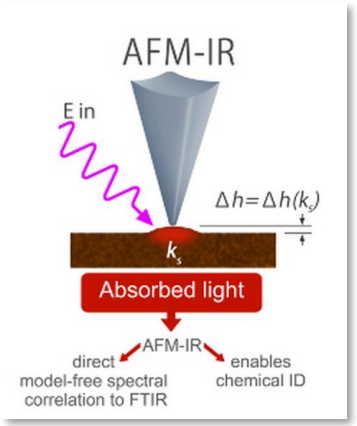

和FTIR类似

亚20纳米的光学分辨率

获得复杂的光学信息，间接得到化学信息

对于**无机，二维材料**以及**光子材料**适用性好

非常直接的红外吸收光谱和成像

非常准确，和FTIR光谱一致性极好

对于**有机，聚合物，高分子**适用性好

nature photonics

LETTERS

PUBLISHED ONLINE: 19 JANUARY 2014 | DOI: 10.1038/NPHOTON.2013.373

Tip-enhanced infrared nanospectroscopy via molecular expansion force detection

Mid-infrared absorption spectroscopy in the molecular fingerprint region is widely used for chemical identification and quantitative analysis employing infrared absorption spectra databases. The ability to perform mid-infrared spectroscopy with nanometre spatial resolution is highly desirable for applications in materials and life sciences. At present, scattering near-field scanning optical microscopy[1-6] is considered to be the most sensitive technique for nanoscale mid-infrared spectroscopy under ambient conditions. Here, we demonstrate that nanoscale mid-infrared spectra can be obtained with comparable or higher sensitivity by detecting mechanical forces exerted by molecules on the atomic force microscope tip on light excitation. The mechanical approach to mid-infrared nanospectroscopy results in a simple optical set-up that, unlike scattering near-field scanning optical microscopy, requires no cryogenically cooled mid-infrared detectors, is easy to align, and is not affected by sample scattering.

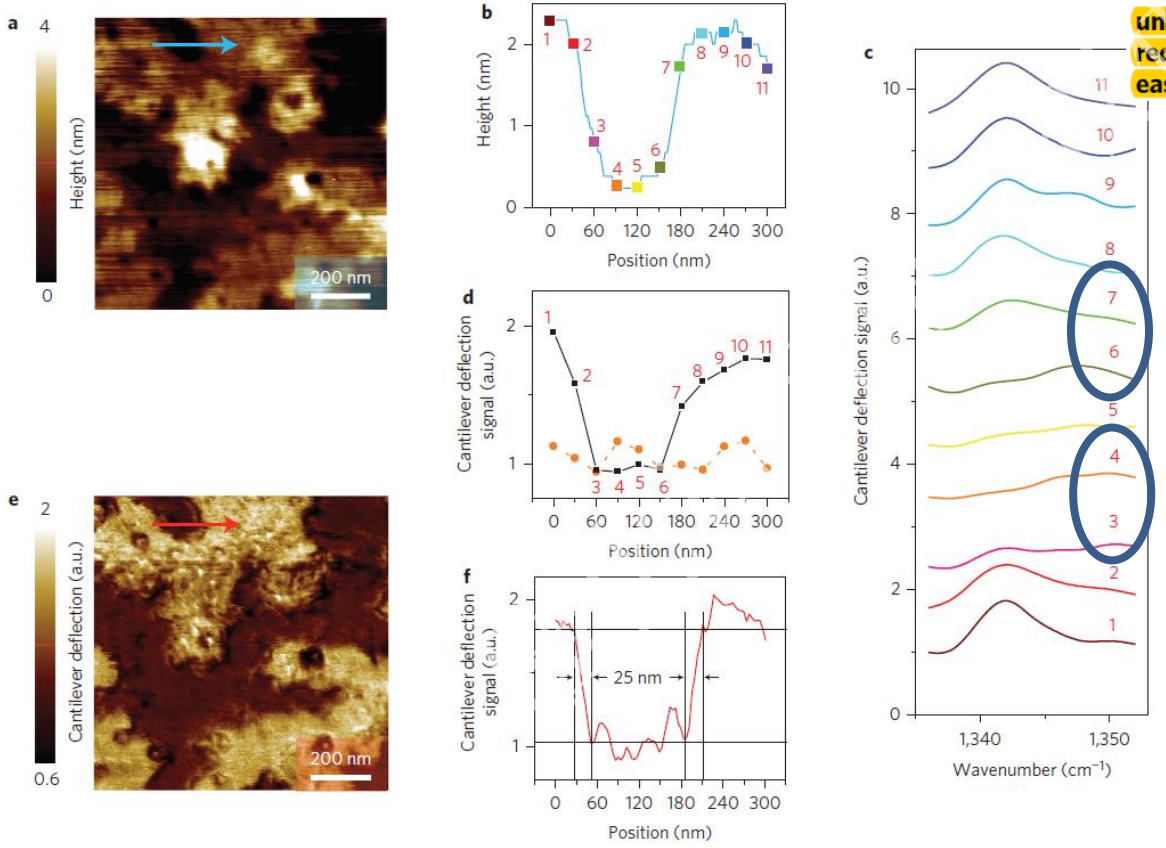

PTIR实现了SNOM可比的灵敏度：

1）单分子层灵敏度

2）25纳米红外光谱空间分辨率

SNOM和AFM-IR技术的差别以及应用差别？

纳米红外光谱近期展望

---无偏移的高信噪比光谱

--- 超快红外光谱

---10纳米化学成像

---1000~3600cm-1超宽光谱范围

---同时得到化学和纳米力学信息

Infrared Spectroscopy of Molecular Submonolayers on Surfaces by Infrared Scanning Tunneling Microscopy: Tetramantane on Au(111)

IR-STM

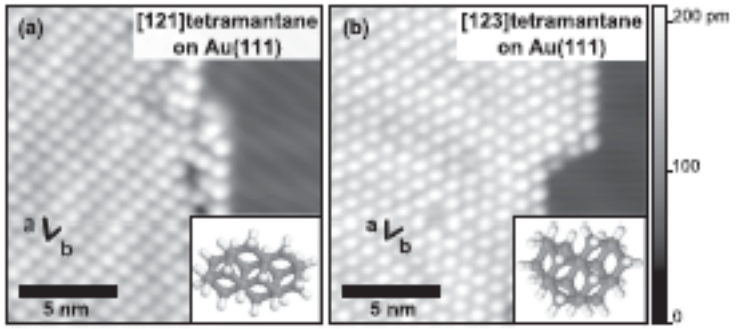

FIG. 1. (a) STM topography of [121]tetramantane molecules on Au(111) ($V_{sample} = 1.0$ V, $I = 50$ pA, $T = 13$ K). The molecular lattice has an oblique structure with lattice constants $|\mathbf{a}| = 11.1 \pm 0.1$ Å, $|\mathbf{b}| = 8.3 \pm 0.1$ Å, and an interior angle of $59° \pm 1°$. The inset shows a model of [121]tetramantane (gray and white balls represent carbon and hydrogen atoms). (b) STM topography of [123]tetramantane on a Au(111) surface ($V_{sample} = -2.0$ V, $I = 100$ pA, $T = 13$ K). Within experimental resolution, [123]tetramantane molecules form a hexagonal

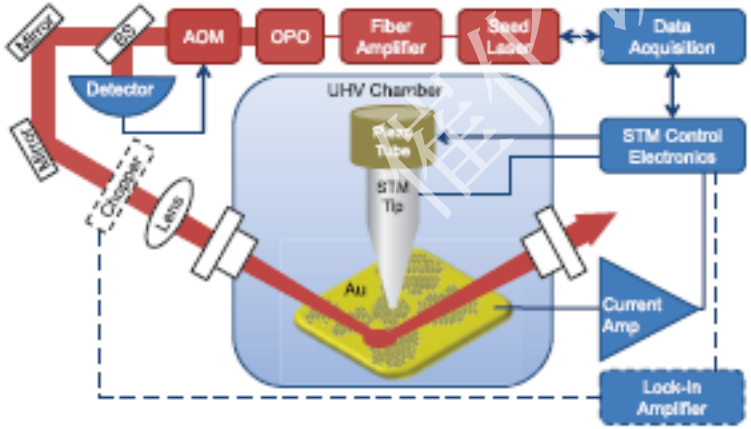

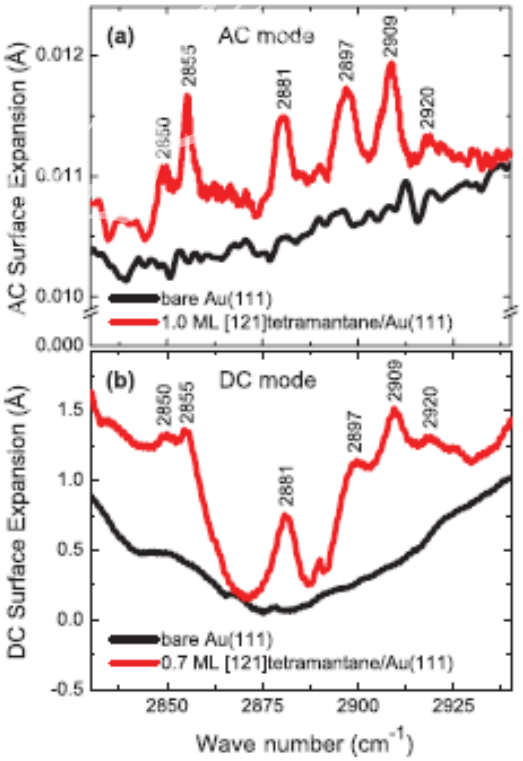

FIG. 3 (color). (a) Differential ac surface expansion due to absorption of modulated IR light, measured via lock-in amplifier for constant-current STM Z signal (chopper modulation frequency ~13 Hz, lock-in amplifier time constant 3 s). The black (lower) and red (upper) lines show ac surface expansion of bare gold and [121]tetramantane-decorated gold, respectively. (b) dc surface expansion of bare gold (black lower line) and [121] tetramantane-decorated gold (red upper line) as a function of incident IR frequency, measured via constant-current STM Z signal.

SX-STM

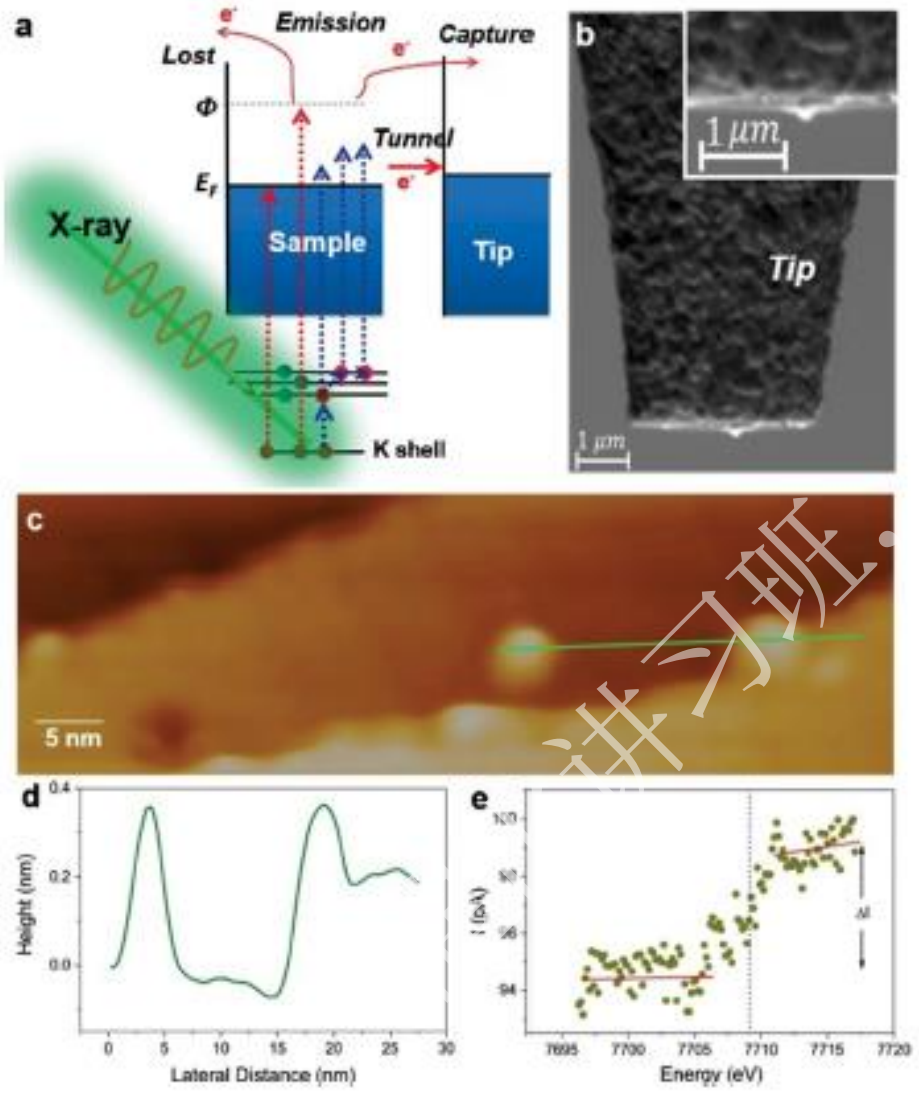

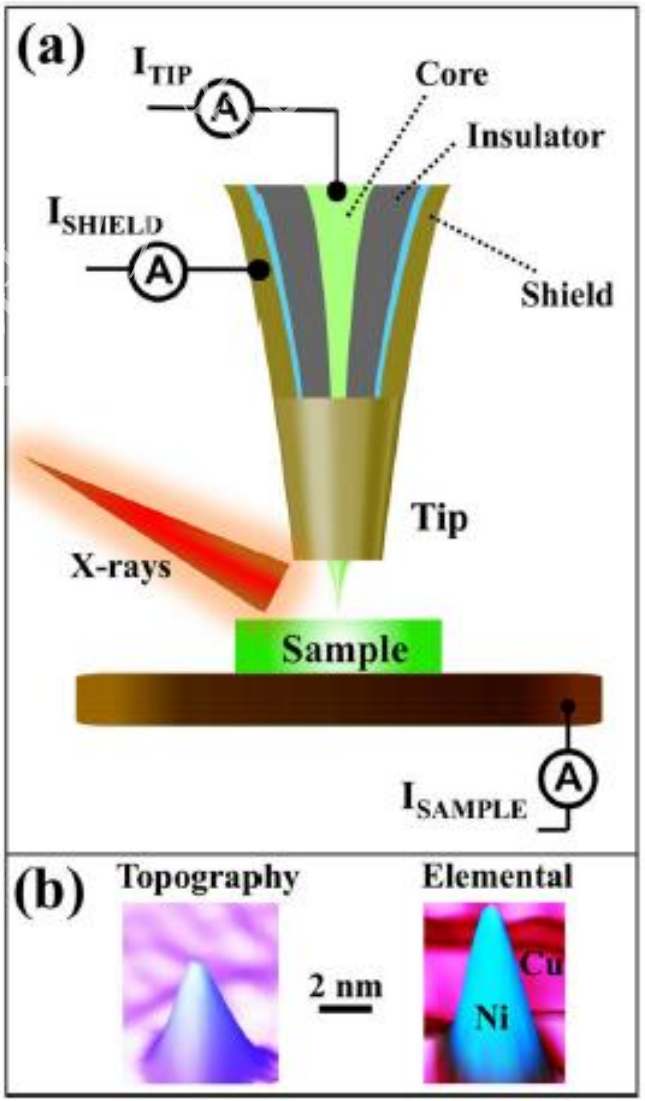

Hla et al.

深入催化反应的时间和空间尺度

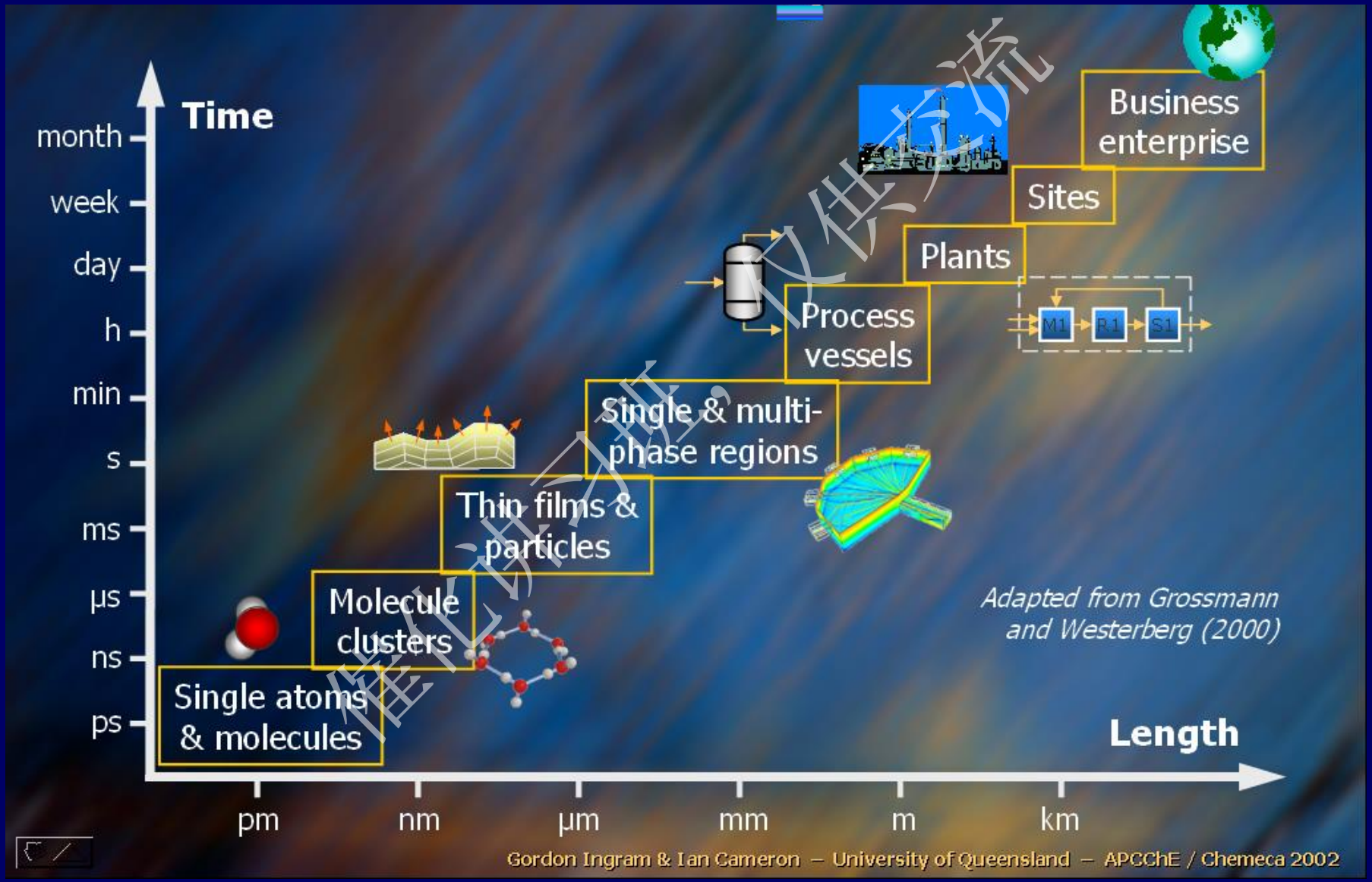

单纳米粒子表界面催化过程的原位观测

❑结合STM和自由电子激光红外光谱的tip增强表征方法

STM缺乏表面反应的化学信息

Tip增强的光学成像，其分辨率主要受针尖Apex限制

观测单个纳米粒子或者局域结构/活性位

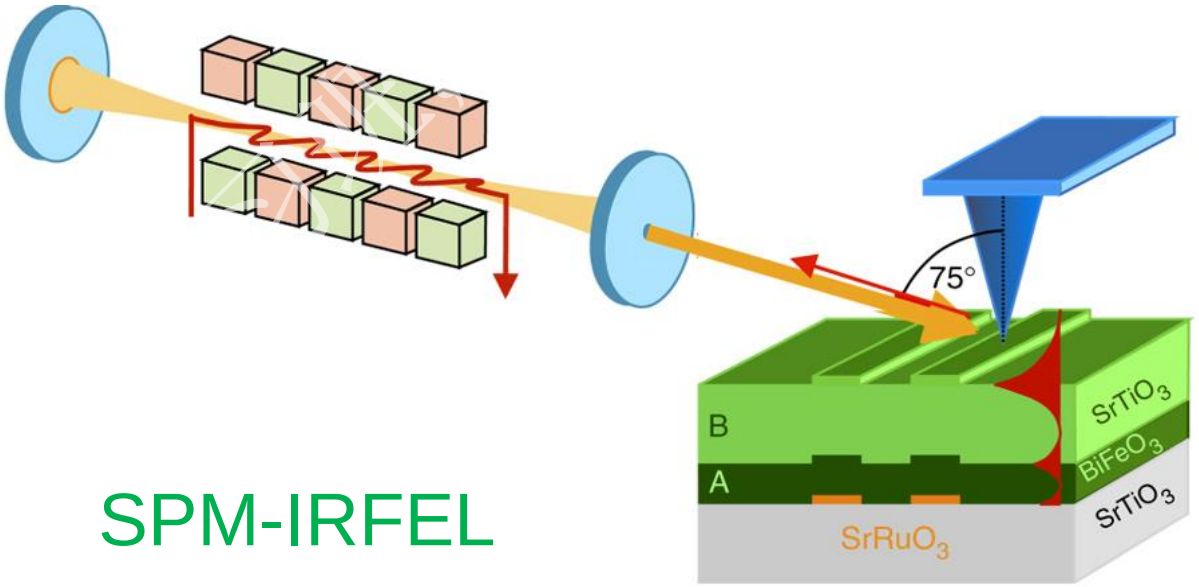

SPM-IRFEL

Thanks for Your Attention 谢谢!

Postdoc positions available!

Salary (200k-300k RMB/year + full compensasion by CAS + One Bedroom Apartment)